HYDROGEN REACTIONS WITH GERMANIUM SILICATE GLASSES

BY

ELIZABETH M. BIRTCH

A THESIS

SUBMITTED TO THE FACULTY OF

ALFRED UNIVERSITY

IN PARTIAL FULFILLMENT OF THE REQUIREMENTS
FOR THE DEGREE OF

DOCTOR OF PHILOSOPHY

IN

GLASS SCIENCE

ALFRED, NEW YORK

SEPTEMBER, 2006

HYDROGEN REACTIONS WITH GERMANIUM SILICATE GLASSES

BY

ELIZABETH BIRTCH

B.S. ALFRED UNIVERSITY (2002)

SIGNATURE OF AUTHOR (Signature on File)

APPROVED BY (Signature on File)
JAMES E. SHELBY, ADVISOR

(Signature on File)
THOMAS P. SEWARD, ADVISORY COMMITTEE

(Signature on File)
MATTHEW M. HALL, ADVISORY COMMITTEE

(Signature on File)
ALEXIS G. CLARE, ADVISORY COMMITTEE

(Signature on File)
CHAIR, ORAL THESIS DEFENSE

ACCEPTED BY (Signature on File)
ALASTAIR N. CORMACK, DEAN
KAZUO INAMORI SCHOOL OF ENGINEERING

ACCEPTED BY (Signature on File)
WILLIAM M. HALL, ASSOCIATE PROVOST
FOR GRADUATE AND PROFESSIONAL PROGRAMS
ALFRED UNIVERSITY

ACKNOWLEDGMENTS

First and foremost I would like to express my most sincere gratitude to my academic advisor and dear friend, James Shelby. Thank you for providing me with the experiences and opportunities necessary for a great career in the field of glass science. A very special thank you goes out to Mom, Dad, Jess, Andy and Luke, without your continued love and support I would not be where I am today.

I would also like to thank Marc Whalen from Corning Incorporated for providing the glass used in my research. My advisory committee members (Dr. Thomas Seward, Dr. Alexis Clare, and Dr. Matthew Hall) also deserve a sincere thank you for their invaluable input and guidance while preparing this thesis. Others who contributed to this work through support in specific characterization techniques include; Swavek Zdzieszynski and Dr. Scott Misture (XRD), Gerry Wynick and Ward Votava (ESEM/EDS), and Juergen Walker (Confocal Raman Spectroscopy). Pat LaCourse also deserves recognition for helping with the formatting of this thesis.

It is great to have such a wonderful opportunity to thank all of my friends who have had a significant influence and impact on my research and graduate career through insightful conversations; Fabienne, Michelene, MJ, Melissann, Melodie, Mandi, Doug, Doug, Chris, Bryan, Dan and Nate. Thanks to all of you for helping me get through the course work and various research endeavors.

TABLE OF CONTENTS

LIST OF TABLES

LIST OF FIGURES

Note regarding color figures: For convenience of reproduction, this thesis is available in PDF format at Scholes Library, Alfred, NY

ABSTRACT

The effect of processing technique and the presence of striations in glasses on the properties and behavior of binary GeO_2-SiO_2 is reported. Optical images of the as-received binary GeO_2-SiO_2 glasses prepared by OVD show concentric circular striations observed as a refractive index pattern resulting from the layer-by-layer deposition processing technique. The composition of two different binary GeO_2-SiO_2 glasses was examined using electron microprobe analysis. The environmental scanning electron microscope (ESEM) was used to characterize the striations after etching. The density, refractive index, and thermal expansion coefficient of binary GeO_2-SiO_2 glasses have been measured and found to be relatively insensitive to the presence of striations.

Treatment of 100 mol% SiO_2, 6 mol% GeO_2-94 mol% SiO_2 and 14.6 mol% GeO_2-85.4 mol% SiO_2 glasses was monitored using infrared spectroscopy and optical spectrometry as a function of time under a H_2 atmosphere (700 Torr) at 500ºC, 600ºC, 700ºC and 800ºC. Hydrogen reactions with binary GeO_2-SiO_2 glasses to form hydroxyl species, monitored using infrared spectroscopy, are a function of time, temperature and germanium content. The effect of GeO_2 concentration on hydroxyl formation is evident as induced hydroxyl formation increases with increasing GeO_2 concentration. The rate of hydroxyl formation increases with increasing temperature for both binary GeO_2-SiO_2 glasses. Hydroxyl concentration is uniform throughout the thickness of the sample at saturation. Hydride species do not form during heat treatment in hydrogen at any of the temperatures in either of the binary GeO_2-SiO_2 glasses, as indicated in the lack of change in their infrared spectra.

The change in concentration of reduced germanium species in the glass caused by hydrogen diffusion is monitored using optical spectroscopy and is a function of time, temperature and germanium content. This reaction is associated with an intense change in color of the glass from colorless to brown. The effect of GeO_2 concentration on color formation is evident, as induced color formation increases with increasing GeO_2 concentration. The rate of color formation increases with increasing temperature for both binary GeO_2-SiO_2 glasses. A detailed analysis of the changes in the optical spectra resulting from hydrogen reactions is provided. Color formation is confined to the exposed surface of each sample. Color concentration is not uniform across the surface of the sample, but varies systematically with areas of non-uniform concentration in the samples. This reaction is associated with an induced crystallization. A detailed analysis of the induced crystallization resulting from hydrogen reactions, using X-ray diffraction and Raman spectroscopy, is provided. Induced crystal formation is confined to the exposed surface of each sample and is not uniform across the surface of the sample, but it varies systematically with areas of non-uniform concentration in the samples, similar to the results observed with color formation.

Hydrogen treatment of pure GeO_2 glasses was monitored as a function of time under a hydrogen atmosphere (700 Torr) at 400°C, 450°C and 500°C. Pure GeO_2 glasses heat treated in the presence of hydrogen readily react to form reduced germanium species confined to the surface of each sample, including crystals of pure germanium.

CHAPTER 1: INTRODUCTION

This research started as an effort to obtain a fundamental understanding of hydrogen reactions silica glasses with a number of different dopants. The focus of the research was quickly narrowed, however, by the discovery of the unexpected sensitivity of binary GeO_2-SiO_2 glasses to reaction with hydrogen. Other doped silica glasses showed relatively little reaction with hydrogen, but the binary GeO_2-SiO_2 glasses showed unanticipated changes in the appearance of samples, suggesting possible reactions with hydrogen. GeO_2-SiO_2 glasses developed a dark brown color with progressive treatment in hydrogen. Infrared measurements revealed the formation of a significant amount of hydroxyl associated with both germanium and silicon species in the glass. These remarkable results were not anticipated and suggested further investigation.

The work presented here represents an exploratory study of the interactions of hydrogen with binary GeO_2-SiO_2 glasses at elevated temperature. This thesis encompasses a series of studies orchestrated to further clarify the chemical reaction between hydrogen and binary GeO_2-SiO_2 glasses. A few of the specific topics addressed include: the difference in reaction rate between binary GeO_2-SiO_2 and pure SiO_2 glasses, the effect of temperature on the reaction process, and the source of the color formation. Another important property of the glasses studied is that they have striations resulting from the process by which they are fabricated. What effect would the presence of striations have on this reaction process? The chapters of this thesis include a detailed discussion of the each of these effects, preceded by a thorough investigation of the properties of the glass samples.

This thesis reports the results of an extensive study on hydrogen reactions with binary GeO_2-SiO_2 glasses. Many different defect centers and structural imperfections in this glass system have been observed, monitored and identified. Perhaps most significant conclusion of this research is that hydrogen-induced color formation results from formation of nanocrystalline germanium species in the near surface of the glass samples.

CHAPTER 2: LITERATURE REVIEW

This literature review presents a brief overview of existing applications of binary GeO_2-SiO_2 glasses, as well as a summary of active areas of current research including potential applications. This short introduction to the material is followed by a fundamental description of the binary GeO_2-SiO_2 glass structure and the processing techniques necessary to produce the high purity glass used in this research. A short description of the interactions of light with glass is presented, followed by a more detailed review of measurement techniques used throughout this thesis, identification of defect species known to exist in this glass system and spectral analysis techniques related to this research. Finally, analysis techniques used to identify crystal formation in the glass are discussed, with a short summary of the properties of crystal phases observed in this research.

2.1. Current Applications of Binary GeO_2-SiO_2 Glass

As a result of their remarkable durability, compositional purity and superior optical quality, binary GeO_2-SiO_2 glasses have found many applications in modern technology. Perhaps the most important and best-known application is the use of binary GeO_2-SiO_2 glass as the core composition in optical fibers. The use of binary GeO_2-SiO_2 glass and other doped silica glass compositions allows flexibility in the design of optical fiber systems.

2.1.1. Optical Fiber Design

The theoretical foundation behind the optical fiber communications system is the principal that light in a glass medium can carry information over longer distances with more bandwidth than electrical signals in copper or coaxial mediums. The first challenge in creating optical fiber communication systems was development of a glass pure enough to transmit a light signal over a significant distance without amplification. Early research on glasses used for optical communications dealt with multi-component glasses including soda-lime silicate and borosilicate glass systems. The focus of research then shifted to high-silica content glass systems made by the vapor phase technique when advantages included relatively easy tailoring of refractive index, higher strength and durability, lower

concentration of impurities and, most importantly, low hydroxyl concentration levels were discovered.

The ability to tailor the refractive index of the glass is the most important tool in optical fiber design since the functionality of an optical fiber is based on the principal of total internal reflection. Lightwaves are guided through the core of an optical fiber by reflection at the interface between the core and cladding of the optical fiber. The angle at which the light waves are transmitted enables control over the efficiency of the light propagation. The composition of the core glass relative to that of the cladding determines the fiber's ability to refract the light. The difference in the refractive index of the glass compositions confines the transmitted light to the core of the fiber. Refractive index is the most basic optical property for determination of the appropriate glass for many applications and remains the most measured optical property of glasses.[1] The well-characterized increase of refractive index, with increasing GeO_2 content, attainable using the binary GeO_2-SiO_2 glass system is the primary reason these glasses are so popular in optical fiber design.

The greatest limitation on the use of optical fiber as an optical wave-guide is attenuation, often measured in dB/km. Optical loss can either be from absorption loss or radiative loss. Intrinsic absorption loss is characterized as loss due to interactions between major glass components, for example absorption bands that develop from oscillations of structural units within the glass. Extrinsic absorption is often characterized as loss due to impurities, for example absorption bands that develop from transition metal ions.[2] Radiative loss, or scattering loss, is loss caused by inhomogeneities smaller than the wavelength of light, that arise from density and compositional fluctuations that are frozen into the glass structure upon cooling. Glass fabrication methods, composition and fiber design are all possible sources of optical loss. Improvements in loss quality can be made through characterization of defects and impurities. Defects and structural imperfections within the glass network pose a serious threat to the required low transmission loss necessary to achieve significant signal retention over long distances. The elimination of these defects opens up the communications windows at 1310 and 1550 nm where the lowest intrinsic loss is achievable. The challenge to improve optical fibers and develop high purity glass has

resulted in glass manufacturing techniques far beyond conventional glass melting methods involving melting reagent grade powder components.

2.1.2. Basics of Fiber Bragg Gratings

The capability to manufacture optical fibers with complex compositional profiles, including the binary GeO_2-SiO_2 core with a pure SiO_2 cladding, lead to the discovery of fiber Bragg gratings. Fiber Bragg grating technology has its origins in the discovery of photosensitivity of binary GeO_2-SiO_2 glass by Hill et al.[3] in 1978. Binary GeO_2-SiO_2 glasses have a unique response to ultraviolet light, enabling an induced, permanent increase in refractive index upon exposure to ultraviolet light. The observation of this unique response presented scientists with the challenge of creating a useful application. In 1989, it was found[4] that a permanent periodic modulation of the refractive index in the core of a photosensitive fiber could be produced by transverse illumination with an interference pattern created by a pair of strong UV-laser beams. Fiber Bragg gratings are formed when a series of traverse planes, characterized by a permanent periodic modulation of the refractive index, are created within the binary GeO_2-SiO_2 core of a singlemode optical fiber. Light propagating through the core of the optic fiber will be reflected by the interfaces between regions having different refraction indices. For most wavelerngths, the reflected light is out of phase with the incident light resulting in extinction, however, for a specific wavelength, the Bragg wavelength λ_{Bragg}, the light reflected by the periodically varying index of refraction will be in phase and will add constructively. This phenomenon results in a characteristic minimum in transmission spectrum as well as a peak in the reflection spectrum that is characteristic of the spacing between the lines. Obvious applications of this technology arise in the form of sensors used to measure strain, i.e. tension or compression of the Bragg grating will result in a change in the special arrangement of the lines, ultimately resulting in a change in the measured reflection spectrum. Fiber Bragg gratings are now components for a wide range of applications in the areas of telecommunications, lasers and sensors.

In 1993 Lemaire et al.[5] discovered that high pressure hydrogen loading of the fiber prior to UV laser exposure enhances the photosensitivity and thermal sensitivity of the binary GeO_2-SiO_2 glasses. In fact, the process of creating various refractive index

modifications and achieving submicrometer spatial resolution now relies on loading optical fibers with molecular hydrogen prior to exposure to UV light or heat.[6] The chemical reactions that occur between the structural imperfections in the glass network and hydrogen with exposure to heat or UV light are of primary importance for the understanding of the mechanisms for increased photosensitivity due to hydrogen and not yet fully clarified.[7]

2.1.3. Current Research: Nanocomposite Materials

Nanocomposite materials consisting of very small colloidal particles dispersed in a host matrix have been the topic of a very active area of research for the last decade. The popularity of this field continues to grow. Current interest of such nanocomposite materials arises from potential applications in chemical catalysis or magnetic, electronic or photonic (nonlinear optical) materials. More specifically, nanocrystals of homopolar semiconductors, like silicon and germanium, embedded in a silicon dioxide matrix, have been studied extensively for their luminescence and charge retention properties for integration as optoelectronic and microelectronic devices and complimentary metal-oxide-semiconductor (CMOS) applications.[8] Nanocrystals embedded within SiO_2 can be successfully fabricated by a number of different methods, including plasma deposition from silane,[9] dc sputtering deposition in a reactive oxygen environment,[10] rapid thermal annealing,[10] termination of glass-melt reaction,[9] sol-gel processing[11] and ion implantation.[12] In recent years, ion implantation with subsequent annealing has been determined to be the fabrication method best suited for CMOS nanocrystal memory fabrication.[8]

2.2. Binary GeO_2-SiO_2 Glass Structure

Vitreous GeO_2 has a structure very similar to that of vitreous SiO_2. The basic building block of both of these glasses in the pure form is a cation-oxygen tetrahedron unit.[a] Networks consist of tetrahedra connected at all four corners just as in the

[a] In multi-component glass systems germanium can be found in either 4 or 6 fold coordination if a modifier is present.

corresponding crystals, but the vitreous networks are not periodic and symmetrical as in the crystal. The networks extend in 3D such that the average behavior in all directions is the same, i.e. properties of the glass are isotropic. Silicon and germanium are both considered glass formers in the binary GeO_2-SiO_2 glass system with a structure consisting of a fully linked network made up of a random mixture of GeO_2 and SiO_2 tetrahera, as shown in the illustration in Figure 2.1. Such structural units are often referred to as Q_4 units, indicating four-fold cation coordination. Each oxygen atom is shared by two silicon or germanium atoms, which occupy the center of the fully linked tetrahedra. The germanium ion is larger in diameter than silicon and the Ge-O bond distance is greater, with a bond length of ~0.173 nm, than that of the Si-O bond at, ~0.162 nm.[1] The average Ge-O-Ge bond angle is also smaller than the average Si-O-Si bond angle. Gas diffusion studies suggest that the structure of vitreous GeO_2 is more compact than that of vitreous SiO_2, resulting in a slightly lower free or interstitial volume in vitreous GeO_2. The lower melting temperature of GeO_2 as compared to that of SiO_2 indicates that the Ge-O bond is considerably weaker than the Si-O bond. Simple ionic field strength arguments would lead to the same conclusion. Structural defects are more common in vitreous GeO_2 than in vitreous SiO_2, with a measurable concentration of Ge-Ge bonds. The two components are mutually soluble in all proportions. Bulk properties, i.e. density and refractive index, vary linearly from one pure glass to the other.[13,14] Although the glasses are not phase separated, it has been suggested, and is supported by some spectral evidence, that intermediate range order groups containing only one species of glass forming oxide exist in the structure.

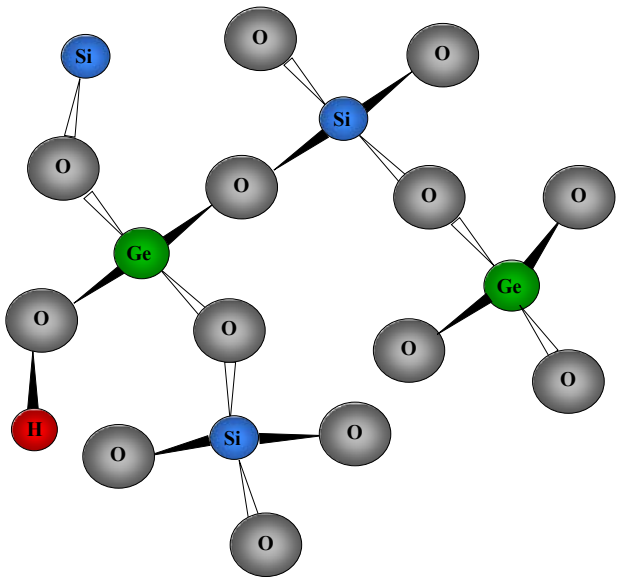

Figure 2.1. Illustration of binary GeO_2-SiO_2 structure.

Fabrication of binary GeO_2-SiO_2 glasses is very difficult due to the extreme temperatures necessary to melt components into a fully dense and transparent glass. Fortunately, the challenge to improve optical fibers and develop high purity glass spurred the development of a number of glass manufacturing techniques that allow for fabrication of high purity doped silica glasses. Development of numerous fabrication techniques for vitreous SiO_2 lead to a classification system to distinguish between different types of commercially available SiO_2 glass with respect to properties and structure.[15] Type I SiO_2 glasses are produced from natural quartz by electrical fusion under vacuum or under an inert gas atmosphere. Contamination in Type I SiO_2 glasses include a relatively high concentration of metallic impurities, and a low hydroxyl content. Type II SiO_2 glasses are produced from quartz crystal powder by flame fusion. Partial volatilization and the absence of a crucible greatly reduces metallic impurities, however, the atmosphere of the hydrogen-oxygen flame results in a relatively high hydroxyl content. Type III SiO_2 glasses are called synthetic vitreous SiO_2 glasses, and are produced by hydrolysis of $SiCl_4$ (high purity organic silanes) sprayed into an oxygen-hydrogen or natural gas-oxygen flame. The use of distilled liquid raw materials results in glass free of metallic impurities, however, for $SiCl_4$ precursors the resulting glass usually has a relatively high chlorine content. The use of the oxygen-hydrogen flame also results in extremely high

hydroxyl content. Type IV SiO_2 glasses are also synthetic glass produced from $SiCl_4$ in a water vapor-free plasma flame. These glasses are similar to the Type III glasses, but have a considerably lower hydroxyl content. Table I summarizes the approximate impurity content of each type of SiO_2 glass, including some of the common commercial product names.

Table 2.I. Summary of Impurity Content of Each Category of Silica Glasses.[15]

Type of Silica	Metallic Impurities (ppm)	Hydroxyl Content (ppm)	Chlorine Content (ppm)	Common Commercial Product Names
Type I	30-100	5 or less	NA	Infrasil, IR-Vitreosil
Type II	less than 30	150-400	NA	Herasil, Homosil, Optosil
Type III	NA	1000	100	Suprasil, Spectrosil, Corning 7940
Type IV	NA	1 or less	200	Suprasil W, Spectrosil WF, Corning 7943

Type III and IV SiO_2 glasses are considered to be best suited for optical applications due to the reduced concentration of most transition metal impurities, which eliminates optical absorption within the transmission window. In particular, Type IV SiO_2 is considered the optimal type of SiO_2, since it has the lowest metallic impurity and hydroxyl concentration of all four types of SiO_2. Process modifications or subsequent treatments of the glasses have also been used to create extremely low hydroxyl content glasses.

2.3. Outside Vapor Deposition Process

The germanium doped silica glasses used in this study were fabricated at Corning Inc. using a doping and redraw process similar to that used in optical fiber production. Manufacturing of an optical fiber usually consists of three steps: laydown, consolidation, and draw. The outside vapor deposition process is the preferred fiber laydown process since it has many advantages over plasma chemical vapor deposition (PCVD) and modified chemical vapor deposition (MCVD). In the OVD process, a rotating bait rod is used to collect fine soot particles of silica and germania from a traversing burner,

illustrated in Figure 2.2. The traversing burner is used as a mixer as ultra-pure processing gasses react in the flame. The process gases include active gases, i.e. the gases that will react to contribute glass-forming species to the chemical composition of the final glass product, such as $SiCl_4$ and $GeCl_4$, and delivery and combustion gasses such as CH_4 and O_2. The optical fiber preform is constructed by accumulating sequential layers of soot from the center outward. Since raw materials used in this process are liquids, purification by distillation radically reduces impurity content. One very important advantage of this process is ability to manufacture a soot perform containing only silica and germania. MCVD requires the use of additional chemicals, like phosphorous, to facilitate soot consolidation and centerline hole closure, resulting in increased attenuation in the presence of radiation and hydrogen.

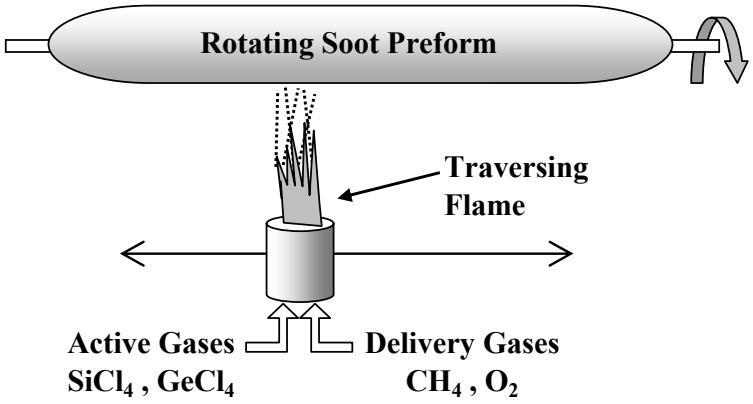

Figure 2.2. Schematioc of outside vapor deposition process.

After the bait rod is removed from the center of the porous preform, the preform is transferred from the OVD lathe to a consolidation furnace for further vapor phase cleaning and drying. As part of the same processing step, the soot preform is then sintered into pure glass in a precisely controlled environment to ensure uniformity, as shown in Figure 2.3. This process may also include a doping process whereby the soot or glass is exposed to alternate gasses to create doped glass compositions. Some common dopants that have been used include TiO_2, GeO_2, P_2O_5, and Al_2O_3, which increase the refractive index, or B_2O_3 and F dopants, which decrease the index. These dopants can be used in a variety of combinations to create different fiber profiles. The centerline of the

perform is then exposed to an etch gas prior to hole closure to remove any remnants of the bait rod. Centerline hole closure in the OVD process is exceptional, resulting in a very smooth and compositionally uniform index profile. The ability to manufacture glass with very high purity levels is another advantage of the OVD method. Unlike inside vapor deposition methods, i.e. MCVD and PVCD, that are formed in a glass tube, often manufactured by a third party supplier, OVD performs are formed directly from the chemical raw materials.

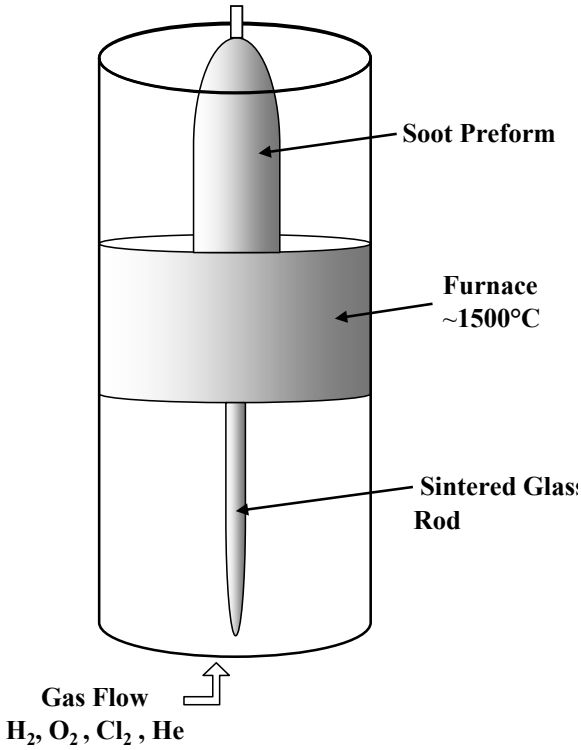

Figure 2.3. Schematic of consolidation process. Porous soot preform prepared via OVD is subsequently lowered into a furnace where it is sintered into a dense glass rod at approximately 1500°C under an atmosphere composed of a mixture of gases.

2.4. Interactions of Light with Glass: Multi-Phonon Edge and UV Band Edge

Electromagnetic radiation of any wavelength impinged on a glass results in an interaction between the material structure and the radiation. The nature of the interaction varies with the energy of the incident radiation, characteristic energy levels associated with the material and the presence of defects or inclusions in the structure. Optical

characteristics of transmission, absorption and reflection are fundamentally related to the interaction of the atomic structure of the glass and the energy of the incident radiation.

In the optical spectrum of most glasses, the frequency region with the maximum intrinsic transparency is referred to as the optic window. The broad transmission range in frequency is bound on the long-wavelength side by the infrared band edge, also known as the multi-phonon edge, and on the short wavelength side by the ultraviolet band edge, also known as the electronic edge. All transparent materials have an inherent ultraviolet and infrared band edge, marked by an intense absorption of light resulting from the intrinsic structure and composition of the material.[16]

The multiphonon edge results from the intense absorption of light by structural vibrations with characteristic dipole moments. Most structural units within a glass have characteristic dipole moments and the frequency of the multiphonon edge is a strong function of the glass composition. The vibrational frequency is a strong function of the bond strength and the mass of the atoms involved in the bond, therefore the glasses containing heavier ions with weaker bonds will result in a low frequency shift of the multiphonon edge. The multiphonon edge is not significantly affected by the presence of defects and minor structural imperfections in the glass.

The ultraviolet band edge is a result of band gap absorption when electrons are excited and move from a filled valance band to an empty conduction band. In oxide glasses, the absorption edge results from the energy required to liberate an electron from the network forming anion, i.e. oxygen. The ultraviolet band edge for pure silica results from the excitation of an electron from a bonded oxygen atom in the network, since silica has a 4+ charge and is not as readily excitable. The ultraviolet edge, or band gap energy, for most oxide glasses typically occurs in the ultraviolet region of the electromagnetic spectrum. Impurities, defects and minor perturbations of the network structure have a dominating influence on the UV band edge frequency.[2] Electron excitation is possible because there are inherent defects and disruptions of the continuous random network within the glass structure. The true ultraviolet edge of most commercial glasses is often obscured by the presence of intense charge transfer bands due to intrinsic impurities that become an effective UV edge. This artificial shifting of the effective UV band edge to high wavelengths can result from disruptions of the silica network caused by the presence

intrinsic defects or alkali impurities. For example, when alkali impurities are incorporated into the silica network, non-bridging oxygens are formed. The electron from a non-bridging oxygen associated with a defect in the glass is more easily excited than that of typical bonded oxygen atoms and therefore takes less energy to excite, shifting the apparent UV band edge to lower frequencies, higher wavelength**.**

2.5. Optical Absorption Spectroscopy and Glass

Optical spectroscopy probes electronic transitions in glasses, via absorption and emission of visible and UV light. Intrinsic optical absorption features in the visible energy range (759 – 393 nm, 1.6-3.1 eV) are typically a result of disruptions in the fundamental structural oscillators in the material that exhibit intense electromagnetic activity. Impurities, inherent defects and minor disruptions of the network structure can all contribute to spectral features in this spectral region.

2.5.1. Defects in Binary GeO_2-SiO_2

The study of defects in binary GeO_2-SiO_2 glass is not only necessary to evaluate loss and degradation in performance of optical glasses but is of primary importance for the understanding of the mechanisms behind the unique response to ultraviolet irradiation and reactions with hydrogen. The ideal structure of binary GeO_2-SiO_2 glass is a continuous random network made up of germania and silica tetrahedra joined at the corners. This continuous random network of tetrahedral bonds is not energetically stable, therefore defects are incorporated into the structure as an essential component.[1] Some common defects in binary GeO_2-SiO_2 glass are E'centers, oxygen hole centers, peroxy radicals, lone pair centers, oxygen vacancies, and T-T bonds.[b] Defects and inclusions can result in scattering loss and attenuation of propagating light. This scatter and absorption is typically wavelength dependent.

E' centers consist of an unpaired electron in a dangling, tetrahedral (sp^3) orbital, of a single silicon or germanium atom bonded to only three oxygen atoms, otherwise known as a trapped hole, designated by (≡T•).[17] Three variant types of E' centers exist

[b] In binary GeO_2-SiO_2 glasses it is common notation to use "T" to designate either Ge or Si cations.

and are described as E'$_\beta$, E'$_\alpha$, and E'$_\gamma$. Formation of E'$_\alpha$ species occur when oxygen atoms are displaced by knock-on collisions with high energy Compton electrons, allowing a hole to be trapped at the site of a natural oxygen vacancy, as expressed by Reaction 2.1[17]

$$\equiv T\text{-}T\equiv \rightarrow \equiv T\bullet + T\equiv + e^- \qquad (2.1)$$

where the T≡ structure relaxes into a planr configuration of an ionized bond. E'$_\gamma$ are created by a radiolytic process that moves an oxygen atom from an undisturbed network site to a neighboring position, which has to be chemically bonded since the energy produced from an x-ray generated Compton e^- is insufficient to result in a net breakage of bonds. This process can occur in one of two ways, as expressed by Reactions 2.2 and 2.3

$$\equiv T\text{-}O\text{-}T\equiv + h\nu \rightarrow \equiv T\bullet + \equiv T\text{-}O\text{-}O\bullet + e^- \qquad (2.2)$$

$$\equiv T\text{- -}O\text{-}T\equiv \rightarrow \equiv T\bullet + \bullet O\text{-}T\equiv \qquad (2.3)$$

where (+O-O) represents a peroxy bond, or peroxy radical, ≡T- -O-T≡ represents momentary rupture of a strained T-O bond and •O-T≡ represents a non-bridging oxygen hole center. E'$_\beta$ formation occurs when mobile hydrogens react with a three coordinated silicon or germanium, which cause a pre-existing defect sites in the un-irradiated glass, as expressed in Reaction 2.4[18,19]

$$\equiv T + H^\circ \rightarrow \equiv T\bullet + H^+ \qquad (2.4)$$

The above process can also resulting from long range relaxations when mobile hydrogen reacts with an oxygen vacancy, creating an E'$_\beta$ and hydride species, as expressed by Reaction 2.5.

$$\equiv T\text{-}T\equiv + H^\circ \rightarrow \equiv T\bullet + \equiv T\text{-}H \qquad (2.5)$$

An oxygen hole center represents a hole trapped in the $2p^3$ orbital of a single oxygen bonded to a single silicon, designated by (≡T-O•). One variant of an oxygen hole center, a non-bridging oxygen hole center, is produced in reaction 2.3. Non-bridging oxygen hole centers are also produced when type III silica is x-irradiated at temperatures less than 100K due to hydrolysis of hydroxyl groups,[18,19] as expressed by Reaction 2.6.

$$\equiv Si\text{-}OH \rightarrow \equiv Si\text{-}O\bullet + H^{\circ} \qquad (2.6)$$

A peroxy radical is an oxygen associated hole center, designated by (≡Si-O-O•). Peroxy radicals can form as a co-product when E'γ are formed as shown in equation 2.2. Peroxy radicals also form in un-irradiated, low hydroxyl silica from a precursor structure called a peroxy linkage (≡Si-O-O-Si≡) that traps a hole, as expressed by Reaction 2.7.[17]

$$\equiv Si\text{-}O\text{-}O\text{-}Si\equiv \rightarrow \equiv Si\text{-}O\text{-}O\bullet + \text{-}Si\equiv + e\text{-} \qquad (2.7)$$

The peroxy linkage is a member of a Frenkel defect with a neutral oxygen pair vacancy (≡Si-Si≡) as the counter part. Bleaching, through exposure to oxygen, of an E'_{γ} can also form a peroxy radical, as shown in Reaction 2.8.

$$E'_{\gamma} + O_2 \rightarrow \equiv T\bullet + O_2 \rightarrow \equiv T\text{-}O\text{-}O\bullet \qquad (2.8)$$

Diffusion of hydrogen into silica containing defects can result in an elimination or conversion of the defects. E'centers, oxygen hole centers, and peroxy radicals all react with molecular hydrogen to form SiH or SiOH. E' centers will react with molecular hydrogen to produce SiH as expressed by Reaction 2.9.[18,19]

$$\equiv Si\bullet + H_2 \rightarrow \equiv SiH + H^{\circ} \qquad (2.9)$$

Molecular hydrogen reacts with an OHC as expressed by Reaction 2.10.

$$\equiv Si\text{-}O\bullet + H_2 \rightarrow \equiv Si\text{-}OH + H^{\circ} \qquad (2.10)$$

A peroxy linkage will react with hydrogen to form two hydroxyl groups, as expressed by Reaction 2.11.[19]

$$\equiv Si\text{-}O\text{-}O\text{-}Si\equiv \rightarrow \equiv Si\text{-}OH + HO\text{-}Si \equiv \qquad (2.11)$$

Defects in high purity glasses can be manipulated to obtain the necessary properties for specific glass applications. Hydrogen reactions with radiation induced defects can be beneficial when processing lenses, where good ultraviolet transparency is desired, since hydrogen induced absorption bands appear in the infrared region of the spectrum. Optical fiber applications, however, require an extremely low concentration of hydrogen related defects in glass, since absorption peaks associated with these defects exist within the optical window used for many telecommunications systems.

2.6. Infrared Spectroscopy as a Characterization Tool

Infrared spectroscopy is a relatively inexpensive, non-destructive and important analytical technique used for the determination of several structural features in common glass systems. Absorption or emission spectra resulting from the rotational and vibrational motions of a molecule generally occur in the infrared region of the electromagnetic spectrum. Infrared spectroscopy uses photons to probe material excitations including phonons (atomic vibrations). Polychromatic light at infrared wavelengths is used to couple directly to vibrational modes inherent to the material via the dipole moment associated with the vibrations. Bonds within a glass vibrate at a specific resonant frequency. When a material is exposed to infrared radiation of that frequency, the bond will absorb the energy of the incident photon. Molecular bond vibrations result in a change in dipole moment, which has an inherent electrical field that interacts with the electrical component of electromagnetic radiation. All bonds that have a changing dipole moment and are capable of producing an oscillating electric field will demonstrate this phenomenon. Overtones at frequencies that are integral multiples of the fundamental are also possible, but their contributions to the spectra are much weaker in intensity.

The relative sensitivity of this technique can be shown by the fact that, while there is only approximately 0.025% carbon dioxide in the atmosphere, the presence of this gas is revealed in spectra from every spectrometer in which air is the medium through which the measurement is made. Such spectra contain a very sharp absorption band at 4.26μm (2347 cm^{-1}). This absorption band can provide a simple check of the calibration of the instrument,[20] but it is typically removed with the background prior to the sample measurement.

Infrared spectroscopy is primarily a qualitative measurement, but it can be used for some quantitative measurements when used correctly. It is important to scrutinize the range of validity in terms of accuracy when analysis of infrared absorption spectra is presented, since it is very subject to personal interpretation. A reasonable amount of labor is required to unravel the spectrum of a complex molecule often involving advanced mathematics, such as group theory.[20] The theoretical tools for such analysis are well developed, and the results to be obtained are of such broad interest that the peak assignments are commonly made through assumptions, which often leads to extremely suspect conclusions. Therefore, infrared spectroscopy is often used in conjunction with other analytical methods. Correlations between absorption peaks and vibrations can be confirmed by comparing the results of many analytical methods. Unfortunately, there are some instances where information can only be obtained from infrared analysis and is not available through other means. In spite of complications involving spectral analysis, vibrational spectra can provide an efficient means of detecting changes in material composition and structure with progressive treatments.

2.6.1. Infrared Spectroscopy: Hydrogen Reactions in Glass

Infrared spectroscopy has been used extensively to detect and monitor the presence of water and other hydrogen related species in glasses. Hydroxyl species, often considered unintentional impurities, have a characteristic absorption in the infrared portion of the spectrum. The interaction of gases, such as hydrogen and deuterium with glasses has been studied extensively.[21] When hydroxyl is incorporated in the structure of either pure silica or binary GeO_2-SiO_2 glasses, an infrared active band appears resulting from the stretching vibration between oxygen and hydrogen atoms. Bands due to

hydroxyl species in pure GeO_2 occur at slightly lower frequencies than those for pure SiO_2 because of the nearest neighbor identity. The corresponding maximum intensities for SiOH and GeOH in the pure glass systems are 3672 cm^{-1} and 3562 cm^{-1}, respectively. Both hydrogen and deuterium can be used as a diagnostic tool to further understand the properties of glasses and the effect of water related species on performance of glass systems. Infrared monitoring of hydroxyl formation has played a unique role in the modeling of gas diffusion kinetics. Specific knowledge of how gasses interact with the glass structure can be used to determine the mechanism of redox reactions, including hydroxyl formation and reduction of species in the glass.

Molecular hydrogen can exist in the interstices of the tetrahedral structure of the silica network, and can be detected by infrared spectroscopy and Raman spectroscopy, exhibiting a peak at 4140 cm^{-1}. Symmetric molecules, such as diatomic gas molecules, cannot be analyzed using infrared spectroscopy since two identical atoms are incapable of forming a changing dipole moment, and are therefore considered infrared inactive. Molecular hydrogen dissolved in the free volume of the glass network, however, is actually slightly asymmetric resulting from weak interactions with the glass network. Shelby demonstrated the use of infrared spectroscopy to show the existence of molecular hydrogen, hydroxyl and hydride species in vitreous silica.[22] This study also demonstrated quantitative infrared analysis as the molar extinction coefficient for molecular hydrogen was determined. The molar extinction coefficient can be determined from the best fit straight line through the data when change in absorbance, or fraction of reaction, is plotted as a function of weight loss during removal of hydrogen. In this study it was assumed that weight loss is solely due to the removal of molecular hydrogen and that absorption follows the Beer-Lambert law.

Molecular hydrogen readily dissolves into vitreous SiO_2 or binary GeO_2-SiO_2 glasses and can react with the network to create hydroxyl or hydroxyl/hydride pairs with the influence of ionizing radiation or elevated temperatures. Hydroxyl and hydride have absorption peaks that exist within the optical window and therefore are not desired in glass that is intended for optical transmission purposes. Most molecular hydrogen comes from diffusion into the network from the surface. A wide range of varying hydroxyl content glasses can be made when water reacts with the vitreous network during

processing. For example, during the manufacturing of Type II SiO_2, quartz powder is melted under an atmosphere containing molecular hydrogen. During this process, a significant amount of hydroxyl, greater than 100ppm, is incorporated into the glass network. To remove this hydroxyl, the glass is subsequently heat treated to get a final hydroxyl concentration of less than 10ppm. The untreated glass also contains a significant amount of hydride at a concentration equal to that of the hydroxyl.

When vitreous silica is irradiated with high energy X-rays or γ-rays the concentration of defects increases significantly, since a large number of Si-O-Si bonds are broken.[17] If hydrogen is present during irradiation, as in hydrogen-impregnated silica, the usual formation of defects is suppressed as a result of the formation of hydroxyl and hydride.[19] This form of chemical annealing has an advantage over thermal annealing in that defect removal can be accomplished at much lower temperatures. When an irradiated glass is held at high temperatures, defects will react with hydrogen in the atmosphere to form hydroxyl and hydride groups as shown in equations 2.9 and 2.10, but hydroxyl and hydride species can also be eliminated when a glass is thermally annealed at temperatures greater than 700°C according to Reaction 2.12.

$$SiOH + SiH \rightarrow Si\text{-}O\text{-}Si + H_2 \qquad (2.12)$$

The hydroxyl and hydride species react to form molecular hydrogen, which can diffuse out of the glass structure. Therefore, chemical annealing is not necessary for glass that has to be thermally annealed to remove the hydroxyl and hydride species.

2.6.2. Other Important Effects of Water in Glass

Water in the glass network can have a profound influence on many properties of glasses, including density, refractive index, viscosity, conductivity and crystallization behavior. At high temperatures, water in vitreous silica exists almost entirely as hydroxyl. To understand the influence of hydroxyl concentration on glasses, one must first understand the relative amounts of hydroxyl in each of the four types of SiO_2. Table 2.I shows an approximate range of hydroxyl concentration for each of the four main types of SiO_2. The influence of hydroxyl concentration on the density of vitreous SiO_2 as a

function of fictive temperature for type I, IV and III SiO_2 glasses was determine by Bruekner et al.[23] The high hydroxyl concentration of type III SiO_2 creates an open network structure similar to that of an alkali oxide impurity, but without filling the added free volume since the hydrogen ion is significantly smaller. This model also explains why the natural SiO_2 glasses (type I and II), with a significantly higher alkali concentration, have a higher density than type III.

The refractive index of a glass is inversely proportional to the speed of light. The speed of light decreases when the electrons interact with the electric field of the light. If the atoms of a structure move apart, there is less mass per volume and therefore density decreases. If the density decreases, there are fewer electrons per volume to interact with the light, therefore refractive index and density are proportional. When hydroxyl is present in SiO_2, a certain amount of structural relaxation occurs when the stressed Si-O-Si bonds form hydroxyl groups, allowing the tetrahedra to relax and move apart. When the structure relaxes, the density decreases since there is less mass per unit volume, as does the refractive index since there are fewer electrons per unit volume for the light to interact with.

The profound influence of hydroxyl concentration on structural relaxation also influences the viscosity of SiO_2. High hydroxyl concentration in a SiO_2 glass is associated with an increase in non-bridging units and an open network structure. This structure creates network fragments and preordered arrangements with a greater mobility, which influences long-range cooperative motions governed by viscous flow. Therefore, viscosity decreases as hydroxyl concentration increases and weakens the network structure.

Water-rich SiO_2 glasses have a higher crystallization rate than water-poor samples. SiO_2 glasses treated under in an atmosphere of water vapor also have a higher crystallization rate than SiO_2 samples heat treated in a dry atmosphere at elevated temperatures. Therefore, water vapor and hydroxyl concentration have a catalytic influence on crystallization. In SiO_2 glasses, the crystalline phase has the same composition as the glass phase, and can lead to large changes in the density of the glass.

2.6.3. Reaction Kinetics and the Tarnishing Model

The tarnishing model has been used by many authors to describe the reaction between a gas and the surface of a material. The tarnishing model was originally derived to describe the oxidation of metals.[24] A material reacts with either a gas or liquid and a layer of product forms between the two reactants. The reaction proceeds by diffusion of either, or both of the reactants through the reacted layer. Therefore, the initial reacted layer of the material limits further reaction as diffusion of the gas through the reacted layer must be considered.[25] The rate of layer formation is limited either by diffusion of the gas through the reacted layer or the rate of the reaction between the diffusing material and the other reactants at the opposite interface.[26] Figure 2.4 shows an illustration of a hydrogen gas surface reaction exhibiting tarnishing model behavior. This process can be regarded as reaction front, or moving boundary, consisting of an increased concentration of the species resulting from the reaction, moving through the sample away from the initial surface. The thickness of the product layer will increase with square root time.

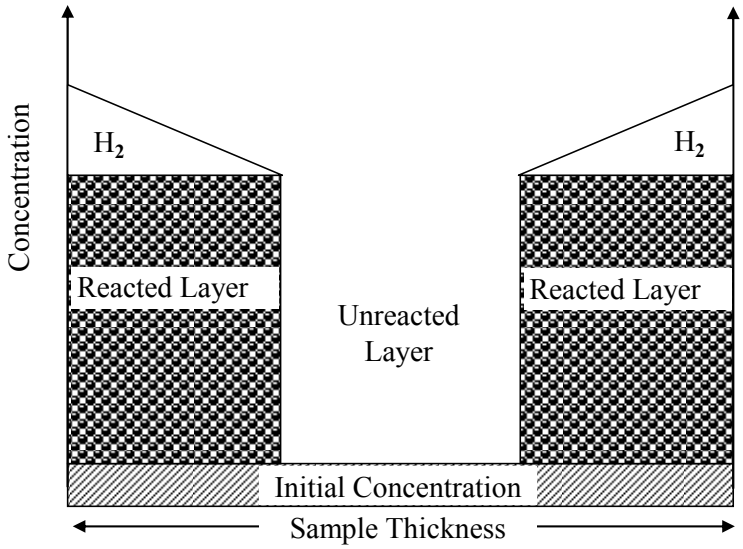

Figure 2.4. Illustration of a gas surface reaction exhibiting tarnishing model behavior for a planar geometry.

Equations used to describe the tarnishing model behavior are obtained through the following derivation. Since the tarnishing model describes a diffusion related process, it is appropriate to begin with the flux equivalent of a moving reaction front:

$$J = C_x \frac{dx}{dt} \tag{2.13}$$

Equation 2.13 can be equated to Fick's first law, modified to fit the tarnishing model,

$$J = -D\frac{dC}{dx} = D\frac{C_s}{X} \tag{2.14}$$

to obtain the expression:

$$C_x \frac{dx}{dt} = D\frac{C_s}{X} \tag{2.15}$$

where D is the diffusion coefficient for the gas in the glass. Rearranging Equation 2.15 and integrating from x = 0 to X and t = 0 to t yields;

$$X^2 = \frac{2DC_s t}{C_x} \tag{2.16}$$

If the dissolved gas obeys Henry's Law (C_s=SP) and using the relationship K = DS, we can substitute and solve for the reaction layer thickness for a planar geometry;

$$X = \sqrt{\frac{2KPt}{C_x}} \tag{2.17}$$

To obtain the equation for the fraction of reaction that has occurred for a planar geometry, Equation 2.17 must be divided by one half the sample thickness and the initial concentration of the product species present in the as-received sample (C_i) must be taken into account. The resulting equation;

$$\frac{2X}{L} = \frac{C - C_i}{C_f - C_i} = \sqrt{\frac{8KPt}{C_x L^2}} \tag{2.18}$$

where the term on the left side equation represents the fraction of reaction, i.e. the change in the concentration of the species being monitored, K is the permeability, P is the pressure of the reacting gas, t is time, L is the thickness of the substrate and C_x is the number of available reaction sites within the substrate material. The equations can be used to determine either the number of reaction sites available for reaction or the permeability of hydrogen in the glass, depending on what is known about the glass and the experimental design.

This formation mechanism of the reacted layer manifests itself in a linear growth when absorbance, i.e. concentration of reactant species, is plotted as a function of square root of time. When the moving reacted layer front from either side of the exposed surfaces of the thin plate meet in the middle, reaction sites are no longer available, the concentration of the reaction product should be constant throughout the thickness of the sample and equilibrium saturation is reached. If a reasonable way to measure the concentration of the reaction product is available, then a plot of fraction of reaction as a function of square root time will be similar to that shown in Figure 2.5.

It has been established that spectral data can be used to model hydrogen diffusion kinetics using the tarnishing model. Infrared spectroscopy is used to measure hydroxyl formation resulting from diffusion of hydrogen into a glass, through the exposed surface, at elevated temperatures and subsequently reacting with the glass structure to form hydroxyl species. Hydroxyl formation will occur at the exposed surfaces of the glass samples until reaction sites are no longer available, then a moving front of hydroxyl formation will continue to form inside the glass sample, moving inward from the exposed surfaces of the thin glass plate. The progress of this continuous reaction can be monitored using infrared spectroscopy as the concentration of the reaction product will increase as the layer front moves inward from each surface. Saturation will occur when the hydroxyl concentration is constant throughout the thickness of the sample, the infrared band will no longer grow

with further treatment, and the absorbance as a function of square root of time will level off at a constant value.

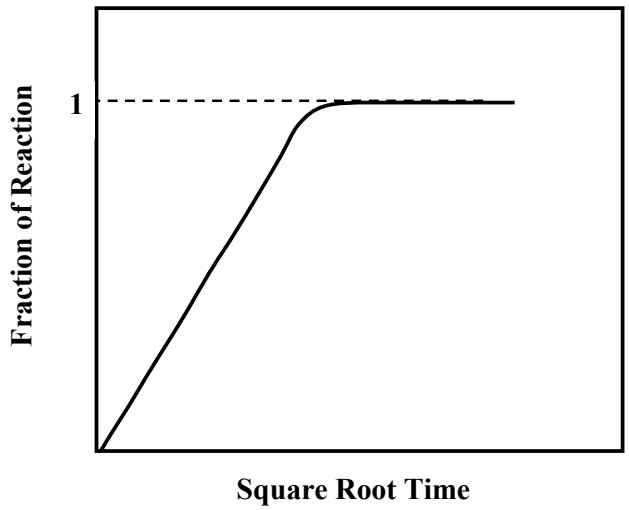

Figure 2.5. Schematic of a plot fraction of reaction as a function of square root time.

Spectral absorption data used for this technique, however, must be considered with extreme caution. Use of the tarnishing model can only be considered when absorption bands are properly deconvoluted or measured in such a way to represent only one particular species, either the reaction product or one of the other reactants. Absorption bands with spectral features from other species in the glass superimposed cannot be used. Once an absorption band is properly isolated and identified as being representative of either a reactant or product of the reaction being studied, then the maximum peak intensity can be used to monitor the fraction of the reaction as a function of time. As stated previously, however, a reasonable amount of labor is involved in the deconvolution of absorption spectra and peak assignments are commonly made through assumptions, which usually leads to extremely suspect conclusions. In the case of hydroxyl formation in binary GeO_2-SiO_2 glasses, for example, researchers[27] have deconvoluted the hydroxyl band into as many as four different hydroxyl related species.

Recently, it has been shown that, in the case of hydroxyl formation in glasses, the tarnishing model can still be considered if the integrated area under the peak is used to monitor the formation of hydroxyl species. Using integrated area instead of peak height

is convenient since deconvolution is not necessary, however, the resulting analysis can only be discussed in terms of total hydroxyl species formed, i.e. there is no distinction between different hydroxyl species.

2.7. Crystallization in Glasses

Crystallization in glasses may result in the formation of a composite structure. This crystallization process can be characterized as either devitrification (generally un-controlled crystallization of the glass) or formation of a glass-ceramic (controlled crystallization). A glass-ceramic can be produced with very fine and uniform grain sizes. The combination of multiple phases allows for adjustment and manipulation of a variety of important material properties. In the strictest sense, however, glasses for which only a relatively thin surface layer is crystallized should not perhaps be described as glass-ceramics,[28] but such composite structures also exhibit very interesting properties different from those of the glass or the crystal formed. The mechanism through which surface crystallized glasses are produced closely resembles the glass-ceramic process and the crystallization processes can be similar to or identical to those occurring in glass-ceramics of similar composition. The nuclei involved need not even have the same composition as that of the growing crystal, as is frequently the case for heterogeneous nucleation, particularly at surfaces.

Changes in the physical characteristics and properties of the glass-ceramic can often be compared with those of the glass from which they were derived. One particularly common change brought about by the heat-treatment of a glass to induce crystallization is the conversion of a transparent glass to an opaque polycrystalline material. The opacity of the glass-ceramic results from the scattering of light at the interfaces between the adjacent crystals and between crystals and the residual glass phase, due to differences in the refractive indices of the phases. If a beam of light enters a glass medium, scattering of the light in directions away from that of the incident beam will occur due to point-to-point variations in the refractive index of the medium. Scattering centers also arise from density fluctuations, but such centers are small relative to the wavelength of light. In addition to the obvious change in optical appearance of the glass sample, examination under high magnification reveals the surfaces of treated

glasses are not as smooth as the parent glass, resulting from the stresses generated as a result of volume changes associated with the growth of crystals within the glass. The formation of large crystals may lead to generation of prohibitively high stresses, which could result in fracture of the glass.

One important aspect of high temperature treatment of glasses concerns the possibility of chemical reduction of certain glass constituents, resulting from the reducing conditions of the atmosphere. Controlled crystallization is very sensitive to the furnace atmosphere, and the state of oxidation or reduction must be regulated if controlled nucleation is to be achieved. A number of metallic ions can be dissolved in molten glass and remain in solution when the glass is cooled resulting in a transparent glass. Upon reheating to temperatures near the glass transition temperature, however, a color will develop and this process is known as "stiking". For example, glasses containing cadmium sulphide exhibit this effect as a colorless glass is formed after melting and cooling, but a rich yellow color develops after reheating, due to the formation of colloidal precipitate of cadmium sulphide. The unique properties associated with colloidal crystal formation within a glassy matrix has been an active area of research for many years, however, many of the reaction mechanisms and subsequent composite properties remain unexplained. The formation of colloids in a glass is actually a crystallization process, however, most researchers report the effect of the presence of the colloids on optical properties of the glass rather than crystallization kinetics or mechanisms of crystal growth.

2.7.1. Reduction of Glass Constituents and Subsequent Crystallization

Hydrogen induced color formation in transparent glasses is often indicative of colloid formation. The presence of colloidal particles in glass is not uncommon when ions within the glass have been exposed to a reducing environment. Many different metallic species have been established to form colloidal metal particles in glass. This short review of previously reduced species in glass summarizes some of the techniques used to reduce specific constituents in the glass and resulting properties of colloidal metal particles embedded in a glassy matrix.

Complete reduction of glass modifying and intermediate species has been observed in many glass forming systems. Glass modifiers are cations in the glass that form highly ionic bonds with oxygen and exist within the free volume of the glass network creating non-bridging oxygens (NBO's) in silicate glasses.[1] Species that bond with a high ionic character tend to not be network formers because ionic bonds are non-directional i.e. the ions are too weak to exert orientational or directional influence on the anions. Glass modifying species that have been reduced in a hydrogen atmosphere to the atomic state in glass include gold,[29] silver,[29,30] copper,[31-33] nickel,[34] platinum[29] and cobalt.[35] Intermediate species in the glass are cations forming slightly more covalent bonds with oxygen that tend to replace glass-forming bonds and eliminate NBO's. Intermediate ions will compete with network-forming cations and, depending on the cation-to-oxygen ratio, they are able to form tetrahedral structures within the glass. Bismuth,[36-38] antimony,[36-39] arsenic[36,39,40] and lead[37,38,41] are all intermediate glass species that have also been reduced to the atomic state.

The formation of colloidal metal particles in a glass can be achieved through the addition of reducing agents to a glass batch containing the ionic form of the desired metal. Gold colloids in glass are most commonly made through a process called striking, whereby a clear, colorless glass with a gold content of 0.01% or less, in the ionic form, is reheated up to only 600 or 700°C where gold is no longer soluble.[29] The nucleation of gold crystals in the glass is facilitated by the presence of antimony or cerium oxides, which create a reducing environment in the glass. The gold nanocrystals grow in size with cumulative treatment time. Silver colloids can be made in a similar fashion.

Reduction of constituent species in solid glass samples at elevated temperatures can also be achieved through careful regulation of a reducing furnace atmosphere. The use of hydrogen gas to create a reducing atmosphere at temperatures around the glass transition temperature of the glass has also been used to successfully produce colloids in glass. In 1946, Bastress[38] studied the effect of the glass matrix on the reducibility of constituent oxides in the glass, including Ag, Bi, Sb and Pb, by exposing powdered glass to hydrogen at elevated temperatures. Batress found that the reducibility of silver ions increased as the basicity of the glass increased, i.e. concentration of alkali and alkaline earth increases. Batress[38] also observed that reduction of Bi, Sb and Pb resulted in a gray

color formation of the powered glass. A few years later, Green and Blodgett[37] studied the reduction of Pb, Bi and Sb using electrical conductivity measurements. Glass plates containing Pb, Bi and Sb ions, treated in a hydrogen atmosphere at elevated temperatures, around the glass transformation region, had a reduced surface layer on all exposed surfaces. Electrical resistance measurements of the surface layer resulted in primarily electric conduction as opposed to ionic conduction. The clear colorless glass samples also exhibited a range in color formation from light brown to black with increased time and temperature of treatment. The color formation was also confined to the exposed surfaces of the samples, where even the most intense black coating was reported to be only 0.001 inches thick. Kohli et al.[40] found similar results in the reduction of arsenic by a similar process, however the hydrogen-induced coloration was not attributed to the formation of colloidal species in the glass, but instead was attributed to the partial reduction of As (V) to As (III) with concurrent formation of hydroxyl. Tuzzolo et al.[39] later suggests the complete reduction of both As and Sb species in the glass. In a further study of the reduction of As, Sb and Bi, Tuzzolo et al.[36] suggests the complete reduction of Sb and Bi to the metallic state, and the formation of particles of amorphous As with similar reduction experiments.

More recently, the focus of reducible species in glass has shifted to the reduction of glass modifying species through reaction with hydrogen gas, with possible applications evolving from the properties of the controlled growth of metallic nanocrystals confined within the a glassy matrix. Estournes et al.[33] demonstrated the reduction of Cu to the metallic state. The reduction of Ni was then accomplished and the properties of the Ni and Cu metallic species, confined within the glass, were compared.[34] Glasses with reduced Ni species exhibit a magnetic behavior dependent on the size of the nanocrystal formed. Reduction of both glasses showed the formation of the reduced surface layer on each of the exposed surface associated with an intense color formation. In a study on the formation of copper colloids by hydrogen reduction in sodium borate glasses, Edson[31] and Shelby[32] showed that bromine additions inhibit the formation of Cu colloids. Miller[35] showed that reduction of Ni and Co species in borosilicate glasses can be monitored using electron spin resonance (ESR) and magnetic measurements.

Color in glasses can result from the presence of colloidal metal particles. The coloration mechanism is referred to as Mie scattering in which the theory of plasma resonance absorption is applied. In this theory, free electrons are treated as plasma confined to the colloid surface. The electric currents producing the high reflectivity in bulk metals cannot develop in small particles less than one tenth the wavelength of light and only absorption is seen. This effect is often called Mie scattering and is derived from a plasma-resonance absorption, with the free electrons being treated as a bound plasma oscillating at the plasma resonance frequency. Conduction band electrons are not confined to the colloid surface and are available to contribute to plasmon resonance. The size and morphology of the colloidal particle determines the resonant frequency and resulting absorption spectra. The resulting coloration is typically dark brown or black, although gold, copper and silver colloids are exceptions.

Blue scattering can be observed from particles as large 300 nm down to particles just a few atoms or molecules in size. The exact color depends in a complex way on the size, distribution of size, arrangement and shape of the scattering particles. When the size of the scattering particles approaches and then becomes larger than the wavelength of incident light, the Rayleigh approach to scattering no longer applies.[29] In 1908, a German physicist G. Mie solved Maxwell's equation for small spherical particles. When Mie scattering is considered for particles smaller than the wavelength of light and twice the wavelength of light, scattering becomes much more intense and much more predominant in the forward direction as the particle size increases. With increasing particle size, the scattering also becomes much less strongly dependant on the wavelength, but in a more complex manner. Therefore the scattering is no longer predominantly blue but shows different colors, mostly red and green bands. If there is a distribution in size or a difference in shape among particles present, bands will overlap resulting a featureless optical absorption spectra showing absorption at all wavelengths. Mie scattering calculations are extremely complex and the difficulty only increases with non-spherical particles and size distributions and the inability to determine the correct dielectric constant as a function of wavelength for both the colloidal particle and the matrix material.

2.8. X-ray Diffraction to Study Crystals in Glasses

It is well known[28,42,43] that crystalline substances give sharp X-ray diffraction spectra which can be used as a positive means of identifying crystals by comparison with a standard data base. On the other hand, glasses show a rather diffuse X-ray diffraction pattern with complete absence of sharp lines. Amorphous solids and liquids both have structures characterized by an almost complete lack of periodicity with a tendency to order only in the sense that the atoms are fairly tightly packed together showing a statistical preference for a particular interatomic separation distance, resulting in an X-ray scattering curve with nothing more than one or two broad maxima.[42] XRD measurements, therefore, provide an excellent means for investigation of crystallization of glasses.

Although XRD analysis can be used in a number of different ways to characterize crystal formation within a glass substrate, beyond simple crystal identification, many of the techniques have limitations. There must be at least a few percent of crystal in the glass in order to study crystallization using XRD. Crystal identity can be determined with reasonable accuracy when the position and relative intensity of the diffraction peaks is compared to a known database. In rare cases, after the composition of the crystal phase is identified, crystal orientation can be determined when X-ray diffraction is measured on the surface of a crystallized sample. If the crystals are oriented with respect to the diffraction plane, only crystal planes parallel to the diffraction plane will diffract, or appear, in the diffraction pattern. Evaluation of the missing peaks can be used to determine the orientation of the crystals in the sample. The intensity of the peaks does not tell anything about the crystal size, but the shape of the peak can be used to yeild some information about the size of the crystals. In general, a broad peak represents small particles, or crystals, while a narrow, sharp peak represents larger particles. If a glass contains multiple different crystals, or different phases, the the diffraction pattern will be more complex leading to an increased difficulty in phase identification.

2.9. Raman Spectroscopy

Micro-Raman spectroscopy, i.e. use of a Raman equipped microscope, is sensitive to local structure and is especially useful for detecting, identifying, and monitoring spatial

variations as well as changes in chemical composition and structure in glasses. Raman spectroscopy is often complimentary to infrared spectroscopy when characterization of a glass system is required. Raman scattering spectra contain an enormous amount of information about the microscopic morphology of a glass. Unfortunately, decoding the information is a major task. Well characterized vibrational properties deduced from Raman spectra can, however, reveal a significant amount of information about bonding in materials, including information about long versus short range order, symmetry, structure and coordination numbers without significant assumptions and deconvolution. For example, very broad spectral features are generally characteristic of highly disordered solids while narrow structural features are indicative of crystals. Impurities and defects often display distinctive vibrational signatures depending on the host material and specific environment in the host. Features in the vibrational spectra may also reveal the presence of multiple phases in a sample.

Raman spectroscopy measures a change in polarizability with vibration while infrared spectroscopy requires a change in dipole moment. Monochromatic light, generally in the visible region of the spectrum, is used to couple with vibrational modes through nonlinear polarizability associated with the vibrational modes. The excitation of the vibrational modes is manifested by a frequency-shifted spectrum of scattered light. Spontaneous Raman scattering is a process in which vibrational excitations are either created (Stokes), resulting in down shifting of the scattered light frequency; or annihilated (anit-Stokes), resulting in an upshift of the scattered frequency. The source of a Raman signal is scatter, not absorption as in infrared spectroscopy, and can therefore have a significantly different maximum peak intensity than the absorption signal for the same species in infrared. This difference results in a potential change in intensity of band without significant shift in the frequency of the band position. The Raman signal is measured as a shift in the frequency of the incident beam. This shift in frequency is identical to the frequency required to couple with a dipole moment for infrared active modes. The incident photon in Raman spectroscopy causes a vibration, similar to that of infrared, and the light emitted from the characteristic vibration has the same frequency as the infrared vibration. It is important to note that not all Raman modes are infrared active, i.e. select Raman modes will not have a corresponding infrared absorption. Even

though Raman and infrared spectroscopy have been shown to be complimentary in many instances, false interpretation and error is still common.

The Raman microprobe couples an optical microscope and a conventional Raman spectrometer. Tightly focused, short-wavelength laser sources enable focused measurements with submicron resolution. The microprobe is also designed to scan samples spatially while probing very small volumes, allowing for examination of variations in properties as a function of position. The microprobe has become an increasingly popular tool for studying variations in composition and structure on a micron scale.

2.10 Characterization Techniques and Experimental Design

Characterization techniques such as FTIR, UV-Vis, XRD, ESEM, Raman spectroscopy, as well as many other complimentary techniques, provide crucial information regarding basic material properties and reaction mechanisms when used correctly. It is important to scrutinize the range of validity in terms of accuracy when analysis of any characterization technique is presented. There is often a reasonable amount of labor required to extract useful information and, even though the theoretical tools for such analysis are well-developed, the results to be obtained are of such considerable interest that analysis can be subject to personal interpretation, which leads to extremely suspect conclusions.

Often the most difficult, ambiguous and questionable step in data analysis is the struggle to obtain the perfect curve fit. A better curve fit can always be obtained by adjusting fitting parameters, such as; peak position, number of components, full width at half maximum (FWHM) values and percent Lorentzian or Gausian character.[44] Perhaps the most obvious way to remove this ambiguity in data analysis is to use complimentary characterization techniques to confirm analytical conclusions and assignments. If a complimentary technique does not exist, however, most characterization techniques can provide an efficient means of detecting changes in material composition and basic properties with progressive treatments. Experimental design that includes comparison of data obtained from monitoring gradual changes in the properties of samples with progressive treatment is another way to avoid the necessity of making suspect band

assignments and analytical conclusions. Many of the experiments presented in this work are constructed in such a manor; i.e. characterization techniques without available complimentary techniques are used to monitor changes in material properties with progressive treatment. Any band assignment or pattern fitting is presented in such a way to provide a consistent and reasonable explanation of the experimental data.

2.11. References

1. J.E. Shelby, *Introduction to Glass Science and Technology;* pp. 78-97,196. Royal Society of Chemistry, Cambridge, UK, 1997.

2. K.J. Beales and C.R. Day, "A Review of Glass Fibers for Optical Communications," *Phys. Chem. Glasses,* **21** [1] 5-21 (1980).

3. K.O. Hill, Y. Fujii, D.C. Johnson, and B.S. Kawasaki, "Photosensitivity in Optical Fiber Waveguides: Application to Reflection Filter Fabrication," *Appl. Phys. Lett.,* **32** [10] 647-9 (1978).

4. G. Meltz, W.W. Morey, and W.H. Glenn, "Formation of Bragg Gratings in Optical Fibers by a Transverse Holographic Method," *Opt. Lett.,* **14** [15] 823-5 (1989).

5. P.J. Lemaire, R.M. Atkins, V. Mizrahi, and W.A. Reed, "High Pressure Hydrogen Loading as a Technique for Achieving Ultrahigh UV Photosensitivity and Thermal Sensitivity in Germania Doped Optical Fibers," *Electron. Lett.,* **29** [13] 1191-3 (1993).

6. B.I. Greene, D.M. Krol, S.G. Kosinski, P.J. Lemaire, and P.N. Saeta, "Thermal and Photo-Initiated Reactions of H_2 with Germanosilicate Optical Fibers," *J. Non-Cryst. Solids,* **168** [1-2] 195-9 (1994).

7. P. Cordier, C. Dalle, C. Depecker, P. Bernage, M. Douay, P. Niay, J.-F. Bayon, and L. Dong, "UV-Induced Reaction of H_2 with Germanosilicate and Aluminosilicate Glasses," *J. Non-Cryst. Solids,* **224** [3] 277-82 (1998).

8. S. Duguay, J.J. Grob, A. Slaoui, Y. Le Gall, and M. Amann-Liess, "Structural and Electrical Properties of Ge Nanocrystals Embedded in SiO_2 by Ion Implantation and Annealing," *J. Appl. Phys.,* **97** [10] 104330 5pp. (2005).

9. P. Mutti, G. Ghislotti, S. Bertoni, L. Bonoldi, G.F. Cerofolini, L. Meda, E. Grilli, and M. Guzzi, "Room-Temperature Visible Luminescence from Silicon Nanocrystals in Silicon Implanted SiO_2 Layers," *Appl. Phys. Lett.,* **66** [7] 851-3 (1995).

10. V. Ng, S.P. Ng, H.H. Thio, W.K. Choi, A.T.S. Wee, and Y.X. Jie, "Luminescence and X-Ray Diffraction Studies of Ge Nanocrystals in Amorphous Silicon Oxide," *Mater. Sci. Eng., A,* **A286** [1] 161-4 (2000).

11. H. Yang, X. Wang, H. Shi, F. Wang, X. Gu, and X. Yao, "Sol-Gel Preparation of Ge Nanocrystals Embedded in SiO_2 Glasses," *J. Cryst. Growth,* **236** [1-3] 371-5 (2002).

12. K. Kawamura, Y. Kameshima, H. Hosono, and H. Kawazoe, "Proton-Implantation-Induced Optical Phenomena in SiO_2:GeO_2 Glasses: Formation of Photosensitive Defects and Nanometer Sized Ge Crystals," *Mater. Sci. Eng., B,* **54** [1-2] 18-23 (1998).

13. E.M. Birtch, J.E. Shelby, and J.M. Whalen, "Properties of Binary GeO_2-SiO_2 Glasses," *Phys. Chem. Glasses: Eur. J. Glass Sci. Technol. B,* **47** [2] 182-5 (2006).

14. Y.Y. Huang, A. Sarkar, and P.C. Schultz, "Relationship between Composition, Density and Refractive Index for Germania Silica Glasses," *J. Non-Cryst. Solids,* **27** [1] 29-37 (1978).

15. R. Brueckner, "Properties and Structure of Vitreous Silica. I," *J. Non-Cryst. Solids,* **5** [2] 123-75 (1970).

16. *Infrared Fiber Optics*. Edited by J.S. Sanghera and I.D. Aggarwal. CRC Press, Boca Raton, FL, 1998.

17. D.L. Griscom, "Defect Structure of Glasses. Some Outstanding Questions in Regard to Vitreous Silica," *J. Non-Cryst. Solids,* **73** [1-3] 51-77 (1985).

18. J.E. Shelby, "Reaction of Hydrogen with Optical Defects in Glasses," *J. Am. Ceram. Soc.,* **67** [5] C93-4 (1984).

19. J.E. Shelby, "Radiation Effects in Hydrogen-Impregnated Vitreous Silica," *J. Appl. Phys.,* **50** [5] 3702-6 (1979).

20. *Experimental Techniques of Glass Science*. Edited by C.J. Simmons and O.H. El-Bayoumi. American Ceramic Society, Westerville, OH, 1993.

21. J. Stone, "Interactions of Hydrogen and Deuterium with Silica Optical Fibers: A Review," *J. Lightwave Technol.,* **LT-5** [5] 712-33 (1987).

22. J.E. Shelby, "Protonic Species in Vitreous Silica," *J. Non-Cryst. Solids,* **179,** 138-47 (1994).

23. R. Brueckner, "Effect of Hydroxyl Content in the Structure of Silica Glasses," *Glastech. Ber.,* **43** [1] 8-12 (1970).

24. F. Booth, "A Note on the Theory of Surface Diffusion Reactions," *Trans. Faraday Soc.,* **44,** 796-801 (1948).

25. J. Crank, *The Mathematics of Diffusion,* 2nd ed.*;* pp. 37,305. Oxford University Press, New York, 1975.

26. J.E. Shelby, *Handbook of Gas Diffusion in Solids and Melts;* pp. 8-10. ASM International, Materials Park, OH, 1996.

27. V.G. Plotnichenko, V.O. Sokolov, and E.M. Dianov, "Hydroxyl Groups in Germanosilicate Glasses," *J. Non-Cryst. Solids,* **278** [1-3] 85-98 (2000).

28. P.W. McMillan, *Glass-Ceramics;* p. 121. Academic Press, London, 1964.

29. K. Nassau, *The Physics and Chemistry of Color: The Fifteen Causes of Color,* 2nd ed.*;* pp. 305-6. John Wiley & Sons, New York, 2001.

30. J.E. Shelby and J. Vitko, Jr., "Colloidal Silver Formation at the Surface of Float Glass," *J. Non-Cryst. Solids,* **50** [1] 107-17 (1982).

31. D.L. Edson, "Effect of Halogen Substitutions on the Formation of Copper Colloids by Hydrogen Reduction in Sodium Borate Glasses"; Ph.D. Thesis. Alfred University, Alfred, NY, 2003.

32. D.L. Edson and J.E. Shelby, "Effects of Bromine Additions on the Formation of Copper Colloids by Hydrogen Reduction in Sodium Borate Glasses," *Phys. Chem. Glasses,* **44** [3] 220-4 (2003).

33. C. Estournes, N. Cornu, and J.L. Guille, "Reduction of Copper in Soda-Lime-Silicate Glass by Hydrogen," *J. Non-Cryst. Solids,* **170** [3] 287-94 (1994).

34. C. Estournes, T. Lutz, and J.L. Guille, "Reduction of Nickel in Soda-Lime-Silicate Glass by Hydrogen," *J. Non-Cryst. Solids,* **197** [2,3] 192-6 (1996).

35. M.E. Miller, "Formation of Transition-Metal Crystallites in Glass"; M. S. Thesis. Alfred University, Alfred, NY, 2005.

36. M.R. Tuzzolo and J.E. Shelby, "Hydrogen-Induced Formation of Colloids of Arsenic, Antimony, and Bismuth in Oxide Glasses," *J. Non-Cryst. Solids,* **143** [2-3] 181-90 (1992).

37. R.L. Green and K. Blodgett, "Electrically Conducting Glasses," *J. Am. Ceram. Soc.,* **31** [4] 89-100 (1948).

38. A.W. Bastress, "Influence of Glass Compositions on Reducibility of Ag+, Bi+++, Sb+++, and Pb++," *J. Am. Ceram. Soc.,* **30** [2] 52-3 (1947).

39. M.R. Tuzzolo, J.T. Kohli, and J.E. Shelby, "Hydrogen-Induced Absorption in Glasses Containing Arsenic and Antimony," *Proc. SPIE-Int. Soc. Opt. Eng.,* **1327,** 2-9 (1990).

40. J.T. Kohli, B.M. Wright, J.M. Jewell, and J.E. Shelby, "Hydrogen-Induced Coloration of Glasses Containing Arsenic," *Phys. Chem. Glasses,* **31** [4] 133-7 (1990).

41. K.B. Blodgett, "Surface Conductivity of Lead Silicate Glass after Hydrogen Treatment," *J. Am. Ceram. Soc.,* **34** [1] 14-27 (1951).

42. *Elements of X-Ray Diffraction,* 3rd ed.; p. 321. Edited by B.D. Cullity and S.R. Stock. Addison-Wesley Publishing, Menlo Park, CA, 2001.

43. *Introduction to X-Ray Powder Diffractometry*; pp. 25, 89-90. Edited by R. Jenkins and R. Snyder. John Wiley & Sons, New York, 1996.

44. P.W. Wang, Y. Qi, and D.O. Henderson, "Oxygen Bonding in GeO_2 Glass," *J. Non-Cryst. Solids,* **224** [1] 31-5 (1998).

CHAPTER 3: EXPERIMENTAL PROCEDURE

3.1. Introduction

The general procedures used to characterize and observe changes in the measured properties of the glasses used in this study are described in this chapter. Unique variations from the techniques described in this chapter will be discussed in the chapter in which they were used.

3.2. Glass Preparation

Binary GeO_2-SiO_2 glasses used in experiments described in this thesis (100 mol% SiO_2, 6 mol% GeO_2-94 mol% SiO_2 and 14.6 mol% GeO_2-85.4 mol% SiO_2) were produced at Corning Incorporated. Glasses were fabricated using a doping and redraw process similar to that used in fiber production. The silica and germania were co-deposited as a soot to form the porous preform. The porous material was then consolidated to a glass and drawn into a hollow cane.

Glass samples used in this study were cut to plates of desired thickness from the bulk glass using a low-speed diamond saw, with a kerosene/water solution as the cutting fluid. Dimensions of the glass plates cut from the hollow canes are shown in Figure 3.1. The 6 mol% GeO2-94 mol% SiO_2 glass samples had a larger diameter than the 14.6 mol% GeO2-85.4 mol% SiO_2 glass samples. The samples were subsequently ground and polished using a series of SiC grit papers and 0.5 μm cerium oxide polishing compound. Sample thickness was measured using a micrometer and recorded to within 0.01 mm. All measurements were made on optically polished plates unless otherwise stated.

GeO_2 glasses were prepared from reagent grade GeO_2 powder. A batch of 12 grams of glass was melted in a Pt crucible at 1500°C in an ambient atmosphere for approximately 30 minutes. Further remelting[c] at 1400°C for 15 minutes was used to completely remove bubbles from the glass.[1] After fining, the crucible was removed from the furnace, allowed to cool to room temperature, and the glass was removed from the crucible. The resulting glass was colorless and free of bubbles. Samples were annealed

[c] Special caution must be exercised when melting pure GeO_2 in a platinum crucible at excessive temperatures or in reducing environments. Jackson et al. reported that melting at high temperatures can result in reduction of germanium to the metallic state, forming a low temperature eutectic with platinum subsequently destroying the crucible.

by reheating to their glass transformation temperature, holding for 30 minutes and then cooling at 1 K/min to room temperature. Samples were cut from the annealed glasses using a low speed diamond saw, with isopropal alcohol as the cutting fluid to avoid problems associated with the hygroscopic nature of the glass. The samples were subsequently ground and polished using a series of SiC grit papers and 0.5 μm cerium oxide polishing compound, again using isopropal alcohol as the lubricant. Sample thickness was measured using a micrometer and recorded to within 0.01 mm.

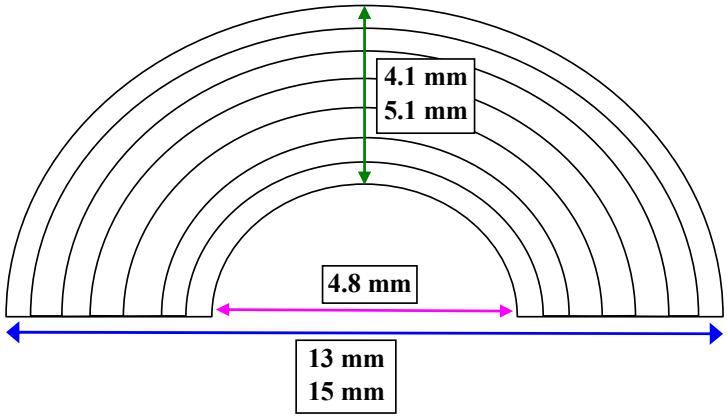

Figure 3.1. Schematic of deminsions of the glass plates cut from the hollow canes. The 6 mol% GeO_2-94 mol% SiO_2 glass samples had a larger diameter than the 14.6 mol% GeO_2-85.4 mol% SiO_2 glass samples.

3.3. Property Measurements

Density of the binary GeO_2-SiO_2 glasses and the pure SiO_2 glass was measured using the Archimedes' Method with kerosene as the immersion liquid. The density of a vitreous silica standard is reproducible to within ±0.001 g/cm^3 when measured using this method. Refractive indices (±0.0001) were measured on polished plates using an Abbe refractometer (AO scientific Instruments Mark II model) equipped with a sodium lamp (589.3nm). Electron microprobe measurements were done at Corning Inc. Measurements were made radially, on the bulk glass rod, in 50 μm increments from the inner edge to the outer edge as shown in Figure 3.2.

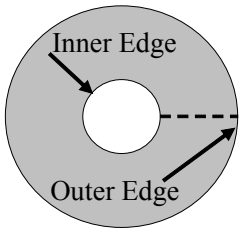

Figure 3.2. Schematic of glass sample profile where the dotted line shows the position of the microprobe measurement along the radial profile of the glass samples.

Thermal expansion coefficients were measured using a vitreous silica push-rod dilatometer using bars typically 3 mm on a side and 15 to 20 mm long and a heating rate of 4 K/min. The average thermal expansion coefficient between 100 and 400°C is reproducible to within ±0.2 ppm/K.

3.4. Etching Experiments

Hydrofluoric acid was used to etch the surface of the as-received binary GeO_2-SiO_2 glasses to accentuate the structural features. The as-received glasses were cut into plates, approximately one millimeter thick, and soaked in 9% HF acid solution with constant agitation for 45 minutes at room temperature. The resulting etched as-received glasses were subsequently examined using the environmental scanning electron microscope (ESEM), as described below.

3.5. Reaction Kinetics Experiments

Treatments in a controlled atmosphere were carried out in the apparatus shown in Figure 3.3. Samples were placed on a platinum setter in a vitreous silica tube (3.6cm I.D., 3.8cm O.D. and 40cm long) attached to a gas handling apparatus. The vitreous silica tube is evacuated via vacuum pump. The preheated horizontal tube furnace was positioned around the evacuated silica sample chamber. Temperatures (500, 600, 700, or 800°C) were continuously monitored by a thermocouple inside the sample chamber, directly above the samples. After the desired temperature was reached, hydrogen gas was introduced into the sample chamber. Sample temperature was held constant to within

±5K throughout the treatment. Each sample was treated isothermally for the desired amount of time under 93 ± 1 kPa of hydrogen.

The apparatus allows for the use of any gas composition for treatment of glass samples at elevated temperatures. Progressive reaction in an atmosphere of deuterium gas was also observed. When treatment under a deuterium atmosphere is used, the same procedures described above are used, except deuterium gas is used instead of hydrogen gas. Extended isothermal treatment under vacuum and ambient atmospheres were also conducted. Isothermal treatments under vacuum are performed when the vacuum pump is on and the silica tube is under vacuum for the duration of the treatment. Treatments in an ambient atmosphere are performed when the silica tube is left open to ambient air, i.e. the sample is exposed to ambient air throughout the duration of the treatment.

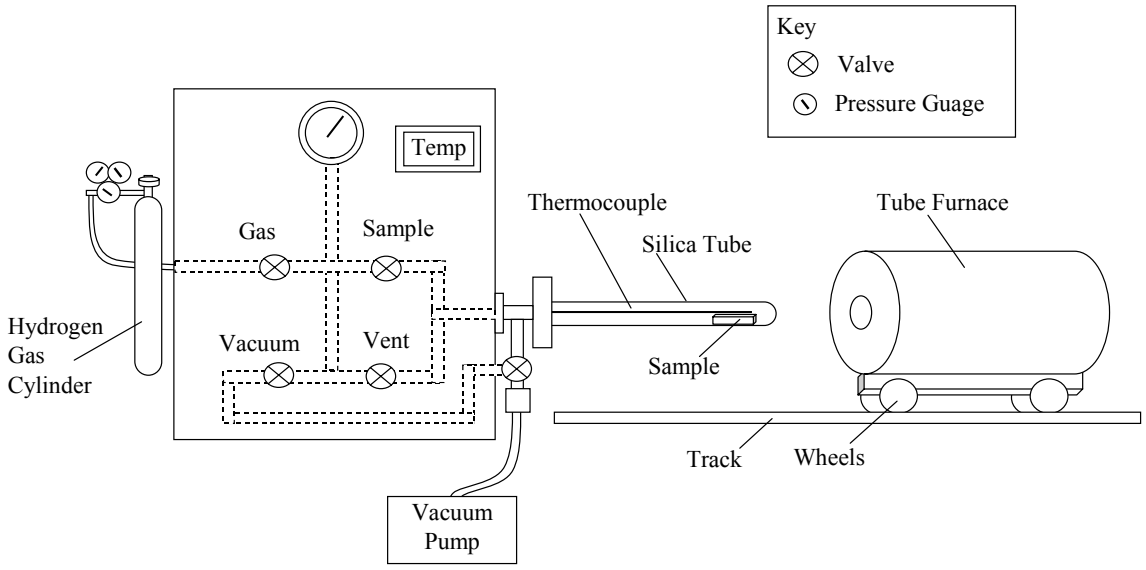

Figure 3.3. Schematic of the hydrogen treatment apparatus.

3.6. Characterization Measurements

3.6.1 Spectroscopy (Fourier Transform Infrared and Ultraviolet/Visible)

Infrared absorption spectra measurements were conducted at room temperature to monitor changes in the concentration of hydroxyl and hydride species in the binary

GeO_2-SiO_2 glasses with progressive treatment in hydrogen at elevated temperatures. Fourier Transform Infrared Spectroscopy (FTIR) absorption spectra over the spectral range from 4200 to 2000 cm^{-1} were obtained for each sample using a Thermo Nicolet Avatar 360 FT-IR spectrometer. Infrared absorption spectra were measured before the initial heat treatment and after each subsequent heat treatment. Since treatment times were cumulative, variations between samples do not exist for this work.

Optical absorption measurements of glass plates were made before and after treatments and were conducted at room temperature to monitor changes in the optical properties of the binary GeO_2-SiO_2 glasses with progressive treatment in hydrogen at elevated temperatures. Absorbances are reproducible to within ±0.01. UV-Vis absorption spectra over the spectral range from 200 to 1100 nm were obtained for each sample using a Perkin-Elmer Lambda 40 UV-Vis spectrometer to study the absorbance change relative to the untreated sample. Optical absorption spectra were measured before the initial heat treatment and after each subsequent heat treatment. Since treatment times were cumulative, variations between samples do not exist for this work.

3.6.2. Optical Microscopy

The optical microscope is perhaps the most important tool for bulk characterization of materials. Images in both transmission and reflection mode were used in this thesis to observe and characterize the as-received glass samples and monitor changes in the appearance of the glass samples with progressive treatment in hydrogen at elevated temperatures. Important parameters such as illumination mode, magnification and color enhancements are reported with every image presented. The use of optical microscopy to study crystallization of glasses, however, was limited since many of the crystals formed in this study are so small that they are below the limit of resolution of the microscope. For this reason, an electron microscope was employed to permit closer examination of interesting structural features.

3.6.3. Environmental Scanning Electron Microscopy

Careful attention must be used when preparing glass samples for examination with an electron microscope in order to obtain micrographs that do not exhibit features

resulting from the preparation method, such as glass fragments on a fractured surface or dust and debris on the sample surface. The use of a Phillips environmental scanning electron microscope (ESEM) allows for observation of samples in a low vacuum environment. Without the charging effects associated with high vacuum systems, examination of nonconducting samples without sputtered conducting surfaces is possible. Examination of samples surfaces without contamination and the ability to avoid the use of replicas greatly reduces the presence of false features and artifacts associated with sample preparation techniques.

The ESEM was used to investigate the possible presence of crystalline phases, including colloidal particles, formed during hydrogen reaction experiments with binary GeO_2-SiO_2 glasses. The as-received glass samples were examined in low vacuum mode to investigate structural features of the glass samples prior to treatment. The as-received glass samples were also etched in a 9 wt % hydrofluoric acid solution to accentuate the structural features of the bulk glass samples and subsequently examined using the ESEM. The treated glass samples were also examined in low vacuum mode, allowing for examination of uncontaminated, non-sputtered glass samples to investigate morphology and depth of crystallization at the exposed surfaces of each of the treated glass samples. An accelerating potential of either 20 or 30 kV and a spot size of 3.0 nm or 4.0 nm was used for all images, unless otherwise noted. Images obtained with the ESEM were taken in either secondary electron mode or backscatter electron mode; the mode used is noted in the figure caption of each image.

3.6.4. X-ray Diffraction

X-ray diffraction (XRD) measurements provide an excellent means for investigation of crystallization of glasses. It is well known[2-4] that crystalline substances give sharp XRD spectra, while glasses show a rather diffuse X-ray diffraction pattern with complete absence of sharp lines. The sharp lines present in the XRD pattern are characteristic of a specific crystalline material and can be used as a positive means of identifying crystals by comparison with standard data from International Centre for Diffraction Data (ICDD) powder diffraction files. XRD measurements were performed on selected samples to investigate the possible presence of crystalline phases, including

colloidal particles, formed during hydrogen reaction experiments. Phase identification XRD measurements were performed in a Siemens D500 equipped with an mBraun position-sensitive detector. Samples were positioned with the crystalline surface of the bulk samples at the plane of diffraction. Scans were conducted using a scan speed of 3 degrees 2θ/minute from 20 to 120 degrees 2θ. Due to the very small quantity of each phase present, a long count time was necessary. In every measurement, the x-ray tube was operated at 40 kV and 20 mA with a copper target.

3.6.5. Raman Spectroscopy

The possible presence of crystalline phases, including colloidal particles, formed during hydrogen reaction experiments was also examined using Raman spectroscopy. A Raman microscope couples an optical microscope and a conventional Raman spectrometer, as shown in Figure 3.4. Tightly focused, short-wavelength laser sources enable focused measurements with submicron resolution. Raman scattering measurements were made in a conventional 90° scattering configuration with a CRW 200 Confocal Raman Microscope. Data reported were obtained at room temperature for spectra excited by the 532 nm line of a frequency doubled Nd:YAG laser. The Raman frequency shifts were calibrated between runs using a silicon plate standard. The Raman spectrum of silicon has a characteristic Si line at 520 cm^{-1}, which was used for calibration purposes, as well as to maximize the signal intensity by adjusting the laser power. A liquid nitrogen cooled silicon CCD matrix was used and the spectral resolution was approximately 1 cm^{-1}.

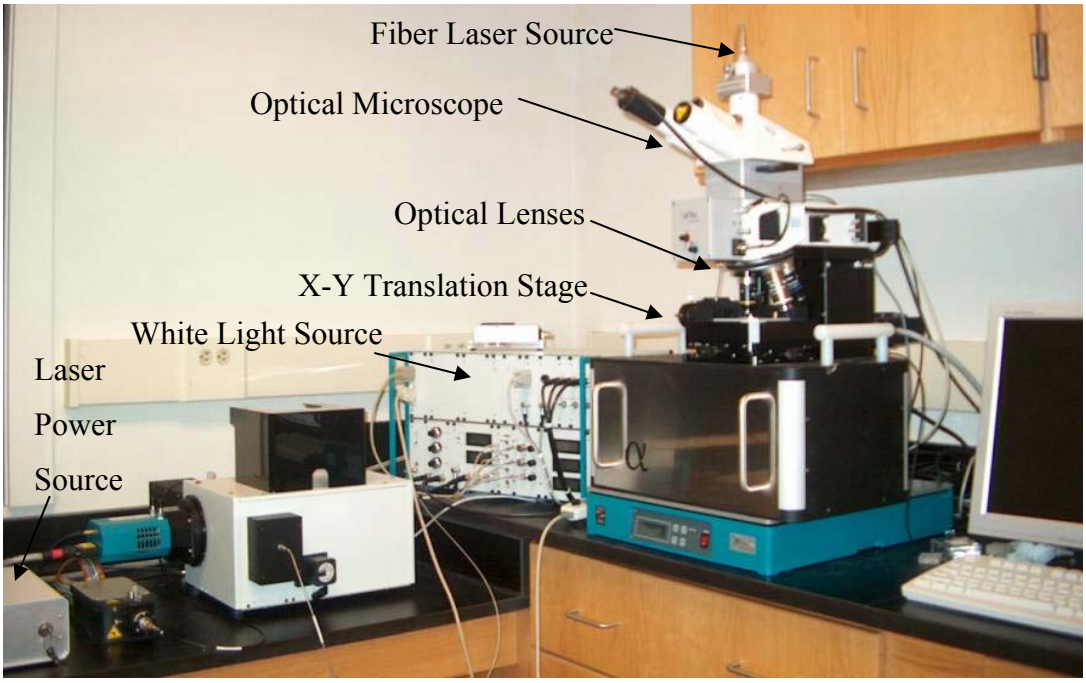

Figure 3.4. Image of the Raman microprobe measurement system, illustrating the use of an optical microscope and a conventional Raman spectrometer.

The confocal Raman microscope is also designed to scan samples spatially while probing very small volumes, allowing for examination of variations in properties as a function of position since it is equipped with a translation stage. The piezoelectric scan table incorporates a 3-axis flexure stage whereby piezotranslators are employed as the drive and guidance systems to provide submicron resolution and stability since each axis has a separate sensor. Using this feature, two dimensional maps displaying the intensity of a single Raman line can be obtained. In the most sensitive mode, called Raman fast imaging, the spectrometer is tuned to a select Raman line and the light from this Raman line is directed to the photon counting Avalanche Photodiode Detector (APD). The result is an image showing the lateral distribution of the chemical species responsible for the selected Raman line based on the intensity of the select Raman line.

3.7. Conductivity Measurements

Although the apparatus used in this study was originally set-up to measure isothermal direct current electrical resistivity of glasses, it also provides a convenient way to monitor the continuity of a conductive surface film. The apparatus allows for insertion

of a plate glass sample into a simple series circuit that consists of a standard resistor and a 9 Volt battery. A schematic of the DC circuit used is shown in Figure 3.5. Insertion of an glass sample into the circuit will form a barrier to the passage of electric current since glasses are dielectric materials. Introduction of a glass sample with a continuous conductive film over the entire surface will complete the circuit, resulting in a measurable drop in voltage across the sample. Measurement of the voltage drop across the sample allows determination of the on-set of surface conductivity. Direct current electrical resistance measurements were performed at room. Use of this measurement apparatus to measure direct current conductivities values as a function of temperature is described in detail elsewhere.[5]

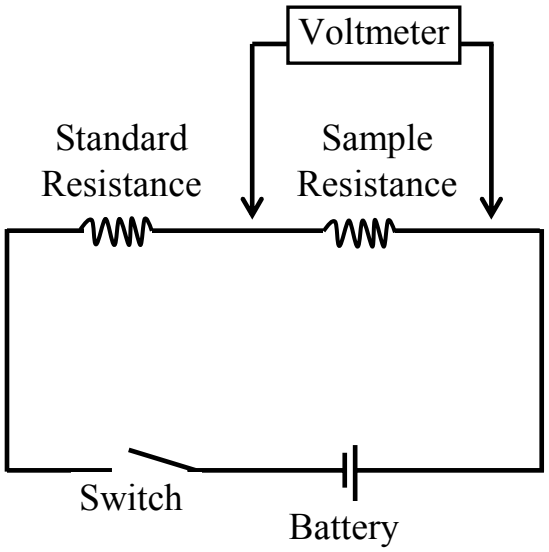

Figure 3.5. Schematic of the direct current circuit used to measure the resistance of the treated glass samples.

3.8. References

1. J.M. Jackson, M.E. Wells, G. Kordas, D.L. Kinser, R.A. Weeks, and R.H. Magruder III, "Preparation Effects on the UV Optical Properties of GeO_2 Glasses," *J. Appl. Phys.,* **58** [6] 2308-11 (1985).

2. *Elements of X-Ray Diffraction,* 3rd ed.; p. 321. Edited by B.D. Cullity and S.R. Stock. Addison-Wesley Publishing, Menlo Park, CA, 2001.

3. P.W. McMillan, *Glass-Ceramics;* p. 121. Academic Press, London, 1964.

4. *Introduction to X-Ray Powder Diffractometry*; pp. 25, 89-90. Edited by R. Jenkins and R. Snyder. John Wiley & Sons, New York, 1996.

5. J.C. Lapp and J.E. Shelby, "DC Electrical Conductivity in Sodium and Potassium Galliosilicate Glasses," *Adv. Ceram. Mater.,* **1** [2] 174-8 (1986).

CHAPTER 4: PROPERTIES OF BINARY GEO_2-SIO_2 GLASSES: IMPORTANCE OF PROCESSING TECHNIQUE

Abstract

The effect of processing technique and the presence of striations in glasses produced from outside vapor deposition (OVD) and consolidation method on the properties and behavior of binary GeO_2-SiO_2 is often ignored. Optical images of the as-received binary GeO_2-SiO_2 glasses prepared by OVD show concentric circular striations observed as a refractive index pattern resulting from the layer-by-layer deposition processing technique. The environmental scanning electron microscope (ESEM) was used to characterize the striations after etching the glass in 9 % hydrofluoric acid solution. The composition of two different binary GeO_2-SiO_2 glasses was examined using electron microprobe analysis. The density, refractive index, and thermal expansion coefficient of binary GeO_2-SiO_2 glasses have been measured and found to be relatively insensitive to the presence of striations. Results indicate that the density and refractive index of these glasses are additive as a function of the molar composition of the glass. The thermal expansion coefficient of these glasses exhibits a slightly positive deviation from additivity. Infrared spectroscopy indicates that these glasses have a very low hydroxyl content. The presence of the striations is evident in the optical absorption spectra as a uniform wavelength-independent scattering loss.

4.1. Introduction

Binary GeO_2-SiO_2 glass is widely used for the core of optical fibers, especially those used for Bragg gratings.[1] As a result, there is considerable interest in the basic properties and the effect of processing on the properties of binary GeO_2-SiO_2 glasses. The very high viscosities of binary GeO_2-SiO_2 melts makes it difficult to produce quality glasses covering a wide range of compositions using traditional powder melting methods. As a result, researchers have developed a variety of techniques to fabricate binary GeO_2-SiO_2 glasses. The diversity in manufacturing techniques and resulting as-prepared binary GeO_2-SiO_2 glasses raises questions concerning the quality and comparability of property data reported for these glasses.

A survey of literature through Sci-Glass[d] to find published density and refractive index values for binary GeO_2-SiO_2 glasses yielded the following papers. Kolesova and Sher[2] were first to reported refractive indices of synthesized GeO_2-SiO_2 glasses from 0.6 to 90 mol% GeO_2. Fleming[3,4] reported the properties, including density and refractive index, of binary GeO_2-SiO_2 glasses prepared by a radio frequency plasma fusion of a powder feed. Predetermined amounts of $Ge(OCH_3)_4$ or $GeCl_4$ and $Si(OCH_3)_4$ were mixed in a flask, resulting in a homogeneous fluid that was subsequently injected into a bath of ammoniated triply distilled water. The resulting hydrous oxide, in gel form, was filtered and dried in an oven at 200°C. The resulting powder was then calcined in a fused silica dish in an electric furnace under an ambient atmosphere. The powder was subsequently injected into a radio frequency plasma torch aimed at a pedestal. The resulting glass boule was then annealed in an electric furnace. Minor loss of volatile constituents during powder preparation and fusion of the powders is mentioned in the discussion. Volatilization was determined to be the cause of a subsequent surface degradation observed in the final glass producing an effect, identified as "orange peel". X-ray fluorescence results showed minor, smooth deviation in composition from the boule center to the outside. This minor composition fluctuation was not great enough to

[d] Sci-Glass is a data base with property-composition search capabilities allowing one to acquire data published in less common journals, in conference proceedings, or in languages other than that of the searcher, however in depth descriptions were not provided for the fabrication techniques of some research presented in this paper.

cause measurable change in the properties examined. Wood and Fleming[5] published a second study reporting property values for more binary GeO_2-SiO_2 glasses made using the same procedure.

The properties of glasses prepared by a flame deposition technique, similar to that used in the present study, were reported by Huang et al.[6] A porous soot preform of pure GeO_2-SiO_2 glass was prepared by a vapor-phase oxidation process using vapor mixtures of $GeCl_4$ and $SiCl_4$ mixed in a traversing burner to deposit pure glass spheres onto a rotating bait rod with a traversing burner. The soot preform was subsequently sintered into a high quality bubble-free glass in a He-atmosphere. Huang et al. reported experimental data for the refractive index and density of numerous bulk GeO_2-SiO_2 glasses and found that, as the GeO_2 content of the binary glasses increases, the density increases, with an approximately linear relationship between them. A similar trend was also reported for the refractive index. Kobayashi et al.[7] and Takahashi and Shibata[8] also reported a few values for the refractive index of binary GeO_2-SiO_2 glasses made by a similar vapor phase axial deposition process.

Binary GeO_2-SiO_2 glasses studied at Corning Glass Works[9] were melted in a platinum crucible in an electric furnace at 1200-1650 °C for 6-10 hours. Refractive index measurements were performed on annealed glass samples. The glass compositions studied were those used for optical fiber applications. Galant[10] also studied the properties of bulk binary GeO_2-SiO_2 glasses prepared by melting in a molybdenum crucible, which implies that the glasses were made from a mixture of powders. Galant reported density and refractive index values for binary GeO_2-SiO_2 glasses with GeO_2 content varying from 2.5 to 64.3 mol% GeO_2.

Each of the processing techniques described above has an influence on the final properties of the as-prepared binary GeO_2-SiO_2 glasses. Currently, outside vapor deposition, described by Huang et.al,[6] is one of the most common processing techniques used to fabricate binary GeO_2-SiO_2 glasses. A detailed explanation of this processing technique was provided in Chapter 2. A remnant refractive index pattern resulting from the layer-by-layer deposition process has been reported by Borrelli et al.[11] The present paper presents results of a survey of existing property data for as-prepared GeO_2-SiO_2 glasses,[2-10,12] combined with new data, which clarifies the compositional dependence of

several properties of these glasses. The influence of the fabrication technique is considered and ability to compare binary GeO_2-SiO_2 glass properties is discussed.

4.2. Experimental Procedures

The binary glasses studied here were produced (100 mol% SiO_2, 6 mol% GeO_2-94 mol% SiO_2 and 14.6 mol% GeO_2-85.4 mol% SiO_2 glasses) at Corning Incorporated. The vitreous germania sample was produced using 99.999 % purity powder at Alfred University by melting in a Pt crucible in air at 1500°C. Other binary glasses considered here were provided by J. W. Fleming (4.1, 7.0, 11.2, 13.5, 31.0 mol% GeO_2) and were made using the process described above.

Samples used in this study were cut to the desired thickness from the bulk glass cane using a low-speed diamond saw and were ground and polished using SiC grit paper and 0.5 μm alumina paste. Sample thickness was measured using a micrometer and recorded to within 0.01 mm. Electron microprobe data was provided by Corning Inc. Infrared absorption spectra were measured and absorbances are reproducible to within ±0.01. Density (±0.001) was measured using the Archimedes' Method with kerosene as the immersion liquid. Refractive indices (±0.0001) were measured on polished plates using an Abbe refractometer. Thermal expansion coefficients were measured (±0.2 ppm/K) using a vitreous silica push-rod dilatometer at a heating rate of 4 K/min. Images of the striations in the as-received glass were obtained using transmitted light optical microscopy. The magnification of the image will be stated in the figure caption of the micrograph.

The environmental scanning electron microscope (ESEM) was used to further characterize the as-received glasses. All images were taken in low vacuum mode, allowing observation of uncontaminated, uncoated glass surfaces. The magnification, voltage and detection mode are stated in the figure caption of each micrograph.

Hydrofluoric acid was used to etch the surface of the binary GeO_2-SiO_2 glasses. The as-received glasses were cut into plates using a low speed diamond saw and soaked in 9 wt % HF acid solution with constant agitation for 45 minutes at room temperature. After etching, the ESEM was used to investigate the effect of etching on striations in the

as-received glass samples. Since the ESEM was operated in low vacuum mode, coating was not necessary to obtain an image.

4.3. Results

4.3.1. Electron Microprobe Data for As-Received Glasses

Electron microprobe data were provided by Corning Incorporated. Measurements were made radially in 50 μm increments from the inner edge to the outer edge of cut plates, as shown in Figure 4.1. The composition of the as-received low and high germania glasses was determined to be 6 mol% GeO_2-94 mol% SiO_2 and 14.6 mol% GeO_2-85.4 mol% SiO_2, respectively. The open and filled data points represent measurements made for two different sections along the length of the cane material from each glass and illustrate the uniformity of germania content over the length of the glass rod. Chlorine content was also measured by electron microprobe at Corning, Incorporated. The chlorine content of each of the binary GeO_2-SiO_2 glasses was less than 100 wt ppm.

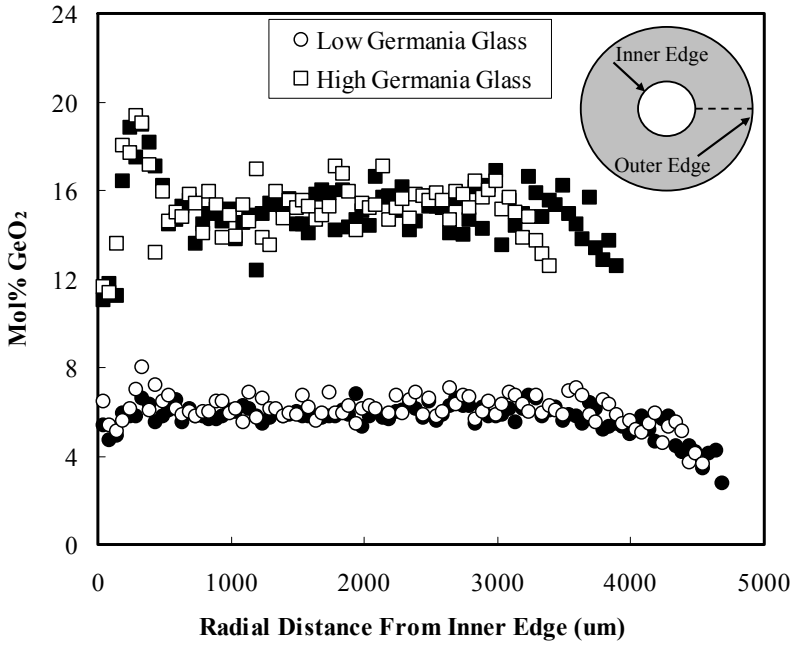

Figure 4.1. Electron microprobe analysis of Gemania content in the as-received binary GeO_2-SiO_2 glasses. The open and filled data points represent measurements made from two different sections along the length of the cane material for each of binary GeO_2-SiO_2 glass rods.

4.3.2. Optical and Environmental Scanning Electron Microscopy

Although the electron microprobe data are fairly uniform, with no resolvable concentration pattern, there is a visually observable radial refractive index pattern in the glasses. Binary GeO_2-SiO_2 glasses manufactured using a layer-by-layer deposition processing technique have a remnant refractive index pattern. This effect has been observed elsewhere.[11] Throughout the duration of this thesis, this refractive index pattern will be referred to as striations. For plates of the as-received glasses cut from the bulk material, the pattern appears as circular striations, as shown schematically in Figure 4.2. This refractive index pattern is quite significant and on a large enough scale that it is readily discernable by eye. Micrographs of the striations observed in the as-received a) 6 mol% GeO_2-94 mol% SiO_2 and b) 14.6 mol% GeO_2-85.4 mol% SiO_2 glasses were obtained using transmitted light and the 16X objective of an optical microscope and are shown in Figure 4.3. The micrographs are labeled with scale bars showing that distance between the striations is approximately 35 μm.

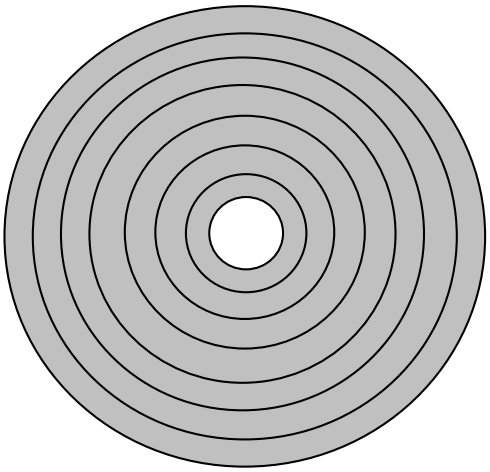

Figure 4.2. Schematic of striation orientation on as-received samples cut from cane material provided by Corning Incorporated.

Environmental scanning electron microscopy (ESEM) was performed to investigate the morphology of the striations in the as-received glass using both secondary electron and back scatter electron mode. The backscatter electron micrograph of as-

received, cut and polished, 14.6 mol% GeO_2-85.4 mol% SiO_2 glass taken at 406X magnification is shown in Figure 4.4. The bright lines in the back scatter image represent regions of the sample with a higher average atomic number. These bright lines correspond well with the 35 μm repetitive pattern of the radial striations observed in the optical micrographs. The difference in intensity of backscatter light suggests a radial, concentric compositional variation in the glass. These results suggest that the bright lines in the ESEM micrographs represent regions of higher germanium content, since germanium has a higher atomic number than silicon.

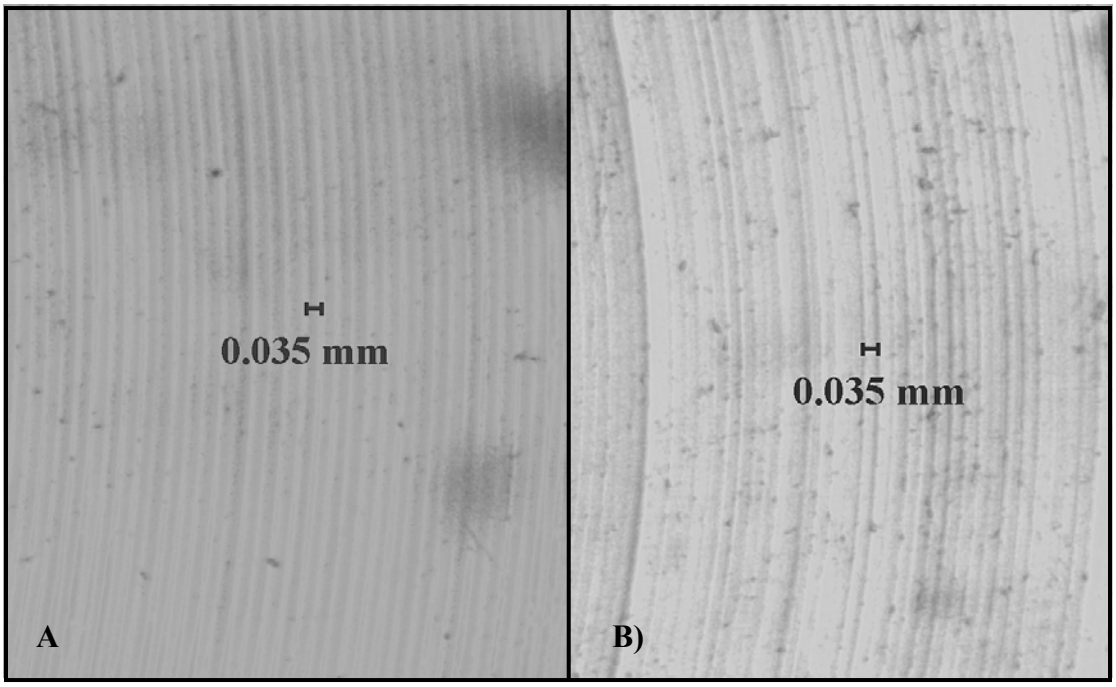

Figure 4.3. Optical micrograph of as-received A) 6 mol% GeO_2-94 mol% SiO_2 and B) 14.6 mol% GeO_2-85.4 mol% SiO_2 glasses.

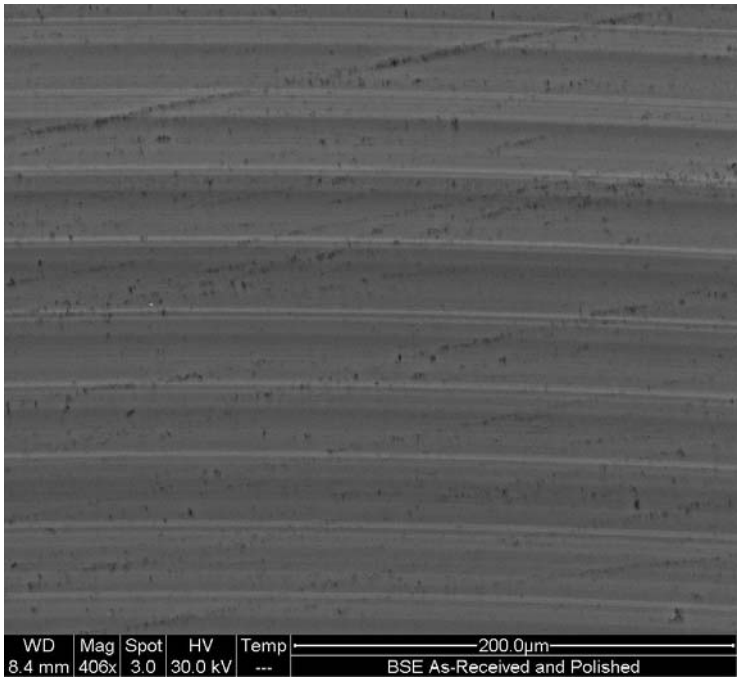

Figure 4.4. Back scatter electron micrograph of as-received, cut and polished, 14.6 mol% GeO_2-85.4 mol% SiO_2 glass taken in low vacuum mode, 406X magnification and a voltage of 30 kV.

4.3.3. Etching the As-Received Glasses

Controlled etching of the as-received glass samples was used to accentuate structural features of the glass based on the simple fact that different glass composition etch at different rates. Polished plates of the as-received glasses were etched in hydrofluoric acid and observed using the ESEM to investigate the possibility of a difference in etch rate along the striations. After 45 minutes in 9 wt % hydrofluoric solution, the presence of the striations is enhanced as preferential etching occurs along the striations. The presence of a pronounced concentric repetitive pattern with a 35 µm interval is evident in Figure 4.5. The a) backscatter electron and b) secondary electron micrographs of an as-received, etched fracture surface of a 6 mol% GeO_2-94 mol% SiO_2 glass taken with a 588X magnification (Figure 4.5) are complimentary. Although backscatter electron imaging is used for compositional analysis, topography can affect the image. The backscatter electron image shows dark lines with a 35 µm interval. The bright lines in the secondary electron image also have a repetitive 35 µm interval.

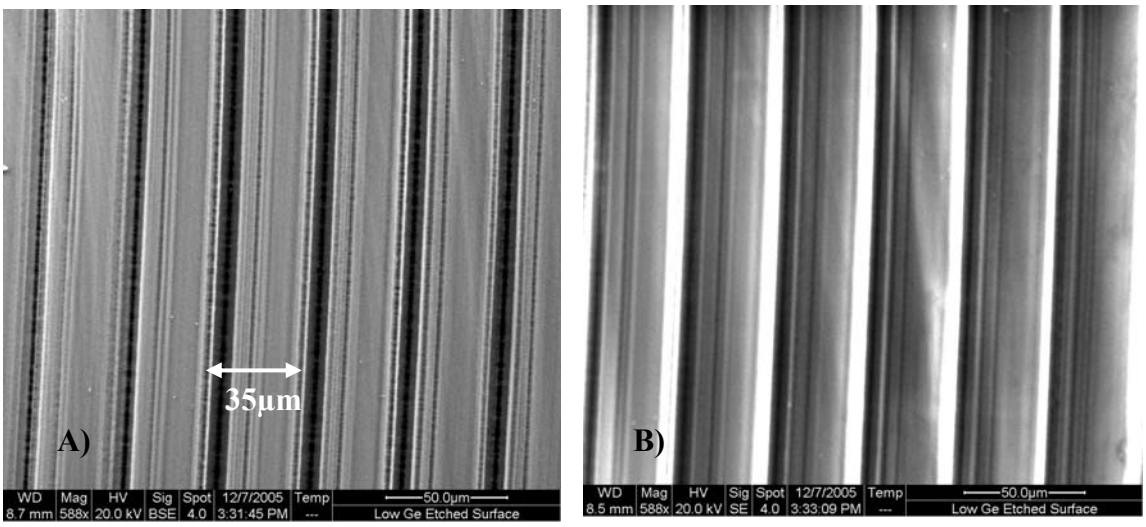

Figure 4.5. A) Backscatter electron and B) secondary electron micrograph of as-received, cut and etched, 6 mol% GeO_2-94 mol% SiO_2 glass taken in low vacuum mode, 588X magnification and a voltage of 20 kV.

When the etched glass is tilted at some arbitrary angle from the detector, the preferential etching pattern along the striations is a bit more obvious. Figure 4.6 shows the secondary electron micrograph of an as-received, etched fracture surface of the 14.6 mol% GeO_2-85.4 mol% SiO_2 glass taken at 980X magnification. The image clearly shows that the glass etches at different rates in a pattern that coincides with the remnant refractive index pattern observed in the optical microscope images. Figure 4.7 shows the overall view of the fractured surface observed in Figure 4.6 at a lower magnification without tilt. This back scatter electron micrograph of the as-received, etched fractured surface of the 14.6 mol% GeO_2-85.4 mol% SiO_2 glass shows the bright lines of the higher atomic number composition in the lower left corner and the depth of etching and difference in etch rates in the fractured area in the upper left corner. This image shows that the area with the fastest etch rate, i.e. the most glass removed, coincides with the bright lines in the as-received and polished glass image.

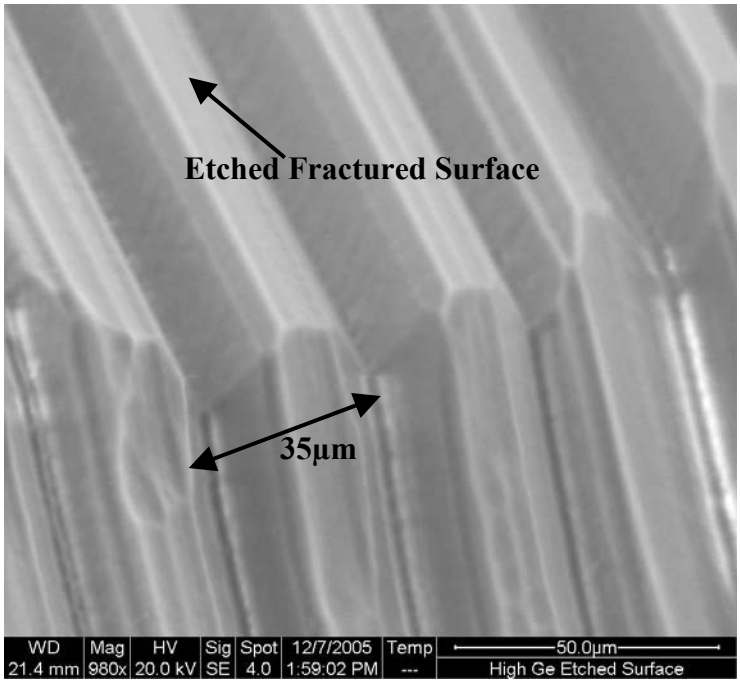

Figure 4.6. Secondary electron micrograph of as-received, etched fracture surface, 14.6 mol% GeO_2-85.4 mol% SiO_2 glass taken in low vacuum mode, 980X magnification and a voltage of 20 kV.

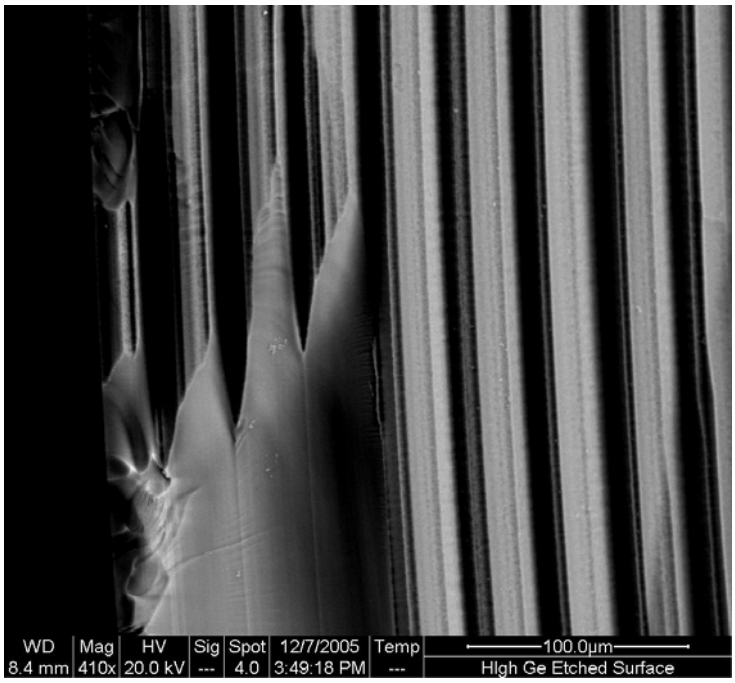

Figure 4.7. Back scatter electron micrograph of as-received, etched fracture surface, 14.6 mol% GeO_2-85.4 mol% SiO_2 glass taken in low vacuum mode, 410X magnification and a voltage of 20 kV.

4.3.4. Property Measurements Insensitive to the Presence of Striations

Although the existence of striations is irrefutable, some glass properties should not be affected by their presence. It is well established [1,13,14] that certain bulk glass properties are relatively insensitive to the presence of inhomogeneities in the glass that are small compared to the size of the sample, including phase separation and details of morphology. This category of properties includes density, refractive index, and thermal expansion coefficient, since they do not involve mass transport over significant distances. These properties reflect an average composition of the sample since they are determined though an averaging, or weighted sum of the properties of the two phases present. Although these glasses are not phase separated, a definite morphology presents itself as a radial composition fluctuation.

The refractive index is the most widely reported property of the GeO_2-SiO_2 glasses. The refractive index of a glass is a strong function of composition, but is relatively insensitive to the presence of inhomogeneities within the sample. The results of nine studies,[2-10] consisting of binary GeO_2-SiO_2 glasses fabricated from a variety of techniques, are combined with those of the present study in Figure 4.8. Although there is some scatter about the line, the results can be fit by a straight line connecting the value for vitreous silica with that for vitreous germania, i.e. the refractive index is an additive property of these glasses. The fact that the results of the present study fall within experimental error on the additive property line is consistent with the suggestion that refractive index measurements are insensitive to the presence of striations.

Data for the density of these glasses (Figure 4.9) are more limited than refractive index data, with only four prior sources of information.[4,6,10,12] Once again, a straight line connecting the values for the single component glasses provides an excellent fit to the data. It follows that density is also an additive property of these glasses.

There are even less prior data available for the thermal expansion coefficient for these glasses (Figure 4.10).[4,6,12] No data exist for compositions lying between 31 and 100 mol% germania. Results of the present study agree well with those of Huang, et al.[6] but appear to be slightly higher than those of Fleming.[4] While the departure from the additivity line is small, there does appear to be a systematic positive departure from additivity for the thermal expansion coefficient of GeO_2-SiO_2 glasses.

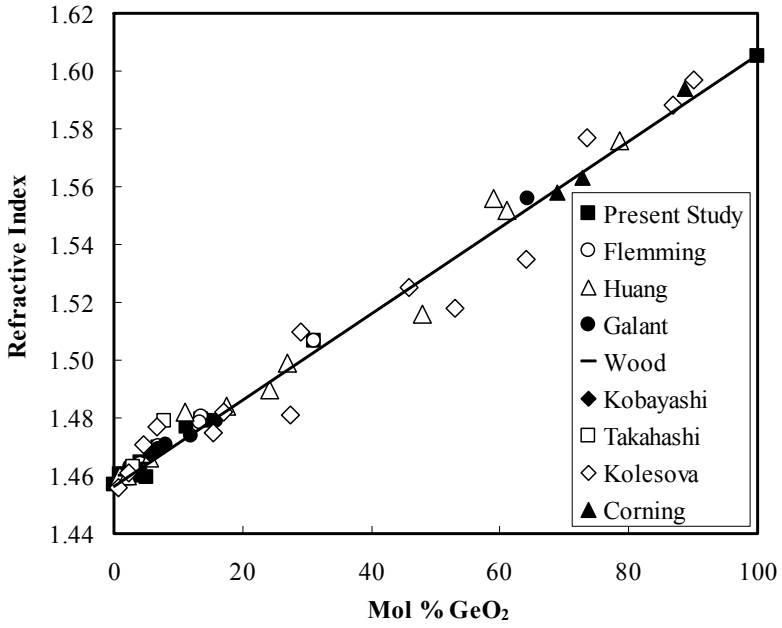

Figure 4.8. Effect of composition on the refractive index of binary GeO_2-SiO_2 glasses.[2,4-10]

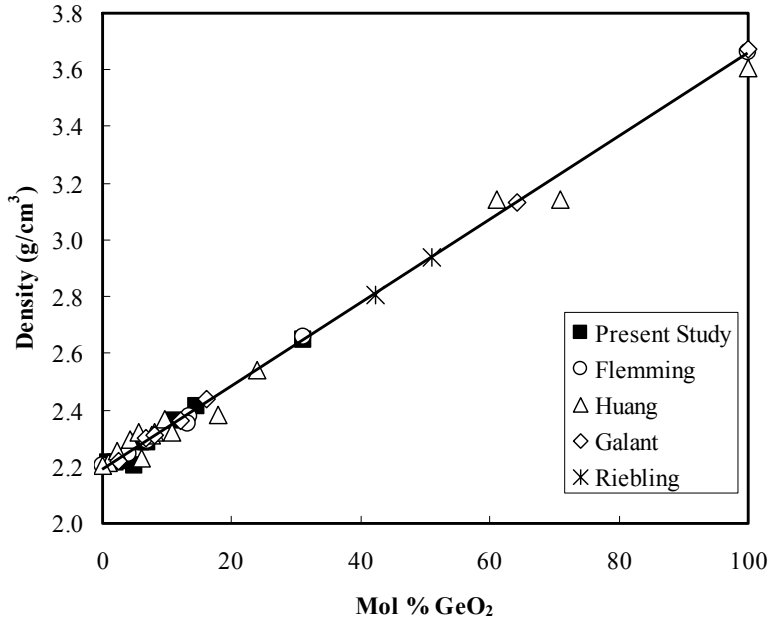

Figure 4.9. Effect of composition on the density of binary GeO_2-SiO_2 glasses.[4,6,10,12]

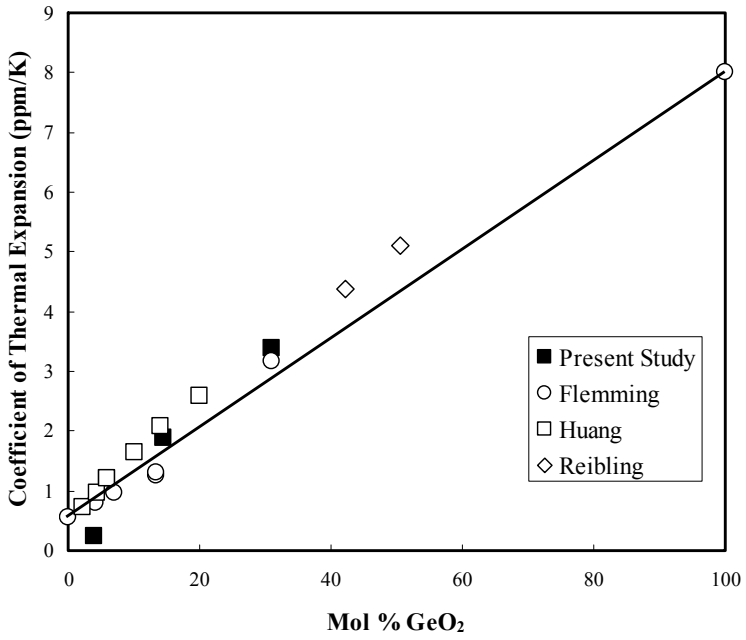

Figure 4.10. Effect of composition on the thermal expansion coefficient of binary GeO_2-SiO_2 glasses.[4,6,12]

4.3.5. Infrared Spectroscopy Measurements

One of the most important advantages of glasses manufactured using the OVD and consolidation technique is the ability to make glass with an extremely low hydroxyl concentration. It is well known[15-20] that hydroxyl species in binary GeO_2-SiO_2 glasses contribute to the formation of the broad absorption band extending from about 3750 to 3400 cm^{-1}. Infrared spectra for each of the as-received binary GeO_2-SiO_2 glasses (Figure 4.11) show an extremely low (less than 10 ppm) hydroxyl content. It is evident that the striations have no significant effect on the resulting infrared spectra within the resolution of the instrument.

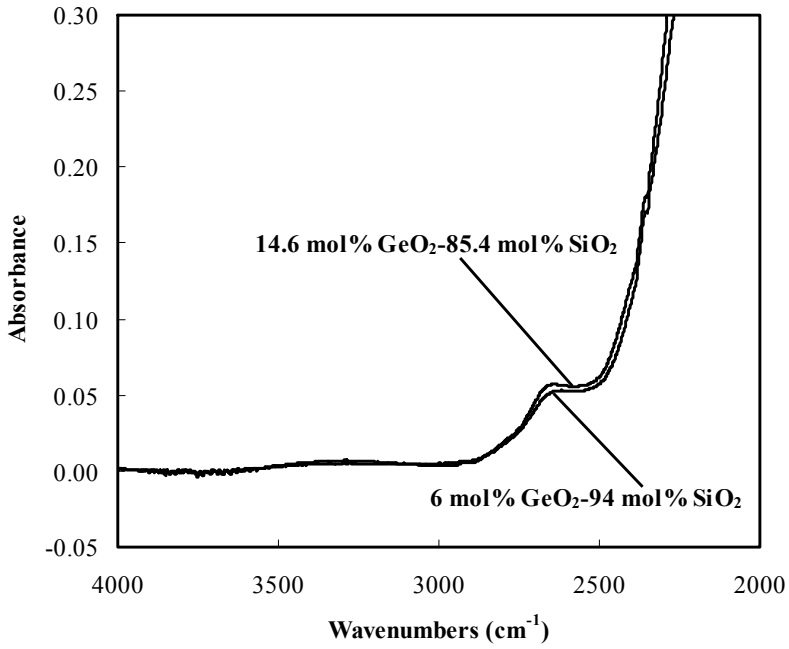

Figure 4.11. Infrared spectra from 2000 to 4000 cm^{-1} for each of the as-received binary GeO_2-SiO_2 glasses.

4.3.6. UV-Vis Spectroscopy Measurements

UV-Vis spectra of the as-received binary GeO_2-SiO_2 glasses (Figure 4.12) show an offset in the baseline absorption resulting from inherent scatter in each of the samples. This intrinsic, wavelength independent increase in absorbance is independent of thickness and results from the remnant refractive-index pattern from the layer-by-layer deposition technique used to produce the glasses. The spatial resolution of the striations, 35 μm, is too large to create a wavelength dependent spectral feature. A change in refractive index oriented parallel with the incident beam, however, will cause a diffraction effect resulting from reflection and refraction. Orientation of the striations relative to the incident beam will have some effect on the magnitude of scatter in the visible region of the spectrum. In order to establish that the increase in absorbance results from the concentric radial striations, the UV-Vis spectra of a binary GeO_2-SiO_2 glass made from a different process,[4] described previously, which has no striations is also included in Figure 4.12. The difference in the baseline value between the glasses is obvious. The band centered at

approximately 240 nm is a characteristic feature of binary GeO_2-SiO_2. The origin of this band will be discussed in a later Chapter 6.

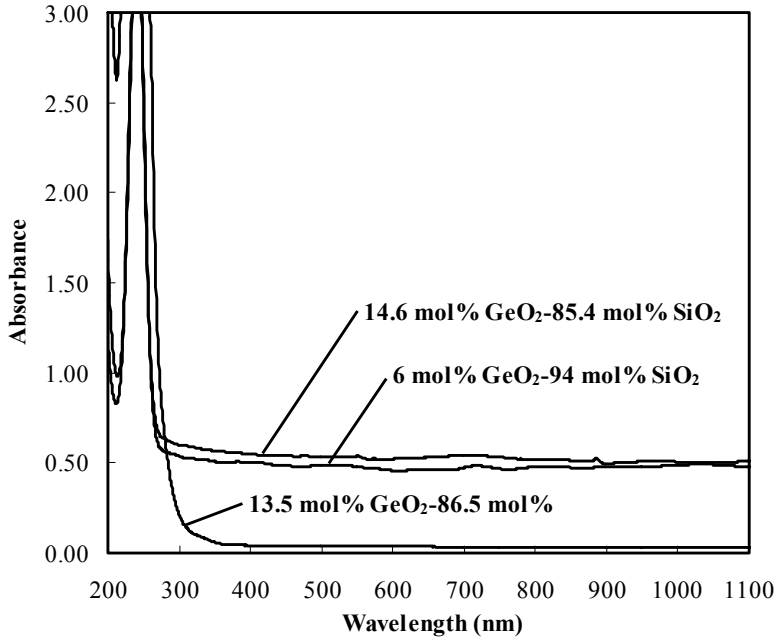

Figure 4.12. UV-Vis spectra from 200 to 1100 nm for each of the as-received binary GeO_2-SiO_2 glasses.

4.4. Discussion

The presence of the striations in the glass is irrefutable. The increment of the microprobe measurements was 50 μm, which is significantly larger than the 35 μm increment of the striations. Closer examination of the microprobe data suggests that there is a fluctuation in the germanium concentration, but the increment of the measurement is much larger than the periodicity of the striations. The microprobe data, while inadequate for characterization of the germanium concentration fluctuations, are still valuable for determining the average germanium concentration for each of the binary GeO_2-SiO_2. Optical micrographs, as well as ESEM images, of the as-received glasses provide excellent confirmation and evidence of the 35 μm periodicity of the striations.

Since all cation-anion-cation bonds in these glasses should be bridging bonds, weathering or etching of these glasses must be related to preferential attack of the weaker of the Ge-O and Si-O bonds. The lower melting temperature of GeO_2 as compared to that of SiO_2 indicates that the Ge-O bond is considerably weaker than the Si-O bond. Simple ionic field strength arguments would lead to the same conclusion. This hypothesis suggests that the regions of the glass samples etched at a faster rate would have a higher germanium concentration. This hypothesis is consistent with the relative position of the bright line features of the ESEM micrographs for the as-received glasses, indicating regions of higher atomic number, i.e. a higher concentration of germanium than the surrounding glass. The bright lines, or areas of higher germania content, correspond well with the areas showing a faster etch rate.

There is no doubt that the presence of the striations in the glass is a direct result of the layer-by-layer process used to fabricate them. The OVD process is the most common process used to manufacture optical fiber products, however, little information is available in the literature about the presence and characterization of striations in the glass. The presence of compositional fluctuations in the glass is often ignored. It is possible that the presence of radial striations is not detrimental to the utility of optical fibers since the striations are symmetric and coaxial with the direction of light travel through the fiber and the spacing of the concentric striae in the preform is reduced several orders of magnitude during fiber draw. The fiber preform, which is several inches in diameter, is drawn down to a fiber that is typically only hundreds of microns in diameter. Therefore the resulting striae in the fiber are less than a wavelength apart and the lightwave travels through a medium of average effective index.

The relationship between the density and the refractive index and the glass composition of the binary GeO_2-SiO_2 glasses are those expected for a continuous, random mixture of the structural units of the network, suggesting that the structure of these glasses can be described by a random mixture of Ge-O and Si-O tetrahedra. Unfortunately, density and refractive index measurements can not be used to determine the presence of phase separations, since a similar trend might be expected for clustering or phase separation in these glasses (density and refractive index are not very sensitive to the presence of phase separation). Similar property trends have been reported

elsewhere[2,3,6] and correspond well with the data presented here. Scatter about the straight line connecting the value for vitreous silica with that for vitreous germania can be attributed to differences in glass resulting from the processing technique including thermal history, hydroxyl content and impurity concentration.

It is less likely that the systematic positive departure from additivity observed for the thermal expansion coefficient is a direct result of differences in the processing technique. This trend was also observed by Huang et al.,[6] who suggested that binary GeO_2-SiO_2 glasses cannot be considered an ideal mixture of the respective single components. In a study of the high frequency region of the infrared spectra, Borrelli[21] found that simple superposition of the spectra of pure GeO_2 and pure SiO_2 does not correspond well with that of the binary GeO_2-SiO_2 glasses, suggesting that the binary glasses have an interconnected structure rather than a structure where segregation of the GeO_2 and SiO_2 phases occur. The small departure from additivity found for the thermal expansion coefficient, which is also not very sensitive to clustering or phase separation, is not large enough to clarify these structural questions. Although a definite morphology presents itself as radial striations, these glasses are not phase separated in the traditional sense; the glass was just formed this way. This glass definitely has a nonhomogeneous structure at the macroscopic level.

4.5. Conclusions

The presence of striations in binary GeO_2-SiO_2 glasses can be observed using optical microscopy and backscatter mode in the ESEM. Preferential etching along the striations can be explained by the decreased durability of the weaker Ge-O bonds concentrated along the striations. The results of the present study are consistent with a structural model for GeO_2-SiO_2 glasses which consists of a random mixture of Ge-O and Si-O tetrahedra with an interconnected structure.

4.6. References

1. J.E. Shelby, *Introduction to Glass Science and Technology;* pp. 78-97,196. Royal Society of Chemistry, Cambridge, UK, 1997.

2. V.A. Kolesova and E.S. Sher, "Two-Component Glasses of the Germanium Dioxide-Silicon Dioxide System," *Izv. Akad. Nauk SSSR, Neorg. Mater.,* **9** [6] 1018-20 (1973).

3. J.W. Fleming, Bell Laboratories, Murray Hill, NJ, 1947, Private Communication.

4. J.W. Fleming, "Material and Mode Dispersion in GeO_2 B_2O_3 SiO_2 Glasses," *J. Am. Ceram. Soc.,* **59** [11-12] 503-7 (1976).

5. D.L. Wood and J.W. Fleming, "Computerized Refractive Index Measurements for Bulk Materials at UV, Visible and IR Wavelengths," *Rev. Sci. Instrum.,* **53** [1] 43-7 (1982).

6. Y.Y. Huang, A. Sarkar, and P.C. Schultz, "Relationship between Composition, Density and Refractive Index for Germania Silica Glasses," *J. Non-Cryst. Solids,* **27** [1] 29-37 (1978).

7. S. Kobayashi, N. Shibata, S. Shibata, and T. Izawa, "Characteristics of Optical Fibers in Infrared Wavelength Region," *Rev. Electr. Commun. Lab.,* **26** [3-4] 453-67 (1978).

8. S. Takahashi and S. Shibata, "Thermal Variation of Attenuation for Optical Fibers," *J. Non-Cryst. Solids,* **30** [3] 359-70 (1979).

9. Corning Glass Works, GB Patent No. 1521826 C1 2 C 03 C 3/16, *Abridg. Specif.*, 1978, pp. 4664,

10. E.I. Galant, *Fiz. Khim. Stekla,* **6** [1] 121 (1980). As cited in SciGlass 3.5 [CD-ROM]. SciVision, Burlington, MA, 1999.

11. N.F. Borrelli, D.C. Allan, and R.A. Modavis, "Direct Measurement of 248 and 193 nm Excimer-Induced Densification in Silica-Germania Waveguide Blanks," *J. Opt. Soc. Am.,* **16** [10] 1-8 (1999).

12. E.F. Riebling, "Nonideal Mixing in Binary Germania-Silica Glasses," *J. Am. Ceram. Soc.,* **51** [7] 406-7 (1968).

13. O.V. Mazurin and G.P. Roskova, "Properties of Phase-Separated Glasses," pp. 243-89 in *Phase Separation in Glass.* Edited by O. V. Mazurin and E. A. Porai-Koshits. North-Holland, Amsterdam, 1984.

14. M. Tomozawa, "Phase Separation in Glasses," pp. 71-110 in Treatise on Materials Science and Technology, Vol. 17. Edited by M. Tomozawa and R. H. Doremus. Academic Press, New York, 1979.

15. K. Awazu, H. Kawazoe, and M. Yamane, "Simultaneous Generation of Optical Absorption Bands at 5.14 and 0.452 eV in 9 SiO_2:GeO_2 Glasses Heated under an H_2 Atmosphere," *J. Appl. Phys.,* **68** [6] 2713-8 (1990).

16. A.V. Belov, E.M. Dianov, P.N. Lebedev, A.N. Gur'yanov, and V.F. Khopin, "Hydroxyl Group Absorption in Germanium Oxide-Doped Fused Silica Fibers," *Electron. Lett.,* **18** [19] 836-7 (1982).

17. H. Itoh, Y. Ohmori, and M. Nakahara, "Germanium-Dopant Effect on Hydroxyl Loss Increase in Optical Fibers," *J. Lightwave Technol.,* **LT-4** [2] 116-20 (1986).

18. M.K. Schurman and M. Tomozawa, "Equilibrium Oxygen Vacancy Concentrations and Oxidant Diffusion in Germania, Silica, and Germania-Silica Glasses," *J. Non-Cryst. Solids,* **202** [1-2] 93-106 (1996).

19. V.G. Plotnichenko, V.O. Sokolov, and E.M. Dianov, "Hydroxyl Groups in Germanosilicate Glasses," *J. Non-Cryst. Solids,* **278** [1-3] 85-98 (2000).

20. Q. Zeng, J.F. Stebbins, A.D. Heaney, and T. Erdogan, "Hydrogen Speciation in Hydrogen-Loaded, Germania-Doped Silica Glass: A Combined NMR and FTIR Study of the Effects of UV Irradiation and Heat Treatment," *J. Non-Cryst. Solids,* **258** [1-3] 78-91 (1999).

21. N.F. Borrelli, "Infrared Spectra of Silica-Germania Glass," *Phys. Chem. Glasses,* **10** [2] 43-5 (1969).

CHAPTER 5: DIFFUSION CONTROLLED REACTIONS OF MOLECULAR HYDROGEN WITH GERMANIUM DOPED SILICA

Abstract

Hydroxyl species formation in 100 mol% SiO_2, 6 mol% GeO_2-94 mol% SiO_2 and 14.6 mol% GeO_2-85.4 mol% SiO_2 glasses was monitored as a function of time under a hydrogen atmosphere of 700 Torr (pH_2 = 93 kPa) at 500ºC, 600ºC, 700ºC and 800ºC. Hydroxyl formation caused by hydrogen diffusion is measured using infrared spectroscopy. Hydrogen reactions with binary GeO_2-SiO_2 glasses are a function of time, temperature and germanium content. The effect of GeO_2 concentration on hydroxyl formation is evident as induced hydroxyl formation increases with increasing GeO_2 concentration. The rate of hydroxyl formation increases with increasing temperature for both binary GeO_2-SiO_2 glasses. Hydroxyl concentration is uniform throughout the thickness of the sample at saturation. Hydride species do not form during heat treatment in hydrogen at any of the temperatures in either of the binary GeO_2-SiO_2 glasses, as indicated in the lack of change in their infrared spectra.

5.1. Introduction

Hydrogen reactions in binary GeO_2-SiO_2 glasses have been studied extensively since the result is critical for a number of applications. It is well established that hydroxyl formation in binary GeO_2-SiO_2 glasses occurs at a much faster rate than in pure silica.[1,2] Understanding of the kinetics and mechanisms for reactions of molecular hydrogen with binary GeO_2-SiO_2 is important for predicting the performance of optical communication fibers,[3] photo-induced Bragg gratings,[4-6] non-linear optical materials and microelectronic devices.[7,8] There still remains a concern that there might be a small but significant long term loss increase in optical fibers used for communication due to reactions with hydrogen. The concept of increased photosensitivity through hydrogen loading prior to exposure to ultraviolet (UV) light includes the formation of hydroxyl species.[9] Ion implantation of protons into glass has recently attracted much interest as a fabrication technique for nonlinear optical devices and also results in the formation of a significant amount of hydroxyl in binary GeO_2-SiO_2 glasses.[7] With so many applications, a number of experimental studies have been carried out to identify hydroxyl related species in binary GeO_2-SiO_2 glasses and the mechanisms behind their formation, but research has only shown that the reaction mechanisms are extremely complicated and have not yet been fully clarified.

Although there have been a number of studies related to the work presented in this paper, most studies have been conducted on optical fiber or samples with relatively large composition gradients, which makes interpretation difficult. Many earlier studies were based on the considerable interest in hydrogen loss phenomena in optical fibers governed by maximum tolerable loss increases for reliable predictions on long-term performance of cable design.[2,3,8,10,11] Belov et al.[3] investigated hydroxyl absorption in GeO_2-SiO_2 core step index fiber and reported formation of both SiOH and GeOH. Increased GeO_2 content resulted in broadening of the hydroxyl absorption band, as compared to pure silica, which was attributed to the formation of GeOH species since the intensity was dependent on GeO_2 concentration. Mochizuki et al.[8] showed that deuteroxyl formation in GeO_2-SiO_2 fibers can become a barrier to hydroxyl formation and further suggests that protonic species (including deuterium and hydrogen) preferentially react with defect sites in the glass. Tomito et al.[11] observed hydrogen-induced loss phenomena in conventional

GeO_2-doped single mode fibers exposed to hydrogen partial pressures of $0.01 < P_{H_2} < 1.0$ atm at temperatures between 75 and 250°C. In addition to the loss increase due to molecular hydrogen and the formation of hydroxyl species, a spectrally broad background loss increase was observed. The rate of background loss increase was initially high, then gradually diminished, with losses approaching an asymptotic limit. The loss increases were not reversible in that removal of the hydrogen atmosphere did not result in any reduction in loss. These results were attributed to hydrogen reactions with defects in the glass structure, with those defects suggested to be related to germanium. Tomita et al. suggests that the gradual decrease in hydroxyl loss can be related to the decrease in concentration of unreacted defects as the reaction proceeds.

With the suggestion that hydrogen reacts with germanium related defects in binary GeO_2-SiO_2 glasses,[8,11] as well as the discovery of photo induced grating formation enhanced by hydrogen loading,[12] a number of studies involving hydrogen reactions with both gamma and UV irradiated glasses were performed to investigate the interaction between radiation-induced defects and hydrogen.[10,13,14] Itoh et al.[10] studied hydrogen interactions with gamma radiation-induced defect centers in GeO_2-SiO_2 glasses. UV laser irradiation of hydrogen-loaded GeO_2-SiO_2 glasses produced spectral results similar to those found for vitreous silica, with the formation of large amounts of hydroxyl, attributed to both SiOH and GeOH species, where the combination of hydroxyl species is designated as TOH[e] by the authors.[13,14] In this case, however, only GeH was formed during irradiation and no detectable amount of SiH was observed. An isochronal annealing study,[13] using 30 minute treatments at 50 K intervals, of binary GeO_2-SiO_2 glass indicates that the TOH and GeH are thermally stable to ≈400°C. Radiation-induced GeOH is eliminated by heating to 650°C, while some TOH is still present after heating to 1200°C. A shoulder at ≈3200 cm^{-1} on the TOH absorption band is attributed to molecular water.[13,15]

Studies involving irradiated GeO_2-SiO_2 glasses provided some insight into the hydrogen reaction mechanism, however, the increased reactivity of GeO_2-SiO_2 glasses

[e] It is common notation to designate all hydroxyl species in binary GeO_2-SiO_2 glasses as TOH, where T can represent either Ge or Si, and this notation will be used throughout this thesis.

compared to pure silica was still not fully clarified. Even studies involving hydrogen reactions in non-irradiated bulk glass samples present gross inconsistencies in the literature with respect to spectral behavior and band assignment. Itoh et al.[2] deconvoluted the infrared absorption spectra in the region attributed to hydroxyl species into only two separate bands, suggesting that band at 3663 cm^{-1} resulted from the fundamental SiOH absorption and that at 3610 cm^{-1} resulted from the fundamental GeOH absorption. Awazu et al.[1] annealed GeO_2-SiO_2 glass samples in an atmosphere of hydrogen 760 Torr (pH_2 = 101 kPa) at temperatures ranging from 400 to 700ºC. The study involved treatment of 10 mol% GeO_2-90 mol% SiO_2 glass plates cut from preform rods produced by vapor phase axial (VAD) deposition. The glass plates had a parabolic shaped graded index where the maximum concentration of GeO_2 was along the central axis. Awazu and co-workers[1] suggested the presence of 3 bands at 3686, 3630 and 3550 cm^{-1} which contribute to a broad hydroxyl absorption band in the region from 3500 to 3700 cm^{-1}. They attributed these bands to isolated SiOH, geminal SiOH, and GeOH, respectively. In a later paper, Awazu[16] shows infrared results with the suggestion that only two bands contribute to the broad hydroxyl band, a single band at 3675 cm^{-1} for SiOH species and a separate band formed from another process at 3550 cm^{-1}, attributed to GeOH species, with a long tail from hydrogen bonded water species. Schurman and Tomozawa[17] studied the effect of oxygen and water in the melt atmosphere on oxygen vacancy annihilation kinetics in binary GeO_2-SiO_2 glasses. Although the discussion of oxygen vacancies in binary GeO_2-SiO_2 glasses is outside the scope of this paper, Shurman and Tomozawa observed and monitored hydroxyl formation in a 24 mol% GeO_2-76 mol% SiO_2 glass heat-treated in a wet air atmosphere of P_{H_2O} = 20 Torr (P_{H_2O} = 2.67 kPa) for temperatures ranging from 500 to 900°C. Schurman and Tomozawa analyzed the infrared absorption spectra in a similar fashion to Itoh et al., deconvoluting the complex band structure into only two bands, one due to SiOH stretching at 3670 cm^{-1} and a second due to GeOH stretching at 3610 cm^{-1}. The location of the band attributed to SiOH is identical to that found in vitreous silica, while that which is attributed to GeOH is significantly shifted from the reported value[18] of 3560 cm^{-1} for vitreous germania. Shurman and Tomozawa suggest that the shift in the position could be accounted for by the fact that the glass is predominantly silica. Plotnichenko et al.[19] deconvoluted infrared

spectra of a germanosilicate glass into as many as 4 bands in the spectral region attributed to hydroxyl species in the glass. They contend that bands near ≈3673, ≈3625, and ≈3582 cm^{-1} are due to Si-OH groups bound in some manner to different species in the glass network, while bands near ≈3510 cm^{-1} are attributed to Ge-OH groups hydrogen-bonded to the glass network.

There has also been a significant amount of controversy over band assignment in the hydride region of the infrared spectrum. Zeng and co-workers[4] provide a more focused study of infrared band assignment and the associated inconsistencies for binary GeO_2-SiO_2 glasses, including analysis of both UV-irradiated and thermally treated glasses. This study uses high resolution ^1H NMR measurements to support controversial FTIR band assignments. A comparison of the effect of UV irradiation and heat treatment on induced hydrogen speciation is presented. The results included a detailed analysis of hydride species formation, as well as hydroxyl species characterization in GeO_2-SiO_2 glasses. Since argument over the exact band position of hydride species in binary GeO_2-SiO_2 glasses[16,20] is discussed in detail by Zeng et al.,[4] only minor points of the controversy will be discussed here. Greene et al.[20] reported the observation of two bands at 2185 and 2140 cm^{-1} and attributed the bands to GeH and GeH_2, respectively, based on Raman spectral results. In response, Awazu[16] argues the spectral band assignments are reversed from a viewpoint of concentration, and contends that suggested band assignments by Greene et al. are incorrect and the correct assignment for bands at 2185 and 2140 cm^{-1} are GeH_2 and GeH, respectively. Currently, it is agreed that SiH and GeH have characteristic absorption bands at approximately 2250 cm^{-1} and 2180 cm^{-1}, respectively. One of the more important conclusions provided by Zeng et al.[4] was the observation of a significant amount of GeH species formed upon UV-irradiation which is accompanied by a significantly higher concentration of hydroxyl species formation. This implies that reactions that occur when hydrogen loaded binary GeO_2-SiO_2 glasses are exposed to UV-irradiation must include a mechanism that accounts for the 'excess' formation of OH species, i.e. hydroxyl and hydride species are not forming at the same rate and, therefore, are not a result of simply breaking a network forming bond in the glass. The second substantial result presented in this study was that the main difference between heat treated and UV-irradiated samples is the observation of a smaller

concentration of H-bearing species with larger values of the OH/GeH ratio in the heat treated glasses.

Recently, much attention has been focused on ion implantation as a fabrication technique for GeO_2-SiO_2 nanocomposites with nonlinear optical properties. Kawamura et al.[7] recently studied the effect of proton (H^+) implantation on the optical properties of binary GeO_2-SiO_2 glasses prepared by the VAD method. A broad absorption peak at around 3600 cm^{-1} observed in the FTIR absorption spectra of the proton implanted glass was attributed to the superposition of SiOH and GeOH species. An increase in the absorption intensities with increasing implantation fluence was observed although no change in the shape of the absorption band occurred. Kawamura et al. suggest the formation of H_2O that subsequently reacts with the glass network to form SiOH and GeOH species in the glass. Deconvolution of the FTIR absorption spectra is shown in a figure inset where the broad band is separated into only two absorption bands although nothing is stated regarding band assignment. Hydroxyl formation is suggested to be associated with reduction of germanium species in the glass through a proposed reaction mechanism. Micro-Raman spectra of the cross-sectional layers are used to profile the depth of germanium reduction from the surface. Reduced germanium species are confined to the surface, implying that hydroxyl species are also confined to the surface, however, no specific reference or measurement was made to show the actual depth of hydroxyl species formation. There was also no mention of hydride species formation throughout the study.

The effect of hydrogen reactions with bulk glass below T_g on the spectroscopic properties of bulk binary GeO_2-SiO_2 glasses with a uniform concentration profile is reported here. Infrared spectroscopy was used to investigate protonic species formation during reactions with hydrogen. Hydrogen reactions with binary GeO_2-SiO_2 glasses are a function of time, temperature and germanium content. Hydroxyl concentration with progressive hydrogen treatment at 600, 700 and 800ºC is calculated using integrated areas and reported. Complete analysis of these trends and proof that hydroxyl formation is a diffusion-controlled reaction involving hydrogen is presented.

5.2. Experimental Procedure

Binary GeO_2-SiO_2 glasses used in experiments described in this thesis (100 mol% SiO_2, 6 mol% GeO_2-94 mol% SiO_2 and 14.6 mol% GeO_2-85.4 mol% SiO_2) were produced at Corning Incorporated. Glasses were fabricated using a doping and redraw process similar to that used in fiber production. The silica and germania were co-deposited as a soot to form the porous soot preform. The porous material was then consolidated to a glass and drawn into a cane. Samples used in this study were cut to the desired thickness from the bulk glass cane using a low-speed diamond saw and polished using SiC grit paper and 0.5 μm alumina paste. Sample thickness was measured using a micrometer and recorded to within 0.01 mm. All samples used in this study were approximately 1.0 mm thick unless otherwise noted.

Samples were placed on a platinum setter in a vitreous silica tube attached to a gas handling apparatus. The preheated horizontal tube furnace was positioned around the evacuated silica sample chamber. Temperatures (500°C, 600°C, 700°C, or 800°C) were continuously monitored by a thermocouple inside the sample chamber, directly above the samples. After the desired temperature was reached, hydrogen gas was introduced into the sample chamber. Sample temperature was held constant to within ±5K throughout the treatment. Each sample was treated for the desired amount of time under 700 ± 7 Torr (93 ± 1 kPa) of hydrogen partial pressure. A more detailed description, including a schematic of the apparatus, is presented in Chapter 3.

Infrared absorption spectra were measured before the initial heat treatment and after each subsequent heat treatment. Since treatment times were cumulative for each treatment temperature, variations between samples do not exist for this work. Absorbances are reproducible to within ±0.01.

5.3. Results

5.3.1. Hydroxyl Formation at 800°C

In a preliminary study, both binary GeO_2-SiO_2 glasses (6 mol% GeO_2-94 mol% SiO_2 and 14.6 mol% GeO_2-85.4 mol% SiO_2) and a pure SiO_2 glass (100 mol% SiO_2), made using the same procedure were treated at 800°C and 700 torr hydrogen for one

hour. All of the glasses in the as-received condition had a very low hydroxyl content, i.e. less than 10 ppm, and can be considered to have started at the same base value. The hydroxyl peak was not observed in any of the as-received glasses because the hydroxyl concentration was too small to interact with the infrared light for detection above background. Figure 5.1 shows the radical difference in reactions with hydrogen between the pure and doped silica glasses. It is well known[1-3] that germanium doped silica glasses react with hydrogen gas at a much faster rate than pure silica. This study agrees well with previously published data. There is a marked difference in the rate of reaction between the binary GeO_2-SiO_2 glasses and that of pure silica. There is also a significant difference in the hydroxyl environment formed in each of the binary GeO_2-SiO_2 glasses. The results of this preliminary experiment suggested a closer look at the interactions of hydrogen with binary GeO_2-SiO_2 glasses.

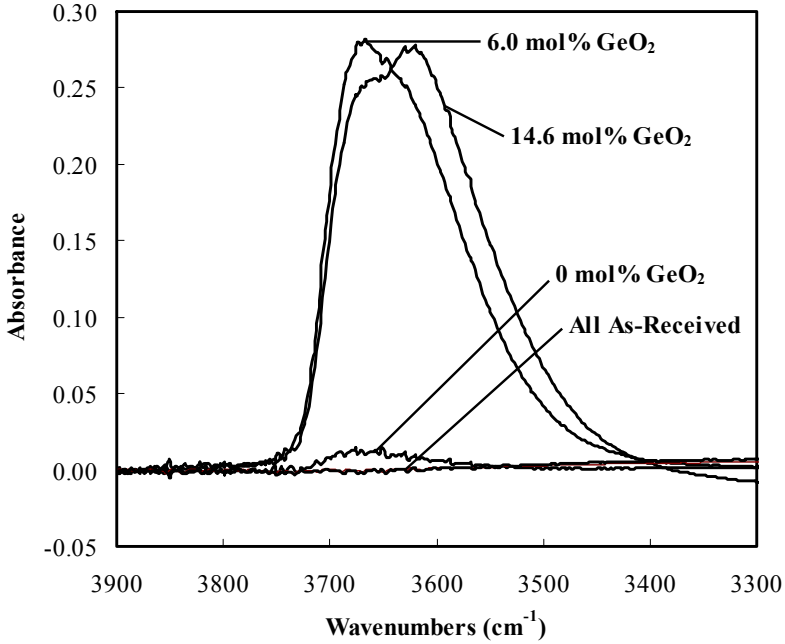

Figure 5.1. Infrared spectra in the hydroxyl/water region for both binary GeO_2-SiO_2 glasses (6 mol% GeO_2-94 mol% SiO_2 and 14.6 mol% GeO_2-85.4 mol% SiO_2) and a pure SiO_2 glass made from the same procedure treated at 800°C and 700 Torr H_2 for one hour.

The treatment of all three samples at 800°C and 700 Torr of hydrogen gas was extended and infrared spectra were measured after progressive hydrogen treatments for

up to 64 hours. Treatment was extended for the pure SiO_2 glass for up to 190 hours and only minimal hydroxyl formation was observed. The infrared spectra for the region from 3900 to 2100 cm^{-1} for each of the binary glasses are shown in Figures 5.2 and 5.3. The samples used in this study for each set of conditions were treated, removed from the furnace, measured and returned to the furnace for further treatment, i.e. the same sample of glass was used throughout the entire study and variations between the glass samples do not exist for this work. With increasing treatment time, there is an increased scattering loss, lifting the infrared spectra at the high frequency end and decreasing with decreasing frequency. This small frequency dependent scattering loss is not included in further data analysis because there is no way to quantitatively determine the exact relationship since the effect is a combination of both scattering and reflection losses. Scatter and reflection losses are a function of wavelength with different wavelength dependencies. In this analysis, the maximum error will be no more than three percent. The values of data with the highest scatter effect, i.e. longest treatment time, will be slightly lower than the actual value, but the effect is so small it will have a negligible effect that is impossible to quantify. The true value is slightly greater than the reported value.

For clarity, the region from 3900 to 3300 cm^{-1}, where absorptions due to hydroxyl species in binary GeO_2-SiO_2 glasses occur,[1-4,17,19] is shown in Figures 5.4 and 5.5 with background subtraction for each the binary glasses. It is clear that at least 2 different species contribute to the formation of the broad band extending from about 3750 to 3400 cm^{-1} with spectral characteristics of both SiOH and GeOH species. Figures 5.4 and 5.5 show the systematic increase in intensity in the spectral regions associated with SiOH and GeOH with progressive hydrogen treatment. The intensities of the bands for of the doped glasses increase in significantly different ways, implying that hydroxyl formation is dependant on germanium concentration. The ratio of the two components of the band reverses with increasing germanium concentration resulting in higher intensity at lower frequency with increasing germanium content. The maximum absorbance indicates the total hydroxyl concentration is smaller in the sample with less germanium, i.e. the total amount of hydroxyl formed during a given treatment is larger for the glass containing more germanium.

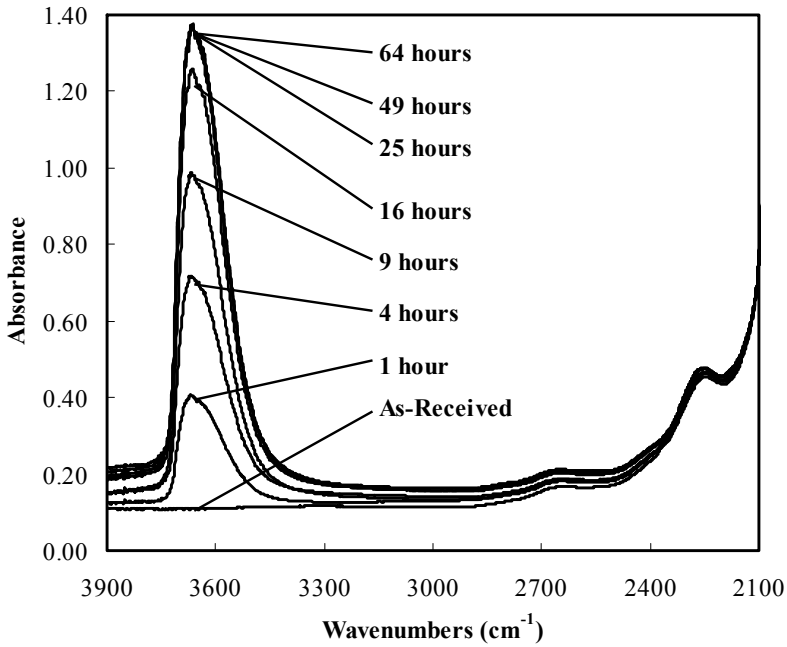

Figure 5.2. Infrared spectra from 2100 cm^{-1} to 3900 cm^{-1} for 6 mol% GeO_2 - 94 mol% SiO_2 glass during progressive hydrogen treatment at 800°C for the indicated cumulative treatment time.

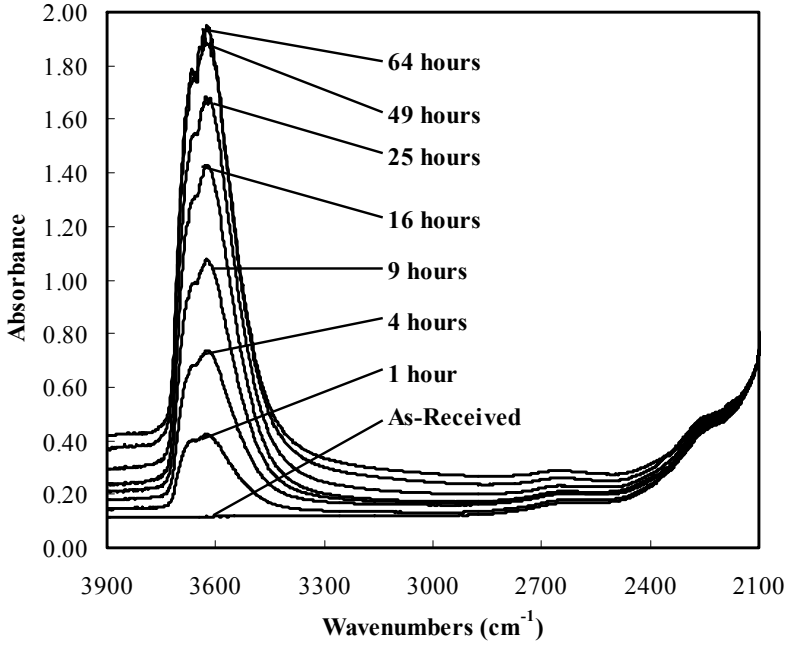

Figure 5.3. Infrared spectra from 2100 cm^{-1} to 3900 cm^{-1} for 14.6 mol% GeO_2 - 85.4 mol% SiO_2 glass during progressive hydrogen treatment at 800°C for the indicated cumulative treatment time.

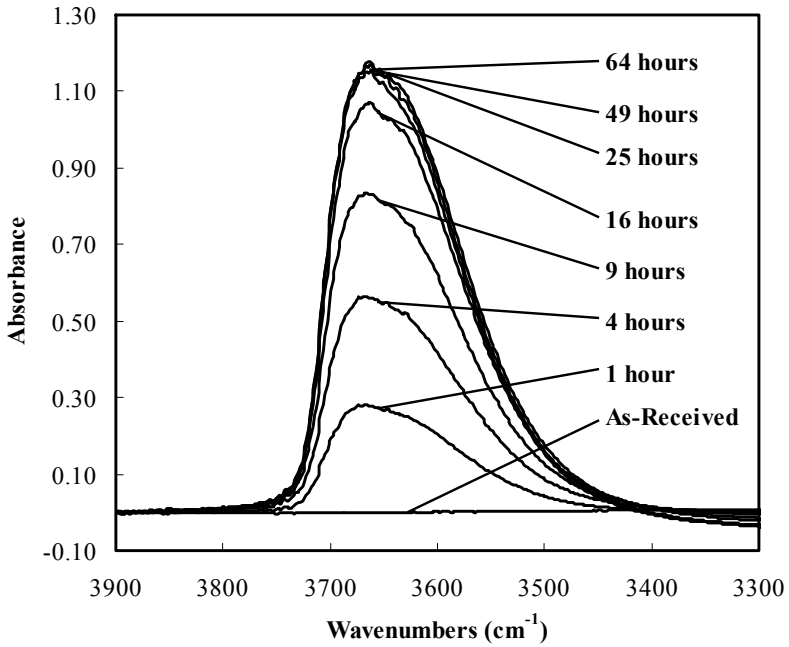

Figure 5.4. Infrared spectra in the hydroxyl/water region for 6 mol% GeO_2 - 94 mol% SiO_2 glass during progressive hydrogen treatment at 800°C for the indicated cumulative treatment time.

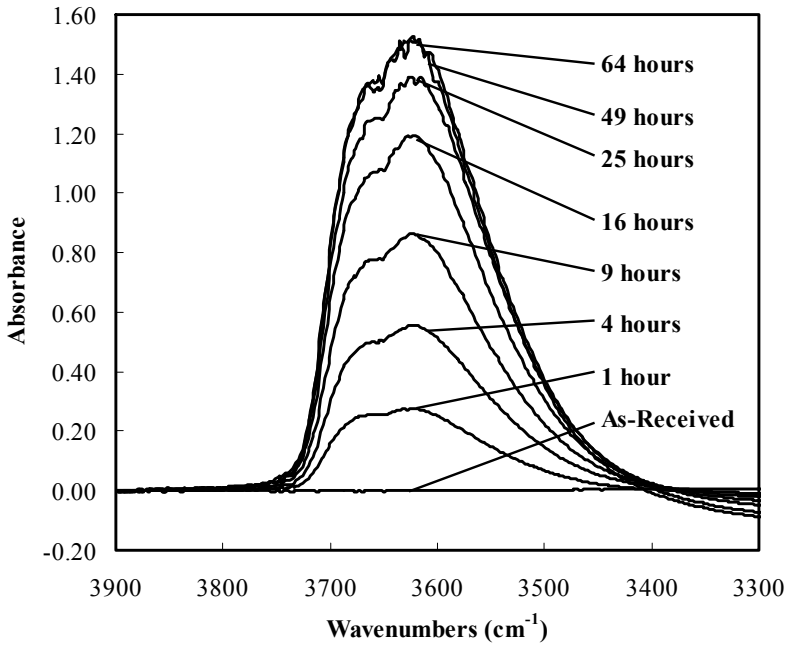

Figure 5.5. Infrared spectra in the hydroxyl/water region for 14.6 mol% GeO_2 - 85.4 mol% SiO_2 glass during progressive hydrogen treatment at 800°C for the indicated cumulative treatment time.

5.3.2. Effect of Temperature on Hydroxyl Formation

One millimeter thick plates of each of the binary GeO_2-SiO_2 glasses were also treated at 700°C, 600°C and 500°C and 700 Torr of hydrogen gas. Infrared spectra taken with progressive treatments at 700°C, 600°C and 500°C are similar in shape and band growth behavior to those observed at 800°C, and are shown in Appendix A. The infrared spectra in the 3900 to 3300 cm^{-1} region are complex, with strong evidence of at least 2 different bands. The absorbances at 3662 cm^{-1} and 3620 cm^{-1}, which are positions of the maximum intensities for the 6 mol% GeO_2 - 94 mol% SiO_2 glass and the 14.6 mol% GeO_2-85.4 mol% SiO_2 glass treated at 800°C, respectively, were plotted as a function of square root time to show the progressive growth of hydroxyl band. Figure 5.6 shows the effect of time on the absorbance at 3662 cm^{-1}, the region of the hydroxyl band most affected by the formation of SiOH species, and Figure 5.7 shows the effect of time on the absorbance at 3620 cm^{-1}, the region of the hydroxyl band most affected by the formation of GeOH species. The filled points represent the absorbance at the chosen frequency for the 14.6 mol% GeO_2-85.4 mol% SiO_2 glasses and the open points represent absorbance at the chosen frequency for the 6 mol% GeO_2-94 mol% SiO_2 glasses. The stars along the x-axis of the plot represent the absorbance at the chosen frequency for the pure silica glass treated at 800°C. This figure clearly shows the radically different range in absorption between the pure silica glass and that of the germania-doped glasses. It is obvious that pure silica does not react as readily with hydrogen gas.

In general, the rate of hydroxyl formation increases with increasing temperature for both binary GeO_2-SiO_2 glasses. Figures 5.6 and 5.7 also show the effect of temperature on the formation of hydroxyl species in each of the binary GeO_2-SiO_2 glasses. The influence of temperature on the data clearly suggests a diffusion mechanism where the glass treated at higher temperatures reacts at a much faster rate i.e. each of the glasses treated at 800°C reach saturation faster then those treated at 700°C, etc.

Closer examination of Figure 5.6, showing the region of the hydroxyl band most affected by the formation of SiOH species, shows some rather interesting results. Overall one could conclude that the final amount of hydroxyl species contributing to this region of the hydroxyl band forms independently of germanium concentration since the final concentration is similar for each glass. Clearly, data shown for the 6 mol% GeO_2 - 94

mol% SiO_2 glass treated at 500°C do not indicate that sufficient time has been allowed to reach equilibrium saturation, which is confirmed by results not shown here. While not shown in Figure 5.6, data were obtained for up to 256 hours for samples treated at 500°C, which show the continual approach toward equilibrium. The 14.6 mol% GeO_2-85.4 mol% SiO_2 glass treated at 800°C, however, may be showing abnormally high hydroxyl formation as a result of the significant crystallization and color formation discussed in subsequent chapters. Another important result presented in Figure 5.6 is the observation that germanium concentration has an increasing effect on the rate of hydroxyl formation as the temperature decreases, i.e. germanium concentration has little to no effect on the rate of hydroxyl formation for samples treated at 800°C but has a drastic effect on the rate of formation for samples treated at 500°C.

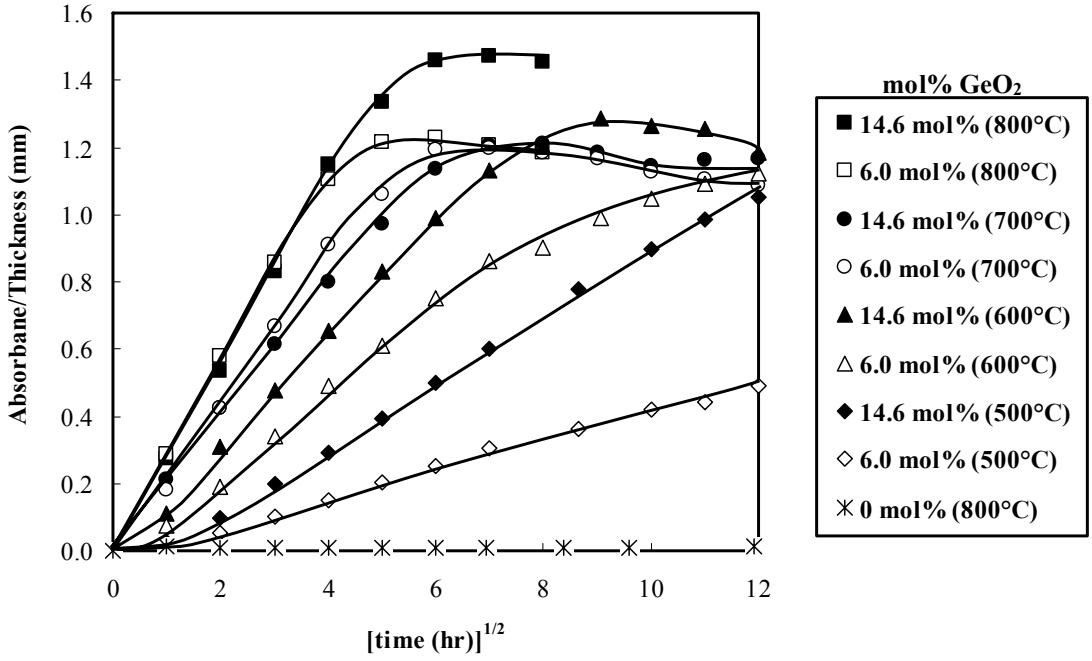

Figure 5.6. The effect of square root time on the absorbance at 3662 cm^{-1}. The filled points represent the intensity for the 14.6 mol% GeO_2-85.4 mol% SiO_2 glasses and the open points represent peak intensity for the 6 mol% GeO_2-94 mol% SiO_2 glasses. The open squares along the axis of the plot represent the intensity of the pure silica glass. Lines are a guide to the eye.

Figure 5.7, showing the region of the hydroxyl band most affected by the formation of GeOH species, clearly shows that the final amount of hydroxyl species

contributing to this region of the broad band are influenced by germanium content in the glass, i.e. the contribution from the GeOH band increases with increasing germanium content. The only obvious results that do not exactly follow these trends are again the 6 mol% GeO_2 - 94 mol% SiO_2 glass treated at the lowest temperature (500°C) and the 14.6 mol% GeO_2-85.4 mol% SiO_2 glass treated at the highest temperature (800°C) for the reasons given above. The temperature dependence of the rate of hydroxyl formation is also observed in Figure 5.7 as the germanium concentration again has an increasing effect on the rate of hydroxyl formation as the temperature decreases. There is even a slight germanium concentration effect on the samples treated at 800°C which was not observed in Figure 5.6.

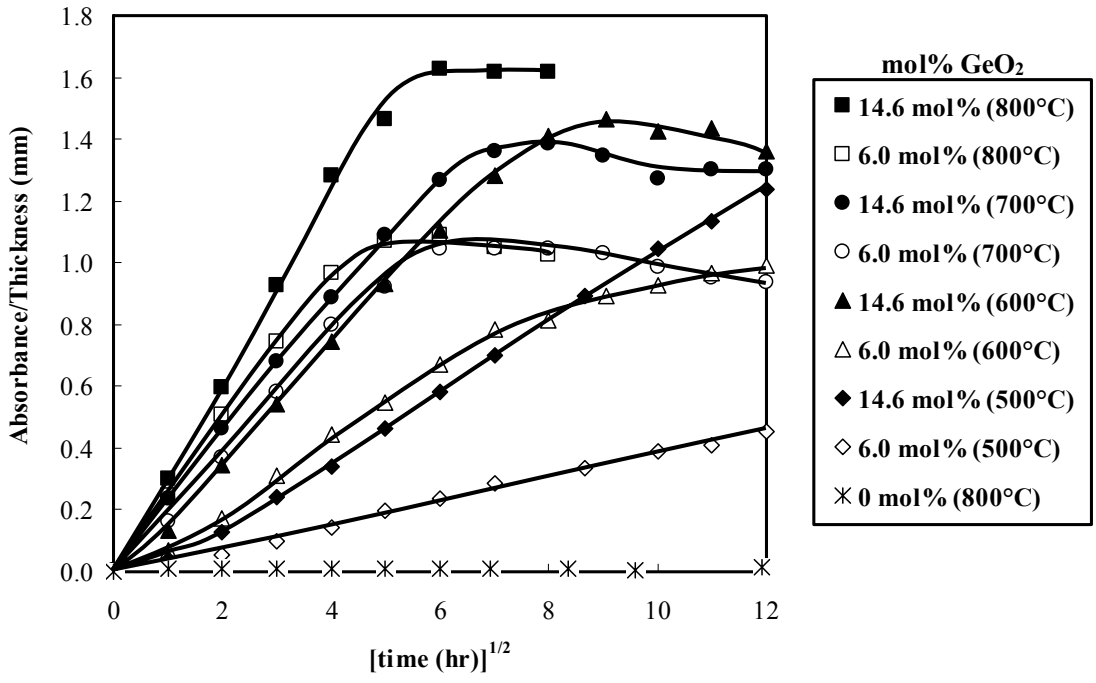

Figure 5.7. The effect of square root time on the absorbance at 3620 cm^{-1}. The filled points represent the intensity for the 14.6 mol% GeO_2-85.4 mol% SiO_2 glasses and the open points represent peak intensity for the 6 mol% GeO_2-94 mol% SiO_2 glasses. The open squares along the axis of the plot represent the intensity of the pure silica glass. Lines are a guide to the eye.

In general, a linear relationship between absorbance and square root time is observed at shorter times. The linear relationship between absorbance and square root time suggests the possibility that hydrogen reaction with the binary GeO_2-SiO_2 glasses to

form hydroxyl can be discussed through application of the tarnishing model. Closer examination of the results for the lowest treatment temperatures (500°C and 600°C), however, show evidence of an incubation time, i.e. a period of time at the beginning of the treatment during which the kinetics are adjusting before the reaction occurs with the square root of time progression. The presence of an incubation period indicates that hydroxyl formation does not occur the instant the sample is exposed to hydrogen at elevated temperatures, implying that the reaction itself lags the supply of hydrogen to the reaction sites.

5.3.3. Integrated Area to Determine Absolute Hydroxyl Formation

Evaluating the broad hydroxyl band by area is convenient for total hydroxyl content, but tells nothing from a mechanistic standpoint for the formation of different hydroxyl species. The integrated area under the broad band extending from about 3880 to 3430 cm^{-1} also shows the effect of temperature on the formation of hydroxyl species, Figure 5.8, as each of the glasses treated at 800°C reach saturation faster then those treated at 700°C etc. Once again the filled points represent the integrated area with progressive treatment for the 14.6 mol% GeO_2-85.4 mol% SiO_2 glasses and the open points represent the integrated area for the 6 mol% GeO_2-94 mol% SiO_2 glasses. The maximum in integrated area indicates the total hydroxyl concentration is smaller in the sample with less germanium, i.e. the total amount of hydroxyl formed during a given treatment is higher for glasses with a higher germanium content. One particularly interesting feature of this figure is that the integrated area for each of the two different glasses appears to be approaching some constant value. This would suggest that there is a fixed number of reaction sites available for reaction with hydrogen regardless of treatment temperature and there are more reaction sites in the higher germanium glass. A fixed number of reaction sites available for hydroxyl formation is essential for application of the tarnishing model to analyze hydrogen diffusion kinetics.

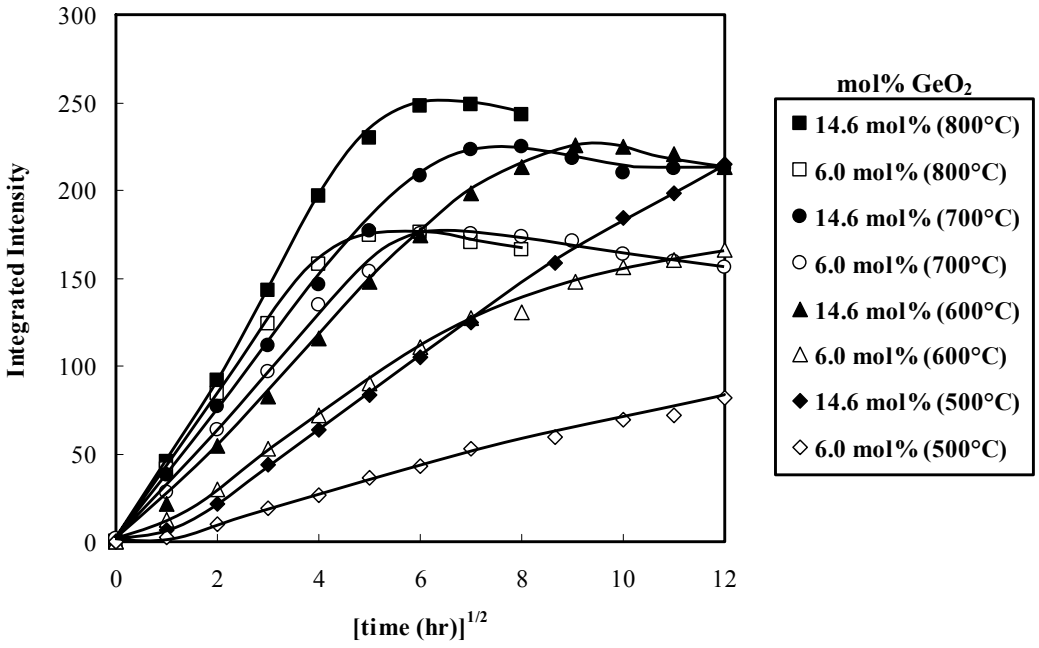

Figure 5.8. The effect of square root time on the integrated area under the broad band extending from about 3750 to 3400 cm^{-1}. The filled points represent the integrated intensity for the 14.6 mol% GeO_2-85.4 mol% SiO_2 glasses and the open points represent integrated intensity for the 6 mol% GeO_2-94 mol% SiO_2 glasses. Lines are a guide to the eye.

The inaccuracies involved with deconvolution of the hydroxyl band can be avoided through the use of an integrated extinction coefficient for determination of total hydroxyl content in the glass. A method for estimating the integrated extinction coefficient for binary GeO_2-SiO_2 glasses was suggested by Zeng et al.[4] and was originally presented by Libowitzky and Rossman.[21] One major assumption necessary for application of this method is that the integrated absorption coefficient for the band due to water species in glass can be determined solely from the position of the median band energy of half area under the absorption band, i.e. the integrated absorption coefficient for the band due to water species in a glass is independent of glass composition. Using the correlation between integrated extinction coefficient and the median wavenumber of the hydroxyl stretching band, Libowitzky and Rossman[21] developed an expression to determine ε_i

$$\varepsilon_i = 123.3\left(3753 - \nu\right) \tag{5.1}$$

where ε_i is the integrated extinction coefficient in (L/mol OH-cm_L-cm_f)[f] and ν is the median wavenumber of the absorption band. The factor of 123.3 is exactly half of 246.6, the factor determined by Libowitzky and Rossman[21] and used for determination of water species in the glass. On a molar basis, the difference between formation of hydroxyl versus water is a factor of two i.e. two OH will form from one H_2O in the glass since the second oxygen is provided by the glass network and, on a molar basis, the source of the second oxygen is insignificant. Figure 5.9 shows the median band energy for the glass composition with progressive hydrogen treatment, the filled points representing the median band energy for the 14.6 mol% GeO_2-85.4 mol% SiO_2 glasses and the open points representing the median band energy for the 6 mol% GeO_2-94 mol% SiO_2 glasses. Application of this method requires that the band does not change in shape with progressive formation of hydroxyl species, i.e. the position of the median band energy does not change with treatment time. There is obviously a significant change in the band shape with progressive treatment for the samples treated at 500ºC, the band shifts approximately 10 cm^{-1} around 25 hours of treatment. The peak shift could be a result of the inability to determine the area of the hydroxyl peak at very short treatment times resulting from the extremely small amount of hydroxyl present. With such a small amount of hydroxyl there is significantly more error involved in determination of the median band energy, therefore the data for the samples treated at 500°C will be omitted from this discussion. The small change in median band energy for the glasses treated at 600, 700 and 800ºC is within the error of the measurement and can be used for determination of integrated extinction coefficients. The median band energy and resulting integrated absorption coefficient for the 14.6 mol% GeO_2-85.4 mol% SiO_2 glass and the 6 mol% GeO_2-94 mol% SiO_2 glass are listed in Table 5.I.

[f] The subscript "L" and "f" on the cm unit indicates the origin of the unit i.e. is used to distinguish between units of length (L) or frequency (f).

Table 5.I. Median Band Energy and Calculated Integrated Absorption Coefficient for 14.6 mol% GeO_2-85.4 mol% SiO_2 Glass and 6 mol% GeO_2-94 mol% SiO_2 Glass.

Glass Composition	Median Band Energy (cm^{-1})	Integrated Absorption Coefficient (L/mol OH-cm_L-cm_f)
14.6 mol% GeO_2-85.4 mol% SiO_2	3631	15042.6
6.0 mol% GeO_2-94 mol% SiO_2	3616	16892.1

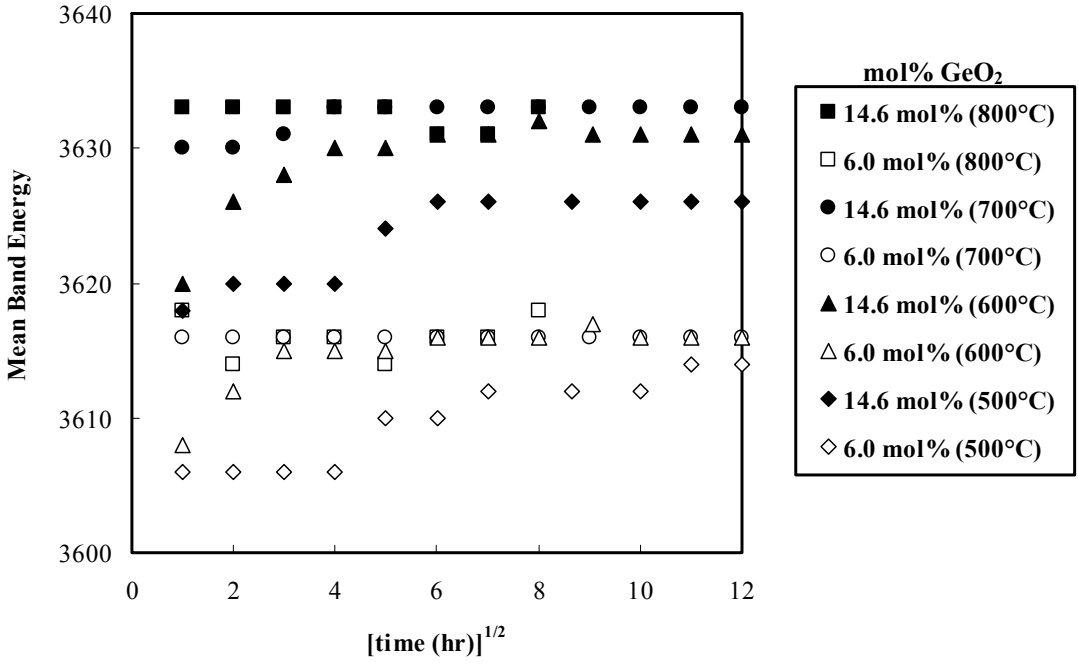

Figure 5.9. The effect of square root time on the median band energy for the broad band extending from about 3750 to 3400 cm^{-1}. The filled points represent the median band position for the 14.6 mol% GeO_2-85.4 mol% SiO_2 glasses and the open points represent peak median band position for the 6 mol% GeO_2-94 mol% SiO_2 glasses.

The concentration of hydroxyl present in the glass with progressive treatment can be determined using a form of the Beer-Lambert Law[22] based on the integrated absorption[21]

$$A_i = c\,t\,\varepsilon_i \tag{5.2}$$

The Beer-Lambert Law can be rearranged and written in a form that is more appropriate for direct determination of the fraction concentration of hydroxyl in the glass;

$$c = A_i\left[\frac{34}{1000\;t\,D_g\;\varepsilon_i}\right] \tag{5.3}$$

where c is the weight fraction concentration of hydroxyl in the glass in (grams of OH/grams of glass), A_i is the integrated intensity or area under the infrared absorption band extending from about 3750 to 3400 cm^{-1} (the cm_f^{-1} unit comes from the increment of the measurement in the sum of intensity), t (cm_L) is the path length of light through the thickness of the sample, D_g is the density of the glass (measured values reported in Chapter 3 were used for calculations) and ε_i is the integrated extinction coefficient from Table I in (L/mol OH-cm_L-cm_f). The factor of 1000 is included in the equation to allow for conversion between the units for density (cm^3) and integrated extinction coefficient (L) i.e. there are 1000 mL in 1 L. The term 34 (g of OH/mol of OH)[g] is included to obtain concentration results in weight rather than mol units since hydroxyl concentration is generally reported in weight units.[23-26] The calculated concentration of hydroxyl species formed in each of the binary GeO_2-SiO_2 glasses with progressive hydrogen treatment is plotted as function of square root time in Figure 5.10. Once again the filled points represent the integrated area with progressive treatment for the 14.6 mol% GeO_2-85.4 mol% SiO_2 glasses and the open points represent the integrated area for the 6 mol%

[g] On a weight basis the factor for determination of hydroxyl in the glass is 34 (g of OH/mol of OH), which is not a factor of two larger than the typical value of 18 (g of OH/mol of OH) used for water calculations. This discrepancy comes from the fact there are two hydroxyl species forming and oxygen for one hydroxyl unit is provided by the glass, which is significant on a weight basis.

GeO_2-94 mol% SiO_2 glasses. The effect of temperature on the formation of hydroxyl species is evident as each of the glasses treated at 800°C reach saturation faster then those treated at 700°C etc. The maximum in hydroxyl concentration indicates that the total hydroxyl concentration is smaller in the sample with less germanium, i.e. the total amount of hydroxyl formed during a given treatment is larger for the glass containing more germania. One particularly interesting feature of this figure is that the hydroxyl concentration for each of the two different glasses appears to be approaching some constant value, with exception of the high germanium glass treated at 800°C, which would suggest that there is a fixed number of reaction sites available for reaction with hydrogen regardless of treatment temperature. Knowing the amount of hydroxyl formation with progressive hydrogen treatment is somewhat meaningless without knowing the distribution of hydroxyl formation throughout the thickness of the glass sample.

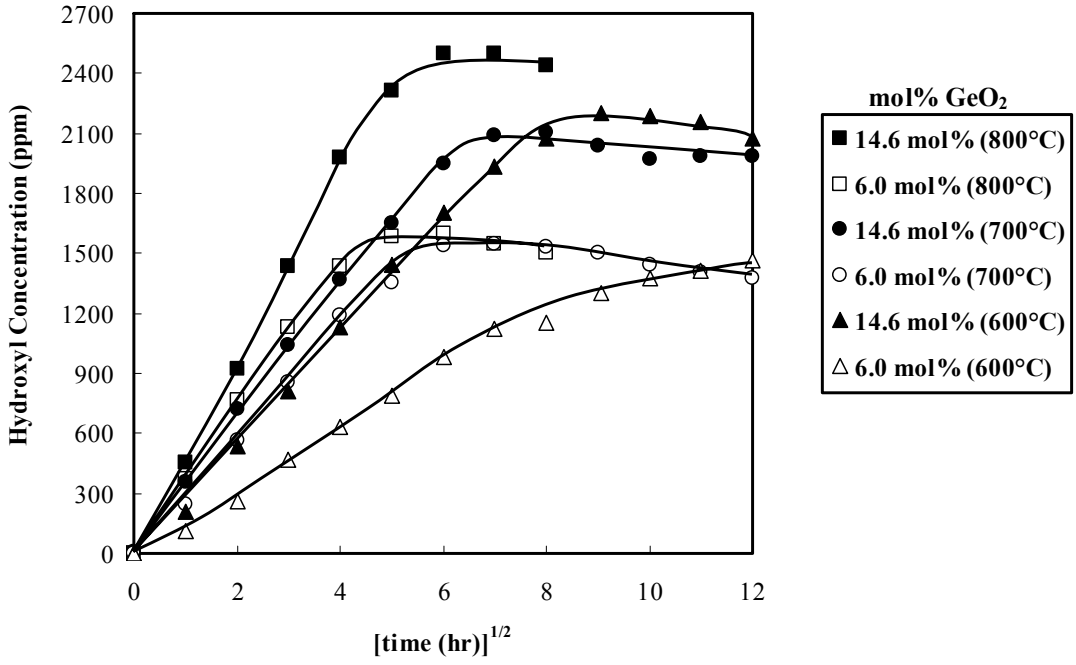

Figure 5.10. The effect of square root time on the hydroxyl concentration in ppm. The filled points represent the median band position for the 14.6 mol% GeO_2-85.4 mol% SiO_2 glasses and the open points represent peak median band position for the 6 mol% GeO_2-94 mol% SiO_2 glasses. Lines are a guide to the eye.

5.3.4. Section Experiments by Mechanical Thinning

Sectioning experiments by mechanical thinning can be used to determine the extent of hydroxylation throughout the experiment. A sample of 14.6 mol% GeO_2-85.4 mol% SiO_2 glass was treated at 800°C and 700 Torr of hydrogen for only 2 hours, i.e. the sample was removed from the furnace before it had reached saturation. Mechanical polishing of one of the reacted surfaces was performed and infrared spectra were measured with progressive removal of the exposed surface. Hydroxyl confined to the near surface region would show no change in absorbance after removal of the reacted layer. The change in absorbance at 3672 cm^{-1} as a function of decreasing thickness, Figure 5.11, shows that hydroxyl formation is confined to the exposed surfaces of the glass sample, i.e. extends only partially through the thickness of the glass samples. The region of constant hydroxyl concentration, i.e. no change in intensity with progressive polishing, that occurs after removal of approximately 200 μm of glass indicates that there is no hydroxyl formation in the center of the glass plate and the measured intensity is representative of the hydroxyl confined to the as-treated, non-polished side of the plate.

Constant hydroxyl concentration throughout the thickness of the sample results in a linear relationship when absorbance is plotted as a function of decreasing thickness. In order to determine the extent of hydroxyl formation at saturation, a randomly chosen treated sample was progressively polished from one side in ≈30 μm increments and infrared spectra were obtained. Figure 5.12 shows the effect of thickness (mm) on absorbance at 3672 cm^{-1} with progressive polishing, of a one millimeter thick sample of 6 mol% GeO_2-94 mol% SiO_2 glass treated at 700°C and 700 Torr of hydrogen for 144 hours, i.e. saturation. The shape of the infrared curve in the region from 3750 to 3400 cm^{-1} does not change with progressive polishing indicating that the concentration of different hydroxyl species in the glass does not change from the surface to the center of the sample. The linear relationship between maximum intensity and thickness of the sample demonstrates that the concentration of hydroxyl is, in fact, uniform through the sample thickness at saturation.

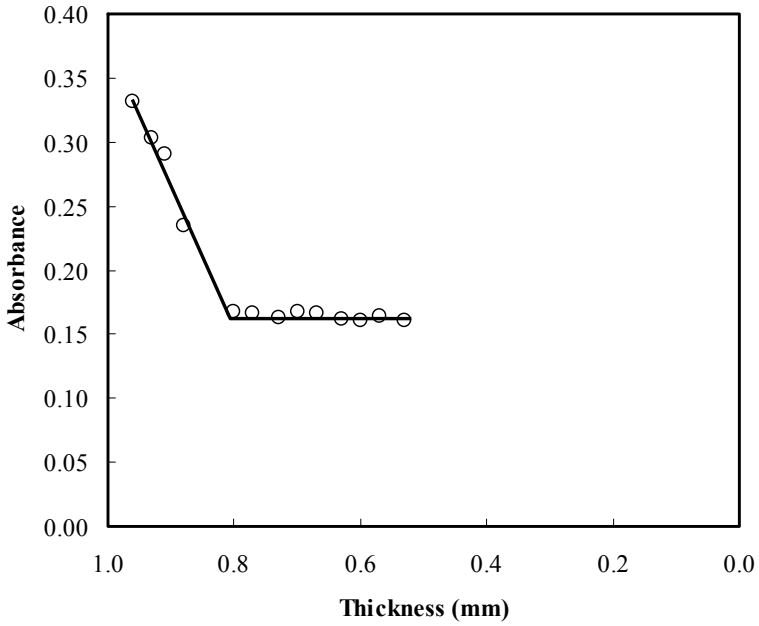

Figure 5.11. Effect of thickness (mm) on absorbance at 3672 cm^{-1} with progressive polishing of a one millimeter thick sample of 14.6 mol% GeO_2-85.4 mol% SiO_2 glass treated at 800°C and 700 Torr of hydrogen for 2 hours. Lines are a guide to the eye.

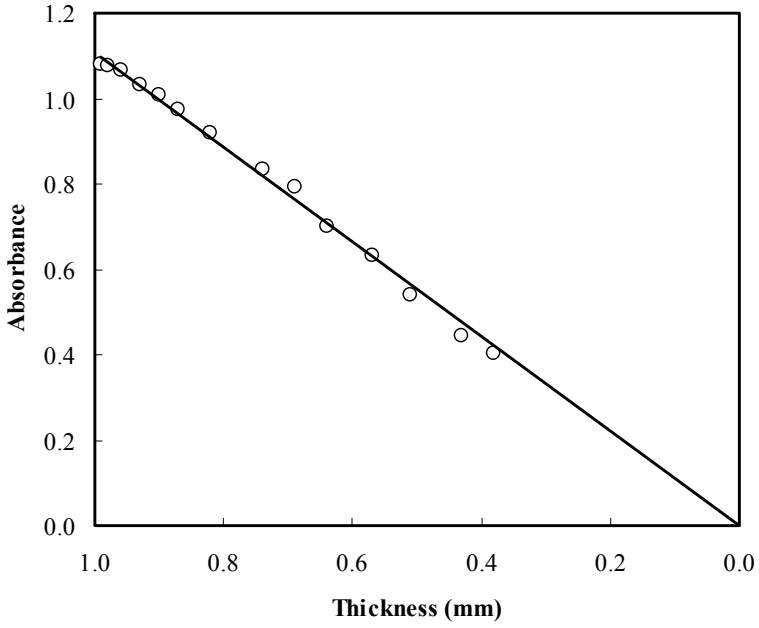

Figure 5.12. Effect of thickness (mm) on maximum peak intensity at 3672 cm^{-1} with progressive polishing of a one millimeter thick sample of 6 mol% GeO_2-94 mol% SiO_2 glass treated at 700°C and 700 Torr of hydrogen for 144 hours.

5.3.5. No Significant Formation of Hydride Species

The lower frequency region of the fundamental infrared spectrum can be used to detect and monitor the presence of hydride species in the glass. It is well established that a band at ≈2250 cm^{-1} is indicative of the presence of SiH in the glass.[25,27] This band occurs at almost the same frequency as a band at ≈2260 cm^{-1}, which is due to the first overtone of the fundamental Si-O-Si stretching vibration at ≈1120 cm^{-1}.[28,29] The argument over the exact band position of hydride species in binary GeO_2-SiO_2 glasses is discussed in detail by Zeng et al.[4] Currently it is agreed that SiH and GeH have characteristic absorption bands at approximately 2250 and 2180 cm^{-1},[4,20] respectively.

The infrared spectra in the hydride region, from 2500 to 2100 cm^{-1}, for 6 mol% GeO_2 - 94 mol% SiO_2 glass and the 14.6 mol% GeO_2-85.4 mol% SiO_2 glass treated at 800°C are shown in Figures 5.13 and 5.14, respectively. Only the as-received and 64 hour spectra are included, all other treatments with a square root time progression fall in between and were omitted to eliminate clutter. The infrared spectra in the hydride region, from 2500 to 2100 cm^{-1}, for 6 mol% GeO_2 - 94 mol% SiO_2 glass and the 14.6 mol% GeO_2-85.4 mol% SiO_2 glass treated at 600°C are shown in Figures 5.15 and 5.16, respectively. Only the as-received and 144 hour spectra are included, all other treatments with a square root time progression fall in between and were omitted to eliminate clutter. In Figures 5.13 - 5.16 the first overtone of the fundamental Si-O-Si stretching vibration at ≈2260 cm^{-1} band is present and the effect of germanium concentration on the shape of the band is obvious in the as-received spectra. The band is significantly smaller in the higher germanium content glass, indicating that there are fewer Si-O-Si bonds present. The presence of carbon dioxide in the atmosphere, the medium through which the measurement was made, is the source for the artifact observed at approximately 2347 cm^{-1} and is a result of insufficient background subtraction during the measurement.

The hydride region of the spectrum for the 14.6 mol% GeO_2-85.4 mol% SiO_2 glass treated at 800°C is the only set of spectra that show a significant change in the absorption behavior. The difference observed in the line shape is not indicative of an absorption band. The reason for the actual change in shape of this band is very difficult

to discuss at this time because the effect of crystallization and subsequent roughening of the sample on the absorbance cannot be determined.

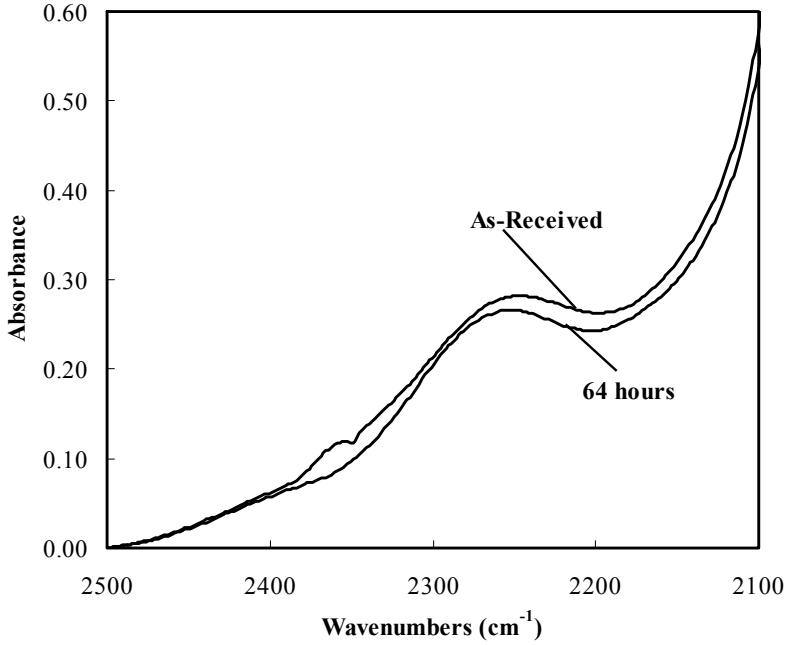

Figure 5.13. Infrared spectra in the hydride region for 6 mol% GeO_2 - 94 mol% SiO_2 glass during progressive hydrogen treatment at 800°C for the indicated cumulative treatment time.

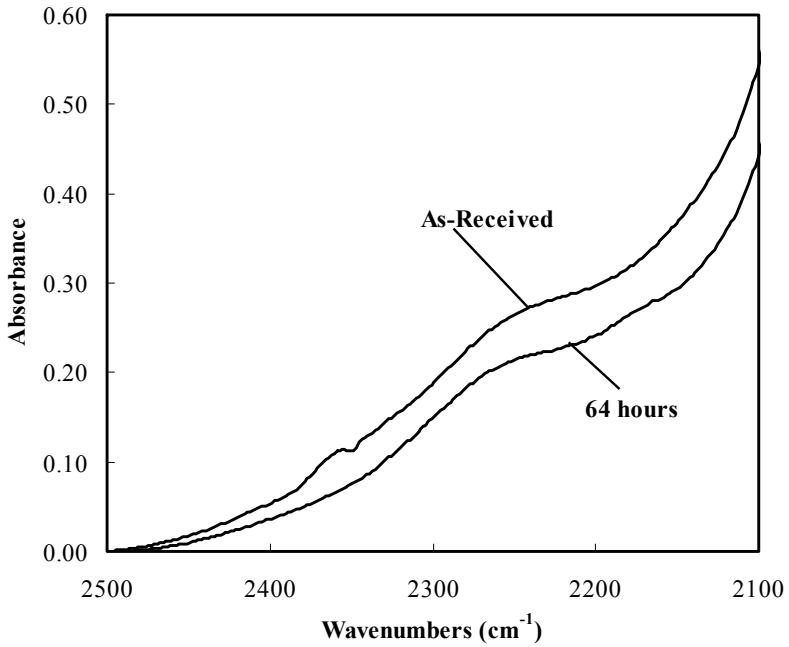

Figure 5.14. Infrared spectra in the hydride region for 14.6 mol% GeO_2-85.4 mol% SiO_2 glass during progressive hydrogen treatment at 800°C for the indicated cumulative treatment time.

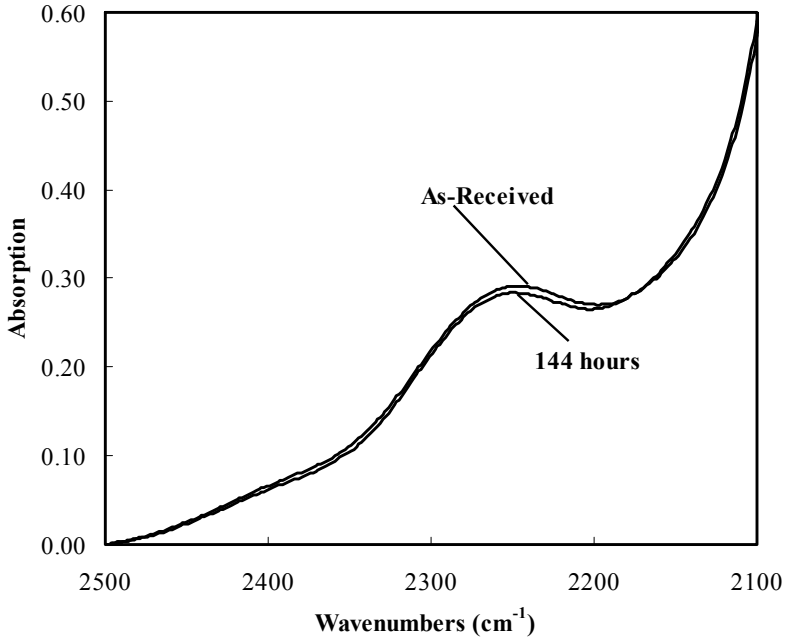

Figure 5.15. Infrared spectra in the hydride region for 6 mol% GeO_2 - 94 mol% SiO_2 glass during progressive hydrogen treatment at 600°C for the indicated cumulative treatment time.

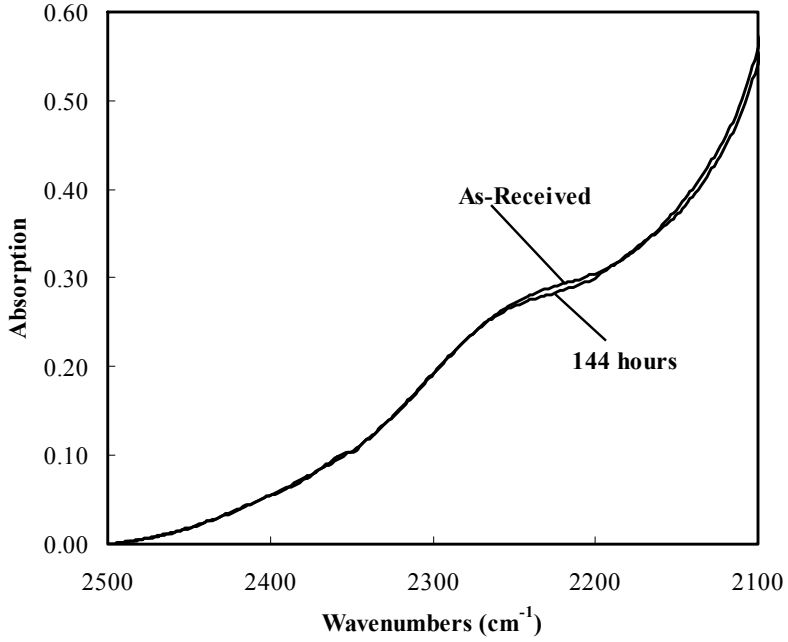

Figure 5.16. Infrared spectra in the hydride region for 14.6 mol% GeO_2 - 85.4 mol% SiO_2 glass during progressive hydrogen treatment at 600°C for the indicated cumulative treatment time.

In this region of the infrared spectra, the line shape remains constant with progressive hydrogen treatment for both of the binary GeO_2-SiO_2 glasses treated at 600°C. With no detectable effect and no significant change in band shape with progressive treatment, it is evident that SiH and GeH species are not forming in this process. There is no evidence to support the formation of bands at 2250 or 2180 cm^{-1} representing SiH and GeH, respectively. Infrared spectra taken for progressive treatments at 700°C, and 500°C, Appendix A, are similar in shape and band growth behavior to those observed at 600°C. If there is any effect, it is extremely small, indicating only a minor change in the amount of species absorbing in this spectral region.

5.3.6. Treatments with Deuterium

Deuterium is often used to further clarify the formation of different species in a glass.[30-33] Shifts in band position in the infrared spectra result from the heavier mass of the deuterium atom as compared to the hydrogen atom. When the as-received binary

GeO_2-SiO_2 glasses are treated with deuterium, rather than hydrogen, at 800°C, the infrared spectra shown in Figure 5.17 and 5.18 were obtained for the 6 mol% GeO_2-94 mol% SiO_2 and 14.6 mol% GeO_2-85.4 mol% SiO_2 glasses, respectively, for treatment up to 64 hours. The samples used in this study were treated, removed from the furnace, measured and returned to the furnace for further treatment, i.e. the same sample of glass was used throughout the entire study and variations between the glass samples do not exist for this work. With increasing treatment time, there is a scattering effect lifting the infrared spectra in the high frequency end and falling off in effect with decreasing frequency, similar to that discussed earlier for hydroxyl formation. Both of the glasses in the as-received condition had very low hydroxyl and deuteroxyl contents. A complex deuteroxyl band, similar in shape to that of the previously discussed hydroxyl band, can be identified at ≈2690 cm^{-1}. A small amount of hydroxyl formation is observed in Figures 5.17 and 5.18. There is about 3% hydrogen in standard isotopically "pure" deuterium, which results in the formation of the small hydroxyl band observed.

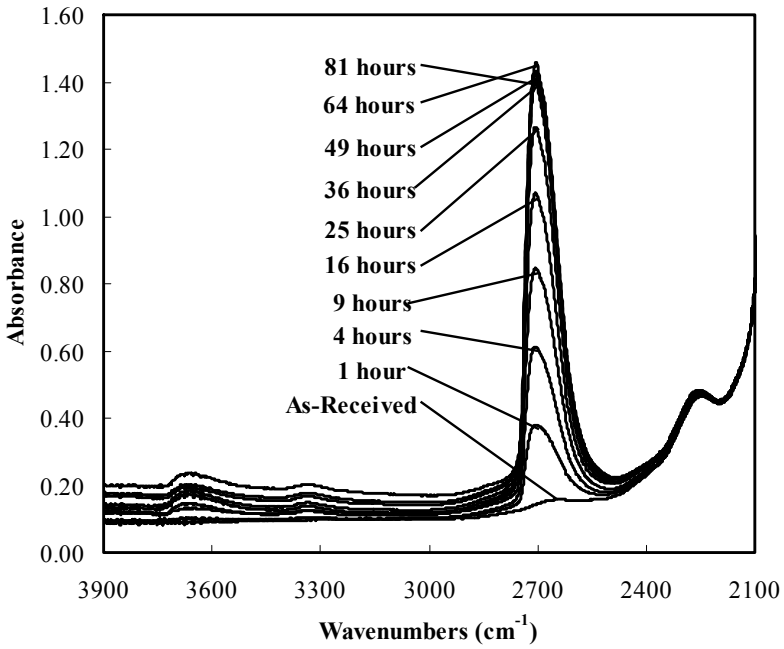

Figure 5.17. Infrared spectra from 2100 cm^{-1} to 3900 cm^{-1} for 6 mol% GeO_2 - 94 mol% SiO_2 glass during progressive deuterium treatment at 800°C for the indicated cumulative treatment time.

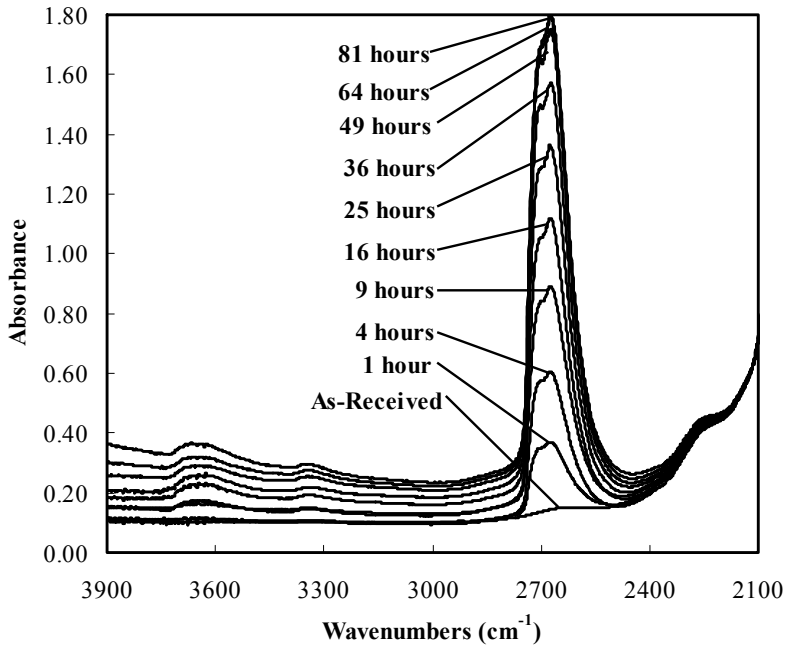

Figure 5.18. Infrared spectra from 2100 cm^{-1} to 3900 cm^{-1} for 14.6 mol% GeO_2 - 85.4 mol% SiO_2 glass during progressive deuterium treatment at 800°C for the indicated cumulative treatment time.

Perhaps the most important conclusion from progressive treatment with deuterium gas can be drawn from evaluation of the peak shape. Comparison of the peak shapes for the progressive hydrogen and deuterium treatments at the same temperature and pressure conditions show that the deuteroxyl band is narrower than the hydroxyl band suggesting that there are, in fact, at least two different species forming and all of the contributing species are not shifting their infrared bands the same amount with deuterium reactions. Small shifts in the band position for deuteroxyl, like hydroxyl, is only affected by the identity of the species on the other side of the oxygen i.e. the nearest neighbor identity.

Closer examination of the region from 2450 to 2850 cm^{-1}, where absorptions due to deuteroxyl species in binary GeO_2-SiO_2 glasses occur,[8,32,33] is shown in Figures 5.19 and 5.20 with background subtraction for each the binary glasses. It is clear that there are at least two different species contributing to the formation of the broad band extending from about 2750 to 2550 cm^{-1} with spectral characteristics of both SiOD and GeOD species. The intensities of the bands for the doped glasses increase in significantly different ways, implying that deuteroxyl formation is dependant on germanium

concentration. The ratio of the two components of the band reverses with increasing germanium concentration, resulting in higher intensity at lower frequency with increasing germanium content, similar to the trends observed for hydroxyl formation.

The maximum band intensities for the 6 mol% GeO_2 - 94 mol% SiO_2 glass and the 14.6 mol% GeO_2-85.4 mol% SiO_2 glass treated at 800°C in hydrogen was determined to occur at 3662 cm^{-1} and 3620 cm^{-1}, respectively. The maximum band intensities for the 6 mol% GeO_2 - 94 mol% SiO_2 glass and the 14.6 mol% GeO_2-85.4 mol% SiO_2 glass treated at 800°C in deuterium was determined to occur at 2704 cm^{-1} and 2675 cm^{-1}, respectively. Figure 5.21 shows the effect of time on the absorbance at 3662 cm^{-1} for treatments in hydrogen, the region of the hydroxyl band most affected by the formation of SiOH species, plotted with the absorbance at 2704 cm^{-1} for treatments in deuterium, the region of the deuteroxyl band most affected by SiOD species. Figure 5.22 shows the effect of time on the absorbance at 3620 cm^{-1} for treatments in hydrogen, the region of the hydroxyl band most affected by the formation of GeOH species, plotted with the absorbance at 2704 cm^{-1} for treatments in deuterium, the region of the deuteroxyl band most affected by GeOD species. The filled points represent the absorbance at the chosen frequency for the 14.6 mol% GeO_2-85.4 mol% SiO_2 glasses and the open points represent absorbance at the chosen frequency for the 6 mol% GeO_2-94 mol% SiO_2 glasses. Figures 5.21 and 5.22 show the difference between progressive hydroxyl and deuteroxyl formation for each of the binary GeO_2-SiO_2 glasses. Figures 5.21 and 5.22 show the systematic increase in intensity in the spectral regions associated with hydroxyl and deuteroxyl species with progressive hydrogen and deuterium treatment at 800°C. The 14.6 mol% GeO_2-85.4 mol% SiO_2 glass treated at 800°C discussed earlier in hydrogen showed a deviation from the observed trends in final hydroxyl concentration for similar treatment at other temperatures. The final hydroxyl content for the 14.6 mol% GeO_2-85.4 mol% SiO_2 glass shows a remarkable correspondence with that of the glass treated in deuterium. The reason given for the observed higher hydroxyl concentration at saturation also applies to the 14.6 mol% GeO_2-85.4 mol% SiO_2 glasses treated in deuterium, significant crystallization and color formation resulted in reflection and scattering effects that may have an influence on the final measured hydroxyl concentration.

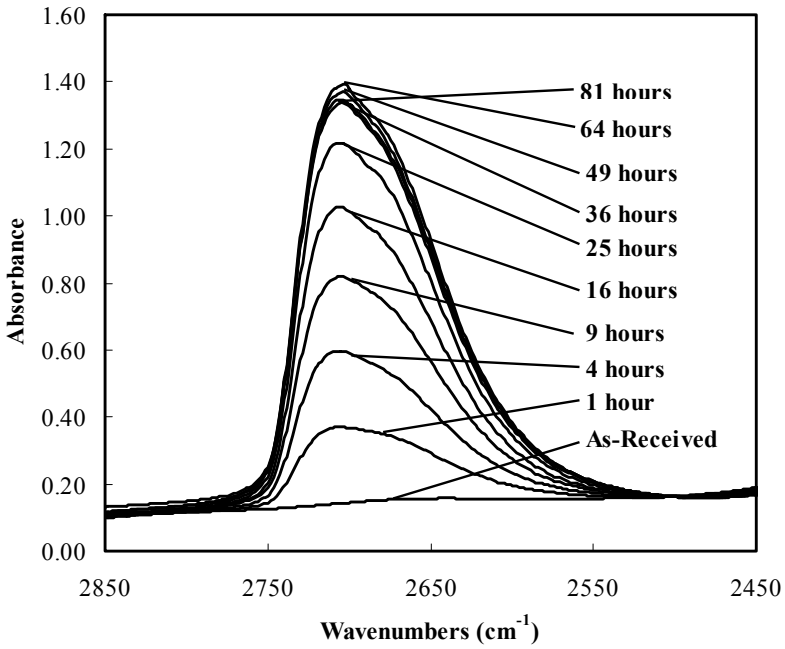

Figure 5.19. Infrared spectra in the deuteroxyl region for 6 mol% GeO_2 - 94 mol% SiO_2 glass during progressive deuterium treatment at 800°C for the indicated cumulative treatment time.

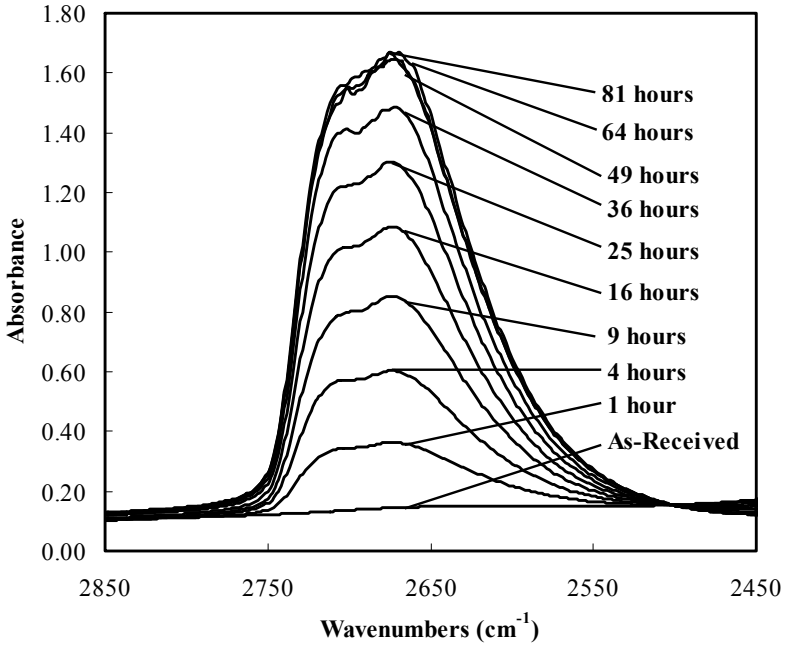

Figure 5.20. Infrared spectra in the deuteroxyl region for 14.6 mol% GeO_2 - 85.4 mol% SiO_2 glass during progressive deuterium treatment at 800°C for the indicated cumulative treatment time.

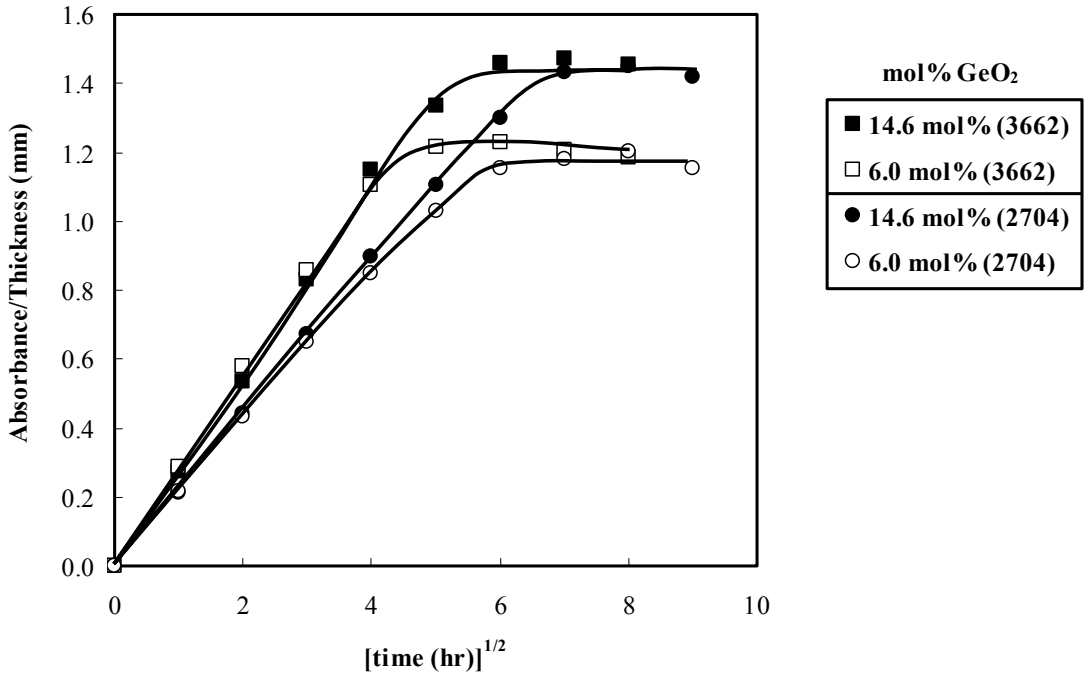

Figure 5.21. The effect of square root time on the absorbance at 3662 cm^{-1} for hydrogen treatment (squares) and 2704 cm^{-1} for deuterium treatment (circles) at 800°C. The filled points represent the intensity for the 14.6 mol% GeO_2-85.4 mol% SiO_2 glasses and the open points represent peak intensity for the 6 mol% GeO_2-94 mol% SiO_2 glasses. Lines are a guide to the eye.

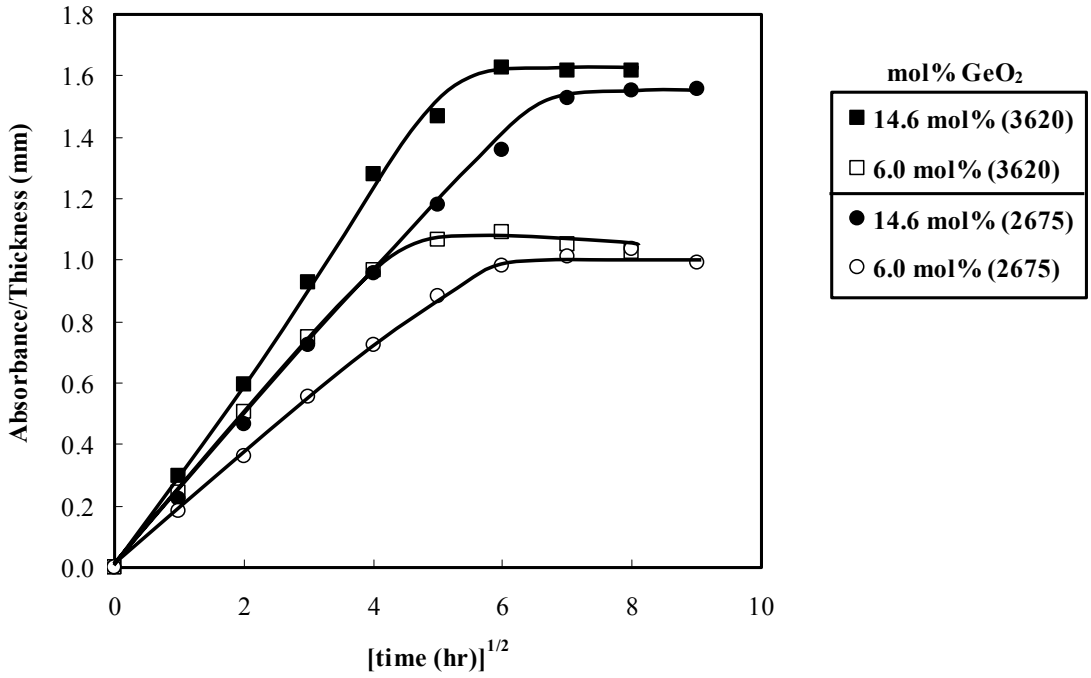

Figure 5.22. The effect of square root time on the absorbance at 3620 cm^{-1} for hydrogen treatment (squares) and 2675 cm^{-1} for deuterium treatment (circles) at 800°C. The filled points represent the intensity for the 14.6 mol% GeO_2-85.4 mol% SiO_2 glasses and the open points represent peak intensity for the 6 mol% GeO_2-94 mol% SiO_2 glasses. Lines are a guide to the eye.

The maximum absorbance indicates the total hydroxyl concentration is smaller in the sample with less germanium, i.e. the total amount of hydroxyl formed during a given treatment is larger for the glass containing more germanium.[h] The rate of deuteroxyl species formation is significantly slower than that of hydroxyl species formation.

It is well known that diffusion of deuterium is slower than hydrogen in pure silica glass[32,33] and these results are consistent with this study. It has been shown that deuterium diffusion is a factor of square root two times slower than hydrogen diffusion in pure silica glass.[34] The factor difference between deuterium and hydrogen diffusion could not be reported with confidence here since there was a minor fluctuation in the temperature control between the hydrogen and deuterium studies.

[h] It should be noted that hydroxyl (deuteroxyl) extinction coefficient is different for each of the binary GeO_2 - SiO_2 glasses and direct comparison of final absorbance values between the glasses must be considered with caution.

The absorption coefficient of OD is about 0.994 that of OH for pure silica,[34] which would manifest itself in only a minor difference in the final height values with similar concentrations of each species present in the glass. The final hydroxyl and corresponding deuteroxyl content for each of the binary GeO_2-SiO_2 glasses shows a remarkable agreement between the hydrogen and deuterium studies. The linear relationship between absorbance and square root of time suggests the expected possibility that deuterium reaction with the binary GeO_2-SiO_2 glasses to form deuteroxyl can also be discussed through application of the tarnishing model.

5.3.7. Treatments in Vacuum and Ambient Air

Each of the as-received binary GeO_2-SiO_2 glasses were treated at 800°C in both vacuum and ambient air to ensure that hydroxyl formation results from the presence of excess hydrogen in the atmosphere. No detectable formation of hydroxyl or hydride species was observed after 100 hours of treatment in vacuum. After 69 hours of treatment in ambient air, infrared spectra showed only minimal hydroxyl formation with no hydride formation.

5.3.8. Dehydroxylation Studies

In a preliminary dehydroxylation study, 0.5 mm thick samples of the binary GeO_2-SiO_2 glasses treated progressively at 600°C for up to 144 hours were vacuum baked at 600°C for extended periods of time to examine the stability of hydroxyl formation. The infrared spectra in the hydroxyl/water region for 6 mol% GeO_2 - 94 mol% SiO_2 glass and the 14.6 mol% GeO_2-85.4 mol% SiO_2 glass after progressive vacuum treatment at 600°C are shown in Figures 5.23 and 5.24, respectively. With progressive dehydroxylation, the peak shape did not change, indicating that both contributing species are removed at the same rate, i.e. the removal of hydroxyl species from the glass is not dependent on nearest neighbor cation identity. This result shows that the species contributing to the broad band extending from about 3750 to 3400 cm^{-1} will vary at the same rate with progressive hydrogen treatment and subsequent removal. There is however a large difference between the rate of formation and removal of hydroxyl species. Removal of hydroxyl species occurs at a much slower rate, since 300

hours in vacuum is a much larger amount of time than that needed to form the hydroxyl. A large fraction of the hydroxyl formed at 600°C appears to be extremely stable suggesting that part of the hydroxyl formation is an irreversible process. The integrated area under the broad band extending from about 3880 to 3430 cm^{-1} can be used to determine the percent of the hydroxyl formed at saturation that is extremely stable and will not be removed with vacuum treatment. The percent of stable hydroxyl formation after 300 hours in vacuum at 600°C for the 6 mol% GeO_2 - 94 mol% SiO_2 glass was approximately 67% while only 53% remained stable for the 14.6 mol% GeO_2-85.4 mol% SiO_2 glass. No detectable amount of hydride was formed during progressive dehydroxylation.

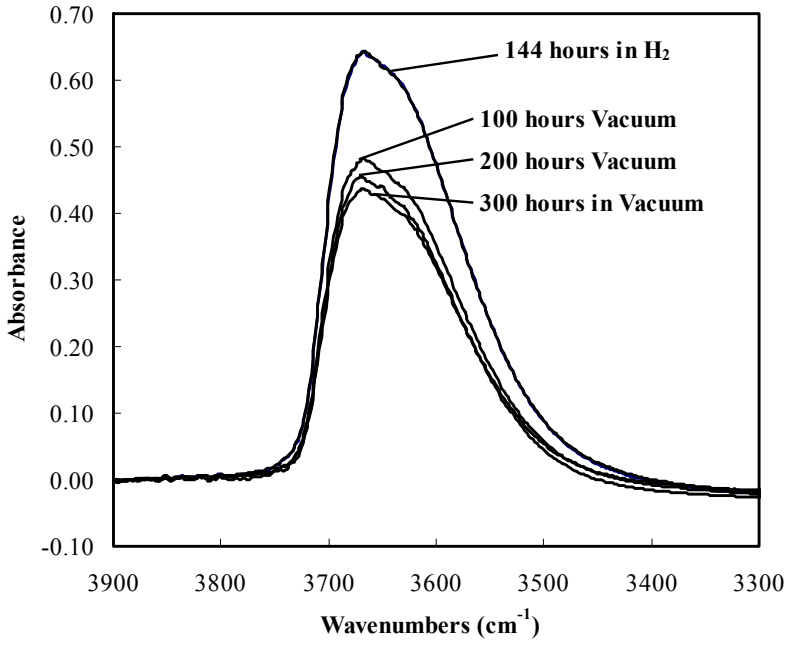

Figure 5.23. Infrared spectra in the hydroxyl/water region for 6 mol% GeO_2 - 94 mol% SiO_2 glass during progressive vacuum treatment at 600°C for the indicated cumulative treatment time.

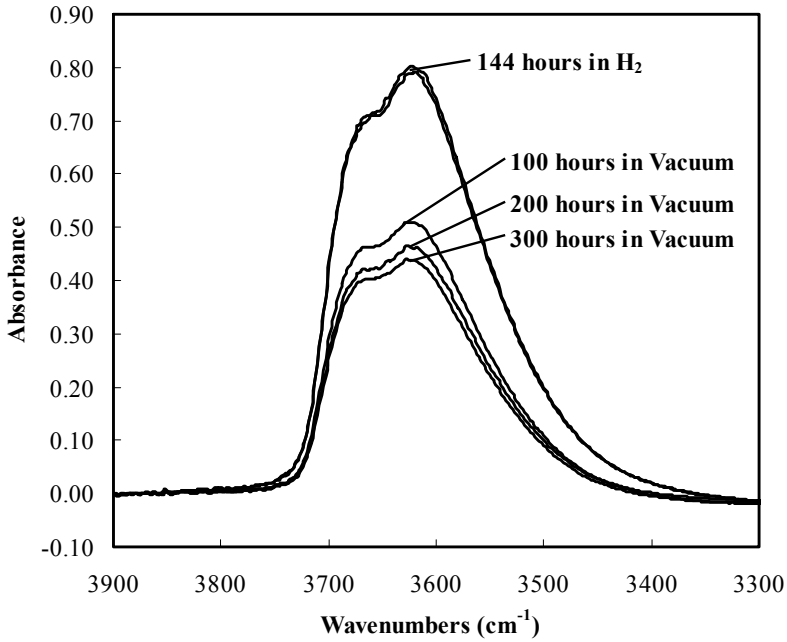

Figure 5.24. Infrared spectra in the hydroxyl/water region for 14.6 mol% GeO_2 - 85.4 mol% SiO_2 glass during progressive vacuum treatment at 600°C for the indicated cumulative treatment time.

5.4. Discussion

It should be noted that all binary GeO_2-SiO_2 glass samples treated in hydrogen at temperatures between 500°C and 800°C showed color formation and crystal formation, as well as hydroxyl formation. The color formation and corresponding crystal formation will be discussed in detail in later chapters. Color formation and crystallization became more significant with increasing treatment temperature and increasing germanium content, and the effect is apparent in the amount of scattering loss in the infrared spectra. The fact that color formation and crystallization do not occur to the same extent for all samples makes interpretation and direct comparison of acquired data more complex, however with background subtraction and separation of such effects many qualitative conclusions about hydroxyl formation are presented.

5.4.1. Qualitative Observations Consistent with Other Related Studies

Hydroxyl formation in binary GeO_2-SiO_2 glasses has been observed in a number of other studies.[1-4,17,19] Although results of previous hydrogen treatment studies cannot

be compared directly with those of the present study because of the use of fibers and graded concentration profiles, the trends with progressive treatment in hydrogen found here are similar to those of the earlier studies. A likely cause of differences in results between studies is that the GeO_2 content, sample geometry and treatment conditions are not consistent between various studies.

Although there are inconsistencies among treatment conditions, a few major results are constant for all studies. It is well known that binary GeO_2-SiO_2 glasses react with hydrogen at a much faster rate then pure SiO_2 glasses, with a significantly more complex hydroxyl environment involving characteristics of both GeOH and SiOH species. This observation is consistent throughout all published research on the topic,[1,2] including this study. The changes in shape and position of the hydroxyl band with increasing germanium content is also fairly consistent.[1,4] Plotnichenko et al.[19] observed that the shape of the hydroxyl band in binary GeO_2-SiO_2 made from the VAD technique changes with increasing germanium content. The results presented here agree well with this observation. This change in band shape was not recognized in binary GeO_2-SiO_2 glasses made by the MCVD method or glasses made by melting a mixture of GeO_2 and SiO_2 powder. In fact, Plotnichenko[19] shows that the change in band shape with germanium content is only present in glasses prepared by the VAD method. The observation that the shape of the hydroxyl band does not change with progressive hydrogen treatment, but the intensity of the band increases with treatment time has also been reported.[1] Shurman and Tomozawa[17] have also shown that the shape of the hydroxyl band does not change with progressive treatment in water at elevated temperatures. Growth of the band without shape change implies that all hydroxyl species contributing to the band are forming at the same rate i.e. generation of SiOH and GeOH species occur at the same rate during treatment in a hydrogen atmosphere. This observation suggests that reaction is occurring at the same kind of site, and if GeOH and SiOH species are forming, then the hydrogen must be reacting with the Ge-O-Si bond, breaking the bond at the Ge-O bond. Without the formation of hydride species, however, there must be another component to the reaction mechanism or a subsequent reaction that eliminates hydride formation. Perhaps the presence of defect sites in the glass has an influence on the hydroxyl formation reaction. Another important observation that is

consistent with this work and others[2,3] is that the growth in intensity of the hydroxyl band, and therefore the concentration of hydroxyl species formed, increases with increasing germanium content.

Contrary to experimental observation of hydride formation in UV-irradiated, hydrogen impregnated binary GeO_2-SiO_2 glasses, thermally induced H-bearing species showed no detectable formation of either GeH or SiH. These results are somewhat consistent with Zeng et al.[4] who observe larger values of the OH/GeH ratio in the heat treated glasses as compared to the corresponding UV-irradiated glasses. UV-irradiated glasses also show a change in band shape with increasing exposure to UV-irradiation as the absorption increase due to GeOH happens more rapidly than for SiOH, indicating that the generation of both groups occurs at different rates during exposure.[9] This effect is obviously not observed in thermally induced hydroxyl species as the band shape does not change with time at temperature, suggesting that SiOH and GeOH species are forming at the same rate.

5.4.2. Application of the Tarnishing Model

Spectral data can be used to model hydrogen diffusion kinetics with application of the tarnishing model.[23,24,26,35,36] This model was originally derived to describe the oxidation or tarnishing of metals.[37,38] In this model, gas diffuses into the free volume of the glass through the exposed surfaces. The gas then reacts with sites in the glass, creating a reacted layer front that moves toward the center of the thin glass plate from each of the exposed surfaces. Further reaction within the material is limited by the diffusion of the gas through the reacted surface layer. This model assumes that the rate of reaction is controlled by the diffusion rate of hydrogen to the reaction site. The equation that describes the tarnishing model is:

$$\left(\frac{C - C_i}{C_f - C_i}\right) = \sqrt{\frac{8KPt}{L^2 C_x}} \tag{5.4}$$

where the term on the left side of Equation 5.4 represents the fraction of reaction, i.e. the change in the concentration of the species being monitored, K is the gas permeability, P

is the pressure of the reacting gas, t is time, L is the thickness of the substrate and C_x is the concentration of available reaction sites within the substrate material. This formation mechanism manifests itself in a linear increase in fraction of reaction when absorbance, i.e. concentration of reactant species, is plotted as a function of square root time. When the moving reacted layer fronts from either side of the exposed surface of the thin plate meet in the middle of the plate, reaction sites are no longer available, the concentration of the reaction product should be constant throughout the thickness of the sample and equilibrium saturation is reached. For this particular application, saturation will occur when the hydroxyl concentration is constant throughout the thickness of the sample, the infrared band will no longer grow with further treatment and the absorbance as a function of square root time will level off at a constant value. The presence of a fixed number of reaction sites implies that the reaction can only occur until all of those sites are eliminated, i.e. a finite concentration of hydroxyl will be formed regardless of reaction temperature.[25] The concept of a fixed number of reaction sites for hydroxyl formation was also suggested by Mochizuki et al.,[8] who claimed that the number of reaction sites is, in fact, associated with defect centers in the glass and, furthermore, the defects themselves are associated with the presence of germanium in the glass.

In this study, all of the as-received glasses had extremely low hydroxyl contents, i.e. lower than the resolvable detection limits of the instrument, therefore simple evaluation of absolute absorbance is equal to the fraction of reaction. The growth of the hydroxyl band shows a remarkable fit to the tarnishing model. Hydroxyl formation occurs from each of the exposed surfaces with a reacted layer front moving toward the center of the sample (Figure 5.11 and 5.12). For each of the given experiments, temperature (in the permeability term), pressure, and thickness were held constant and time was the only variable. The results of this study clearly show that hydrogen reactions with binary GeO_2-SiO_2 glass to form hydroxyl species are diffusion-controlled reactions involving diffusion of hydrogen to the reaction sites followed by formation of a reaction layer front at the exposed surfaces.

To the author's knowledge, the tarnishing model has not previously been used to describe the formation of hydroxyl species in binary GeO_2-SiO_2 glasses. The only study with which this study can be compared was performed at significantly shorter treatment

times, resulting in extremely small reported absorbance values.[1] Awazu et al. reported that the infrared absorption of T-OH groups forms simultaneously with the optical absorption band at 5.14 eV (242 nm) in binary GeO_2-SiO_2 glasses during treatment under a hydrogen atmosphere, after stating that the 5.14 eV peak growth does not obey the $t^{1/2}$ rule. With further analysis, Awazu et al.[1] claim that there is a linear relationship between hydroxyl formation and the absorption coefficient for the 5.14 eV band, suggesting that the structural imperfection responsible for the 5.14 eV band forms simultaneously with TOH groups, at 400°C, 500°C, 550°C and 600°C. In summary, Awazu and co-workers imply that the formation of TOH species in their study does not follow the $t^{1/2}$ dependence and therefore hydroxyl formation is not a diffusion-controlled process, but a reaction-controlled process. Results presented in this study, however, indicate that hydroxyl formation at the lowest treatment temperatures (500°C and 600°C) show evidence of an incubation time, i.e. period of time during which the kinetics are adjusting, before the reaction occurs with the square root of time. The presence of an incubation period shows that hydroxyl formation does not occur the instant that the sample is exposed to hydrogen at elevated temperatures, implying that the reaction itself lags behind the supply of hydrogen to the reaction sites and hydroxyl formation is a reaction-controlled process. Since the treatment times used in the study presented by Awazu et al. were within the treatment time for the observed incubation period of the results presented here, it is not possible to directly compare the short term and long term reaction results of the two studies, simply because the effects observed for extended treatment times are inconsistent with those for short treatment times. In fact, the results for this study could be consistent with those from Awazu et al. since an incubation period suggests a reaction-controlled process. The square root of time dependence after the incubation period means that once the reaction begins to occur, supply of the reactant, hydrogen, is a factor in hydroxyl formation. This square root of time dependence with extended treatment does not prove that hydroxyl formation is a diffusion-controlled process; it could simply mean that some specific hydrogen concentration must be achieved before the reaction can occur.

Progressive hydrogen treatments of binary GeO_2-SiO_2 glasses at high temperatures (700°C and 800°C) clearly indicate a diffusion-controlled process. Without

the presence of an incubation period, the hydroxyl formation reaction shows an immediate square root of time dependence that is maintained until equilibrium saturation is achieved. Sectioning experiments performed on the 14.6 mol% GeO_2-85.4 mol% SiO_2 glass treated for only 2 hours, where treatment was stopped before equilibrium saturation was achieved, at 800°C and 700 Torr of hydrogen demonstrate the use of infrared spectroscopy to prove the formation of a reaction layer front at the exposed surfaces of the sample. The tarnishing model can be applied to hydrogen reactions with binary GeO_2-SiO_2 glasses at 700°C and 800°C, illustrating that hydroxyl formation is a diffusion-controlled process.

5.5. Conclusions

Treatment of binary GeO_2-SiO_2 glasses under a hydrogen atmosphere (pH_2 = 93 kPa) at elevated temperatures results in the extensive formation of hydroxyl species with little to no hydride formation. Hydrogen reactions in binary GeO_2-SiO_2 glasses resulting in the formation of hydroxyl species are a function of time, temperature and germanium content. Induced hydroxyl formation increases with increasing GeO_2 concentration. The rate of hydroxyl formation increases with increasing temperature. Hydroxyl formation increases with time until saturation, at which point hydroxyl concentration is uniform throughout the thickness of the sample.

5.6. References

1. K. Awazu, H. Kawazoe, and M. Yamane, "Simultaneous Generation of Optical Absorption Bands at 5.14 and 0.452 eV in 9 SiO_2:GeO_2 Glasses Heated under an H_2 Atmosphere," *J. Appl. Phys.,* **68** [6] 2713-8 (1990).

2. H. Itoh, Y. Ohmori, and M. Nakahara, "Germanium-Dopant Effect on Hydroxyl Loss Increase in Optical Fibers," *J. Lightwave Technol.,* **LT-4** [2] 116-20 (1986).

3. A.V. Belov, E.M. Dianov, P.N. Lebedev, A.N. Gur'yanov, and V.F. Khopin, "Hydroxyl Group Absorption in Germanium Oxide-Doped Fused Silica Fibers," *Electron. Lett.,* **18** [19] 836-7 (1982).

4. Q. Zeng, J.F. Stebbins, A.D. Heaney, and T. Erdogan, "Hydrogen Speciation in Hydrogen-Loaded, Germania-Doped Silica Glass: A Combined NMR and FTIR Study of the Effects of UV Irradiation and Heat Treatment," *J. Non-Cryst. Solids,* **258** [1-3] 78-91 (1999).

5. R.M. Atkins, P.J. Lemaire, T. Erdogan, and V. Mizrahi, "Mechanisms of Enhanced UV Photosensitivity Via Hydrogen Loading in Germanosilicate Glasses," *Electron. Lett.,* **29** [14] 1234-5 (1993).

6. P.J. Lemaire, R.M. Atkins, V. Mizrahi, and W.A. Reed, "High Pressure Hydrogen Loading as a Technique for Achieving Ultrahigh UV Photosensitivity and Thermal Sensitivity in Germania Doped Optical Fibers," *Electron. Lett.,* **29** [13] 1191-3 (1993).

7. K. Kawamura, Y. Kameshima, H. Hosono, and H. Kawazoe, "Proton-Implantation-Induced Optical Phenomena in SiO_2:GeO_2 Glasses: Formation of Photosensitive Defects and Nanometer Sized Ge Crystals," *Mater. Sci. Eng., B,* **54** [1-2] 18-23 (1998).

8. K. Mochizuki, Y. Namihira, and M. Kuwazuru, "Absorption Loss in Optical Fibers Due to Hydrogen," *Electron. Lett.,* **20** [13] 550-2 (1984).

9. F.M. Araujo, E. Joanni, M.B. Marques, and O.G. Okhotnikov, "Dynamics of Infrared Absorption Caused by Hydroxyl Groups and Its Effect on Refractive Index Evolution in Ultraviolet Exposed Hydrogen Loaded GeO_2-Doped Fibers," *Appl. Phys. Lett.,* **72** [24] 3109-11 (1998).

10. H. Itoh, M. Shimizu, Y. Ohmori, and M. Nakamura, "Hydrogen Diffusion and Defect Center in Gamma-Irradiated GeO_2-Doped Optical Fiber," *J. Non-Cryst. Solids,* **70** [3] 439-43 (1985).

11. A. Tomita and P.J. Lemaire, "Hydrogen-Induced Loss Increases in Germanium-Doped Single-Mode Optical Fibers: Long-Term Predictions," *Electron. Lett.,* **21** [2] 71-2 (1985).

12. K.O. Hill, Y. Fujii, D.C. Johnson, and B.S. Kawasaki, "Photosensitivity in Optical Fiber Waveguides: Application to Reflection Filter Fabrication," *Appl. Phys. Lett.,* **32** [10] 647-9 (1978).

13. C. Dalle, P. Cordier, C. Depecker, P. Niay, P. Bernage, and M. Douay, "Growth Kinetics and Thermal Stability of UV-Induced H-Bearing Species in Hydrogen Loaded Germanosilicate Glasses," *OSA Trends Opt. Photonics Ser.,* **33,** 346-8 (2000).

14. P. Cordier, C. Dalle, C. Depecker, P. Bernage, M. Douay, P. Niay, J.-F. Bayon, and L. Dong, "UV-Induced Reaction of H_2 with Germanosilicate and Aluminosilicate Glasses," *J. Non-Cryst. Solids,* **224** [3] 277-82 (1998).

15. K.M. Davis and M. Tomozawa, "An Infrared Spectroscopic Study of Water-Related Species in Silica Glasses," *J. Non-Cryst. Solids,* **201** [3] 177-98 (1996).

16. K. Awazu, "Comments on 'Thermal and Photo-Initiated Reactions of H_2 with Germanosilicate Optical Fibers'," *J. Non-Cryst. Solids,* **201** [3] 267-71 (1996).

17. M.K. Schurman and M. Tomozawa, "Equilibrium Oxygen Vacancy Concentrations and Oxidant Diffusion in Germania, Silica, and Germania-Silica Glasses," *J. Non-Cryst. Solids,* **202** [1-2] 93-106 (1996).

18. A.J. Cohen and H.L. Smith, "Ultraviolet and Infrared Absorption of Fused Germania," *Phys. Chem. Solids,* **7,** 301-6 (1958).

19. V.G. Plotnichenko, V.O. Sokolov, and E.M. Dianov, "Hydroxyl Groups in Germanosilicate Glasses," *J. Non-Cryst. Solids,* **278** [1-3] 85-98 (2000).

20. B.I. Greene, D.M. Krol, S.G. Kosinski, P.J. Lemaire, and P.N. Saeta, "Thermal and Photo-Initiated Reactions of H_2 with Germanosilicate Optical Fibers," *J. Non-Cryst. Solids,* **168** [1-2] 195-9 (1994).

21. E. Libowitzky and G.R. Rossman, "An IR Absorption Calibration for Water in Minerals," *Am. Mineral.,* **82** [11-12] 1111-5 (1997).

22. J.P. Williams, Y.S. Su, W.R. Strzegowski, B.L. Butler, H.L. Hoover, and V.O. Altemose, "Direct Determination of Water in Glass," *Am. Ceram. Soc. Bull.,* **55** [5] 524-7 (1976).

23. J.E. Shelby, "Reaction of Hydrogen with Hydroxyl-Free Vitreous Silica," *J. Appl. Phys.,* **51** [5] 2589-93 (1980).

24. J.E. Shelby, "Reaction of Hydrogen with Optical Defects in Glasses," *J. Am. Ceram. Soc.,* **67** [5] C93-4 (1984).

25. J.E. Shelby, "Protonic Species in Vitreous Silica," *J. Non-Cryst. Solids,* **179,** 138-47 (1994).

26. C.M. Shaw and J.E. Shelby, "Hydrogen Reactivity as a Structural Probe for Glasses," *Phys. Chem. Glasses,* **34** [1] 35-41 (1993).

27. K.M. Davis and M. Tomozawa, "Water Diffusion into Silica Glass: Structural Changes in Silica Glass and Their Effect on Water Solubility and Diffusivity," *J. Non-Cryst. Solids,* **185** [3] 203-20 (1995).

28. A. Agarwal, K.M. Davis, and M. Tomozawa, "A Simple IR Spectroscopic Method for Determining Fictive Temperature of Silica Glasses," *J. Non-Cryst. Solids,* **185** [1,2] 191-8 (1995).

29. G.H. Sigel, Jr., "Optical Absorption of Glasses," pp. 5-89 in Treatise on Materials Science and Technology, Vol. 12. Edited by M. Tomozawa and R. H. Doremus. Academic Press, New York, 1977.

30. J.E. Shelby and J.C. Lapp, "Helium and Deuterium Migration in Alkali Silicate Glasses," *Phys. Chem. Glasses,* **34** [6] 227-31 (1993).

31. J.E. Shelby, "Helium, Deuterium, and Neon Migration in a Common Borosilicate Glass," *J. Appl. Phys.,* **45** [5] 2146-9 (1974).

32. J.E. Shelby, "Molecular Diffusion and Solubility of Hydrogen Isotopes in Vitreous Silica," *J. Appl. Phys.,* **48** [8] 3387-94 (1977).

33. J.E. Shelby, P.L. Mattern, and D.K. Ottesen, "Radiation-Induced Isotope Exchange in Vitreous Silica," *J. Appl. Phys.,* **50** [8] 5533-5 (1979).

34. J.E. Shelby, "Quantitative Determination of the Deuteroxyl Content of Vitreous Silica," *J. Am. Ceram. Soc.,* **70** [1] C/9-10 (1987).

35. J.E. Shelby and J. Vitko, Jr., "Hydrogen Transport in a Machinable Glass-Ceramic," *J. Non-Cryst. Solids,* **45** [1] 83-92 (1981).

36. J.E. Shelby and J. Vitko, Jr., "The Reduction of Iron in Soda-Lime-Silicate Glasses by Reaction with Hydrogen," *J. Non-Cryst. Solids,* **53** [1-2] 155-63 (1982).

37. J. Crank, *The Mathematics of Diffusion,* 2nd ed.*;* pp. 37,305. Oxford University Press, New York, 1975.

38. F. Booth, "A Note on the Theory of Surface Diffusion Reactions," *Trans. Faraday Soc.,* **44,** 796-801 (1948).

CHAPTER 6: HYDROGEN-INDUCED COLOR FORMATION IN BINARY GEO_2-SIO_2 GLASSES

Abstract

Treatment of 100 mol% SiO_2, 6 mol% GeO_2-94 mol% SiO_2 and 14.6 mol% GeO_2-85.4 mol% SiO_2 glasses was monitored using optical spectrometry as a function of time under a H_2 atmosphere (pH_2 = 93 kPa) at 500ºC, 600ºC, 700ºC and 800ºC. Binary GeO_2-SiO_2 glasses heat treated in the presence of hydrogen react to form reduced germanium species in the glass. This reaction is associated with an intense change in color of the glass from colorless to brown. A detailed analysis of the changes in the optical spectra resulting from hydrogen reactions is provided.

Hydrogen reactions with binary GeO_2-SiO_2 glasses are a function of time, temperature and germanium content. The effect of GeO_2 concentration on color formation is evident, as induced color formation increases with increasing GeO_2 concentration. The rate of color formation increases with increasing temperature for both binary GeO_2-SiO_2 glasses. Color formation is confined to the exposed surface of each sample. Color concentration is not uniform across the surface of the sample, but varies systematically with areas of non-uniform concentration in the samples.

6.1. Introduction

The study of defects and reactions with hydrogen are the most active areas of research involving binary GeO_2-SiO_2 glasses. A majority of the published research on binary GeO_2-SiO_2 glasses has focused on the distinct, intrinsic absorption band centered at approximately 5.14 eV (242nm), with a tail that extends into the visible region of the spectrum. This intense absorption band was first observed in pure SiO_2 glasses obtained by the fusion of quartz in pioneering work by Garino-Canina[1] and Cohen.[2] Garino-Canina[3,4] studied the effect of melt atmosphere on the optical absorption and photoluminescence of fused quartz glass and observed removal of the band at 242 nm and the luminescence when the glass was melted under oxidizing conditions, and reintroduction of the 242 nm band and luminescence when the glass was melted at much higher temperatures under reducing conditions. Garino-Canina[5] later proposed that the 242 nm impurity band in fused silica is due to germanium, since the band intensity varied with additions of varied amounts of germanium. Cohen[2] confirmed the conclusion set forth by Garino-Canina[5] that the 242 nm band results from the presence of germanium impurities in the reduced state in the fused quartz glass. More specifically, Cohen[6] suggests that Ge(II) (Ge^{+2}) is the impurity responsible for the band.

A comprehensive study of the optical properties of pure GeO_2 was proposed to determine whether an absorption band in the region of 242 nm was present. Cohen and Smith[7] were the first to demonstrate photobleaching of an intense absorption band centered at 244.5 nm in pure fused GeO_2, as well as a detailed description of the general features of the optical absorption spectra. It was suggested that the intense band in the as-melted glass results from the presence of reduced germanium species in the glass, more specifically Ge^{+2}, which is the same reduced germanium species responsible for the band at 242 nm in fused SiO_2. Upon exposure to ultraviolet light or x-rays, the band intensity decreases, accompanied by an increase in absorbance below 220 nm, which is in the vacuum ultraviolet region of the spectrum. No further suggestion was offered as to the origin of the photo-induced band in the vacuum ultraviolet. It was also mentioned that no color center bands were produced upon X-ray treatment.

In order to justify the assumption that the band at ~245 nm in pure germania results from the presence of an oxygen vacancy or complex of vacancies Jackson et al.[8]

studied the effect of fusion temperature (T_Φ), oxygen partial pressure during melting and the quenching rate from T_Φ on the optical absorption. The activation energy for the formation of the defect in GeO_2 glasses was reported based on the assumption that absorption could be used to measure the diffusion of oxygen into the melt. Although the data were reported to be inadequate to suggest a specific redox equilibrium reaction in GeO_{2-x} glasses because of the large experimental error, a few important conclusions were drawn. The T_Φ, atmosphere[i] P_{O_2} and the quenching rate dependencies of the 245 nm band are consistent with oxygen vacancies or complex vacancies. Also the P_{O_2} dependence at T_Φ and cooling rate indicates that the defect may be more complex than a single neutral oxygen vacancy, suggesting the possibility of dioxygen or trioxygen vacancies.

The inherent absorption band at 5.14 eV (242nm), with a tail that extends into the visible region, is not only inherent to glasses made from melting of powders, it is also found in glasses prepared using the vapor phase axial deposition (VAD) method, i.e. glass preforms or fibers. The discovery by Hill et al.[9] of the unique refractive index response of binary GeO_2-SiO_2 glasses, made by the VAD method, to ultraviolet (UV) light exposure, spurred a significant interest in the mechanism behind the response. The development of a transverse holographic method[10] to produce periodic refractive index modulation led to the formation of Bragg gratings in binary GeO_2-SiO_2 glass fibers. The discovery of hydrogen enhancement[11] of this effect encouraged a renewed interest in the defects responsible for the intense absorption centered at approximately 242 nm in binary GeO_2-SiO_2 glasses because the responsible defects are considered to be closely related to novel nonlinear optical properties.

Tomita et al.[12] observed hydrogen-induced loss phenomena in conventional GeO_2-doped single mode fibers that were exposed to hydrogen partial pressures of $0.01 < P_{H2} < 1.0$ atm at temperatures between 75 and 250°C. In addition to the loss increase due to molecular hydrogen and the formation of hydroxyl species, a spectrally broad background loss increase was observed. The rate of background loss increase was initially high, but then gradually diminished with losses approaching an asymptotic limit.

---

[i] Jackson et al. suggests caution when melting GeO_2 powder under temperatures exceeding 1650°C or extremely low pressure, i.e. because reducing atmosphere, since this led to the reduction of GeO_2 to Ge metal which formed a low melting eutectic with the platinum crucible subsequently destroying the crucible.

The loss increases were not reversible in that removal of the hydrogen atmosphere did not result in any reduction in absorbance. Hydroxyl growth kinetics exhibited similar behavior. Tomita suggests that the diminishing rates of background loss increase and the lack of reversibility indicates that the hydrogen reacts with defects in the glass structure, further suggesting that the concentration of unreacted defects decreases as the reaction proceeds.

The optical absorption band at ~242 nm in binary GeO_2-SiO_2 glasses was also observed by Kohketsu et al.,[13] who examined the effect of sintering atmosphere on the intensity of the band using UV-Vis spectroscopy and photoluminescence. Glasses prepared under reducing conditions exhibited in a very strong absorption band at 242 nm along with a weak absorption band at 330 nm. Glasses prepared in a helium atmosphere also exhibit a strong band at 242 nm, with no significant absorption at 330 nm. In contrast to this behavior, glasses prepared with oxygen in the sintering atmosphere show only a very weak absorption at 242 nm, with no evidence of a band at 330 nm. Kohketsu et al.[13] report the same conclusion as Cohen,[6] suggesting that the defect responsible for the optical absorption band at 242 nm can be attributed to the presence of reduced species of germanium, more specifically Ge^{+2}, and confirming the band assignment with photoluminescence results.

Awazu and co-workers[14] reported that the optical absorption band at 5.14 eV (242 nm) in binary GeO_2-SiO_2 glasses forms simultaneously with the infrared absorption of TOH[j] groups during annealing in an atmosphere of hydrogen at 760 Torr (pH_2 = 101 kPa) at temperatures ranging from 400 to 700ºC. Their study involved treatment of 10 mol% GeO_2-90 mol% SiO_2 glass plates cut from preform rods produced by vapor phase axial deposition. The glass plates had a parabolic shaped graded index where the maximum concentration of GeO_2 was along the central axis. With progressive hydrogen treatment at 600ºC, the absorption band detected in the as-received samples at 242 nm was reported to grow, becoming off scale for their measurment, accompanied by the appearance of very weak bands at longer wavelengths, i.e. 3.82 eV (325 nm) and 2.70 eV (460 nm), and

[j] It is common notation to designated all hydroxyl species in binary GeO_2-SiO_2 glasses as TOH, where T can represent either Ge or Si. This notation will be used throughout this thesis.

a rise in absorbance at 6.22 eV (200 nm). The authors further state that, upon annealing at 700ºC, induced absorption bands in the VUV region and at 5.14 eV (242 nm) are so intense that the apparent cutoff wavelength is shifted to 4.1 eV (303 nm). For treatments at 500ºC, the authors claim to observe the induced absorption of the 242 nm peak using a 0.5 mm thick sample and state that the peak growth does not obey the $t^{1/2}$ rule and, therefore, growth of the 242 nm band is not a result of a diffusion-controlled process, but reaction-controlled process. Although there is no direct mention of hydrogen-induced color formation in the samples, it is implied that there was at least a slight change in optical appearance as there is mention of tail from the band at around 242 nm extending into the visible region of the spectrum, implying a faint tan to brown color formation.

Hosono and co-workers[15] were the first to set forth the concept that the absorption band at ~5 eV (249 nm) is composed of two types of neutral oxygen vacancies. They proposed that the band at 5.06 eV (246 nm) is due to neutral oxygen monovacancies (NOMV) coordinated by two Ge ions (≡Ge-Ge≡), with a second component existing at 5.16 eV (241 nm) due to Ge^{+2} ions coordinated by two oxygens and two lone pair electrons, labeled a neutral oxygen divacancy (NODV). Band assignments were supported by electron paramagnetic resonance and photoluminescence measurements and experiments based on irradiation with UV light. The peak at 5.06 eV (246 nm) is bleached when illuminated with UV light, accompanied by formation of GeE' centers, determined by electron paramagnetic resonance (EPR) measurements. The band at 5.16 eV (241 nm) is not bleached by illumination with 5 eV (249 nm) light and, since no changes were observed in the photoluminescence spectra, the defect responsible for the 5.16 eV band is considered to be the sole source of the luminescence bands at 3.2 eV (388 nm) and 4.3 eV (289 nm).

Renewed interest in the defects responsible for the 5 eV band based on the suggestion that they are closely related to novel nonlinear optical properties spurred research to clarify changes in concentrations of the contributing defects with treatment in hydrogen. Hosono et al.[16] studied the heat treatment of 5.5 mol% GeO_2-94.5 mol% SiO_2 glass plates cut from preform rods produced by vapor phase axial deposition and subsequently treated in a flow of hydrogen gas (200 mL/min) at 500°C. The authors mention that the germanium concentration was not uniform throughout the rod. The

intensity of the 5 eV band as a function of hydrogen treatment time at 500ºC was monitored for 0.17 and 0.50 mm thick samples. It was determined that intensity of the 242 nm band increased almost linearly with time during an initial stage, then approached a saturation level. Sectioning experiments performed on 0.5 mm thick samples treated in hydrogen showed that the intensity of the 5 eV band decreases linearly with decreasing thickness. The authors suggest that these results indicate that the responsible process is not controlled by diffusion of hydrogen, but by chemical reaction. At the end of the paper, the authors mention that treatment of binary GeO_2-SiO_2 glasses at temperatures greater than 800ºC resulted in an induced brown coloring which they attribute to the formation of germanium particles. Unfortunately, the optical absorption spectra of samples treated at temperatures other than 500ºC were not presented. The authors further state that hydrogen treatment at temperatures less than 300ºC gave no change in optical properties. Honoso et al.[16] concluded that hydrogen treatment temperatures in the range 400 to 700ºC were appropriate for enhancement of UV-bleachable defects.

It is now generally agreed[15-19] that the absorption band at approximately 242 nm is a convolution of two separate bands resulting from two types of oxygen deficient defects;[19] the neutral oxygen monovacancy (Ge-NOMV; ≡Ge-Ge≡ or ≡Ge-Si≡) at 5.06 eV (246 nm) and the neutral oxygen divacancy (Ge-NODV; Ge^{+2} with a lone pair of electrons) at 5.14 eV (242 nm), also known as germanium lone pair center (GLPC, GeO defect).[17] The Ge-NOMV defect is easily bleached by irradiation with a UV laser or lamp and converted to GeE' centers.[19] The response of the NOMV defect is said to be photobleachable, i.e. when illuminated with a 5 eV light, it is converted into a GeE' center, resulting in an absorption band in the vacuum UV region of the spectrum. The NODV or GLPC, with a lone pair electron occupying the uppermost level, emits an intense blue luminescence at 3.2 eV and 4.3 eV, but does not change chemically with UV illumination.[15] This band assignment is well established using many different characterization techniques and experimental observations including photoluminescence[13-15,20] and EPR.[14,15,17,18,21] There is, however, some controversy over the ability to bleach the NODV defect with exposure to UV light. Contrary to previous observation, Awazu et al.[17] proposed that both NOMV and NODV are reduced with illumination, and that there is a one-to-one correlation between the reduction of GLPC's

(NODV) and the generation GeE' centers resulting from reaction with hydrogen molecules in the glass. While discussion of the inconsistencies in UV irradiation of binary GeO_2-SiO_2 glasses is outside the scope of this paper, a few of the reaction mechanisms proposed by researchers in the field correlate well with the results of this study.

One of the more interesting results from the study by Awazu et al.[17] was the discovery of reduction of the 242 nm band with treatment in an oxygen atmosphere at 1000°C. The study involved treatment of a 10 GeO_2 – 90 SiO_2 glass in an oxygen atmosphere of undetermined partial pressure, for up to twelve days at 1000°C. Awazu et al. observed almost complete reduction of the 242 nm band, as well as a decrease in the tail that extends into the UV from VUV. One important observation that is not explicitly stated by Awazu et al.[17] is that the band decreases without any major change in shape, indicating that both NODV and NOMV centers are reacting with the oxygen and subsequently being eliminated at the same rate. The decrease in the intensity of the 242 nm band with oxygen treatment supports the contention that the band results from the presence of oxygen deficient centers in the glass.

The recent hydrogen-induced color observation briefly mentioned by Hosono et al.[16] is not the only mention of color formation in binary GeO_2-SiO_2 glasses. Another mention of an intense color development was presented in a study of ion implantation of 1.5 MeV protons into binary GeO_2-SiO_2 glass substrates prepared by VAD. Kawamura et al.[22] acknowledge the presence of the 5 eV (249 nm) band, comprised of neutral oxygen monovacancies (NOMV) coordinated with two Ge^{4+} ions and Ge^{2+} (with a lone pair) coordinated with two oxygens, in the as-received binary GeO_2-SiO_2 glasses, and show that proton implantation drastically enhances the concentration of both NOMV and NODV defects in the glass. With an increase in fluence, a remarkable increase in optical absorption intensity in the VUV region was observed, with a tail extending to ~2 eV (620 nm). This tail resulted in a change in the color of the glass from transparent to a yellowish-brown. A broad band absorption around 3 eV (413 nm) appearing as a weak shoulder on the 242 nm band was attributed to the presence of germanium nanocrystals. One particularly interesting result of this research is that the germanium nanocrystals

form in the as-implanted glass without post-thermal annealing, which is not true for sputtering, sol-gel technique or even germanium implantation into SiO_2 glass.

Yang et al.[23] prepared binary GeO_2-SiO_2 glasses by combining sol-gel processing and treatment in hydrogen gas. They reported that transparent, as-prepared glasses turned brown with treatment in flowing hydrogen gas. The extent of coloration increased with increased germanium content. Yang suggests the color formation results from the reduction of Ge^{4+} to Ge^{o} in the gel glasses. Yang et al. show that the absorption edge shifts toward shorter wavelengths as the Ge/Si ratio decreases after treatment at 600°C for three hours in hydrogen gas. The absorption edge will also shift toward shorter wavelengths with decreasing temperature and time. The absorption spectra presented show no well-resolved band structure, but have a shoulder at a wavelength shorter than the absorption edge resulting from a wide distribution of germanium nanoparticle size. They explain the blue shift in the absorption edge as an effect of carrier confinement.

In this chapter the effect of hydrogen reactions with bulk binary GeO_2-SiO_2 glasses below T_g on optical absorption is reported. UV-Vis spectroscopy was used to investigate color formation during reactions with hydrogen at elevated temperatures. Hydrogen reactions with binary GeO_2-SiO_2 glasses are a function of time, temperature and germanium content. An analysis of these trends and identification of color producing species is presented.

6.2. Experimental Procedure

Binary GeO_2-SiO_2 glasses used in experiments described in this paper (100 mol% SiO_2, 6 mol% GeO_2-94 mol% SiO_2 and 14.6 mol% GeO_2-85.4 mol% SiO_2) were produced at Corning Incorporated. Glasses were fabricated using a doping and redraw process similar to that used in fiber production. The silica and germania were co-deposited as soot to form the porous preform. The porous material was then consolidated to a glass and drawn into a cane. Samples used in this study were cut to the desired thickness from the bulk glass cane using a low-speed diamond saw and were polished using SiC grit paper and 0.5 μm alumina paste. Sample thickness was measured using a micrometer and recorded to within 0.01 mm.

Samples were placed on a platinum setter in a vitreous silica tube attached to a gas handling apparatus. The preheated horizontal tube furnace was positioned around the evacuated silica sample chamber. Temperatures (500°C, 600°C, 700°C, or 800°C) were continuously monitored by a thermocouple inside the sample chamber, directly above the samples. After the desired temperature was reached, hydrogen gas was introduced into the sample chamber. Sample temperature was held constant to within ±5K throughout the treatment. Each sample was treated for the desired amount of time under 700 Torr (93 ± 1 kPa) of hydrogen partial pressure. A more detailed description, including a schematic of the apparatus, is presented in an earlier section, Chapter 3.

Optical absorption spectra were measured before the initial heat treatment and after each subsequent heat treatment. Since treatment times were cumulative, variations between samples do not exist for this work. Absorbances are reproducible to within ±0.01.

6.3. Results

6.3.1. Color Formation at 800°C

Hydrogen-induced color formation is observed with progressive treatment of binary GeO_2-SiO_2 glasses at elevated temperatures in a hydrogen environment. There is significant change in color of the samples with increasing treatment time for each of the binary GeO_2-SiO_2 glasses, as is shown in Figure 6.1. The images show the progressive hydrogen-induced color formation with increasing treatment at 600°C and 700 Torr of hydrogen for the indicated cumulative treatment times. This hydrogen-induced color effect is less dramatic in the lower germanium content glasses but still exists. The clear, as-received 14.6 mol% GeO_2-85.4 mol% SiO_2 glass sample becomes almost opaque as the intense brown color develops with increasing treatment time. Examination of the treated sample surface of the 6 mol% GeO_2-94 mol% SiO_2 glass treated at 800ºC and 700 Torr of hydrogen for 100 hours, Figure 6.2, shows that the color formation enhances the observation of the striations. The micrograph is labeled with a scale bar showing that the distance between the striations is approximately 35 μm. Figures 6.3 and 6.4 show the

optical absorption spectra obtained for the 6 mol% GeO_2-94 mol% SiO_2 and 14.6 mol% GeO_2-85.4 mol% SiO_2 glass treated at 800°C and 700 Torr of hydrogen for a total of 64 hours, respectively. Optical absorption spectral results correlate directly with the change in color of the samples with increasing treatment time. There is a considerable difference between the two different binary GeO_2-SiO_2 glasses in the way the band changes shape. The 14.6 mol% GeO_2-85.4 mol% SiO_2 glass darkens at a much faster rate than the 6 mol% GeO_2-94 mol% SiO_2 glass. The offset in the baseline due to scattering observed in the optical absorption spectra of the as-received samples was explained in Chapter 4. The band at approximately 242 nm, detected in the as-received samples, is significantly affected by treatment with hydrogen in both glasses. There is also a considerable difference in the growth of the band with increasing treatment time between the two different binary GeO_2-SiO_2 glasses. As is consistent with Awazu et al.[14] and Jackson et al.,[8] it is difficult to observe the growth of the 242 nm band since the band grows rapidly, forcing the peak optical density beyond the measurement limit of the equipment. Figures 6.3 and 6.4 also show the non-uniform growth in absorbance over the entire visible region with progressive treatment in hydrogen. Although there may be a small contribution to the color formation due to growth of the 242 nm band, with a high wavelength tail extending into the visible region of the spectrum, it is obvious that the color formation is not completely due to growth of this band.

6 mol% GeO_2 - 94 mol% SiO_2

14.6 mol% GeO_2 - 85.4 mol% SiO_2

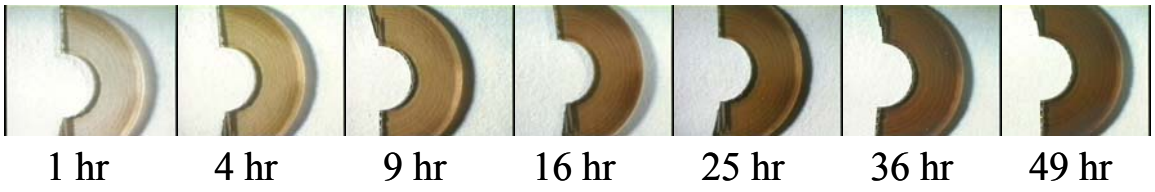

Figure 6.1. Color change with progressive hydrogen treatment at 600°C for the indicated cumulative treatment time.

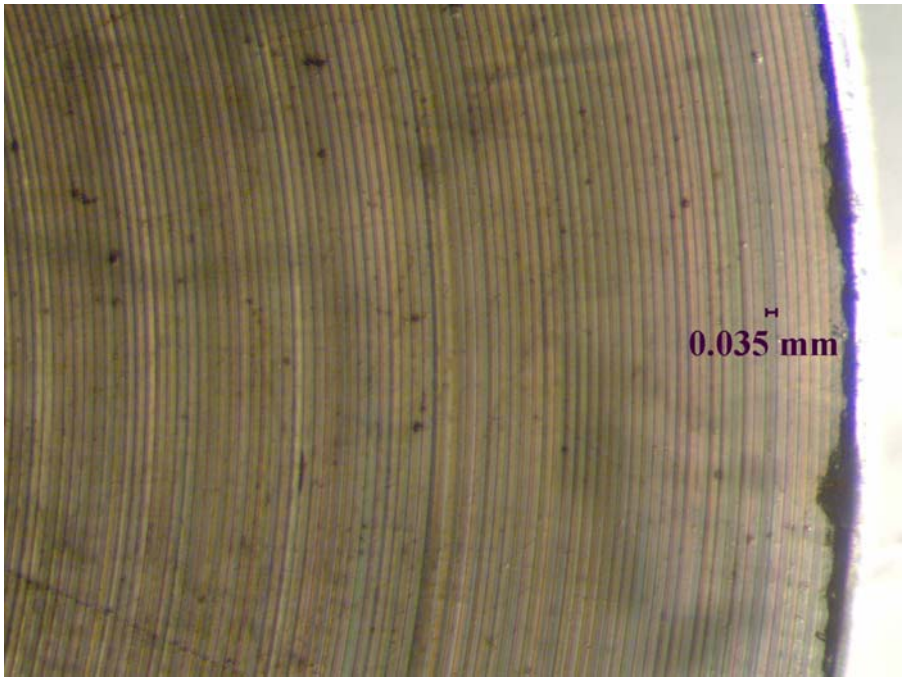

Figure 6.2. Optical micrograph of 6 mol% GeO_2 - 94 mol% SiO_2 glass after 100 hours of hydrogen treatment at 800°C.

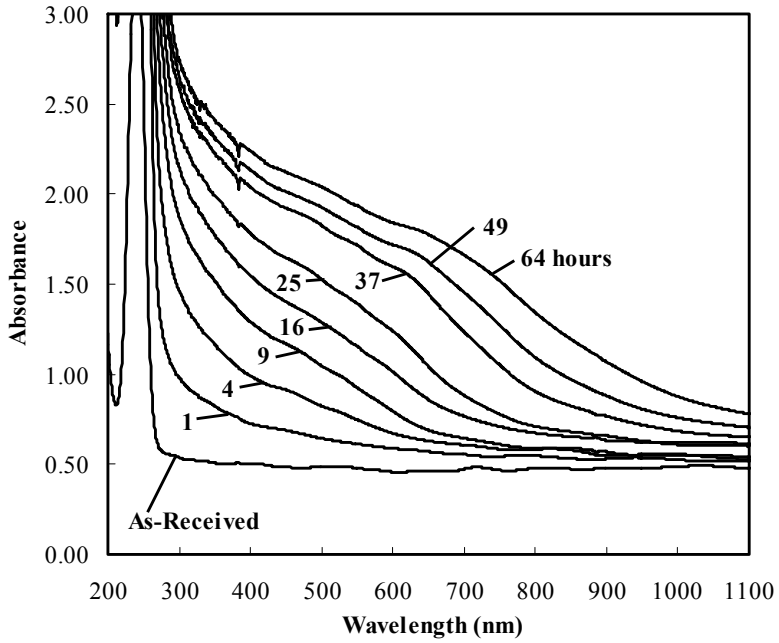

Figure 6.3. Optical absorption spectra for 6 mol% GeO_2 - 94 mol% SiO_2 glass during progressive hydrogen treatment at 800°C for the indicated cumulative treatment time (hours).

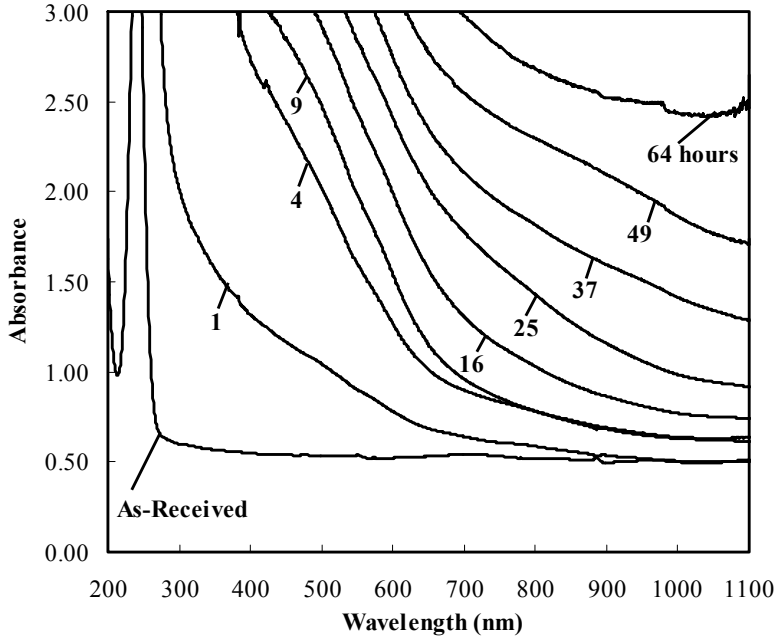

Figure 6.4. Optical absorption spectra for 14.6 mol% GeO_2 - 85.4 mol% SiO_2 glass during progressive hydrogen treatment at 800°C for the indicated cumulative treatment time (hours).

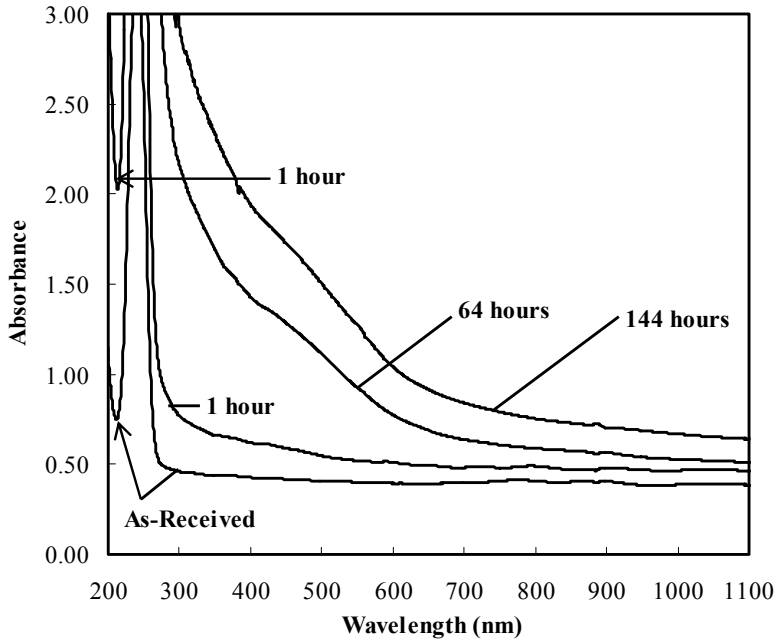

Figure 6.5. Optical absorption spectra for 6 mol% GeO_2 - 94 mol% SiO_2 glass during progressive hydrogen treatment at 700°C for the indicated cumulative treatment time.

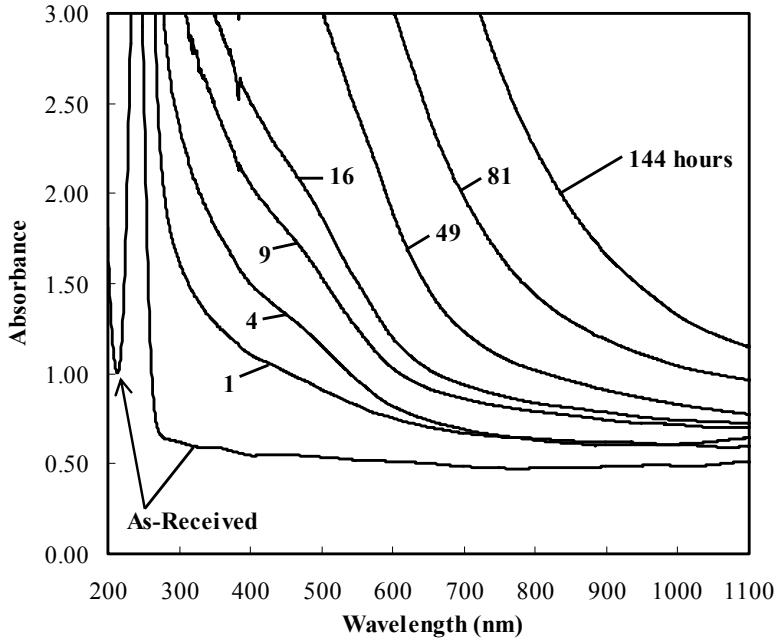

Figure 6.6. Optical absorption spectra for 14.6 mol% GeO_2 - 85.4 mol% SiO_2 glass during progressive hydrogen treatment at 700°C for the indicated cumulative treatment time.

6.3.2. Effect of Temperature on Color Formation

The effect of temperature on the color formation is apparent when the optical absorption spectra of the binary GeO_2-SiO_2 glasses treated at 800°C are compared with the optical absorption spectra of the binary GeO_2-SiO_2 glasses treated at 700, 600 and 500°C. Figures 6.5 and 6.6 show the optical absorption spectra of the 6 mol% GeO_2-94 mol% SiO_2 and 14.6 mol% GeO_2-85.4 mol% SiO_2 glasses, respectively, during progressive hydrogen treatment at 700°C for up to 144 hours. Figures 6.7 and 6.8 show the optical absorption spectra of the 6 mol% GeO_2-94 mol% SiO_2 and 14.6 mol% GeO_2-85.4 mol% SiO_2 glasses, respectively, during progressive hydrogen treatment at 600°C for up to 144 hours. Figures 6.9 and 6.10 show the optical absorption spectra of the 6 mol% GeO_2-94 mol% SiO_2 and 14.6 mol% GeO_2-85.4 mol% SiO_2 glasses, respectively, during progressive hydrogen treatment at 500°C for up to 256 hours. The samples used in this study for each set of conditions were treated, removed from the furnace, measured and returned to the furnace for further treatment, i.e. the same sample of glass was used at each temperature throughout the entire study, so variations between the glass samples exist only between the temperatures and not a given temperature. While measurements were made between each progressive treatment for samples treated at 700, 600 and 500°C, select spectra have been omitted to eliminate clutter.

Since the intensity of the band at 242 nm is greater than the detectable limit of the instrument after only a short period of treatment time, the minimum at 210 nm can be used to indirectly indicate the growth of the 242 nm band. The change in the minimum at 210 nm for the samples treated at 500°C is revealed in Figures 6.9 and 6.10. The change in the minimum absorbance at 210 nm is readily observable and labeled for up to 100 hours for the 6 mol% GeO_2-94 mol% SiO_2 and up to 4 hours for the 14.6 mol% GeO_2-85.4 mol% SiO_2 glasses. The increase in the intensity at the minimum is consistent with growth of the 242 nm band and shows that the band is growing with progressive hydrogen treatment. Clearly this band grows faster for the 14.6 mol% GeO_2-85.4 mol% SiO_2 glass, as this minimum can only be observed in the samples treated at 500ºC. The minimum is off scale after only one hour of treatment for all other temperatures.

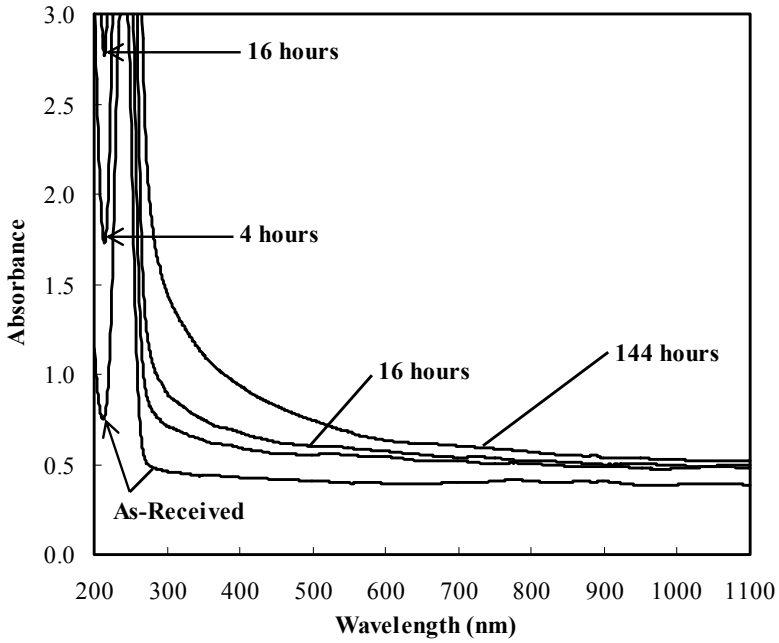

Figure 6.7. Optical absorption spectra for 6 mol% GeO_2 - 94 mol% SiO_2 glass during progressive hydrogen treatment at 600°C for the indicated cumulative treatment time.

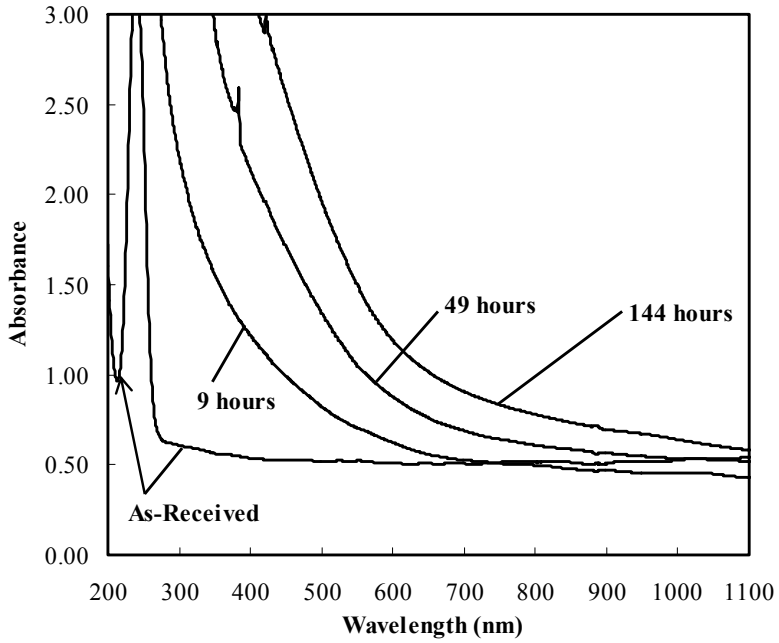

Figure 6.8. Optical absorption spectra for 14.6 mol% GeO_2 - 85.4 mol% SiO_2 glass during progressive hydrogen treatment at 600°C for the indicated cumulative treatment time.

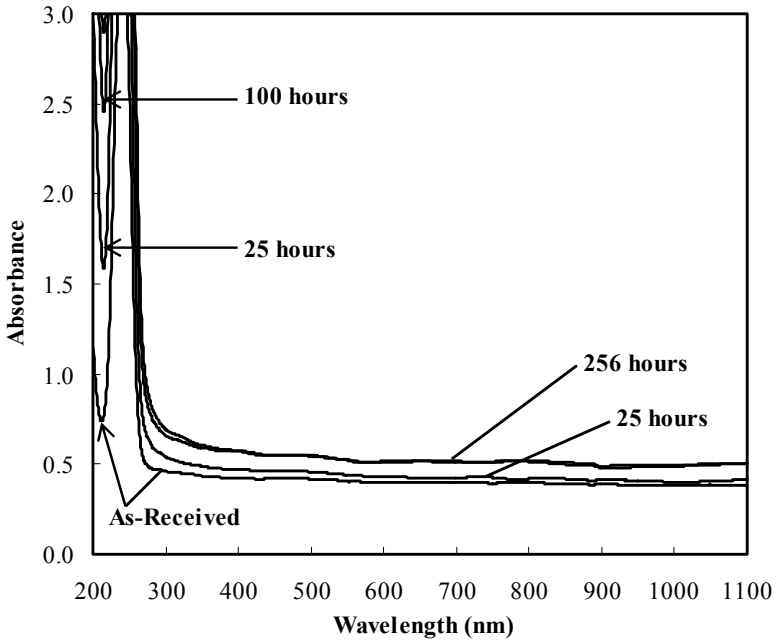

Figure 6.9. Optical absorption spectra for 6 mol% GeO_2 - 94 mol% SiO_2 glass during progressive hydrogen treatment at 500°C for the indicated cumulative treatment time.

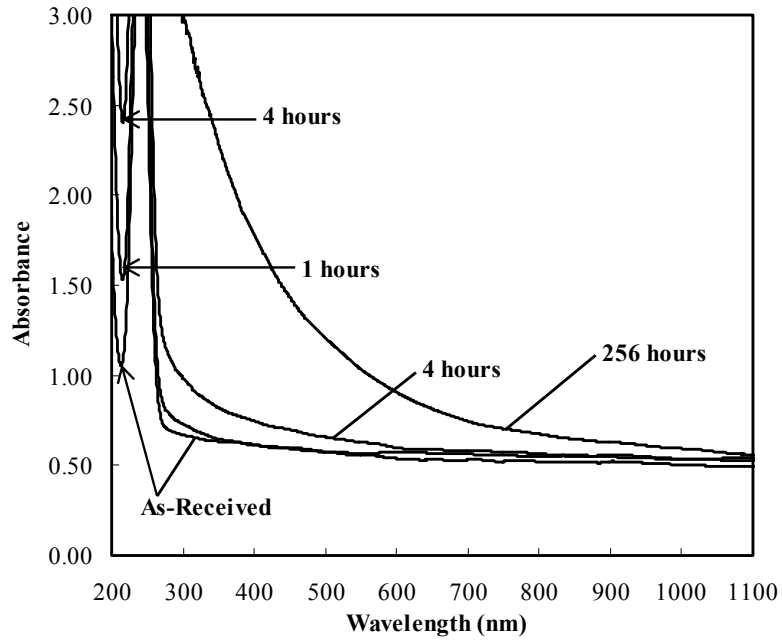

Figure 6.10. Optical absorption spectra for 14.6 mol% GeO_2 - 85.4 mol% SiO_2 glass during progressive hydrogen treatment at 500°C for the indicated cumulative treatment time.

In each of the samples, hydrogen-induced darkening increases with increasing treatment time, and the rate of color formation increases with increasing treatment temperature. There is a considerable difference in the non-uniform growth in absorbance over the entire visible region with progressive treatment in hydrogen between the two different binary GeO_2-SiO_2 glasses, for each treatment temperature. In general, the darkening is more significant in the samples with a higher germanium content for all treatment temperatures. All absorption spectra show no well-resolved band structure, with the effective absorption edge shifting to longer wavelengths with progressive hydrogen treatment for each temperature. Although there are no well-resolved bands, the optical absorption spectra of the glasses treated at 800°C and 700°C are not completely featureless. The development of a shoulder at longer wavelengths than the apparent absorption edge can be observed in Figures 6.3 - 6.6. Samples treated at 600°C and 500°C do not show significant development of longer wavelength bands on the shoulder of the apparent absorption edge, in fact, the featureless spectra shown in Figures 6.7 - 6.10 show the shift in the apparent absorption edge could almost be interpreted completely as growth of 242 nm band with a tail extending into the visible region of the spectrum. The significant difference in the way the optical absorption spectra change between the two different concentrations with progressive treatment is perhaps most effectively shown in the samples treated at 500ºC for up to 256 hours. The 6 mol% GeO_2-94 mol% SiO_2 glass shows minimal growth in absorbance over the entire visible region with progressive treatment, while the 14.6 mol% GeO_2-85.4 mol% SiO_2 glass shows a more significant growth in absorbance over the entire visible region.

To better illustrate the relative effect of darkening with progressive treatment and the effect of temperature on the hydrogen-induced color formation for the 6 mol% GeO_2-94 mol% SiO_2 and 14.6 mol% GeO_2-85.4 mol% SiO_2 glasses, absorbance values at 600 nm were plotted as a function of square root time in Figures 6.11 and 6.12, respectively. Values above an absorbance of 3.0 are off scale for the instrument and cannot be measured. A wavelength of 600 nm was arbitrarily chosen to demonstrate that growth in absorbance as a function of square root time is, in fact, not linear, i.e. representative of a diffusion controlled process, and there is no recognizable correlation in growth between

different treatment temperatures and absolutely no correlation between UV-Vis induced species and induced hydroxyl growth.

6.3.3. Color Confined to Surface

One of the most intriguing observations about the color formation is the fact that for all treatment temperatures and in both of the binary GeO_2-SiO_2 glasses, the color formation that corresponds to the extreme growth in absorbance over the entire visible region with progressive treatment is confined to the surfaces of the glass samples that are exposed to hydrogen. Close inspection of the treated glass samples shows intense color formation on both of the cut and polished surfaces, as well as on the as-received and fractured surfaces, i.e. color formation occurrs on all surfaces exposed to hydrogen at elevated temperatures. This observation eliminates the possibility that hydrogen reaction and subsequent color formation is associated with surface altering procedures such as cutting and polishing.

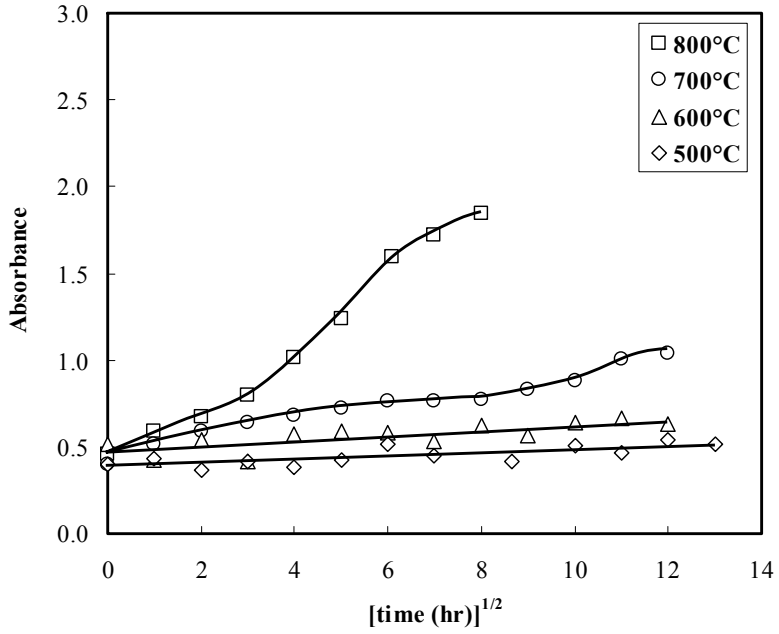

Figure 6.11. Effect of square root time on the absorbance at 600 nm for 6 mol% GeO_2 - 94 mol% SiO_2 glass during progressive hydrogen treatment at the indicated temperature. Lines are a guide to the eye.

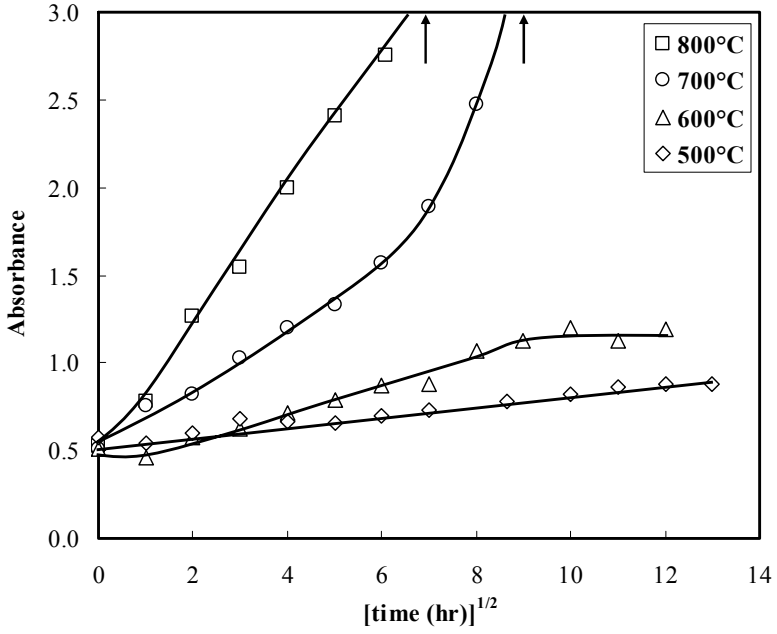

Figure 6.12. Effect of square root time on the absorbance at 600 nm for 14.6 mol% GeO_2 - 85.4 mol% SiO_2 glass during progressive hydrogen treatment at the indicated temperature.

In a limited study of the depth of color formation, one millimeter thick plates of each of the as-received binary GeO_2-SiO_2 glasses were treated under a hydrogen atmosphere (pH_2 = 93 kPa) at 800°C for 100 hours. After 100 hours of treatment in hydrogen, the optical absorption spectra of the treated glasses were measured. The spectra indicate a significant amount of color formation. The optical absorption spectra of the 6 mol% GeO_2-94 mol% SiO_2 glass is shown in Figure 6.13. The 14.6 mol% GeO_2-85.4 mol% SiO_2 glass was optically opaque, showing no detectable transmitted light, i.e. detection of transmitted light for this glass was beyond the measurement limit of the spectrometer. Each of the treated glasses was then polished on the previously cut and polished surfaces until no color was present. Removal of 45 micrometers from the surface of the 6 mol% GeO_2-94 mol% SiO_2 glass and 250 micrometers from the surface of the 14.6 mol% GeO_2-85.4 mol% SiO_2 glass produced optically transparent, colorless glass samples. Subsequent optical absorption measurements revealed growth of the 242 nm band, when compared to the as-received samples, as shown in Figures 6.13 and 6.14 for the 6 mol% GeO_2-94 mol% SiO_2 glass and the 14.6 mol% GeO_2-85.4 mol% SiO_2, respectively. The change in intensity of the 242 nm band with respect to the as-received

samples indicates that oxygen deficient centers are forming throughout the thickness of the sample and are not confined to the surface where the color formation occurs. The lack of significant broadening of the 242 nm band indicates that growth of this band alone is not responsible for the significant darkening observed with progressive treatment of binary GeO_2-SiO_2 glasses in hydrogen at elevated temperatures.

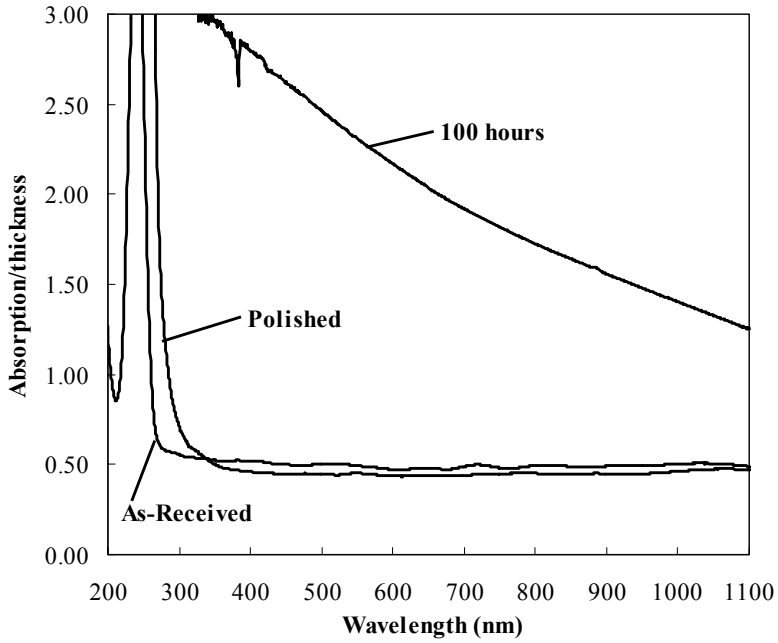

Figure 6.13. Optical absorption spectra for 6 mol% GeO_2 - 94 mol% SiO_2 glass after 100 hour treatment in a hydrogen atmosphere (pH_2 = 93 kPa) at 800°C then polished until colorless.

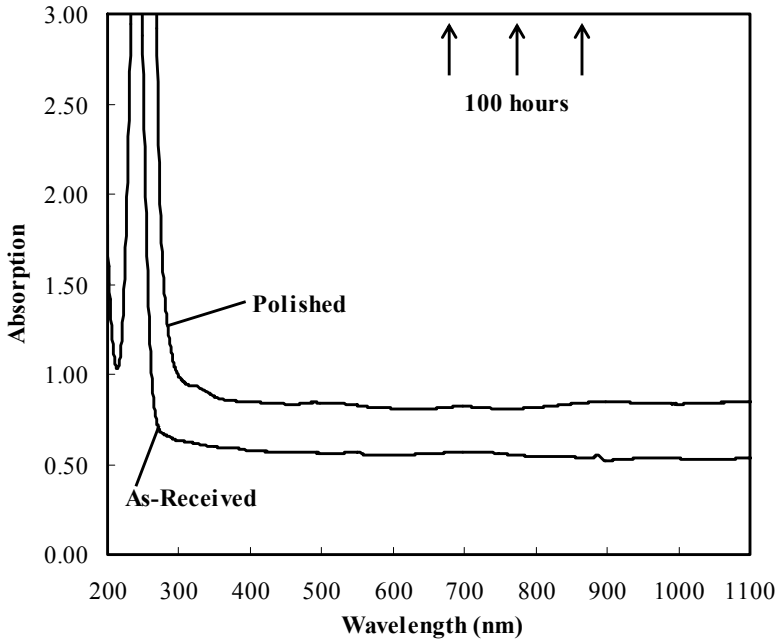

Figure 6.14. Optical absorption spectra for 14.6 mol% GeO_2 - 85.4 mol% SiO_2 glass after 100 hour treatment in a hydrogen atmosphere (pH_2 = 93 kPa) at 800°C then polished until colorless.

6.3.4. Color Associated with Striations

Close examination of the optical micrograph in Figure 6.2 shows that the color formation is most prevalent along the striations. In the previous section it was mentioned that color formation was confined to the surface and that progressive polishing of each surface resulted in optically transparent samples. Polishing of the exposed sample surfaces revealed that, although color formation was uniform over the entire surface, with progressive polishing removal of the uniform layer of color resulted in a sample with alternating rings of colorless and transparent with dark brown glass. The dark brown rings were thin and their position corresponded well with the striations in the glass. This observation indicates that, below the uniform formation of color along the surface, there is a rippled color formation that corresponds well with the striations, i.e. color formation is deeper into the glass, at the exposed surfaces, along the striations. This is a measure of the radial periodic variation in GeO_2 concentration. An effect of the soot lay-down process.

6.3.5. Color Resulting Only with Hydrogen Treatment

Each of the as-received binary GeO_2-SiO_2 glasses were treated at 800°C in a vacuum and ambient air atmosphere to ensure that color formation is a direct result of the presence of hydrogen in the atmosphere. After 100 hours of treatment in vacuum at 800°C, optical absorption spectra show no detectable color formation i.e. there is no detectable change in the spectrum. Treatment in ambient air for 69 hours at 800°C results in optical absorption spectra showing no detectable color formation.

The hydrogen-induced color formation is also irreversible. Optical absorption measurements for 0.5 mm samples after 144 hours of treatment at 600ºC and 700 Torr of hydrogen are shown in Figures 6.15 and 6.16 for the 6 mol% GeO_2-94 mol% SiO_2 glass and the 14.6 mol% GeO_2-85.4 mol% SiO_2, respectively. After 144 hours of progressive treatment under a hydrogen atmosphere (700 Torr), the samples were measured and returned to the furnace for further treatment under vacuum at 600ºC. After 300 hours of treatment in vacuum there was very little to no detectable change in the measured optical absorption spectra, demonstrating that the hydrogen-induced color formation is stable and irreversible with treatment at elevated temperature in vacuum.

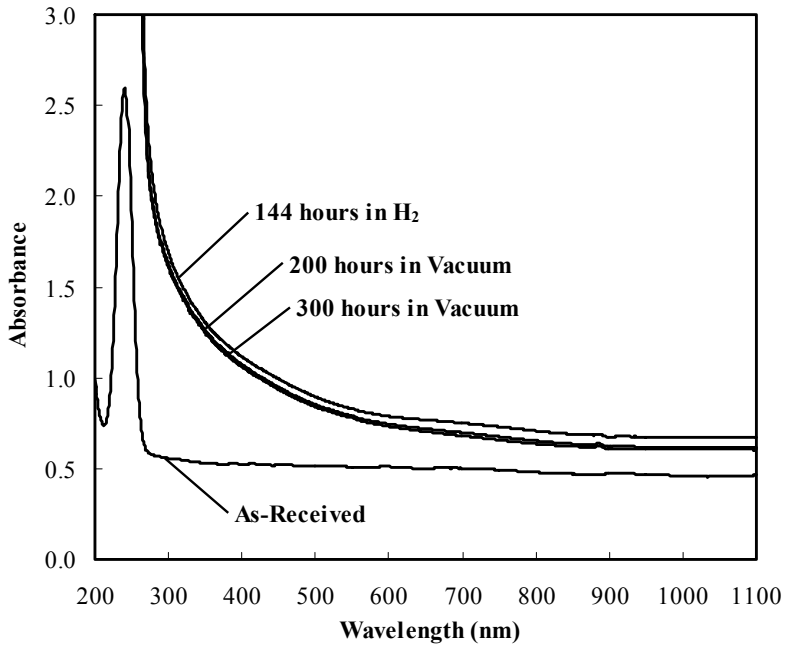

Figure 6.15. Optical absorption spectra for 6 mol% GeO_2 - 94 mol% SiO_2 glass (0.5 mm) after 144 hour treatment in a hydrogen atmosphere (pH_2 = 93 kPa) at 600°C, then treated in vacuum at 600°C for up to 300 hours in 100 hour increments.

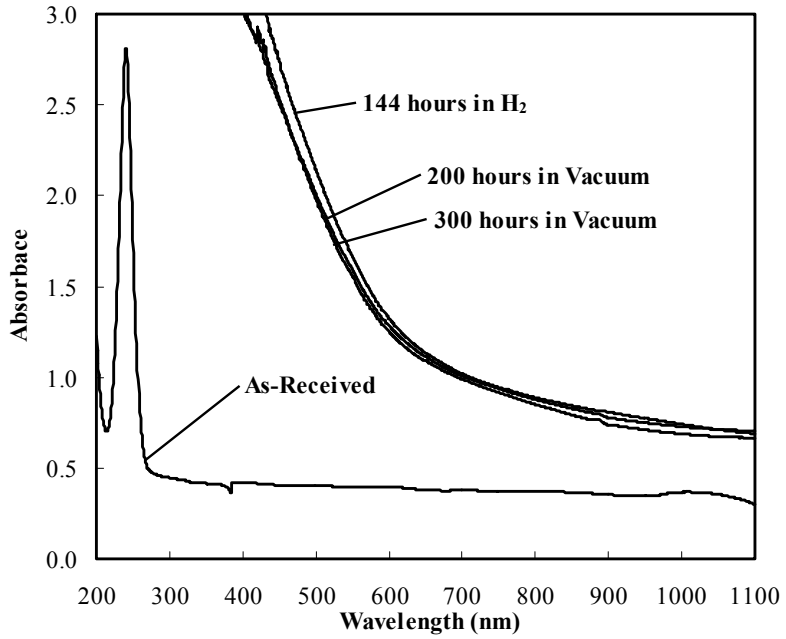

Figure 6.16. Optical absorption spectra for 14.6 mol% GeO_2 - 85.4 mol% SiO_2 glass (0.5 mm) after 144 hour treatment in a hydrogen atmosphere (pH_2 = 93 kPa) at 600°C, then treated in vacuum at 600°C for up to 300 hours in 100 hour increments.

6.3.6. Treatments with Deuterium

When the as-received binary GeO_2-SiO_2 glasses are treated with deuterium, rather than hydrogen, at 800°C, optical absorption spectra, shown in Figure 6.17 and 6.18 were obtained for the 6 mol% GeO_2-94 mol% SiO_2 and 14.6 mol% GeO_2-85.4 mol% SiO_2 glasses, respectively, for treatment up to 64 hours. The samples used in this study were treated, removed from the furnace, measured and returned to the furnace for further treatment, i.e. the same sample of glass was used throughout the entire study and variations between the glass samples do not exist for this work. The optical absorption spectra for the samples treated progressively in deuterium at 800°C are very similar to those treated progressively in hydrogen at 800°C. The induced color effect is less dramatic in the lower germanium content glasses but still exists. The clear, as-received 14.6 mol% GeO_2-85.4 mol% SiO_2 glass sample becomes almost opaque as the intense brown color develops with increasing treatment time. Optical absorption spectral results correlate directly with the change in color of the samples with increasing treatment time. There is a considerable difference between the two different binary GeO_2-SiO_2 glasses in the way the band changes shape, as well as the rate of darking. The 14.6 mol% GeO_2-85.4 mol% SiO_2 glass darkens at a much faster rate than the 6 mol% GeO_2-94 mol% SiO_2 glass. The band at approximately 242nm, detected in the as-received samples, is significantly affected by treatment with deuterium in both glasses. There is also a considerable difference in the growth of the band with increasing treatment time between the two different binary GeO_2-SiO_2 glasses. As is consistent with Awazu et al.[14] and Jackson et al.,[8] it is difficult to observe the growth of the 242 nm band since the band grows rapidly, forcing the peak optical density beyond the measurement limit of the equipment. Figures 6.17 and 6.18 also show the non-uniform growth in absorbance over the entire visible region with progressive treatment in deuterium. Although there may be a small contribution to the color formation due to growth of the 242 nm band, with a high wavelength tail extending into the visible region of the spectrum, it is obvious that the color formation is not completely due to growth of this band.

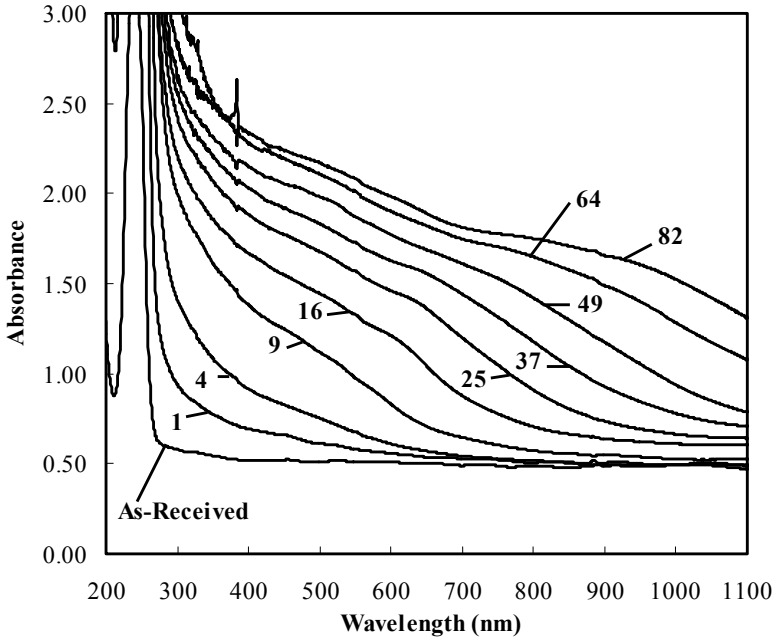

Figure 6.17. Optical absorption spectra for 6 mol% GeO_2 - 94 mol% SiO_2 glass during progressive deuterium treatment at 800°C for the indicated cumulative treatment time (hours).

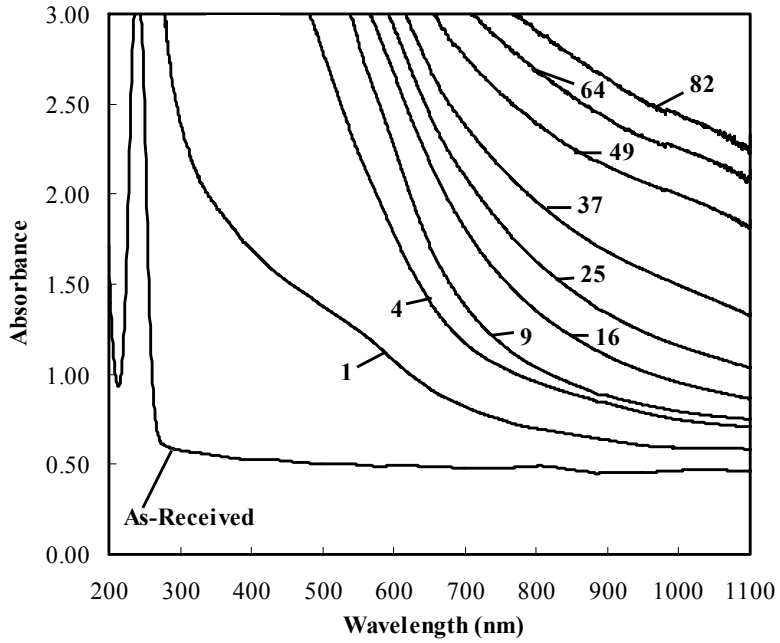

Figure 6.18. Optical absorption spectra for 14.6 mol% GeO_2 - 85.4 mol% SiO_2 glass during progressive deuterium treatment at 800°C for the indicated cumulative treatment time (hours).

6.3.7. Color Inherent to the Glass

A 100 mol% SiO_2 glass, made from the same process, was treated with the binary GeO_2-SiO_2 glasses at 800°C and 700 Torr (pH_2 = 93 kPa) of hydrogen for up to 64 hours. Treatment was subsequently extended for the pure SiO_2 glass for up to 190 hours. After 190 hours of treatment in hydrogen, the 100 mol% SiO_2 showed only minimal hydroxyl formation with no detectable color formation.

This intense hydrogen-induced color formation is inherent to the glass. Binary GeO_2-SiO_2 glasses fabricated from a similar process were also treated at elevated temperatures in a hydrogen atmosphere. Similar color formation was observed on all surfaces exposed to hydrogen. Pieces of binary GeO_2-SiO_2 glasses with a composition gradient were broken from a fiber perform and treated at 800°C for 10 hours. The results from treatment of these glasses, although not as well organized, showed a remarkable correspondence to the general trends observed with treatment of the 6 mol% GeO_2-94 mol% SiO_2 glass and the 14.6 mol% GeO_2-85.4 mol% SiO_2 glasses. Color formation occurred on fractured surfaces, as well as polished surfaces, and the intensity of the color increased with increasing germanium content.

6.4. Discussion

Although the optical properties of binary GeO_2-SiO_2 glasses have been studied extensively, published observations of change in the optical properties with progressive hydrogen treatment at elevated temperatures are limited. The research encompassed in this study is to some extent comparable to three other studies of hydrogen reactions with binary GeO_2-SiO_2 glasses by Awazu et al.,[14] Hosono et al.[16] and Yang et al.,[23] however, inconsistencies in experimental conditions and glass fabrication techniques, as well as the use of glasses with graded indices, adds to the difficulty in quantitative comparison.

6.4.1. Growth of the 242 nm Band

The extinction coefficient of the 242 nm band is extremely high. Since most of the samples used in this study were approximately one millimeter thick, the maximum

peak absorption is too high to be experimentally observable for both of the binary GeO_2-SiO_2 glasses. Since the absorption coefficient of the 240 nm band is so high, an apparent absorption edge develops with progressive hydrogen treatment. In order to clarify the actual position of the maximum intensity of the defect band, examination of 0.5 mm thick samples was necessary. The entire band for each of the binary GeO_2-SiO_2 glasses can be observed in Figures 6.15 and 6.16. The actual band maximum for each of the as-received glasses occurs at 242 nm, which is consistent with the band maximum reported in number of other studies.[1-4,6,14,15] The most interesting aspect of this correlation in band position is that between this study and those of Garino-Canina[1,3,4] and Cohen[2,6] is that these papers involved optical absorption spectral measurements of SiO_2 prepared from natural quartz, claiming that the 242 nm band resulted from impurity germanium content in the glass. This defect band is also readily observable in the spectra of vitreous GeO_2 but the band is shifted from the 242 nm position to slightly higher wavelengths, i.e. 244.5 nm, as reported by Cohen and Smith.[7]

Observation of the growth of the 242 nm band with progressive treatment of binary GeO_2-SiO_2 glasses in a hydrogen atmosphere at elevated temperatures, without subsequent irradiation, is somewhat limited. The only studies with which the optical absorption spectral data of this study can be compared are those by Awazu et al.[14] and Hosono et al.[16] because these studies did not involve exposure of the glass to UV light, which alters the defect population in the glass. Although Hosono et al. did study the effect of subsequent photobleaching after hydrogen treatment, a detailed description of the spectral properties resulting exclusively from hydrogen treatment at elevated temperatures is presented in great detail.

Awazu et al.[14] was able to observe the growth of the 242 nm band at 500°C with a 0.5 mm thick sample for limited treatment time, however, the band still becomes off scale after only two hours, inhibiting further measurement. Awazu et al. reported that an increase in infrared absorption of T-OH groups occurs simultaneously with the growth of the optical absorption band at 5.14 eV (242 nm) in binary GeO_2-SiO_2 glasses during treatment under a hydrogen atmosphere, after stating that the 5.14 eV band growth does not obey the $t^{1/2}$ rule. With further analysis, Awazu et al. claim that there is a linear relationship, that does not follow the $t^{1/2}$ dependence, between hydroxyl formation and

the absorption coefficient for the 5.14 eV band, suggesting that the structural imperfection responsible for the 5.14 eV band forms simultaneously with TOH groups. Such results imply that the entire process is not a diffusion-controlled process, but a reaction-controlled process. In general, the formation of hydroxyl species in the glasses used in this study did follow diffusion-controlled kinetics, as shown in the previous chapter, however, results presented in this study indicate that hydroxyl formation at the lowest treatment temperatures (500°C and 600°C) show evidence of an incubation time, i.e. period of time during which the kinetics are adjusting, before the reaction occurs with the square root of time. The presence of an incubation period shows that hydroxyl formation does not occur the instant that the sample is exposed to hydrogen at elevated temperatures, implying that the reaction itself lags behind the supply of hydrogen to the reaction sites and thus that hydroxyl formation is a reaction-controlled process. Since the treatment times used in the study by Awazu et al.[14] were within the treatment time for the observed incubation period of the results presented here, their conclusions are not valid due to insufficient treatment to observe the diffusion controlled region. In fact, the results for this study are consistent with those from Awazu et al. since an incubation period in hydroxyl formation suggests an initially reaction-controlled process. The square root of time dependence after the incubation period means that, once the reaction begins to occur, supply of the reactant, i.e. hydrogen, is a factor in hydroxyl formation. The square root of time dependence of hydroxyl growth with extended treatment does not prove that hydroxyl formation, and therefore color formation, is a diffusion-controlled process, since it could simply mean that some specific hydrogen concentration must be achieved before the reaction can occur. Quantative comparison of the results between the two studies are difficult to discuss since Awazu et al. used samples with a graded index. Progressive hydrogen treatments of binary GeO_2-SiO_2 glasses at high temperatures (700°C and 800°C) clearly indicate a diffusion-controlled process. Without the presence of an incubation period, the hydroxyl formation reaction shows an immediate square root of time dependence that is maintained until equilibrium saturation is achieved.

Hosono et al.[16] studied the heat treatment of 5.5 mol% GeO_2-94.5 mol% SiO_2 glass plates, a composition similar to the low germanium glass of this study, cut from preform rods produced by vapor phase axial deposition and subsequently treated in a

flow of hydrogen gas (200 mL/min). Although the author does mention that the germanium concentration was not uniform through out the rod, a few qualitative results presented in the study are very similar to those observed in this study. The intensity of the 242 nm band as a function of hydrogen treatment time at 500ºC was monitored for 0.17 and 0.50 mm thick samples. It was determined that intensity of the 242 nm band increased almost linearly with time at an initial stage then approached a saturation level. Sectioning experiments performed on 0.5 mm thick samples treated in hydrogen showed that the intensity of the 5 eV band decreases linearly with decreasing thickness. Hosono et al.[16] suggest that these results indicate that the responsible process is not controlled by diffusion of hydrogen but by reaction. Although no attempt was made in this study to quantitatively monitor the growth of the 242 nm band, the qualitative observation that the band increases in intensity with progressive hydrogen treatment at elevated temperature is consistent with the results presented by Awazu et al.,[14] and in this study.

6.4.2. Color Formation not a Result of Hydroxyl or the 242 nm Band

Observation of infrared spectra show that hydroxyl growth is not nearly as strongly affected by hydrogen treatment as the increase in absorbance in the visible region of the optical absorption spectrum, therefore no direct correlation between hydroxyl formation and color evolution can be established. Figure 6.11 and 6.12 shows that the hydrogen-induced color formation is not linear with respect to square root time and there is no correlation in the difference in absorbance growth between different treatment temperatures and absolutely no correlation between hydrogen-induced color formation and induced hydroxyl absorption. This suggests that hydroxyl and color formation may result from two completely different processes. The samples treated at 500°C contain a large amount of induced hydroxyl with minimal color formation. About half as much hydroxyl is formed at 500ºC with respect to those treated at 800ºC, but the difference in hydrogen-induced color formation is enormous. Infrared measurements show that the concentration of hydroxyl is uniform through the sample thickness, while color formation is restricted to surface of the sample. Clearly the reaction that leads to hydroxyl formation does not lead directly to hydrogen-induced color formation, providing evidence that at least two different mechanisms occur with progressive

hydrogen treatment. This observation does not mean, however, that one reaction is not necessary to promote the other in an elaborate series of reactions, or that many reactions are not occurring simultaneously, but merely that they are not occurring from the same one-step reaction. Perhaps it is most important to suggest that the same reactions are not occurring at all temperatures, based on the simple fact that the data do not support such contentions.

Awazu et al.[14] suggested that some color formation occurs from growth of the 242 nm band with a tail that extends into the visible region of the spectrum. Figures 6.13 and 6.14 show the optical absorption spectra after complete removal of the hydrogen-induced color formation from the surface. The observation that the 242 nm band does not return to the as-received value is evidence for two very important conclusions; (a) oxygen deficient defects are forming throughout the thickness of the glass plate and (b) significant color formation does not result from the tail of 242 nm band into the visible region of the spectrum.

Although most of the results presented by Hosono et al.[16] involved heat treatment of 5.5 mol% GeO_2-94.5 mol% SiO_2 glass plates in a flow of hydrogen gas (200 mL/min) at 500°C, a short paragraph at the end of their publication implies that treatment was carried out over a temperature range of 300 to 800°C. The authors mention that treatment of binary GeO_2-SiO_2 glasses at temperatures greater than 800ºC resulted in an induced brown coloring which they attributed to the formation of germanium particles, which treatment at temperatures less than 300ºC gave no change in optical properties. The optical absorption spectra of samples treated at temperatures other than 500ºC were not presented. Finally, the authors conclude that hydrogen treatment temperatures in the range 400 to 700ºC were appropriate for enhancement of UV-bleachable defects, implying that no color formation results from treatment within this temperature range. Direct comparison of these results and the results presented in this study is difficult due to differences in experimental conditions, i.e. flowing hydrogen versus isobaric pressure conditions, and slightly different glass compositions. The 5.5 mol% GeO_2-94.5 mol% SiO_2 glass used in the study by Hosono et al. is closest in composition to the 6 mol% GeO_2-94 mol% SiO_2 glass used in this study, however, a significant change in color was observed for samples treated at 600, 700 and 800°C in this study. These results are

inconsistent with the results presented by Hosono et al. in that significant color formation was only observed for the 5.5 mol% GeO_2-94.5 mol% SiO_2 glass treated in hydrogen at 800°C. One possible reason for this inconsistency is the difference in the hydrogen pressure during treatment. The second, more significant, reason for the difference in observed effect is the difference in total treatment time. Although the treatment times used by Hosono et al. for temperatures other than 500°C (70 hours) were not mentioned and therefore cannot be compared, the treatment time for the sample treated at 500°C by Hosono et al. was significantly shorter than 256 hours the total time used for the this study,.

Yang et al.[23] also observed color formation in binary GeO_2-SiO_2 glasses made by a sol-gel process and treated under flowing hydrogen, 1.0 L/h (16.7 mL/min), at temperatures ranging from 500 to 700°C. The extent of coloration increased with increasing germanium content in the glass, treatment temperature and time which is consistent with this study. Yang et al. explain changes in optical absorption spectra as shifts in the ultraviolet band edge. Unfortunately, spectra of the as-prepared glasses and discussion of the band at 242 nm is not presented, and discussion of the shift in what should be called the apparent absorption edge, as well as a lack of report of the thickness of the samples used in optical absorption measurements, implies that the band at 242 nm was not observed in this study. The second qualitative observation that is consistent with the present study is that the apparent absorption edge shifts to higher energy with decreasing germanium content, temperature and time in a hydrogen gas atmosphere. Direct comparison of the optical absorption spectra is difficult because of the difference in experimental conditions, including hydrogen pressure and use of flowing hydrogen gas versus isobaric hydrogen gas, and the ambiguities in determination of the composition of the final sol-gel glass. Unfortunately, neither Hosono et al.[16] or Yang et al.[23] mention confinement of color to the surface of the glass samples. There is a good chance that the gel glasses used in the study by Yang et al.[23] were not fully consolidated into a dense glass at 600°C, and a porous glass could potentially have formed coloration throughout the thickness of the glass sample as a significant amount of the glass would have been exposed to the hydrogen gas during treatment.

6.4.3. Hydrogen Induced Color Formation at the Surface

Hydrogen-induced color formation in otherwise transparent glasses is frequently indicative of colloid formation. The presence of colloidal particles in glass is not uncommon when ions within the glass have been exposed to a reducing environment. Complete reduction of modifying species in glass, including gold,[24] silver,[24,25] copper,[26,27] nickel,[28] platinum,[24] and cobalt[29] and intermediate glass species including bismuth,[30-32] antimony,[30-33] arsenic[30,33,34] and lead[31,32,35] to the atomic state has been observed in a variety of different glass systems. The observation of color, confined to surface exposed to hydrogen, resulting from the presence of colloidal species in the glass has also been observed in many of the reduced intermediate glass species.[30,31,33-35]

The glasses studied in this thesis contain only glass forming cations, i.e. silicon and germanium, and the suggestion of complete reduction of a glass forming species is extremely rare. Reduction of a glass forming species in this binary system would require breaking of network forming bonds, as well as complete reduction of a group IV ion. GeO_2 is much less stable that SiO_2, based on consideration of standard free energy of formation of oxides, and thus reduction of GeO_2 to GeO is much easier than reduction of SiO_2 to SiO, and reduction from the tetravalent state to the divalent state is more favorable for both germanium and silicon with increasing temperature.[15] Honoso et al.[16] very briefly mention that the significant brown color formation in the 5.5 mol% GeO_2-94.5 mol% SiO_2 glass samples treated in hydrogen at 800°C and attribute it to the formation of germanium particles, without further mention of measurements or literature that support this contention. A more detailed study of the reduction of germanium species in GeO_2-SiO_2 glasses is presented by Yang et al.[23] and similar conclusions are supported by x-ray diffraction (XRD) and transmission electron micoroscope (TEM) measurements. They presented XRD spectrum of a GeO_2-SiO_2 glass treated at in hydrogen gas at 600°C for 24 hours which shows formation of germanium nanoparticles.

6.4.4. Theoretical Analysis of Optical Absorption Spectra

In subsequent chapters, crystal formation is discussed. It is sufficient at this time to state that color formation is, in fact, associated with colloid formation at the exposed surfaces of the glass samples and the nanocrystal responsible for the color formation is

germanium. It follows that attributing the color formation to the formation of germanium nanocrystals is consistent with this work. Interpretation of the optical absorption spectra, however, is significantly more difficult since no well resolved band structures are presented.

Yang et al.[23] interpret changes in the optical absorption spectra with progressive hydrogen treatment in terms of a quantum confinement effect of electrons and holes in germanium nanocrystals. The apparent absorption edge was attributed to a transition from the highest hole subband level to the lowest electron subband level of a germanium crystal. Unfortunately, without discussion of the effect of the 242 nm band on the position of the apparent absorption edge, this argument is highly speculative. The arguments presented by Yang et al. are not substantiated by any other source or research.

A detailed discussion of the calculation of the expected optical absorption spectrum of germanium nanocrystal colloids is presented by Heath et al.[36] who studied the effect of size distribution on the characterization of germanium nanocrystals. In this study, germanium nanocrystals were synthesized via an ultrasonic-mediated reduction of colloidal suspensions of germanium nanocrystals. The authors state that it is inappropriate to compare the absorption spectrum of bulk germanium to that of nanocrystals, since it is important to include the effect of scattering as well as absorption in the nanocrystal spectrum. The correct way to calculate the spectral properties for nanocrystals would be to use Mie theory for small particles (radius << wavelength of incident light) to account for geometric differences. Mie theory, however, does not include quantum confinement effects of semiconducting materials. Two very important reasons that Mie theory calculations cannot be applied to this research are the presence of a wide size distribution of germanium nanoparticles and the lack of consideration of the matrix phase, i.e. the optical properties of the binary GeO_2-SiO_2 glass, from which the crystals have grown.

Absorption specra similar to those observed in this study were observed by Wilcoxin et al.[37] for germanium nanocrystals grown and purified from a solution-based synthesis process described as inverse micelles, whereby controlled nucleation and growth occur in the interior of nanosize surfactant aggregates. Wilcoxin et al. include a detailed discussion of the influence of quantum confinement on the optical properties of

semiconductors as quantum dots are made smaller and smaller. Although the growth techniques are completely different, making direct comparison of the optical properties unreasonable, there are a few qualitative results that are in good agreement with this study. Germanium nanocrystals formed in a glass matrix produce broad optical absorption features that make definitive interpretation of quantum confinement difficult.[37] Broad optical absorption features are generally representative of a relatively wide crystal size distribution, resulting in an essentially featureless spectrum. The results presented here are consistent with this expectation. The size and shape of the colloidal crystal also has a significant effect in the observed spectral features. Quantum confinement effects, including the blue shift, or shifting of the germanium band structure to higher energies, should become observable only for nanocrystals below 11.5 nm.[37] To the author's knowledge, similar calculations have not been performed for systems involving dispersion of germanium nanocrystals in a glass, probably because of complications involved with matrix affects, the influence of semiconductor quantum confinement effects and the presence of a significant particle size distribution.

6.4.5. Irreversible Process

Tomita et al.[12] observed a broad background loss increase due to hydrogen reactions that occur at germanium related defects in optical fibers. This broad background loss increase was determined to be irreversible, since removal of the hydrogen atmosphere did not result in reduction of the loss. These results are consistent with those observed in this study, where the optical absorption spectra of the glasses treated in hydrogen then subsequently treated in vacuum show no detectable change, even though there was a significant removal of hydroxyl. The 0.5 mm sample of both binary GeO_2-SiO_2 glasses treated in hydrogen at 600°C for 255 hours, then treated for up to 300 hours in vacuum, Figures 6.15 and 6.16, exhibits no detectable change in the optical absorption spectra, i.e. hydrogen-induced absorption and scattering losses in the optical absorption region of the spectrum are not reversible. This result indicates that hydrogen reacts with unstable defects with the glass structure, creating permanent, stable absorption centers in the glass.

6.5. Conclusion

Treatment of 6 mol% GeO_2-94 mol% SiO_2 and 14.6 mol% GeO_2-85.4 mol% SiO_2 glasses under a hydrogen atmosphere (pH_2 = 93 kPa) at elevated temperature results in an intense change in color of the glass from colorless to brown. Hydrogen reactions with binary GeO_2-SiO_2 glasses result in induced color formation as a function of time, temperature and germanium content. The effect GeO_2 concentration on color formation is evident, as induced color formation increases with increasing GeO_2 concentration. The rate of color formation increases with increasing temperature for both binary GeO_2-SiO_2 glasses. Color formation is confined to the exposed surface of each sample. Color concentration is not uniform across the surface of the sample, but varies systematically with areas of non-uniform concentration in the samples.

6.6. References

1. V. Garino-Canina, "Luminescence of Vitreous Silica as a Function of Temperature," *Compt. Rend.,* **238,** 1577-8 (1954).

2. A.J. Cohen, "Impurity Induced Color Centers in Fused Silica," *J. Chem. Phys.,* **23** [4] 765-6 (1955).

3. V. Garino-Canina, "A New Phenomenon Relating to the Absorption Band at 2400 A and the Luminescence of Vitreous Silica," *Compt. Rend.,* **240,** 1331-3 (1955).

4. V. Garino-Canina, "Nature of Absorption Centers in Vitreous Silica," *Compt. Rend.,* **240,** 1765-7 (1955).

5. V. Garino-Canina, "The Absorption Band at 2420 A of Vitreous Silica-Germanium Impurity and Oxygen Deficiency," *Compt. Rend.,* **242,** 1982-4 (1956).

6. A.J. Cohen, "Neutron Specific Color Center in Fused Silica and an Impurity Band of Identical Wave Length," *Phys. Rev.,* **105** [4] 1151-5 (1957).

7. A.J. Cohen and H.L. Smith, "Ultraviolet and Infrared Absorption of Fused Germania," *Phys. Chem. Solids,* **7,** 301-6 (1958).

8. J.M. Jackson, M.E. Wells, G. Kordas, D.L. Kinser, R.A. Weeks, and R.H. Magruder III, "Preparation Effects on the UV Optical Properties of GeO_2 Glasses," *J. Appl. Phys.,* **58** [6] 2308-11 (1985).

9. K.O. Hill, Y. Fujii, D.C. Johnson, and B.S. Kawasaki, "Photosensitivity in Optical Fiber Waveguides: Application to Reflection Filter Fabrication," *Appl. Phys. Lett.,* **32** [10] 647-9 (1978).

10. G. Meltz, W.W. Morey, and W.H. Glenn, "Formation of Bragg Gratings in Optical Fibers by a Transverse Holographic Method," *Opt. Lett.,* **14** [15] 823-5 (1989).

11. P.J. Lemaire, R.M. Atkins, V. Mizrahi, and W.A. Reed, "High Pressure Hydrogen Loading as a Technique for Achieving Ultrahigh UV Photosensitivity and Thermal Sensitivity in Germania Doped Optical Fibers," *Electron. Lett.,* **29** [13] 1191-3 (1993).

12. A. Tomita and P.J. Lemaire, "Hydrogen-Induced Loss Increases in Germanium-Doped Single-Mode Optical Fibers: Long-Term Predictions," *Electron. Lett.,* **21** [2] 71-2 (1985).

13. M. Kohketsu, K. Awazu, H. Kawazoe, and M. Yamane, "Photoluminescence Centers in VAD SiO_2 Glasses Sintered under Reducing or Oxidizing Atmospheres," *Jpn. J. Appl. Phys.,* **28** [4] 615-21 (1989).

14. K. Awazu, H. Kawazoe, and M. Yamane, "Simultaneous Generation of Optical Absorption Bands at 5.14 and 0.452 eV in 9 SiO_2:GeO_2 Glasses Heated under an H_2 Atmosphere," *J. Appl. Phys.,* **68** [6] 2713-8 (1990).

15. H. Hosono, Y. Abe, D.L. Kinser, R.A. Weeks, K. Muta, and H. Kawazoe, "Nature and Origin of the 5 eV Band in SiO_2:GeO_2 Glasses," *Phy. Rev. B,* **46** [18] 11445-51 (1992).

16. H. Hosono, H. Kawazoe, and K. Muta, "Preferred Concentration Enhancement of Photobleachable Defects Responsible for 5 eV Optical Absorption Band in SiO_2:GeO_2 Glass Preform by Heating in a H_2 Atmosphere," *Appl. Phys. Lett.,* **63** [4] 479-81 (1993).

17. K. Awazu, H. Onuki, and K. Muta, "Mechanisms of Photo-Bleaching of 5 eV Optical Absorption Band in Hydrogen Loaded Ge-Doped SiO_2," *J. Non-Cryst. Solids,* **211** [1-2] 158-63 (1997).

18. M. Essid, J. Albert, J.L. Brebner, and K. Awazu, "Correlation between Oxygen-Deficient Center Concentration and KrF Excimer Laser Induced Defects in Thermally Annealed Ge-Doped Optical Fiber Preforms," *J. Non-Cryst. Solids,* **246** [1-2] 39-45 (1999).

19. J. Nishii, A. Chayahara, K. Fukumi, K. Fujii, H. Yamanaka, H. Hosono, and H. Kawazoe, "Comparison of Formation Process of Ultraviolet Induced Color Centers in GeO_2-SiO_2 Glass Fiber Preform and Ge-Implanted SiO_2," *Nucl. Instrum. Methods Phys. Res., Sect. B,* **116** [1-4] 150-3 (1996).

20. M. Kohketsu, K. Awazu, H. Kawazoe, and M. Yamane, "Luminescence Centers in SiO_2 and SiO_2:GeO_2 VAD Rods Sintered under Reducing or Oxidizing Conditions," *J. Non-Cryst. Solids,* **95-96** [Part 2] 679-84 (1987).

21. V.A. Kolesova and E.S. Sher, "Two-Component Glasses of the Germanium Dioxide-Silicon Dioxide System," *Izv. Akad. Nauk SSSR, Neorg. Mater.,* **9** [6] 1018-20 (1973).

22. K. Kawamura, Y. Kameshima, H. Hosono, and H. Kawazoe, "Proton-Implantation-Induced Optical Phenomena in SiO_2:GeO_2 Glasses: Formation of Photosensitive Defects and Nanometer Sized Ge Crystals," *Mater. Sci. Eng., B,* **54** [1-2] 18-23 (1998).

23. H. Yang, X. Wang, H. Shi, F. Wang, X. Gu, and X. Yao, "Sol-Gel Preparation of Ge Nanocrystals Embedded in SiO_2 Glasses," *J. Cryst. Growth,* **236** [1-3] 371-5 (2002).

24. K. Nassau, *The Physics and Chemistry of Color: The Fifteen Causes of Color,* 2nd ed.*;* pp. 305-6. John Wiley & Sons, New York, 2001.

25. J.E. Shelby and J. Vitko, Jr., "Colloidal Silver Formation at the Surface of Float Glass," *J. Non-Cryst. Solids,* **50** [1] 107-17 (1982).

26. D.L. Edson and J.E. Shelby, "Effects of Bromine Additions on the Formation of Copper Colloids by Hydrogen Reduction in Sodium Borate Glasses," *Phys. Chem. Glasses,* **44** [3] 220-4 (2003).

27. C. Estournes, N. Cornu, and J.L. Guille, "Reduction of Copper in Soda-Lime-Silicate Glass by Hydrogen," *J. Non-Cryst. Solids,* **170** [3] 287-94 (1994).

28. C. Estournes, T. Lutz, and J.L. Guille, "Reduction of Nickel in Soda-Lime-Silicate Glass by Hydrogen," *J. Non-Cryst. Solids,* **197** [2,3] 192-6 (1996).

29. M.E. Miller, "Formation of Transition-Metal Crystallites in Glass"; M. S. Thesis. Alfred University, Alfred, NY, 2005.

30. M.R. Tuzzolo and J.E. Shelby, "Hydrogen-Induced Formation of Colloids of Arsenic, Antimony, and Bismuth in Oxide Glasses," *J. Non-Cryst. Solids,* **143** [2-3] 181-90 (1992).

31. R.L. Green and K. Blodgett, "Electrically Conducting Glasses," *J. Am. Ceram. Soc.,* **31** [4] 89-100 (1948).

32. A.W. Bastress, "Influence of Glass Compositions on Reducibility of Ag+, Bi+++, Sb+++, and Pb++," *J. Am. Ceram. Soc.,* **30** [2] 52-3 (1947).

33. M.R. Tuzzolo, J.T. Kohli, and J.E. Shelby, "Hydrogen-Induced Absorption in Glasses Containing Arsenic and Antimony," *Proc. SPIE-Int. Soc. Opt. Eng.,* **1327,** 2-9 (1990).

34. J.T. Kohli, B.M. Wright, J.M. Jewell, and J.E. Shelby, "Hydrogen-Induced Coloration of Glasses Containing Arsenic," *Phys. Chem. Glasses,* **31** [4] 133-7 (1990).

35. K.B. Blodgett, "Surface Conductivity of Lead Silicate Glass after Hydrogen Treatment," *J. Am. Ceram. Soc.,* **34** [1] 14-27 (1951).

36. J.R. Heath, J.J. Shiang, and A.P. Alivisatos, "Germanium Quantum Dots: Optical Properties and Synthesis," *J. Chem. Phys.,* **101** [2] 1607-15 (1994).

37. J.P. Wilcoxon, P.P. Provencio, and G.A. Samara, "Synthesis and Optical Properties of Colloidal Germanium Nanocrystals," *Phys. Rev. B: Condens. Matter Mater. Phys.,* **64** [3] 035417 9pp. (2001).

CHAPTER 7: HYDROGEN-INDUCED CRYSTALLIZATION IN BINARY GEO_2-SIO_2 GLASSES

Abstract

Treatment of 100 mol% SiO_2, 6 mol% GeO_2-94 mol% SiO_2 and 14.6 mol% GeO_2-85.4 mol% SiO_2 glasses was monitored as a function of time under a hydrogen atmosphere (pH_2 = 93 kPa) at 500ºC, 600ºC, 700ºC and 800ºC. Binary GeO_2-SiO_2 glasses heat treated in the presence of hydrogen react to form reduced germanium species in the glass. This reaction is associated with an induced crystallization. A detailed analysis of the induced crystallization resulting from hydrogen reactions is provided. Hydrogen reactions with binary GeO_2-SiO_2 glasses resulting in crystallization are a function of time, temperature and germanium content. Induced crystal formation is confined to the exposed surface of each sample. Induced crystal formation is not uniform across the surface of the sample, but it varies systematically with areas of non-uniform concentration in the samples, similar to the results observed with color formation.

7.1. Introduction

The increased interest in the nonlinear optical properties of semiconductor nanocrystals as small as a few nanometers (also known as quantum dots) embedded in a solid glass matrix has led to the development of specialized characterization techniques. The discovery of a relative sharp Raman line resulting from the presence of germanium nanocrystals embedded in a pure silica thin film has led to the widespread use of Raman spectroscopy to identify and characterize germanium nanocrystals.

Fujii and co-workers[1] studied Raman scattering from germanium quantum dots ranging from 6.1 to 15 nm in size embedded in pure silica thin films. Germanium quantum dots were embedded in thin films by applying a radio frequency co-sputtering technique, where the samples were subsequently annealed at 500-800°C in vacuum. Fujii and co-workers[1] were the first to discover the relative sharp Raman line at approximately 300 cm^{-1} resulting from the presence of germanium nanocrystals embedded in a pure silica thin film. Fujii et al.[1] suggest that the intense, sharp Raman band around 300 cm^{-1} results from surface boundary conditions. Since tightly stacked germanium nanocrystals embedded in the SiO_2 matrix exhibited seemingly weak surface effects. They also suggest that these nanocrystals conserve bulk character, with Raman signals thought to come mainly from the interior of the crystals. Transmission electron microscopy (TEM) measurements were used to determine the actual size of the embedded germanium crystallites. It was reported that the Raman peak broadens and shifts to slightly higher frequencies as the average size of the crystallite decreases. Fujii et al.[1] suggest a way to calculated the size of the germanium nanocrystals from the full width at half maximum (FWHM) values of the 300 cm^{-1} band, using expressions of Raman intensity and phonon confinement functions specified by Campbell and Fauchet[2] and phonon dispersion curves given by Nilsson and Nelin.[3] Although the exact calculations are not shown, a figure with an exponential curve is presented, allowing for extrapolation of particle size based on measured FWHM values.

In a subsequent study of nanocrystalline size dependence of the Raman spectrum, Fujii et al.[4] observed the increase in line width with decreasing size but the downward shift of the peak frequency was not observed. The peak at 300 cm^{-1} was observed to appear with increasing annealing temperatures and they reported that the peak becomes

stronger and the broad band underneath the peak becomes weaker, as the annealing temperature increases.

Meada et al.[5] used Raman spectroscopy to identify germanium nanocrystals embedded in a SiO_2 matrix which were formed by a radio-frequency magnetron co-sputtering technique. Germanium nanocrystals did not form until the sample was treated at 800°C for 30 minutes, as determined by the appearance of the sharp Raman peak at 297.5 cm^{-1}. The FWHM of the peak was determined to be 6.2 cm^{-1}, which corresponds to a average diameter of about 6 nm using the relationship reported by Fujii et al.[1] The calculated germanium nanocrystal size was in good agreement with micrographs of the nanocrystals obtained using high resolution electron microscopic images. The high resolution electron micrographs also showed that the germanium nanocrystals had a spherical morphology with extensive crystallinity.

Recently, much attention has been focused on ion implantation as a fabrication technique for glass with nonlinear optical properties. Raman spectroscopy was used to characterize germanium nanocrystals in a study where ion implantation of 1.5 MeV protons into binary GeO_2-SiO_2 glass substrates prepared by VAD was used to create germanium nanocrystals.[6] One particularly interesting feature of this research is that the germanium nanocrystals form in the as-implanted glass without post-thermal annealing, which is not true for sputtering, sol-gel techniques or even germanium implantation into SiO_2 glass. Kawamura et al.[6] also uses the technique presented by Fujii et al.[1] to estimate the size of nanocrystals based on the FWHM of the band at 300 cm^{-1} in the Raman spectra. Extrapolated values from the relationship presented by Fujii et al.[1] are in good agreement with the reported particle size of 6 to 8 nm determined from the FWHM value of 10 cm^{-1}.

Plotnichenko et al.[7] observed germanium nanocrystals using Raman spectroscopy in binary GeO_2-SiO_2 glass fibers with a graded index, i.e. graded germanium concentration, that were annealed above 1000°C after hydrogen loading. The Raman band with a maximum from 295 to 303 cm^{-1} and a FWHM of 7-12 cm^{-1}, previously attributed to the formation of germanium nanocrystals, was analyzed using the method proposed by Fujii et al.[1] to determine the size of the germanium nanocrystals. Germanium clusters were calculated and reported to be about 10 nm in size.

In all of the studies described above, nothing was mentioned about the optical properties of the glasses, more specifically none of the studies noticed the development of color in the samples with crystal growth. Hosono et al.[8] studied the heat treatment of 5.5 mol% GeO_2-94.5 mol% SiO_2 glass plates cut from preform rods produced by vapor phase axial deposition, with a non-uniform germanium concentration, that were subsequently treated in a flow of hydrogen gas (200 mL/min) at 500°C. At the end of the paper, the authors mention that treatment of binary GeO_2-SiO_2 glasses at temperatures greater than 800ºC resulted in an induced brown coloring which they attribute to the formation of germanium particles. The presence of crystalline phases, however, is not substantiated by additional measurements or referencing sources that support this contention. The authors further state that hydrogen treatment at temperatures less than 300ºC gave no change in optical properties and conclude that hydrogen treatment temperatures in the range 400 to 700ºC were appropriate for enhancement of UV-bleachable defects, implying that crystallization and excessive optical absorption will not occur within this temperature range under flowing hydrogen gas (200 mL/min).

Yang et al.[9] prepared binary GeO_2-SiO_2 glasses by combining sol-gel processing and treatment in hydrogen gas. They reported that transparent as-prepared glasses turned brown with treatment in flowing hydrogen gas and that the extent of coloration increased with increasing germanium content. Yang et al. suggest the color formation results from the reduction of Ge^{4+} to Ge^0 in the gel glasses. Optical absorption spectra presented show no well-resolved band structure, which is attributed to a wide size distribution of germanium nanoparticles. Such conclusions are supported by x-ray diffraction (XRD) and transmission electron micoroscope (TEM) measurements. An XRD spectrum of a GeO_2-SiO_2 glass treated at in hydrogen gas at 600°C for 24 hours show formation of germanium nanoparticles.

In a subsequent study, Yang et al.[10] provide a more detailed study of the reduction of germanium species to the atomic state in binary GeO_2-SiO_2 gel glasses using XRD, TEM, Raman spectroscopy and photoluminescence measurements to characterize germanium nanocrystals embedded in the binary GeO_2-SiO_2 gel glass matrix.

Although the reduction of germanium ions in silica glass is fairly well known, the complete reduction of germanium to the atomic state has not been fully investigated. To

the author's knowledge, examination of germanium nanocrystal formation with hydrogen reduction of binary GeO_2-SiO_2 glasses made from a VAD fabrication technique has not been reported. The effect of hydrogen reactions with bulk glass below T_g and subsequent crystallization is presented here. ESEM images, XRD and Raman spectroscopy is used to determine crystal species formation during reactions with hydrogen. Hydrogen reactions with binary GeO_2-SiO_2 are discussed as a function of time, temperature and germanium content.

7.2. Experimental Procedure

Binary GeO_2-SiO_2 glasses used in experiments described in this thesis (100 mol% SiO_2, 6 mol% GeO_2-94 mol% SiO_2 and 14.6 mol% GeO_2-85.4 mol% SiO_2) were produced at Corning Incorporated. Glasses were fabricated using a doping and redraw process similar to that used in fiber production. The silica and germania were co-deposited as soot to form the porous preform. The porous material was then consolidated to a glass and drawn into a cane. Samples used in this study were cut to the desired thickness from the bulk glass cane using a low-speed diamond saw and polished using SiC grit papers and 0.5 μm alumina paste. Sample thickness was measured using a micrometer and recorded to within 0.01 mm. All samples used in this study were approximately 1.0 mm thick unless otherwise noted.

Samples were placed on a platinum setter in a vitreous silica tube attached to a gas handling apparatus. The preheated horizontal tube furnace was positioned around the evacuated silica sample chamber. Temperatures (500°C, 600°C, 700°C, or 800°C) were continuously monitored by a thermocouple inside the sample chamber, directly above the samples. After the desired temperature was reached, hydrogen gas was introduced into the sample chamber. Sample temperature was held constant to within ±5K throughout the treatment. Each sample was treated for the desired amount of time under 700 ± 7 Torr (93 ± 1 kPa) of hydrogen. A more detailed description, including a schematic of the apparatus, is presented in Chapter 3.

An environmental scanning electron microscope (ESEM) was used to investigate the possible presence of crystalline phases, including colloidal particles, formed during hydrogen reaction experiments. The treated glass samples were examined in low vacuum

mode, allowing for examination of uncontaminated, non-sputter-coated glass samples to investigate morphology and depth of crystallization. Selected samples were sectioned perpendicular to the thickness. Fractured samples for examination of the reacted surface layer were prepared using the technique illustrated in Figure 7.1. The as-received samples, and their corresponding dimensions, are shown at the top of the schematic. The as-received samples, originally circular in shape, were cut in half to conserve sample and create samples with proper dimensions to fit our sample holders. The treated samples were fractured perpendicular to the thickness to investigate the morphology and depth of crystallization. To create a fracture surface, the samples were cut half way through the thickness and fractured by bending. The removed section was mounted on the sample holder with the orientation shown in the last step of the schematic. The treated glass samples were examined in low vacuum mode, allowing for examination of uncontaminated, non-sputtered glass samples to investigate morphology and depth of crystallization at the exposed surfaces of each of the treated glass samples. An accelerating potential of 30 kV was used for all images, unless otherwise noted. Images obtained with the ESEM were taken in either secondary electron mode or backscatter electron mode; the mode used is noted in the figure caption of each image.

X-ray diffraction (XRD) measurements were performed on selected samples to investigate the possible presence of crystalline phases, including colloidal particles, formed during hydrogen reaction experiments. Phase identification XRD measurements were performed using a Siemens D500 equipped with an mBraun position-sensitive detector. Samples were positioned with the crystalline surface of the bulk samples at the plane of diffraction. Scans were conducted using a scan speed of 3 degrees 2θ/minute from 20 to 120 degrees 2θ. Due to the very small quantity of each phase present, a long count time was necessary. In every measurement, the x-ray tube was operated at 40 kV and 20 mA with a copper target. The sharp lines present in the XRD pattern were used for crystal identification through comparison with standard data from International Centre for Diffraction Data (ICDD) powder diffraction files.

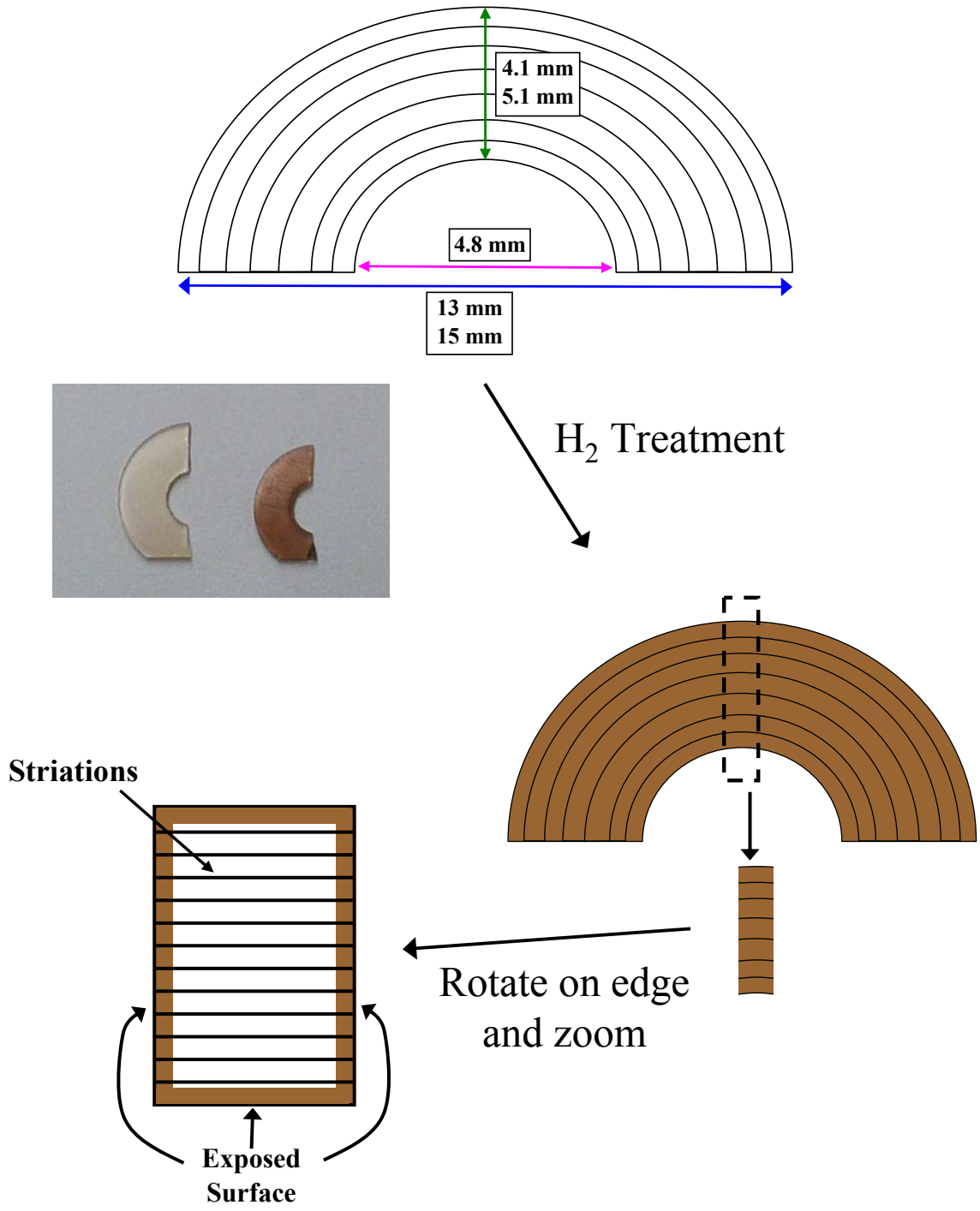

Figure 7.1. Schematic of the procedure used to create fractured samples of the treated binary GeO_2-SiO_2 glasses for ESEM analysis, including length measurements for the as received glass samples. Measurements on the top of the boxes with two values are for the 14.6 mol% GeO_2-85.4 mol% SiO_2 glasses and the values on the bottom are for the 6 mol% GeO_2-94 mol% SiO_2 glasses.

The possible presence of crystalline phases, including colloidal particles, formed during hydrogen reaction experiments was also examined using Raman spectroscopy. Raman scattering measurements were made in a conventional 90° scattering configuration. Data reported were obtained at room temperature, with spectra excited by the 532 nm line of a frequency doubled Nd:YAG laser. The Raman frequency shifts were calibrated between runs using a silicon plate standard. The Raman spectrum of silicon has a characteristic silicon line at 520 cm^{-1}, which was used for calibration purposes, as well as to maximize the signal intensity by adjusting the laser power. A liquid nitrogen cooled silicon CCD matrix was used and the spectral resolution was approximately 1 cm^{-1}.

7.3. Results

7.3.1. Hydrogen-Induced Crystal Formation at 800°C

Spectra and micrographs of samples treated at 800ºC are discussed in the most detail because these samples exhibit the most pronounced crystallization effects. It is easier, therefore, to follow details necessary to examine results for treatment at other temperatures. Figure 7.2 shows the backscatter electron micrograph of the treated surface of a 14.6 mol% GeO_2-85.4 mol% SiO_2 glass treated at 800°C and 700 Torr hydrogen for 100 hours, taken in low vacuum mode, 7615X magnification. The surface of the treated sample shows a significant amount of crystallization, evident as small bright circular features with no clear identifiable morphology. In backscatter electron mode, the bright lines indicate regions of the sample with a higher average atomic number. In this particular micrograph, the bright areas represent regions of crystallization, i.e. crystals in a glass matrix have a higher average atomic number. With higher magnification of the same area on the treated sample surface, Figure 7.3, it is easier to examine the size of the spherically shaped crystal features. Figure 7.3 (A) shows the backscatter electron micrograph of the treated surface of a 14.6 mol% GeO_2-85.4 mol% SiO_2 glass treated at 800°C and 700 Torr hydrogen for 100 hours, taken in low vacuum mode, 51936X

magnification. The circular feature in the surface of the treated sample shows small, slightly unfocused clusters (~200 nm) surrounded by individual, smaller (~30 - 40 nm) crystalline features. Figure 7.3 (B) shows the negative image of (A). The negative image shows the difference in intensity with depth more clearly, confirming the circular morphology of the crystals.

The lack of morphology and uniformity of crystallization observed along the entire surface of the treated sample, however, was not observed at a small fracture on the edge of the sample. A rather strange crystallization pattern was observed, as is shown in Figures 7.4 and 7.5, which show backscatter electron micrographs of a fracture at the edge of a 14.6 mol% GeO_2-85.4 mol% SiO_2 glass treated at 800°C and 700 Torr hydrogen for 64 hours, with a 923X magnification. The angle of the fracture is unknown, but it is clear that the crystallization was deeper along the striations. With further magnification up to 12417X, the octahedral morphology of the crystals becomes more obvious. The presence of a definite morphology below the surface and the increase concentration of crystals along the striations suggested further examination of interior of the treated samples.

The treated samples were fractured perpendicular to the thickness to investigate the morphology and depth of crystallization, as explained in the experimental procedures. Figure 7.6 shows the backscatter electron micrograph of the fractured surface edge of a 14.6 mol% GeO_2-85.4 mol% SiO_2 glass treated at 800°C and 700 Torr hydrogen for 64 hours, with a 1139X magnification. The striations, i.e. compositional variation in the glass with a 35 μm spacing described in detail in Chapter 4, are evident as three bright lines in the image, indicating regions of higher germanium content in the glass. A layer of crystallization, approximately 1- 2 μm in depth, is present along the entire exposed surface of the sample. The white circle outlines an irregular growth of crystals deeper than the 1- 2 μm crystallization layer on the exposed surface of the sample that appears to follows the bright lines of the striations.

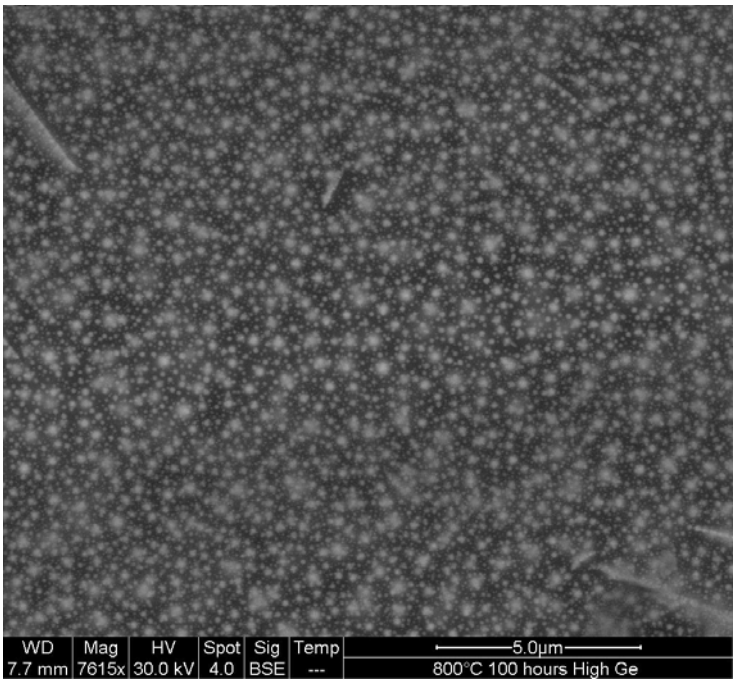

Figure 7.2. Backscatter electron micrograph of the treated surface of a 14.6 mol% GeO_2-85.4 mol% SiO_2 glass treated at 800°C and 700 Torr hydrogen for 100 hours, taken in low vacuum mode, 7615X magnification.

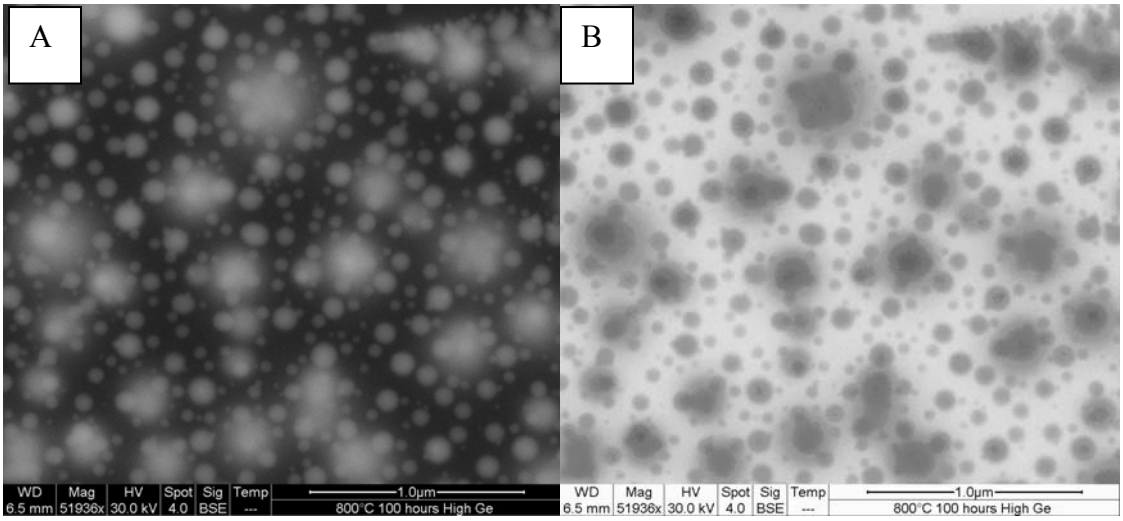

Figure 7.3. A) Backscatter electron micrograph of the treated surface of a 14.6 mol% GeO_2-85.4 mol% SiO_2 glass treated at 800°C and 700 Torr hydrogen for 100 hours, taken in low vacuum mode, 51936X magnification. B) The negative image of A.

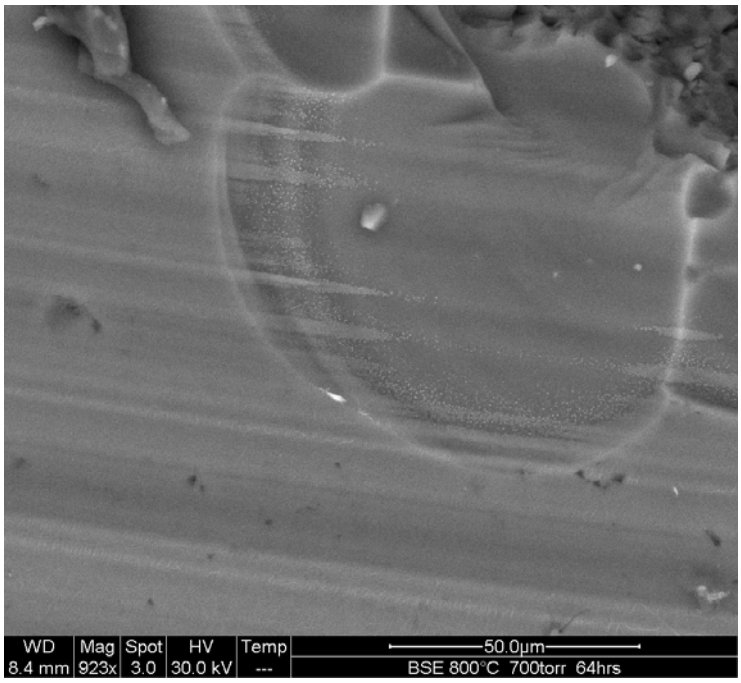

Figure 7.4. Backscatter electron micrograph of a fractured edge of a 14.6 mol% GeO_2-85.4 mol% SiO_2 glass treated at 800°C and 700 Torr hydrogen for 64 hours, taken in low vacuum mode, 923X magnification.

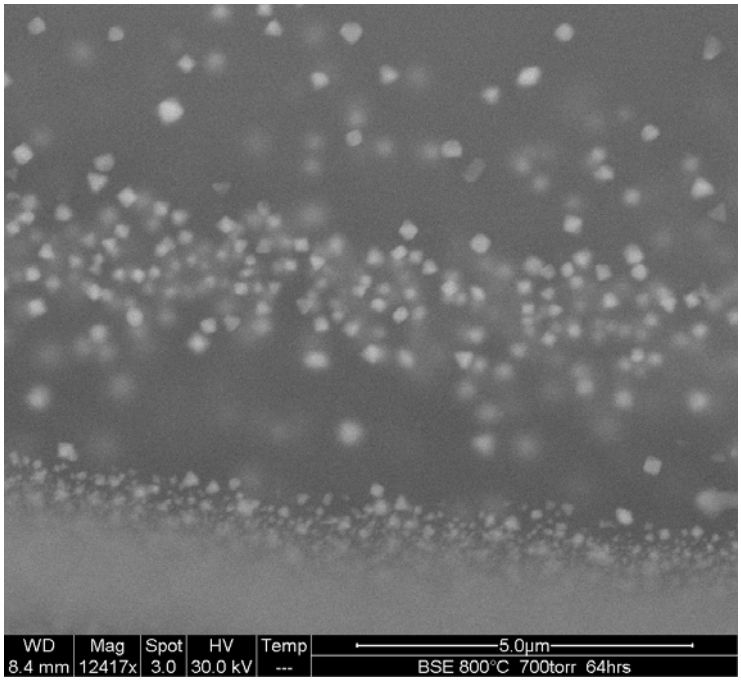

Figure 7.5. Backscatter electron micrograph of a fractured edge of a 14.6 mol% GeO_2-85.4 mol% SiO_2 glass treated at 800°C and 700 Torr hydrogen for 64 hours, taken in low vacuum mode, 12417X magnification.

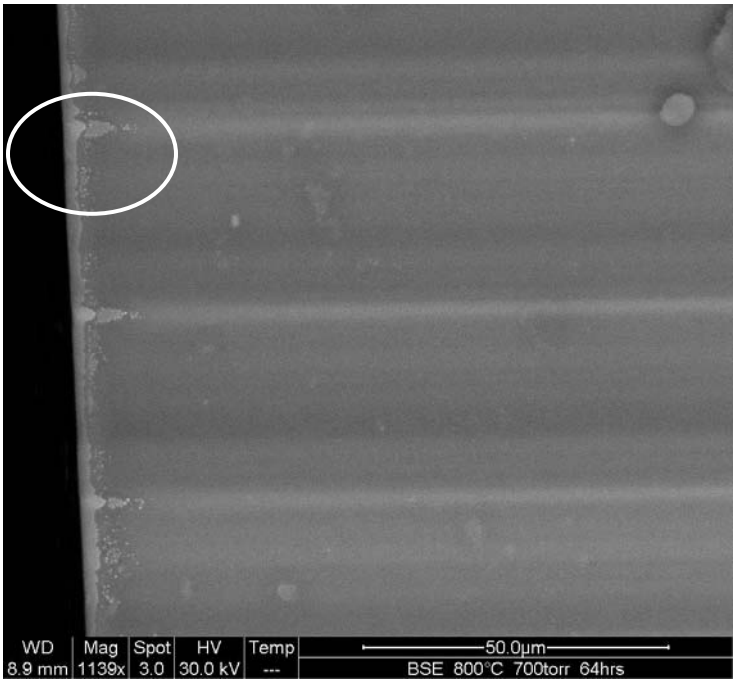

Figure 7.6. Backscatter electron micrograph of the fractured surface edge of a 14.6 mol% GeO_2-85.4 mol% SiO_2 glass treated at 800°C and 700 Torr hydrogen for 64 hours, taken in low vacuum mode, 1139X magnification.

With higher magnification focused on areas of irregular crystal growth following the striations, the development of non-spherical morphology can be observed. Figures 7.7 and 7.8 show the backscatter electron micrograph of the fractured surface edge of a 14.6 mol% GeO_2-85.4 mol% SiO_2 glass treated at 800°C and 700 Torr hydrogen for 64 hours, with a 10840X and 11320X magnification, respectively. It is evident in both images that the presence of striations results in organized crystallization leading to the formation of finite features of subsurface nanocrystal clusters. A definite crystalline morphology is evident with even higher magnification, focused on the crystals formed deeper than the 1- 2 µm crystallization layer on the exposed surface of the sample that appears to follows the bright lines of the striations. Figure 7.9 shows the backscatter electron micrograph of the subsurface nanocrystal clusters of the 14.6 mol% GeO_2-85.4 mol% SiO_2 glass treated at 800°C and 700 Torr hydrogen for 64 hours, with a 30659X magnification. The bright crystal in the center of the magnified micrograph appears to be an octahedral crystal lying on its side. When the magnification is increased to 173434X, all other conditions held constant, the actual size (~400 nm) of the largest crystal can be

determined from the backscatter electron micrograph shown in Figure 7.10. The micrograph in Figure 7.11 shows the backscatter electron micrograph of an inside fracture surface, i.e. the center of the glass sample, of a 14.6 mol% GeO_2-85.4 mol% SiO_2 glass treated at 800°C and 700 Torr hydrogen for 50 hours, with a 500X magnification. No detectable crystallization is observed in this micrograph. Similar micrographs where taken for many glasses treated in hydrogen at 800°C, indicating that significant growth of crystals was confined to the surface of the sample and the interior of the sample, i.e. the section of the sample shielded from exposure to hydrogen, remained glassy. This finding does not mean, however, that nucleation did not occur throughout the thickness of the sample, only that growth of crystals to a size sufficient to be observable by the ESEM happened only at the surfaces of the glass.

In addition to the obvious change in optical appearance of the glass sample, examination under high magnification reveals the surfaces of treated glasses are not as smooth as the parent glass, resulting from the stresses generated as a result of volume changes associated with the growth of crystals within the glass. The formation of large crystals may lead to generation of prohibitively high stresses, which could result in fracture of the glass. There was also a noticeable degree of surface roughening and surface degradation occurring with treatment. The cause of the surface roughening is not yet established. The roughening could be a result of formation and spalling of crystals or preferential etching due to treatments with hydrogen gas itself. Hydrogen can preferentially etch GeO_2 from the surface.

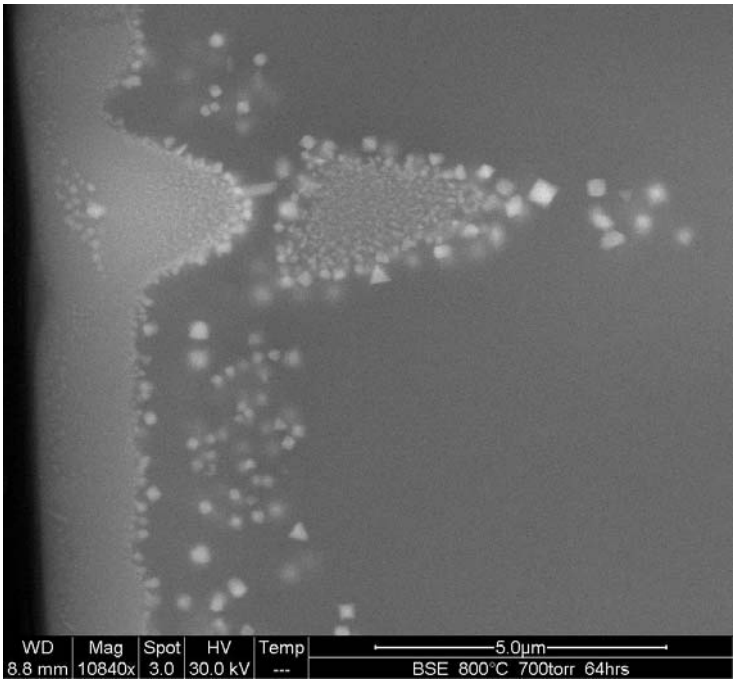

Figure 7.7. Backscatter electron micrograph of the fractured surface edge of a 14.6 mol% GeO_2-85.4 mol% SiO_2 glass treated at 800°C and 700 Torr hydrogen for 64 hours, taken in low vacuum mode, 10840X magnification.

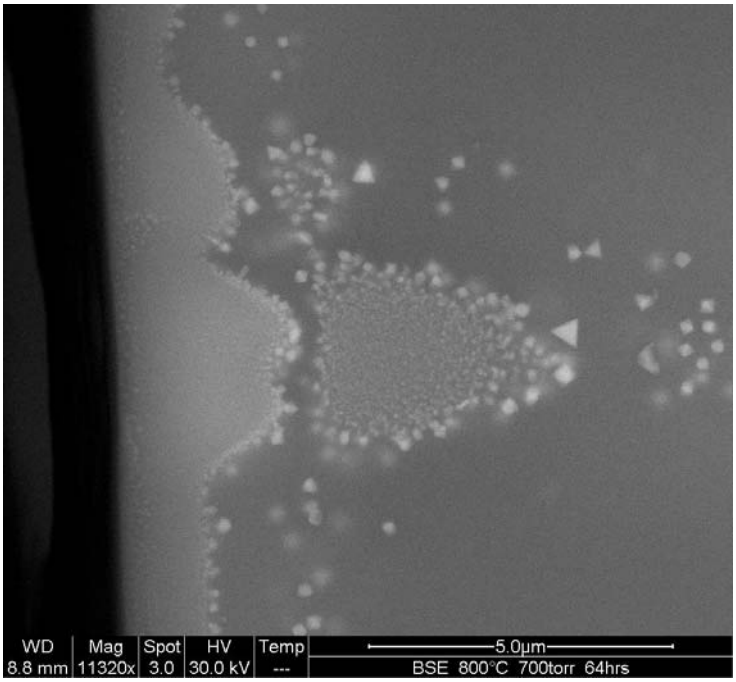

Figure 7.8. Backscatter electron micrograph of the fractured surface edge of a 14.6 mol% GeO_2-85.4 mol% SiO_2 glass treated at 800°C and 700 Torr H_2 for 64 hours, taken in low vacuum mode, 11320X magnification.

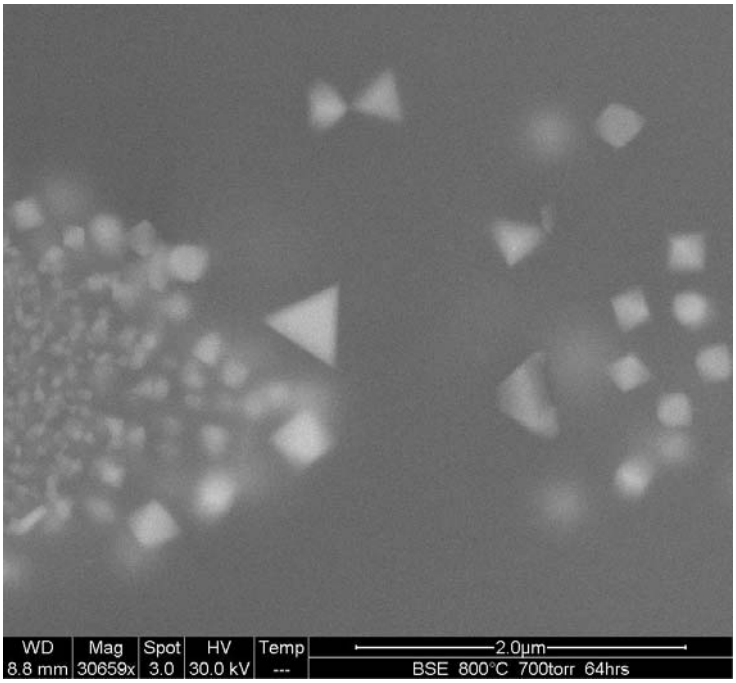

Figure 7.9. Backscatter electron micrograph of the subsurface nanocrytsal clusters of the 14.6 mol% GeO_2-85.4 mol% SiO_2 glass treated at 800°C and 700 Torr hydrogen for 64 hours, taken in low vacuum mode, 30659X magnification.

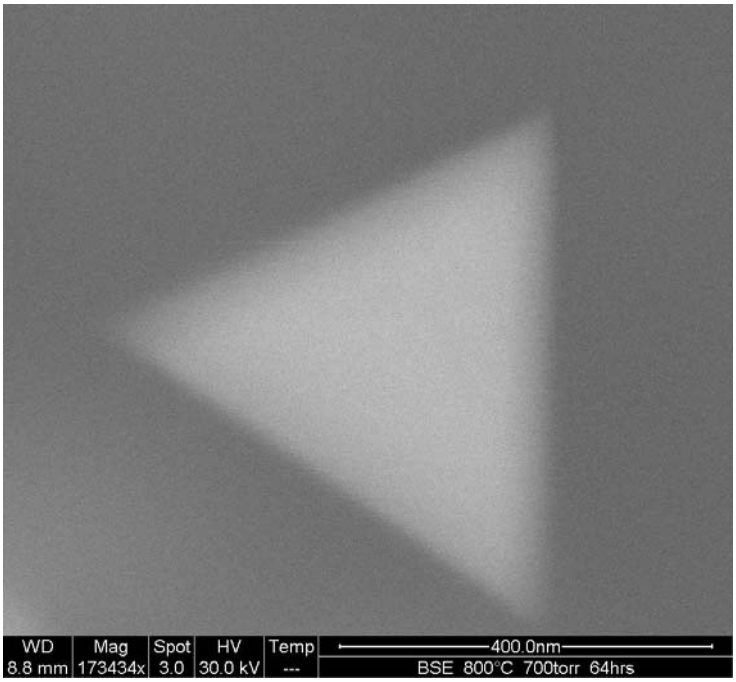

Figure 7.10. Backscatter electron micrograph of nanocrystal formed near the surface of a 14.6 mol% GeO_2-85.4 mol% SiO_2 glass treated at 800°C and 700 Torr hydrogen for 64 hours, taken in low vacuum mode, 173434X magnification.

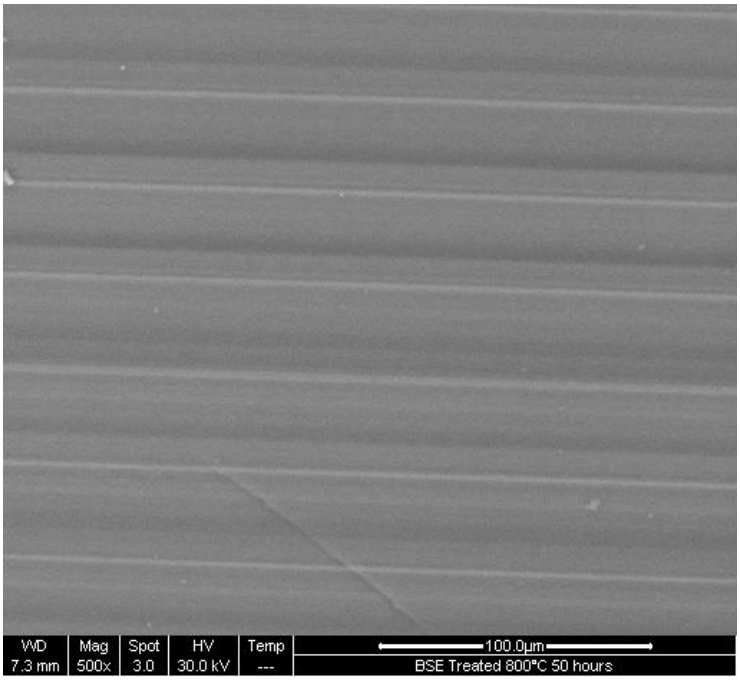

Figure 7.11. Backscatter electron micrograph of an inside fracture surface of a 14.6 mol% GeO_2-85.4 mol% SiO_2 glass treated at 800°C and 700 Torr hydrogen for 50 hours, taken in low vacuum mode, 500X magnification.

7.3.2. Crystallization Associated with Color Formation

The observation of a layer of crystallization at the surface of the sample without detectable crystallization within the surfaces of the sample corresponds well with observation that color formation was also confined to the surfaces that the sample that were exposed to hydrogen at elevated temperatures. Further proof of the color formation is associated with the crystal formation in the samples was observed when a treated sample was progressively polished to examine the depth of color formation. One millimeter thick plates of each of the as-received binary GeO_2-SiO_2 glasses were treated under a hydrogen atmosphere (pH_2 = 93 kPa) at 800°C for 100 hours. Each of the treated glasses was polished on each of the previously cut and polished, hydrogen exposed surfaces to remove the induced color. Progressive polishing of the exposed sample surfaces revealed that, although color formation was uniform over the entire surface, removal of the uniform layer of color resulted in a sample with alternating layers of colorless, transparent glass and dark brown rings. The position of the dark brown stripes corresponds with the striations in the glass. This observation indicates that, below the

uniform formation of color along the surface, rippled bands of color are formed that correspond with the striations, i.e. color formation is deeper along the striations. The sample with the dark brown stripes following the striations was examined using the ESEM. Figure 7.12 shows the backscatter electron micrograph of a 6 mol% GeO_2-94 mol% SiO_2 glass treated at 800°C and 700 Torr hydrogen for 100 hours, taken in low vacuum mode, 1030X magnification. The image clearly shows crystallization confined to the striation as one would expect to observe if the uniform 1 - 2 μm layer in Figure 7.4 was removed. The observation that crystallization and brown color exist only along the striations in this sample substantiated the contention that the dark brown color formation results from the formation of crystals in the glass.

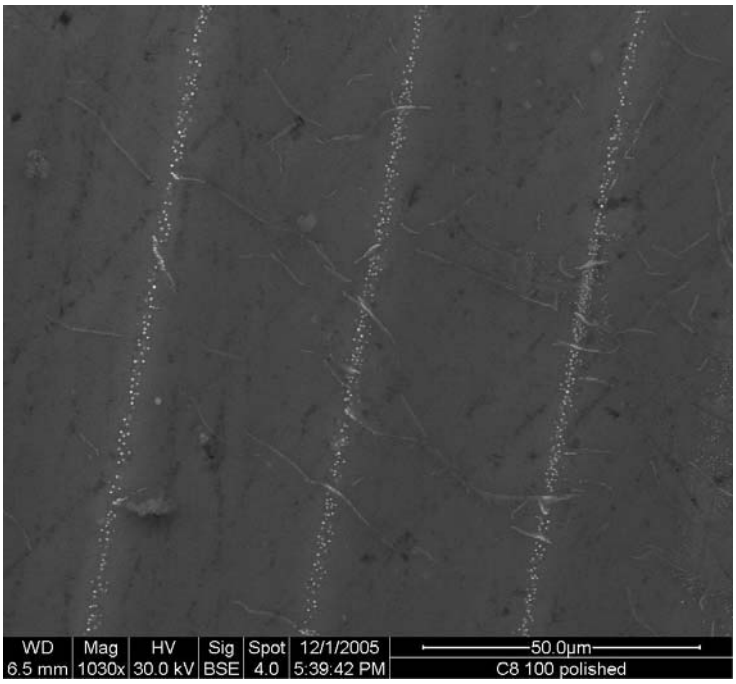

Figure 7.12. Backscatter electron micrograph of a 6 mol% GeO_2-94 mol% SiO_2 glass treated at 800°C and 700 Torr hydrogen for 100 hours with the surface layer polished off, taken in low vacuum mode, 1030X magnification.

7.3.3. X-Ray Diffraction to Identify the Crystal Composition

The presence of crystals embedded within the treated binary GeO_2-SiO_2 glasses, which are large enough to be observed using an ESEM and are concentrated along the striations of higher germanium content, was irrefutable. The identity of the crystalline phase, however, was still unknown. Diffraction patterns were obtained from the reacted surface of selected solid samples to investigate the identity of all crystalline phases present including colloidal particles formed during hydrogen reactions. Figure 7.13 shows the XRD spectra for 14.6 mol% GeO_2-85.4 mol% SiO_2 glass treated at 700°C and 700 Torr hydrogen for a total of 144 hours. The amorphous hump is clearly observable at around 23 degrees 2θ. The dark black lines along the x-axis of the plot represent the peak positions for germanium, obtained from PDF # 00-004-0545, Table 7.I. Five relatively diffuse peaks that correspond well with the expected peak positions for crystalline germanium can be observed in XRD spectra in Figure 7.13, and are assigned to germanium (1 1 1), (2 2 0), (3 1 1), (4 0 0) and (3 3 1) diffraction lines, indicating the presence of crystalline germanium.

Table 7.I. Information Obtained from PDF # 00-004-0545 for Germanium.

Degrees 2θ	**Relative Intensity**	**(h k l)**
27.284	100	(1 1 1)
45.306	57	(2 2 0)
53.683	39	(3 1 1)
66.017	7	(4 0 0)
72.804	10	(3 3 1)

Figures 7.14 – 7.17 show the XRD spectra for binary GeO_2-SiO_2 glasses treated at 500°C, 600°C, 700°C and 800°C, respectively, and 700 Torr hydrogen for the indicated total treatment times. The XRD spectra for different treatment conditions for each temperature are offset to allow comparison between samples treated at the same temperature. The XRD spectra for the as-received glasses are included on each figure to show the samples were x-ray amorphous in the as-received condition. Samples treated at 500°C, Figure 7.14, for 100 hours or 256 hours are also x-ray amorphous, i.e. show no

detectable signs of crystal formation. Figure 7.15, the XRD spectra from glasses treated at 600°C, shows that only the 14.6 mol% GeO_2-85.4 mol% SiO_2 glass treated for 144 hours has a detectable amount of crystalline germanium. Significant germanium crystallization is observed, Figure 7.16, in the both of the 14.6 mol% GeO_2-85.4 mol% SiO_2 glasses treated at 700°C for 100 or 144 hours, however, the 6 mol% GeO_2-94 mol% SiO_2 glass show significant crystallization only in the sample treated for 144 hours. The 6 mol% GeO_2-94 mol% SiO_2 glass treated at 800°C for 100 hours does show, Figure 7.17, significant germanium crystallization, however, the 14.6 mol% GeO_2-85.4 mol% SiO_2 glass treated for 100 hours shows significant formation of a second crystalline phase. The 14.6 mol% GeO_2-85.4 mol% SiO_2 glass treated at 800ºC for 100 hours, plotted separately in Figure 7.18, shows a significant amount of silica cristobalite (SiO_2), PDF # 00-039-1425, summarized in Table 7.II, as well as germanium.

Table 7.II. Information Obtained from PDF # 00-039-1425 for SiO_2, Cristobalite.

Degrees 2θ	**Relative Intensity**	**(h k l)**	**Degrees 2θ**	**Relative Intensity**	**(h k l)**	**Degrees 2θ**	**Relative Intensity**	**(h k l)**
21.985	100	(1 0 1)	51.94	1	(2 2 0)	65.65	1	(2 0 4)
25.32	1	(1 1 0)	52.869	1	(0 0 4)	66.813	1	(2 2 3)
28.439	8	(1 1 1)	54.156	2	(2 0 3)	68.676	2	(2 1 4)
31.462	9	(1 0 2)	56.22	1	(1 0 4)	69.42	1	(3 2 1)
36.08	13	(2 0 0)	57.084	3	(3 0 1)	69.79	1	(3 0 3)
36.381	4	(1 1 2)	57.507	1	(2 1 3)	70.542	1	(1 0 5)
38.41	1	(2 0 1)	58.68	1	(3 1 0)	72.69	1	(3 1 3)
42.656	2	(2 1 1)	58.869	1	(2 2 2)	73.907	1	(3 2 2)
44.843	2	(2 0 2)	60.304	2	(3 1 1)	77.312	1	(2 2 4)
47.063	4	(1 1 3)	62.019	2	(3 0 2)	78.02	1	(4 0 1)
48.611	4	(2 1 2)	65.102	2	(3 1 2)	79.394	1	(4 1 0)

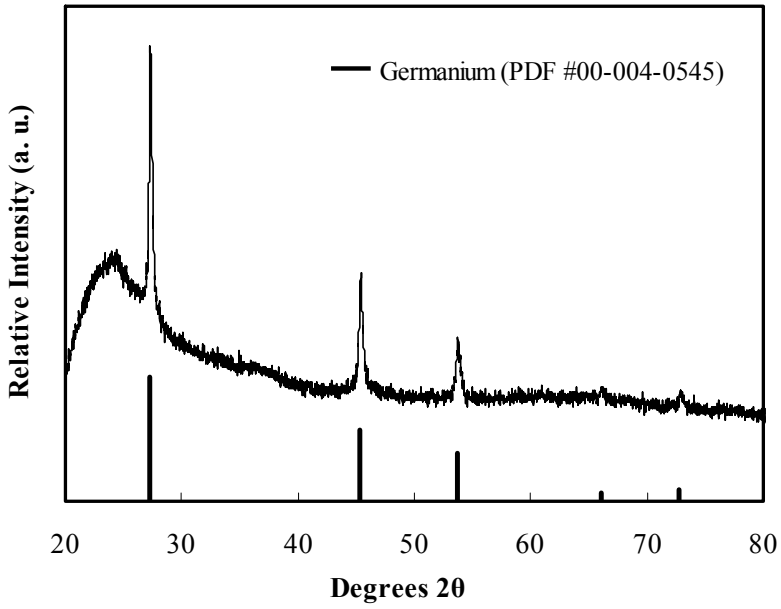

Figure 7.13. XRD pattern for 14.6 mol% GeO_2-85.4 mol% SiO_2 glass treated at 700°C and 700 Torr hydrogen for 144 hours.

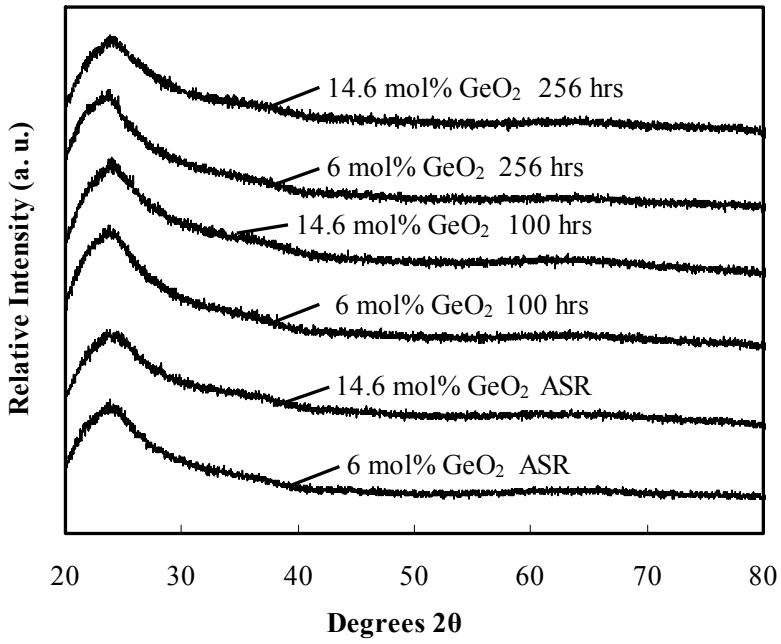

Figure 7.14. XRD pattern for binary GeO_2-SiO_2 glasses treated at 500°C and 700 Torr hydrogen for the indicated total treatment time.

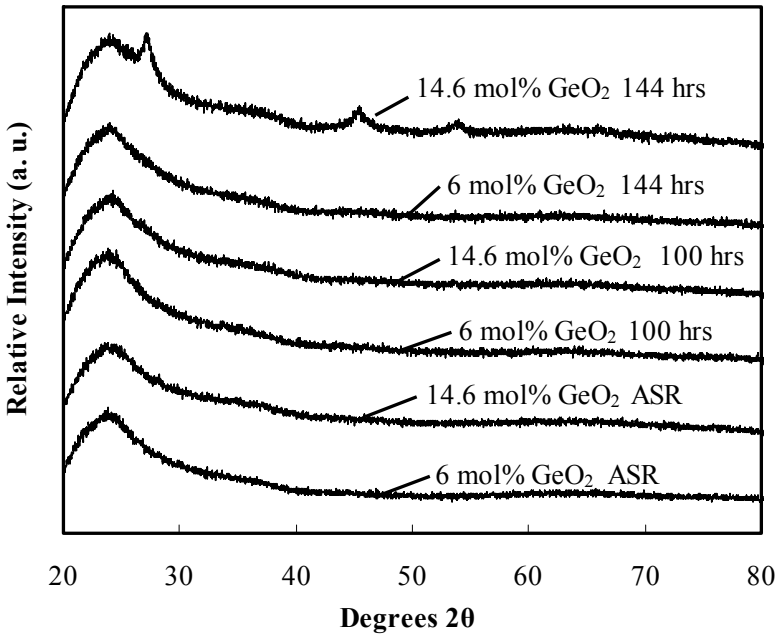

Figure 7.15. XRD pattern for binary GeO_2-SiO_2 glasses treated at 600°C and 700 Torr hydrogen for the indicated total treatment time.

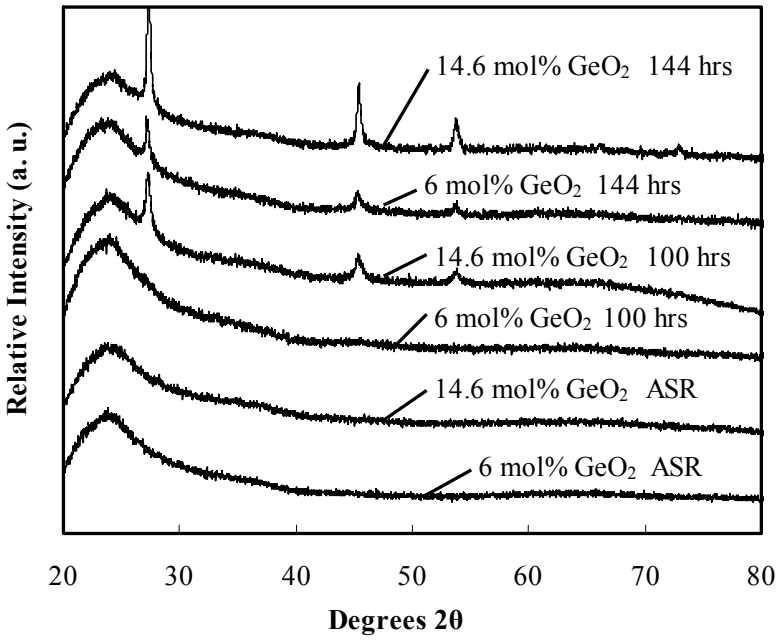

Figure 7.16. XRD pattern for binary GeO_2-SiO_2 glasses treated at 700°C and 700 Torr hydrogen for the indicated total treatment time.

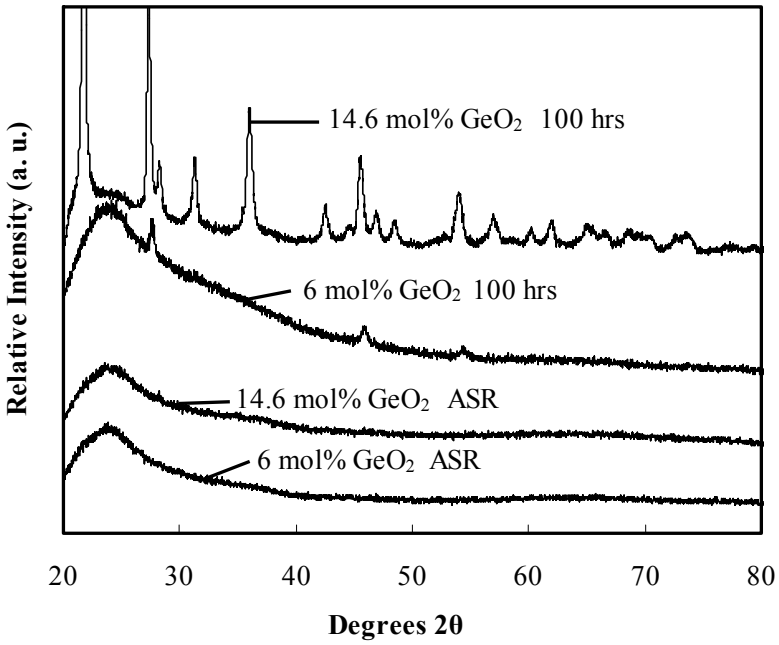

Figure 7.17. XRD pattern for binary GeO_2-SiO_2 glasses treated at 800°C and 700 Torr hydrogen for the indicated total treatment time.

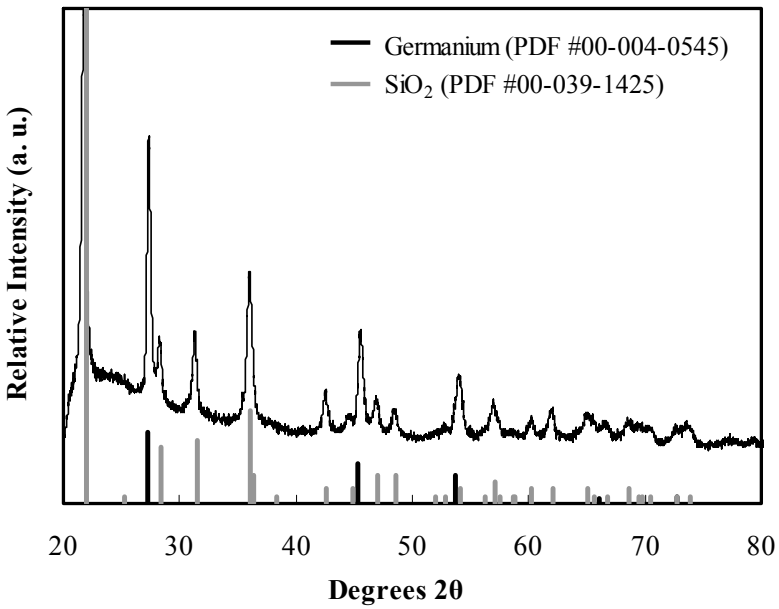

Figure 7.18. XRD pattern for 14.6 mol% GeO_2-85.4 mol% SiO_2 glass treated at 800°C and 700 Torr hydrogen for 100 hours.

The effect of temperature on hydrogen-induced crystal formation is apparent when the XRD patterns of the binary GeO_2-SiO_2 glasses treated at different temperatures are compared. Although no quantitative statements can be made about the extent of crystallization and size of the individual crystals, a few qualitative observations can be made. In general, crystallization develops at a much faster rate at higher temperatures and in the binary glasses with a higher germanium content. As would be expected, longer treatment times also show increased development of crystals in the glass.

7.3.4. Raman Spectroscopy to Confirm the Identity of the Crystal Composition

It has been established that Raman spectroscopy can be used as a tool to observe the formation and growth of germanium nanocrystals in a binary GeO_2-SiO_2 glass matrix.[1,4-7,11] Raman spectroscopy was used to investigate the presence of germanium nanocrystals embedded in the binary GeO_2-SiO_2 glasses treated in this study. A typical Raman spectrum for the 6 mol% GeO_2-94 mol% SiO_2 glass, treated at 800°C and 700 Torr of hydrogen for 64 hours is shown in Figure 7.19. Composite materials, including glass-ceramics, often have identifiable units associated with individual components that contribute distinct features to the Raman spectrum. The intense, sharp band at approximately 300 cm^{-1}, Figure 7.19, indicates the presence of germanium nanocrystals in binary GeO_2-SiO_2 glass. The extreme difference in intensity of the 300 cm^{-1} band as compared to the glass structural bands in the region from 100 to 600 cm^{-1} is obvious.

Raman spectra were obtained from the treated surface of select solid samples to confirm the presence of germanium nanocrystals. Figures 7.20 – 7.23 show the Raman spectra for binary GeO_2-SiO_2 glasses treated at 500°C, 600°C, 700°C and 800°C, respectively, and 700 Torr hydrogen for the indicated total treatment times. Raman spectra for different treatment conditions for each temperature are offset to allow comparison between samples treated at the same temperature. The actual position of the band attributed to the presence of germanium nanocrystals in this study ranges from 292 to 301 cm^{-1}, with no clear trend in the position of the band with respect to treatment temperature, treatment time or crystal size. The band at approximately 300 cm^{-1} is not detected in the as-received samples and only appears after extensive treatment in hydrogen. The intense, sharp band at approximately 300 cm^{-1} is observed in all treated

glasses, except the glasses treated at 500°C for up to 100 hours and the presence of ripple in the spectrum is perhaps questionable. The intensity of the band is significantly affected by treatment with hydrogen. In general, the intensity of the band increases with increasing temperature when compared to the intensity of the structural bands, which form the background in this region.

The effect of temperature on hydrogen-induced crystal formation is apparent when the Raman spectra of the binary GeO_2-SiO_2 glasses treated at different temperatures are compared. Although no quantitative statements can be made about the size of the individual crystals, a few qualitative observations can be made. In general, crystallization develops at a much faster rate at higher temperatures and in the binary glasses with a higher germanium content. As would be expected, longer treatment times also show increased development of crystals embedded in the glass.

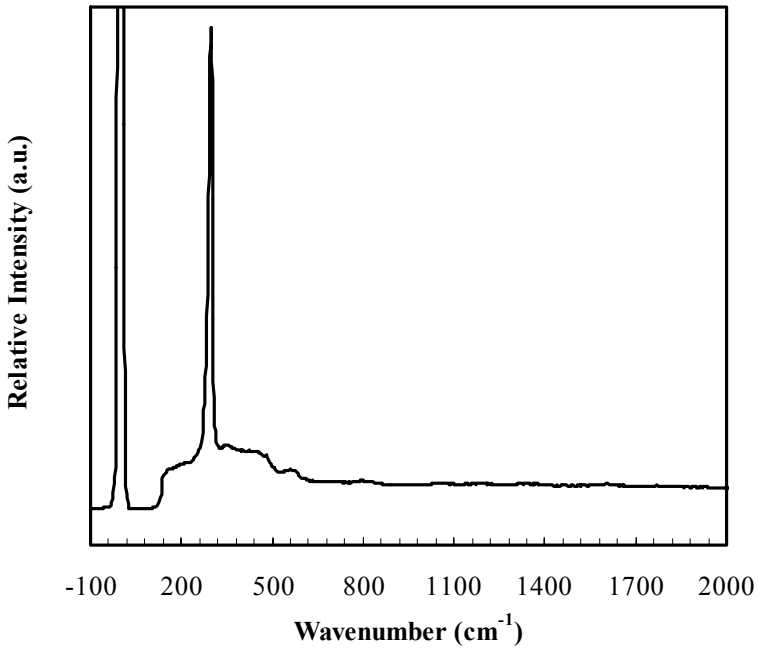

Figure 7.19. Raman spectra for 6 mol% GeO_2-94 mol% SiO_2 glass treated at 800°C and 700 Torr hydrogen for 64 hours.

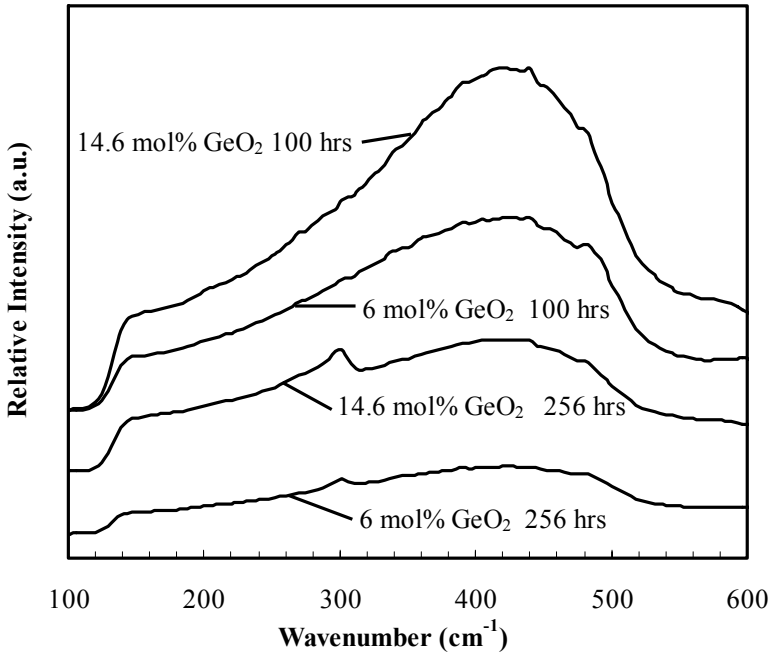

Figure 7.20. Raman spectra for binary GeO_2-SiO_2 glasses treated at 500°C and 700 Torr hydrogen for the indicated total treatment time.

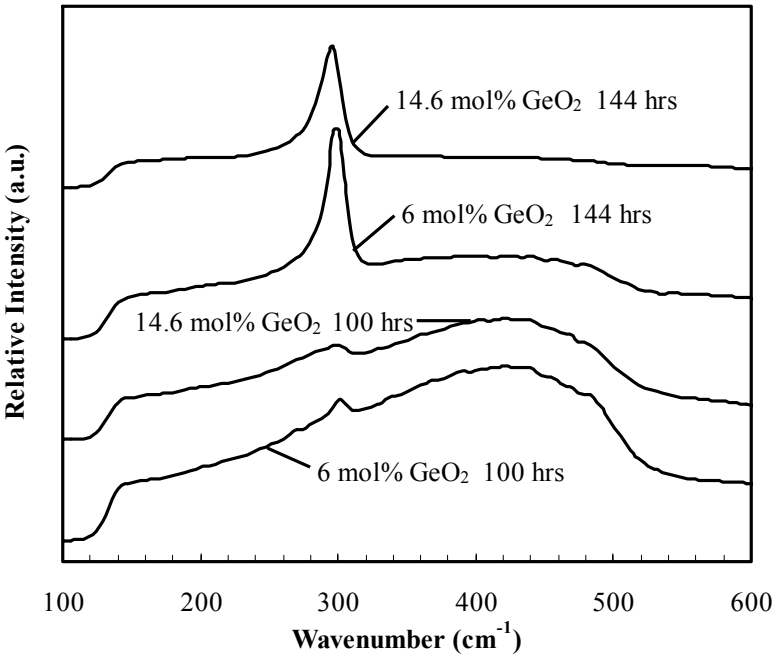

Figure 7.21. Raman spectra for binary GeO_2-SiO_2 glasses treated at 600°C and 700 Torr hydrogen for the indicated total treatment time.

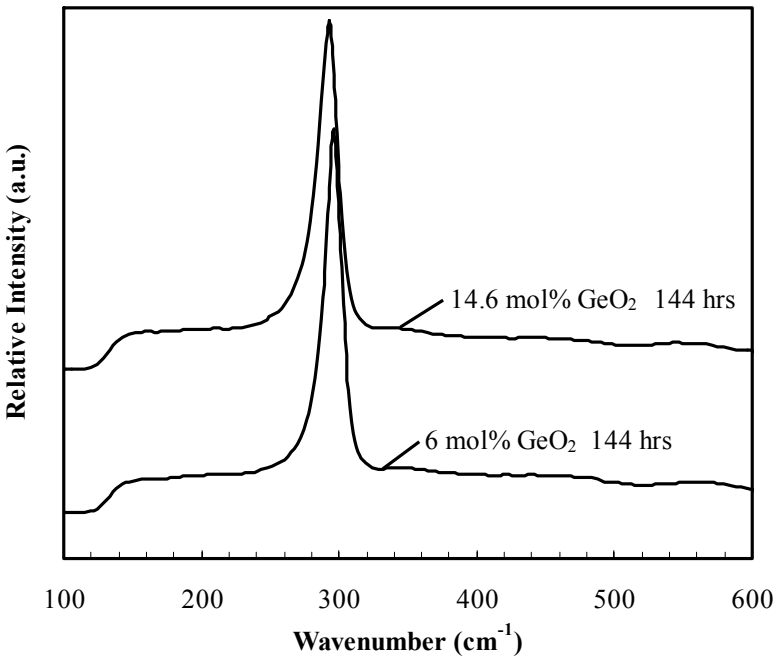

Figure 7.22. Raman spectra for binary GeO_2-SiO_2 glasses treated at 700°C and 700 Torr hydrogen for the indicated total treatment time.

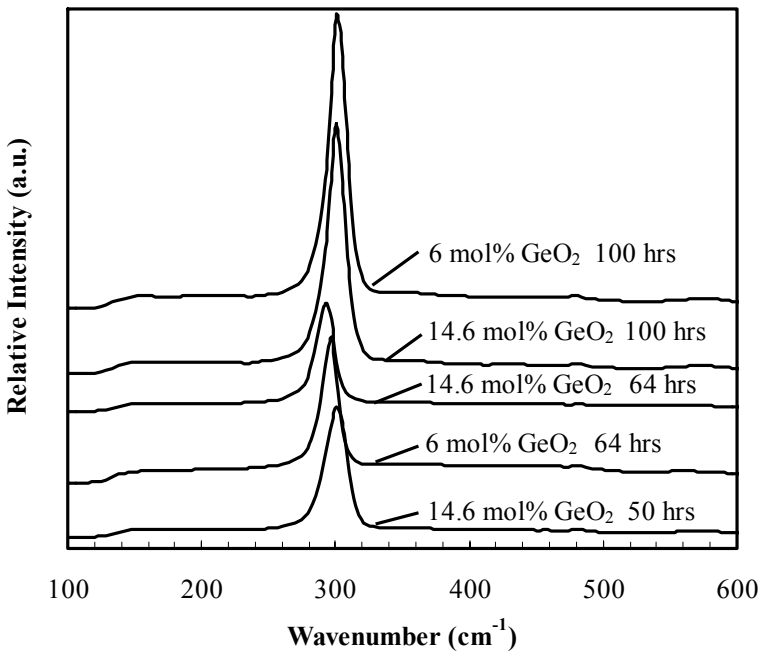

Figure 7.23. Raman spectra for binary GeO_2-SiO_2 glasses treated at 800°C and 700 Torr hydrogen for the indicated total treatment time.

7.3.5. Increased Sensitivity of Raman Spectroscopy Compared to X-ray

The use of Raman spectroscopy to confirm the presence and identity of germanium in the glass samples is invaluable. Table 7.I reports the experimental conditions used to treat the binary glasses and resulting detectable presence of crystallization in the glass as determined from both XRD and Raman spectroscopy. Clearly, Raman spectroscopy is significantly more sensitive to the presence of germanium nanocrystals in the surface of the binary GeO_2-SiO_2 glasses.

Table 7.III. Table of Experimental Conditions and Resulting Detectable Presence of Crystallization Observed in XRD and Raman Spectroscopy.*

6.0 mol % GeO_2				**14.6 mol % GeO_2**			
Temperature (ºC)	Time (hrs)	Crystallization XRD	Crystallization Raman	Temperature (ºC)	Time (hrs)	Crystallization XRD	Crystallization Raman
500	100			500	100		
500	255		X	500	255		X
600	100		X	600	100		X
600	144		X	600	144	X	X
700	100		X	700	100	X	X
700	144	X	X	700	144	X	X
800	64	X	X	800	50	X	X
800	100	X	X	800	100	X	X

* The "X" indicates the observed presence of germanium crystals in the treated surface of the glass.

Increased sensitivity is not the only advantage of Raman spectroscopy over XRD. The Raman microprobe couples an optical microscope and a conventional Raman spectrometer and uses a tightly focused, short-wavelength laser source, enabling focused measurements with micron spatial resolution. The microprobe is also designed to scan samples spatially while probing very small volumes, allowing for examination of variations in properties as a function of position. The Raman microprobe was set-up to raster-scan the surface of a treated sample to investigate the uniformity of crystallization along the as-treated surface. The spectrometer was set to record the peak intensity at 300 cm^{-1} and create an 80 μm by 80 μm image of the peak intensity over the treated surface. Figure 7.24 (a) shows the optical image of the treated surface of the 14.6 mol% GeO_2-

85.4 mol% SiO_2 glass treated at 800°C, 700 Torr of hydrogen for 50 hours. The white box over the image indicates the area over which the microscope scanned. Figure 7.24 (b) shows the 80 μm by 80 μm image of the peak intensity at 300 cm^{-1} measured using the confocal Raman with an automated stage. The scale bar below the image shows the change in color with increasing intensity at 300 cm^{-1}. Observation of the peak intensity at 300 cm^{-1} reveals the concentration of germanium nanocrystals along the surface, i.e. the peak intensity scales with the amount of germanium nanocrystals present. The results show that maximum intensity was highest along the striations of the treated glass surface, as would be expected, since the ESEM images show preferential growth of colloids along the striations.

7.3.6. Deuterium-Induced Crystallization

Supporting evidence of germanium nanocrystal formation, induced by the presence of protonic species, is provided when the binary GeO_2-SiO_2 glasses are treated at elevated temperatures in a deuterium atmosphere. Figure 7.25shows the XRD spectra for binary GeO_2-SiO_2 glasses treated at 800°C and 700 Torr deuterium for 64 hours. The spectra clearly show the presence of crystalline germanium forming in each glass with deuterium treatment. The 14.6 mol% GeO_2-85.4 mol% SiO_2 glass is also beginning to show the presence of cristobalite, with a small diffraction peak forming at approximately 22 degrees two theta. The corresponding Raman spectra, Figure 7.26, also show the presence of germanium nanocrystals in the binary GeO_2-SiO_2 glasses treated at 800°C and 700 Torr deuterium for 64 hours.

7.3.7. Induced Crystallization Resulting Only with Hydrogen Treatment

Each of the as-received binary GeO_2-SiO_2 glasses were treated at 800°C in both vacuum and ambient air atmospheres to ensure that induced crystal formation results from the presence of hydrogen in the atmosphere. XRD and Raman spectra show no detectable amount of induced crystallization after 100 hours of treatment in vacuum at or after 69 hours of treatment in ambient air at 800°C.

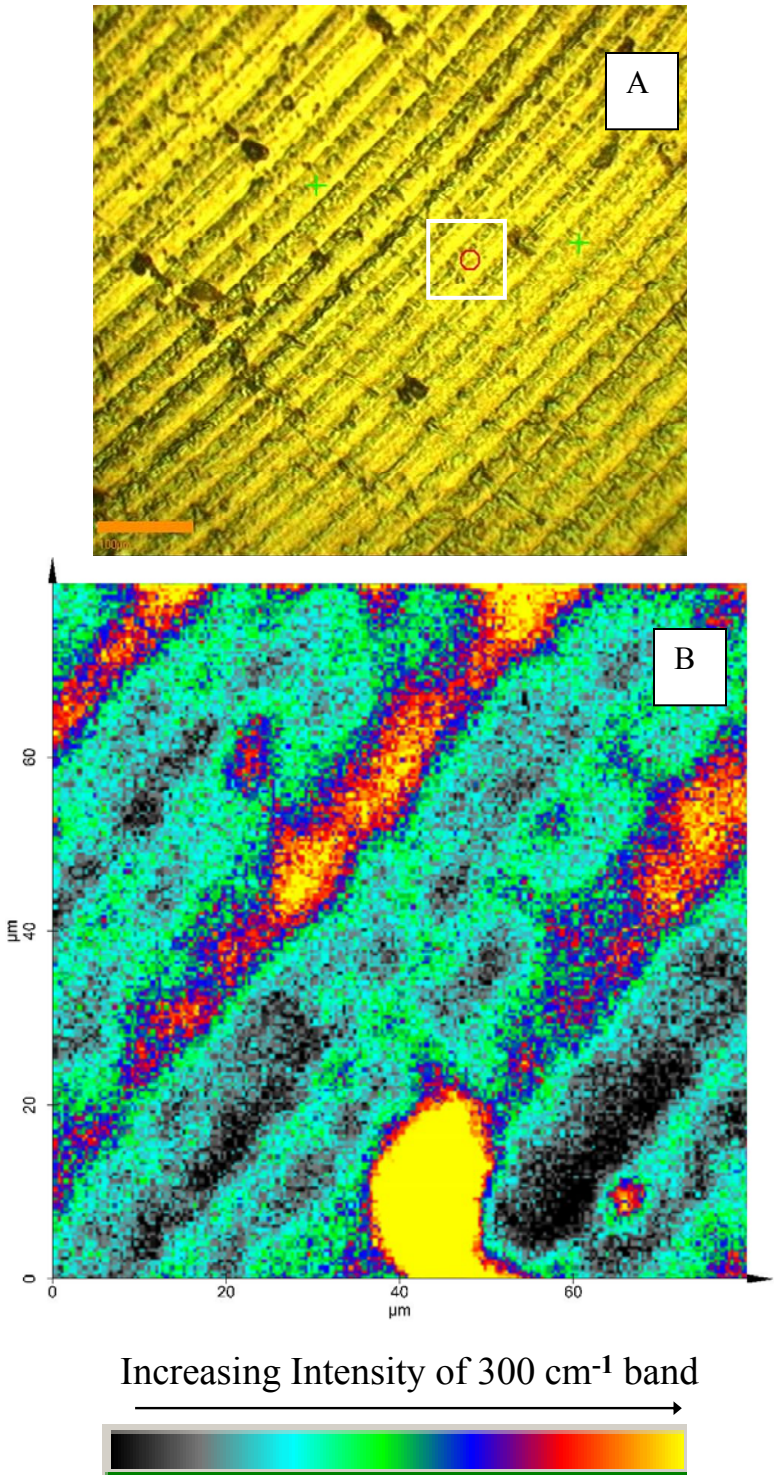

Figure 7.24. (A) Optical image of the treated surface of the 14.6 mol% GeO_2-85.4 mol% SiO_2 glass treated at 800°C, 700 Torr of hydrogen for 50 hours, (B) shows the 80 µm by 80 µm image of the peak intensity at 300 cm^{-1} corresponding with the area outlined in white in image (A).

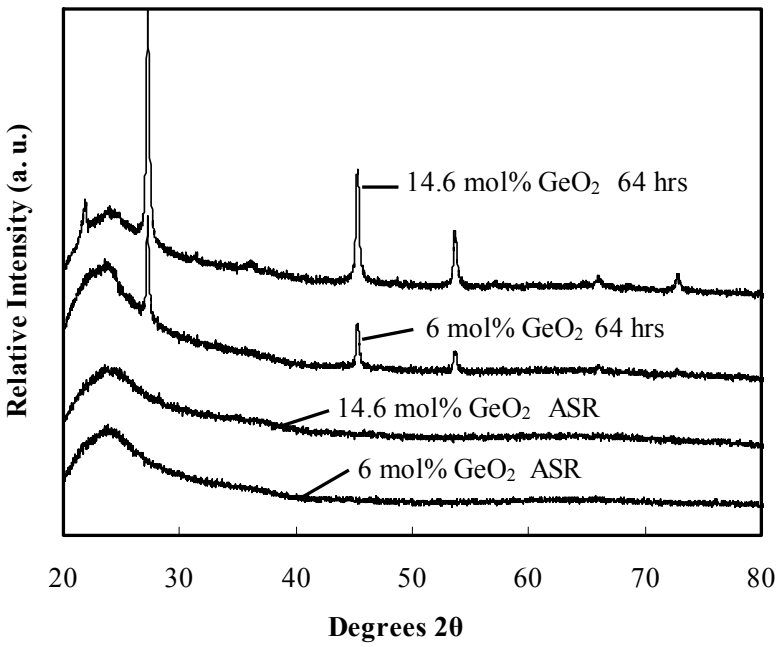

Figure 7.25. XRD spectra for binary GeO_2-SiO_2 glasses treated at 800°C and 700 Torr deuterium for the indicated total treatment time.

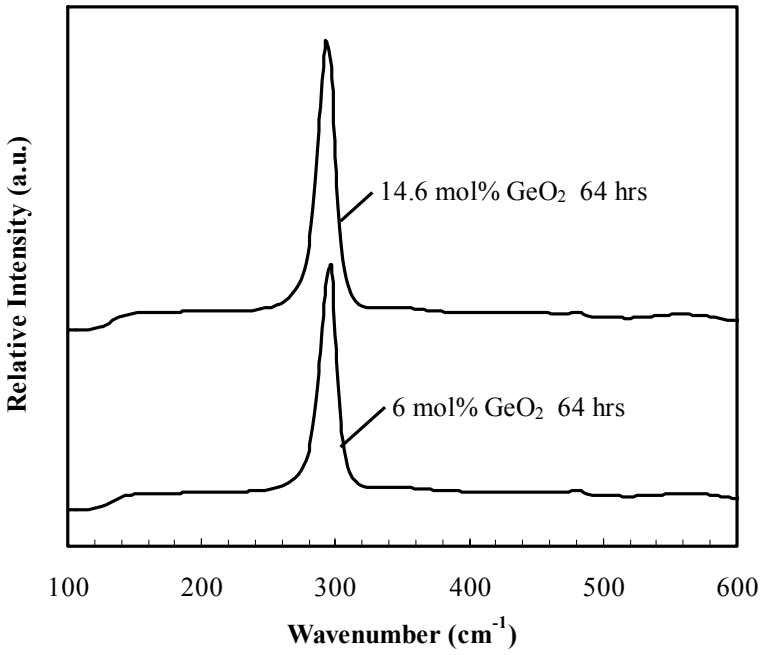

Figure 7.26. Raman spectra for binary GeO_2-SiO_2 glasses treated at 800°C and 700 Torr deuterium for the indicated total treatment time.

7.4. Discussion

7.4.1. Crystal Identification

Raman spectroscopy was used successfully in this study to identify reduced germanium species embedded in the glass. XRD results agreed well with the assignment of the 300 cm^{-1} Raman band, showing only formation of pure germanium crystals in most of the treated glass samples. As stated in the introduction, Fujii et al.[1] report a way to calculated the size of the germanium nanocrystals from the full width at half maximum (FWHM) values of the 300 cm^{-1} band. Although the exact calculations are not presented, a figure with an exponential curve is presented, allowing for extrapolation of particle size based on measured FWHM values. Discussion of the effect of size distribution and stress on the nanocrystal Raman signal is also presented. The presence of a size distribution could also cause non-negligible inhomogeneous broadening of the Raman line, resulting in the inability to use such analysis. FWHM values for the Raman spectra obtained in this study ranged from 17 to 23 cm^{-1}, suggesting an average particle size of 5 nm or less using the extrapolation method suggested by Fujii et al. The extrapolated values could be representative of the spherical germanium clusters observed on the as-treated surfaces of the samples, but the crystals formed only 1 μm below the surface are significantly larger than 5 nm, as shown in ESEM micrographs. Perhaps the sampling depth of the Raman microprobe measurement is significantly less than 1 μm. The ESEM micrographs, however, also show a significant crystal size distribution and Fujii et al.[1] suggested that a large crystal size distribution would cause a non-negligible broadening of the Raman band, also resulting in the inability to use such analysis.

Fujii et al.[1] also tried to find a correlation between peak position and average particle size, however, no such relationship was confirmed in this thesis. It was suggested that a compressive stress could cause a shift in the Raman band to higher wavenumbers and may also affect the band width. The position of the maximum intensity of the Raman band, ranging from 292 to 301 cm^{-1}, for each treatment was determined. No noteworthy relationship between peak position and treatment condition was found. The range in position of the maximum intensity of the Raman band measured in this study does, however, encompass the maximum intensity values reported by a number of other studies,[1,4-7,10] even though, in most cases, the matrix in which the

germanium nanocrystal is embedded is pure SiO_2 glass rather than binary GeO_2-SiO_2 glass. This observation in and of itself is very interesting, since the effect responsible for this enhanced Raman band is a surface scattering effect.

7.4.2. Non-Uniform Morphology and Wide Crystal Size Distribution

Yang et al.[10] claim to observe two different morphologies for the germanium nanocrystals dispersed in a gel glass matrix; (a) cubic germanium nanocrystals with a size of about 23 nm and a less regular shape and (b) amorphous germanium nanoparticles with a diameter of 2.5 – 5 nm and a near spherical shape. The observation of mixed morphology of germanium nanocrystals that varies with size and the presence of a broad size distribution is consistent with this study, as shown by the smaller spherical shaped crystals formed on the surface of the treated samples, Figure 7.3, and the larger octahedral crystals embedded within the glass samples, Figure 7.9. Although germanium has a cubic structure the growth direction could be along the (1 1 1) plane, resulting in octahedral crystal morphology. Yang et al.[10] suggest that germanium atoms first gather to form germanium clusters that subsequently grow into nanocrystalline germanium with a diamond like structure, which is in good agreement with results presented here. The observation of a wide distribution of crystal sizes supports the argument made in Chapter 6 that the broad, featureless optical absorption spectra are representative of a wide distribution of crystal sizes. This result is also consistent with the results observed by Yang et al.[10]

Yang et al.[10] propose that the concentration of germanium nanocrystals increases with increasing germanium content of the as-prepared gel glass. This contention would make sense if the process by which the nanocrystals are formed is the reduction and subsequent diffusion of germanium atoms. Extensive support for this observation is not presented on a quantitative level. Qualitatively, comparison of the XRD patterns for the two different binary glasses treated under the same conditions show more crystalline germanium is present in the glasses with the higher germanium content, i.e. peak intensity is higher. With a wide distribution of crystal size, however, quantitative arguments are unsubstantiated.

Yang et al.[10] mentions the use of the Sherrer equation to analyze crystal size. One must be cautious, however, when using XRD to evaluate a two-phase system consisting of micro or nanocrystals imbedded in amorphous material. The use of the simple Sherrer formula to calculate crystallite size from the full width at half maximum (FWHM) of the Bragg reflection is allowed only if the composite is stress free and the crystallite size is less than about 15-20 nm for the following reasons; (a) mechanical stress contributes to the broadening of Bragg peaks and, if not corrected for, simulates a smaller calculated crystallite size and (b) instrumental broadening becomes appreciable with the FWHM of the Bragg reflection at crystallite size $\geq 30 - 40$ nm and, if not corrected for, also results in a smaller calculated crystallite size.[12] Unfortunately, the use of the Sherrer equation is unreasonable when considered for this study since there is an obvious crystal size distribution, including crystals larger than 40 nm as supported by the ESEM images, as well as the optical absorption spectra. In this study, it is obvious that the crystals are growing inside the glass and therefore may exist under a significant amount of stress. Unfortunately, the magnitude of the stress and subsequent effect on XRD and Raman spectra is difficult to determine.

7.4.3. Penetration of Crystal Growth Along the Striations

To the author's knowledge, organized crystal growth along the striations of vapor phase axial deposition glass has not been reported. The growth of colloids associated with the striations implies that, although the striations may not have a huge effect on fiber optic based applications, the minor composition fluctuations have a significant effect on the way hydrogen reacts with the glass. The presence of a wide distribution of germanium nanocrystals or clusters represents germanium nanocrystals at different stages of the nucleation and growth process. In this particular study, the observation of germanium clusters at the surface of the treated samples and more developed crystals inside the glass would suggest that growth at the surface is either hindered by some other process or started the growth stage after the crystals grown within the glass matrix. Arguments of strain energy could also be used to explain the growth of crystals along the striations, since the striation represent a higher germania content in the glass, and based on arguments presented in Chapter 4, glass with higher germania content should have a

lower viscosity and therefore should be able to relax easier. It is possible that crystals grown along the striations, within the glass sample, developed faster than those at the surface of the glass because of lower strain energy, resulting from the decreased viscosity of glass with a higher germanium content.

7.4.4. Crystals Confined to Surface and Associated with Color

The observation that detectable germanium crystal formation is confined to the surface of the treated samples has also not been reported. While it is not possible to make definitive statements regarding the extent of crystal formation, it is possible to make speculation regarding factors that may contribute to confinement of crystals to the surface of the glass. The fact that the crystals are growing within the glass structure, and therefore under significant strain, could potentially inhibit the growth of crystals anywhere except the surface of the glass, where significant strain can be relieved. Perhaps the strain energy it would take to grow a crystal of significant size deep within the glass, away from the surface, is too high.

On the other hand confinement of crystals to the surface of the glass may be nothing more than just the result of very slow diffusion. The kinetics of the reaction could be such that complete reduction of germanium species throughout the glass could take thousands of hours. On the other hand, maybe reduction of germanium species within the glass may be fairly quick, but the subsequent diffusion of the reduced species in the glass and growth of a crystal is extremely slow. There is, unfortunately, no obvious way to prove these hypotheses using the data presented in this thesis.

The correlation between the crystal formation and observation of color formation in the treated samples, however, is irrefutable. The examination of the sample shown in Figure 7.12 and the observation that brown color exists only where a significant amount of crystallization was observed, results in a strong correlation between color development and crystal formation.

7.5. Conclusion

Treatment of binary GeO_2-SiO_2 glasses under a hydrogen atmosphere (700 Torr) at elevated temperatures results in the formation of germanium nanocrystals as a function of time, temperature and germanium content. Hydrogen-induced germanium nanocrystal formation increases with increasing GeO_2 concentration. The rate of detectable germanium nanocrystal formation increases with increasing temperature. The formation of germanium nanocrystals correlates well with the development of the intense brown color in the binary GeO_2-SiO_2 glasses.

7.6. References

1. M. Fujii, S. Hayashi, and K. Yamamoto, "Raman Scattering from Quantum Dots of Germanium Embedded in Silica Thin Films," *Appl. Phys. Lett.,* **57** [25] 2692-4 (1990).

2. I.H. Campbell and P.M. Fauchet, "The Effects of Microcrystal Size and Shape on the One Phonon Raman Spectra of Crystalline Semiconductors," *Solid State Commun.,* **58** [10] 739-41 (1986).

3. G. Nilsson and G. Nelin, "Phonon Dispersion Relations in Germanium at 80 K," *Phys. Rev. B: Solid State,* **3** [2] 364-9 (1971).

4. M. Fujii, S. Hayashi, and K. Yamamoto, "Growth of Germanium Microcrystals in Silica Thin Film Matrixes: A Raman and Electron Microscopic Study," *Jpn. J. Appl. Phys., Part 1,* **30** [4] 687-94 (1991).

5. Y. Maeda, N. Tsukamoto, Y. Yazawa, Y. Kanemitsu, and Y. Masumoto, "Visible Photoluminescence of Germanium Microcrystals Embedded in Silica Glassy Matrixes," *Appl. Phys. Lett.,* **59** [24] 3168-70 (1991).

6. K. Kawamura, Y. Kameshima, H. Hosono, and H. Kawazoe, "Proton-Implantation-Induced Optical Phenomena in SiO_2:GeO_2 Glasses: Formation of Photosensitive Defects and Nanometer Sized Ge Crystals," *Mater. Sci. Eng., B,* **54** [1-2] 18-23 (1998).

7. V.G. Plotnichenko, A.O. Rybaltovskii, V.O. Sokolov, V.V. Koltashev, A.R. Malosiev, V.K. Popov, and E.M. Dianov, "Role of Hydrogen in Formation of Ge Nanocrystals in Optical Fibres," *J. Non-Cryst. Solids,* **281** [1-3] 25-30 (2001).

8. H. Hosono, H. Kawazoe, and K. Muta, "Preferred Concentration Enhancement of Photobleachable Defects Responsible for 5 eV Optical Absorption Band in SiO_2:GeO_2 Glass Preform by Heating in a H_2 Atmosphere," *Appl. Phys. Lett.,* **63** [4] 479-81 (1993).

9. H. Yang, X. Wang, H. Shi, F. Wang, X. Gu, and X. Yao, "Sol-Gel Preparation of Ge Nanocrystals Embedded in SiO_2 Glasses," *J. Cryst. Growth,* **236** [1-3] 371-5 (2002).

10. H. Yang, R. Yang, X. Wan, and W. Wan, "Structure and Photoluminescence of Ge Nanoparticles with Different Sizes Embedded in SiO_2 Glasses Fabricated by a Sol-Gel Method," *J. Cryst. Growth,* **261** [4] 549-56 (2004).

11. A.K. Dutta, "Visible Photoluminescence from Ge Nanocrystal Embedded into a SiO_2 Matrix Fabricated by Atmospheric Pressure Chemical Vapor Deposition," *Appl. Phys. Lett.,* **68** [9] 1189-91 (1996).

12. S. Veprek, "Chemistry and Solid-State Physics of Microcrystalline Silicon," *Mater. Res. Soc. Symp. Proc.,* **164**, 39-49 (1990).

CHAPTER 8: EXPLORING THE ENDS OF THE BINARY GLASS SYSTEM

Abstract

This chapter presents a survey of preliminary research on the pure glasses that make up the binary glass system discussed in the previous chapters of this thesis. Some of the important property differences between pure SiO_2 and pure GeO_2 glasses are discussed. Most of the hydrogen reaction results presented in this chapter concern only pure GeO_2 glasses, since reactions with hydrogen for pure SiO_2 glasses have been studied extensively and do not need to be repeated here. Treatment of pure SiO_2 and pure GeO_2 glasses was monitored as a function of time under a hydrogen atmosphere (700 Torr) at elevated temperatures. Pure SiO_2 made from the OVD process is relatively inert to hydrogen reaction at elevated temperatures. Pure GeO_2 glasses, however, heat treated in the presence of hydrogen readily react to form reduced germanium species confined to the exposed surface of each sample.

8.1. Introduction

Although it is well known that pure GeO_2 and pure SiO_2 glasses have similar network structures, there are many differences in the fundamental properties of the glasses. The most important difference, and perhaps the primary reason that pure SiO_2 glass has found so many significant applications, is that the durability of SiO_2 glass is far superior to any other glass forming systems.

Vitreous GeO_2 has a structure very similar to that of vitreous SiO_2, in that the basic building block of both of the glasses in the pure form is a network of tetrahedra connected at all four corners. Each oxygen atom is shared by two silicon or germanium atoms, which occupy the centers of the fully linked tetrahedra. The germanium ion is larger in diameter than the silicon ion and hence the Ge-O bond distance is greater, with bond length of ~0.173 nm, than that of the Si-O bond length, ~0.162 nm.[1] The Ge-O-Ge bond angle is also smaller than the Si-O-Si bond angle. Gas diffusion studies suggest that the structure of vitreous GeO_2 is more compact than that of vitreous silica, resulting in a slightly lower free or interstitial volume in vitreous GeO_2. The lower melting temperature of GeO_2 as compared to that of SiO_2 indicates that the Ge-O bond is considerably weaker than the Si-O bond. Simple ionic field strength arguments would lead to the same conclusion.

Structural defects are more common in vitreous GeO_2 than in vitreous SiO_2, with a measurable concentration of Ge-Ge bonds.[1] Oxygen deficient defects in glass have been reported by many glass researchers.[2-14] An intense absorption band at approximately 240 nm (~5 eV) in both GeO_2 and natural SiO_2 glasses has been attributed to oxygen deficient defects related to germanium. A comprehensive discussion on this topic was presented in Chapter 6 and need not be repeated here. It should be sufficient to say that there is general agreement over a broad survey of literature that the intense absorption band in the as-melted glasses results from the presence of reduced germanium species or oxygen-deficient defects related to germanium.

Many researchers have examined the effect of temperature and atmospheric conditions during melting and quenching on the optical absorption of pure GeO_2 glasses. Vergano and Uhlmann[15] examined the effect of oxygen deficiencies in pure GeO_2 glasses, determined by the intensity of the 5 eV band, on crystallization kinetics of

germanium dioxide. They reported that the formation of GeO_2 crystals has a strong correlation with the reduction state of the glass. The growth rate of the crystals was found to increase with increasing reduction of the glass under all cooling conditions, an effect which was attributed to the role of excess germanium in the glass, which lowers the viscosity.

Although the reduction of germanium species in pure GeO_2 glasses is fairly well known, hydrogen reactions with pure GeO_2 glasses below T_g have not been reported. The effect of hydrogen reactions on the optical properties of the glass and subsequent crystallization is presented here. Environmental scanning electron microscopy and x-ray diffraction measurements were used to determine crystal species forming during reactions with hydrogen. Hydrogen reactions with pure GeO_2 glasses are discussed as a function of time and temperature.

8.2. Experimental Procedure

Fourier Transform Infrared Spectroscopy (FTIR) absorption measurements over the spectral range from 4200 to 2000 cm^{-1} were conducted at room temperature to monitor changes in the concentration of hydroxyl and hydride species the GeO_2 and SiO_2 glasses with progressive treatment in hydrogen at elevated temperatures. Optical absorption measurements, over the spectral range from 200 to 1100 nm, of glass plates were conducted at room temperature to monitor changes in the optical properties of the GeO_2 and SiO_2 glasses for the same treatments. Absorbances are reproducible to within ±0.01.

Samples were placed on a platinum setter in a vitreous silica tube attached to a gas handling apparatus. The preheated horizontal tube furnace was positioned around the evacuated silica sample chamber. Temperatures were continuously monitored by a thermocouple inside the sample chamber, directly above the samples. After the desired temperature was reached, hydrogen gas was introduced into the sample chamber. Sample temperature was held constant to within ±5K throughout the treatment. Each sample was treated for the desired amount of time under 93 ± 1 kPa of hydrogen partial pressure. A more detailed description, including a schematic of the apparatus, is given in Chapter 3.

Optical microscopy was used to obtain images to monitor changes in the appearance of the glass samples with progressive treatment in hydrogen at elevated temperatures. All images in this chapter were taken using reflected light. The magnification used is reported in the figure caption of every image presented. The use of optical microscopy to study crystallization of glasses, however, was limited, since many of the crystals formed in this study are so small that they are below the limit of resolution of the microscope. For this reason, the use of an electron microscope was employed to permit closer examination of interesting structural features.

An environmental scanning electron microscope (ESEM) was used to investigate the possible presence of crystalline phases formed during hydrogen reaction experiments. The treated glass samples were examined in low vacuum mode, allowing for examination of uncontaminated, non-sputter-coated glass samples to investigate morphology and depth of crystallization. Select samples were sectioned perpendicular to the thickness and fractured samples for examination of the reacted surface layer were prepared using a technique similar to that illustrated in Figure 7.1. The treated glass samples, varying in shape, were fractured perpendicular to the thickness, approximately 1.0 mm, to investigate the morphology and depth of crystallization. To create a fracture surface, the samples were cut partially through the thickness and broken in bending by hand. The section removed was mounted on the sample holder with the orientation shown in the last step of the schematic in Figure 7.1. Images obtained with the ESEM were taken in either secondary electron mode or backscatter electron mode. The mode used is noted in the figure caption of each image.

X-ray diffraction (XRD) measurements were performed on selected samples to investigate the possible presence of crystalline phases formed during hydrogen reaction experiments. Phase identification XRD measurements were performed in a Siemens D500, with samples positioned with the crystalline surface of the bulk samples at the plane of diffraction. Scans were conducted using a scan speed of 3 degrees 2θ/minute from 20 to 120 degrees 2θ. In every measurement, the x-ray tube was operated at 40 kV and 20 mA with a copper target. The sharp lines present in the XRD pattern were used for crystal identification through comparison with standard data from International Centre for Diffraction Data (ICDD) powder diffraction files.

The formation of a continuous, conductive surface layer was measured using an apparatus that allows for insertion of a plate glass sample into a simple series circuit. A more detailed description of the apparatus used is presented in Chapter 3. Measurement of the voltage drop across the sample shows completion of the circuit and allows determination of the on-set of surface conductivity, i.e. the formation of a continuous electrically conductive surface film. Direct current electrical resistance measurements were performed at room temperature.

8.3. Results

8.3.1. The Differences Between Pure SiO_2 and Pure GeO_2 Glasses

The effect of processing technique on the properties of the final glass product is significant and was discussed in detail in Chapter 4. In this preliminary study, a few of the differences in reaction with hydrogen between a pure SiO_2 glass made from the same process as the binary GeO_2-SiO_2 glasses studied in this thesis are compared to the reactions of a pure GeO_2 glass made from reagent grade powder by melting in a platinum rhodium crucible in an electrically heated furnace. Although the pure glasses used in this study were not made by the same processing technique, there are a few properties of the glasses that can be qualitatively compared and discussed. More importantly, however, the significant difference in the way that each of the glasses react to treatment at elevated temperatures in a hydrogen atmosphere is very interesting and could potential lead to better understanding of reduction processes in binary GeO_2-SiO_2 glasses.

In oxide glasses, the short-wavelength absorption edge results from the energy required to liberate an electron from the network forming anion, oxygen. The short-wavelength band edge for pure silica results from the excitation of an electron from a bonded oxygen atom in the network, since silica has a 4+ charge and is not as readily excitable. The ultraviolet edge, or band gap energy, for most oxide glasses typically occurs in the ultraviolet region of the electromagnetic spectrum. Impurities, defects and minor perturbations of the network structure have a dominating influence on the UV band edge frequency.[16] Electron excitation is possible because there are inherent defects and

disruptions of the continuous random network within the glass structure. The true ultraviolet edge of most glasses is often obscured by the presence of intrinsic impurities resulting in intense charge transfer bands that appears as an effective UV edge. This artificial shifting of the observed UV band edge to longer wavelengths can result from disruptions of the silica network caused by the presence of intrinsic defects or alkali impurities. The electron associated with a defect in the glass structure is more easily exited than that of a typical bonded oxygen atom and therefore takes less energy to excite, shifting the UV band edge to lower frequencies, or longer wavelengths**.**

A great deal of prior research has focused on the optical absorption spectra and the presence of a strong absorption band at approximately 242 nm in the binary GeO_2-SiO_2 glasses.[12-14] This band was observed in the binary glasses and was discussed in detail in Chapter 6. A similar band has also been observed in pure GeO_2 glasses[4,9-11] and a few "pure" SiO_2 glasses.[2,3,6,7] The band at approximately 242 nm is only observed in natural SiO_2 glasses, i.e. Type I or II SiO_2, and not in synthetic silica glasses. The optical absorption spectra of the glasses used in this preliminary study shown in Figure 8.1, however, show no clear band structure at approximately 242 nm. The SiO_2 glass used in this study is a synthetic SiO_2 glass and should not have a band at approximately 242 nm, but the pure GeO_2 glass should, and probably does, have a band at 242 nm, but the extinction due to the 242 nm band is extremely high. The GeO_2 glass sample used to collect the spectrum shown in Figure 8.1 was approximately 0.5 millimeter thick, but the maximum peak absorption was too high to be experimentally observable. Since the absorption due to the 242 nm band is so high, the resulting optical absorption spectra show an apparent absorption edge.

The fundamental properties and reactions with hydrogen for pure SiO_2 glasses have been studied extensively and do not need to be repeated here. A comparison of the reactions under similar conditions is presented to show qualitative differences. The most obvious difference between the two glasses is the decreased durability of the pure GeO_2 glasses when compared to that of the SiO_2 glasses. GeO_2 glasses are very hygroscopic, i.e. extremely susceptible to dissolution in water, limiting the number of techniques used to condition the glass sample and the ability to handle the glasses in an ambient atmosphere without altering the glass surface. In this particular case, water or humidity

in the atmosphere attacks network forming bonds in the glass, ultimately resulting in a layer of reaction product on the surface of the glass sample after extended periods of time. This process is more appropriately called weathering, rather than chemical durability, which usually refers to the interactions of the glass with a liquid, since this layer formation is attributed to the reaction of glass surface with humidity in the air. Examination of a pure GeO_2 glass stored in an ambient atmosphere for ~18 years shows the effect of weathering on this glass. In this particular case, the reacted surface layer on the GeO_2 glass samples appears to be a continuous, opaque, white layer as shown in the optical micrograph in Figure 8.2. Obviously, the formation of this layer seriously degrades the optical appearance of the glass samples as the samples turn from a transparent, colorless sample to an opaque, white sample which appears to be completely crystallized. XRD of the reacted surface of the weathered GeO_2 glass shows that the surface layer is crystalline germanium dioxide, GeO_2, as shown in the XRD pattern in Figure 8.3, including the known pattern of hexagonal GeO_2 crystals, PDF # 00-036-1463. It is important to note that the interior of a fractured, weathered glass sample is vitreous, i.e. the formation of hexagonal GeO_2 crystals, resulting from weathering, is confined to the exposed surfaces of the glass sample.

8.3.2. Pure SiO_2 Relatively Inert to Hydrogen Reaction at Elevated Temperatures

A plate of the as-received SiO_2 glass was treated under a hydrogen atmosphere (pH_2 = 93 kPa) at 800°C for up to 190 hours. Figure 8.4 shows the infrared absorption spectra of the SiO_2 glass with progressive treatment at 800°C and 700 Torr of hydrogen. Only the as-received, 16 hour and 190 hour treatments are included, all other treatments with a square root time progression fall between these curves and were omitted to eliminate clutter. For comparison, the infrared absorption spectra of the as-melted GeO_2 glass is included in Figure 8.4. It is obvious that the as-melted GeO_2 glass has a significantly higher hydroxyl concentration than the as-received SiO_2 glass. Even after 190 hours of treatment in hydrogen, there is only a small amount of hydroxyl formation that is still considerably lower than the hydroxyl content of the as-melted GeO_2 glass. There is no evidence of crystallization in the SiO_2 glasses after extended treatment in a hydrogen atmosphere.

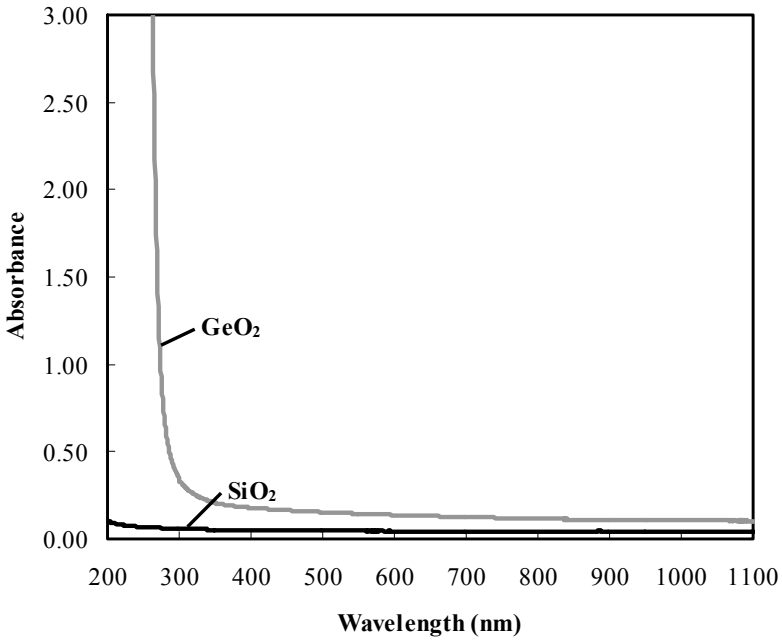

Figure 8.1. Optical absorption spectra for the as-melted pure GeO_2 and as-received pure SiO_2 glass.

Figure 8.2. Optical micrograph, taken in reflected light with the 6.5 X objective, of weathered GeO_2 glass after ~18 years of storage in ambient air.

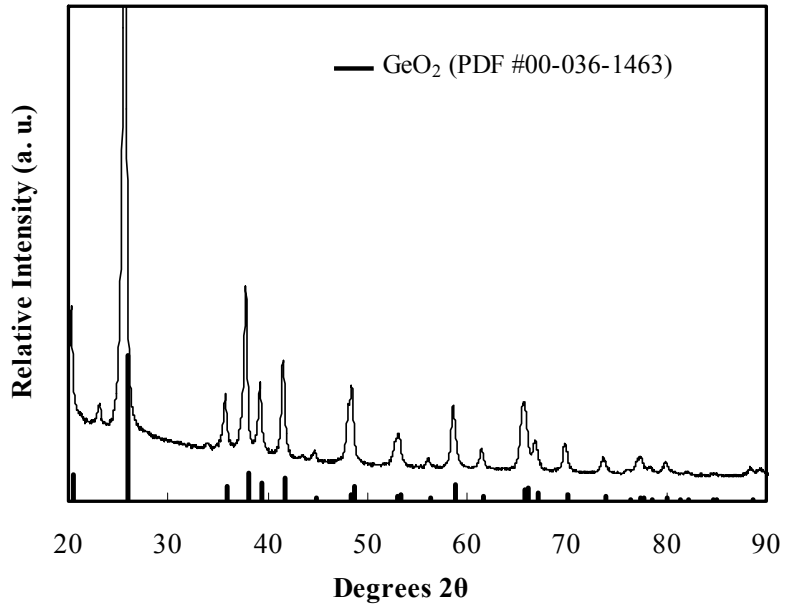

Figure 8.3. XRD pattern for weathered GeO_2 glass after ~18 years of storage in ambient air.

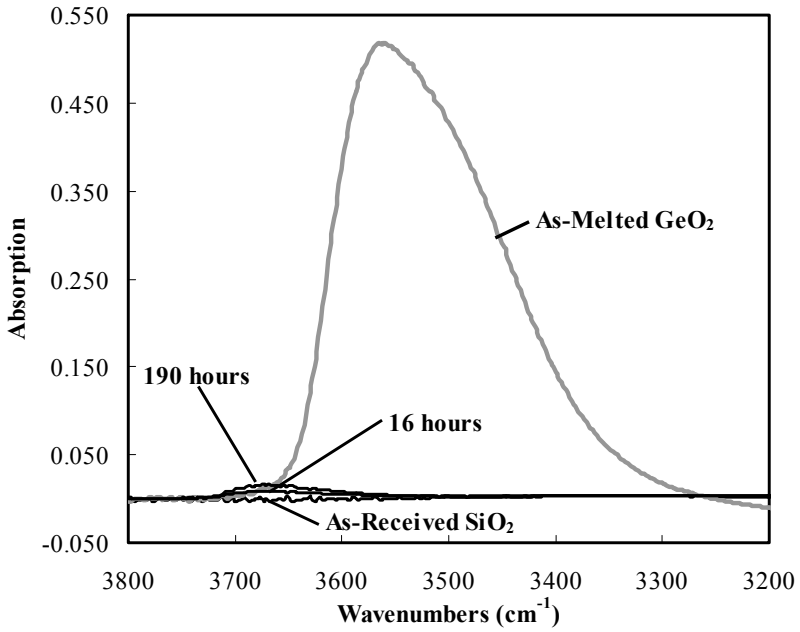

Figure 8.4. Infrared absorption spectra in the hydroxyl/water region for the as-melted GeO_2 and as-received SiO_2 glass. Infrared absorption spectra for the pure SiO_2 glass after progressive hydrogen treatment at 800°C, for the indicated cumulative treatment time, are also included.

8.3.3. Hydrogen-Induced Crystal Formation in Pure GeO_2 Glasses

A one millimeter thick plate of the as-melted GeO_2 glass, with no evidence of a weathered surface layer, was treated under a hydrogen atmosphere (pH_2 = 93 kPa) at 500°C for 2.5 hours. The clear, transparent glass sample was opaque after only 2.5 hours of treatment in hydrogen. ESEM and XRD results show a significant amount of crystal formation. The observation of crystallization is accompanied by the appearance of a shiny, opaque layer, silver/grey in color, on the exposed surfaces of the glass sample after only 2.5 hours. An optical micrograph of the crystallized surface taken in reflected light with a 16 X objective, is shown in Figure 8.5. The fractured edge at the corner of the sample shows that the crystallization occurred at the surface and covers the glass underneath. A backscatter electron micrograph of a fractured surface of the edge of the treated sample further confirms the confinement of the crystallization to the surface layer (Figure 8.6). The darker area in the center of the fractured surface represents the original glass, while the lighter surface layers represent the crystalline phase. At higher magnification, the micrograph shown in Figure 8.7 shows that the thickness of the crystallized layer is approximately 60 μm. No special seeding or surface treatment was necessary to produce surface nucleation.

XRD patterns from the surface of the treated sample were used for identification of the crystalline phase. A representative XRD pattern from the surface of the GeO_2 glass treated in hydrogen at 500°C for 2.5 hours (Figure 8.8) shows the presence of a large amount of pure germanium crystals. The absence of amorphous features in the pattern indicates that the crystallization layer is thicker than the sampling depth of the XRD measurement. The EDS spectra of the treated surface (Figure 8.9) confirms the presence of pure germanium on exposed surfaces of the treated sample. Although EDS spectra lend no information regarding the structure of the pure germanium on the surface of the sample, the fact that the element germanium is the only detectable element at the surface provides evidence that the germanium nanocrystals are forming at the surface. The observed color is also consistent with the semi-metallic appearance of pure germanium.

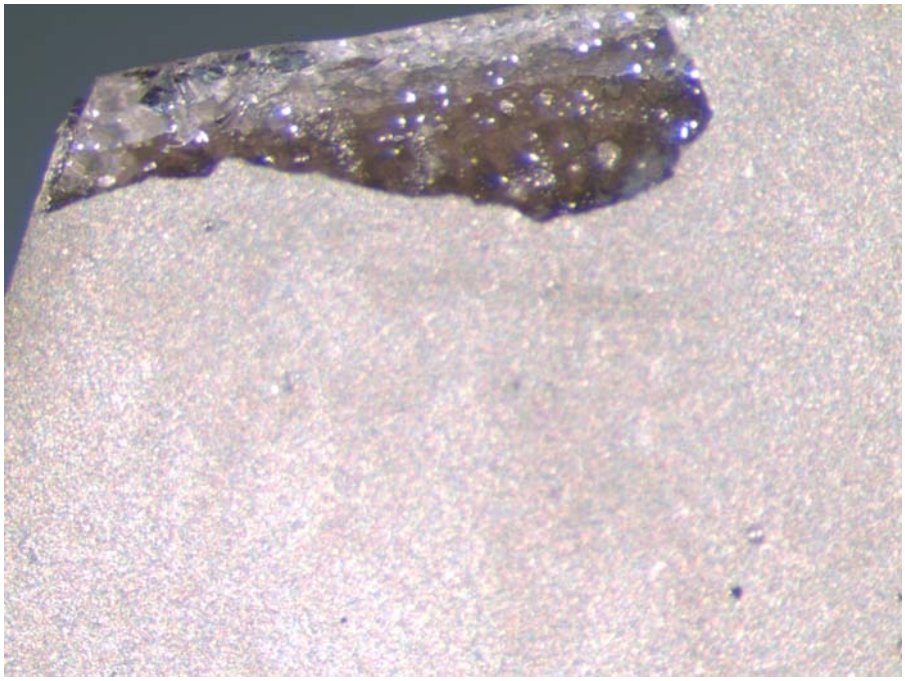

Figure 8.5. Optical micrograph, taken in reflected light with the 16 X objective, of GeO_2 glass treated at 500°C and 700 Torr hydrogen for 2.5 hours.

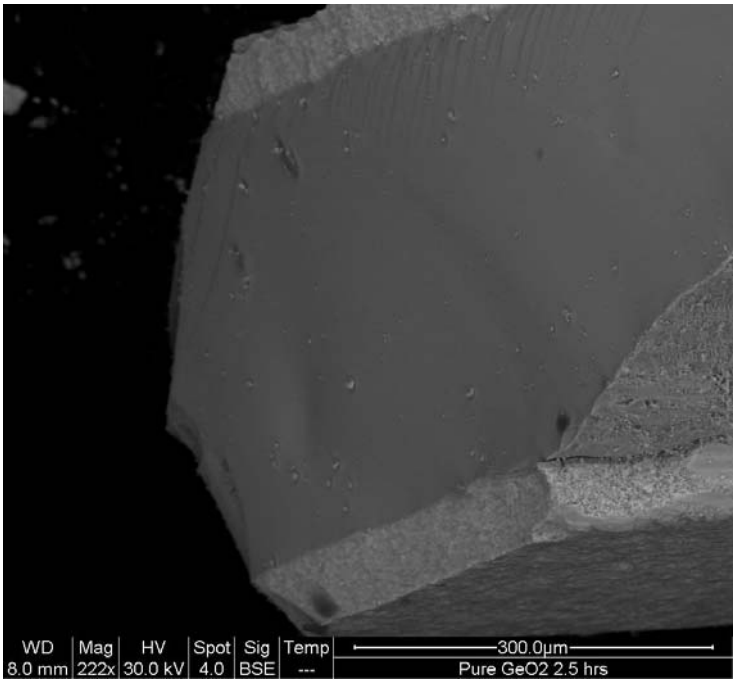

Figure 8.6. Backscatter electron micrograph of the fractured edge of a GeO_2 glass treated at 500°C and 700 Torr hydrogen for 2.5 hours, taken in low vacuum mode, 222X magnification and a voltage of 30 kV.

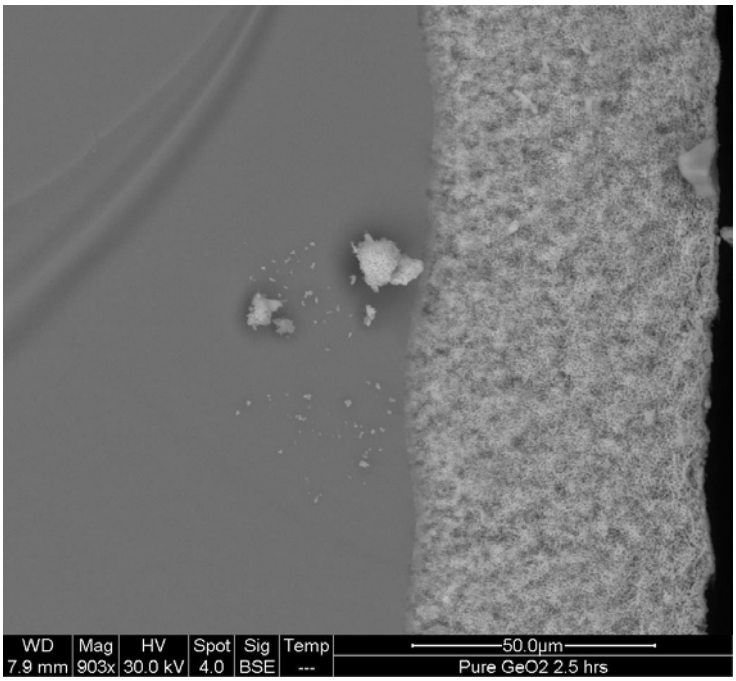

Figure 8.7. Backscatter electron micrograph of the fractured edge of a GeO_2 glass treated at 500°C and 700 Torr hydrogen for 2.5 hours, taken in low vacuum mode, 903X magnification and a voltage of 30 kV.

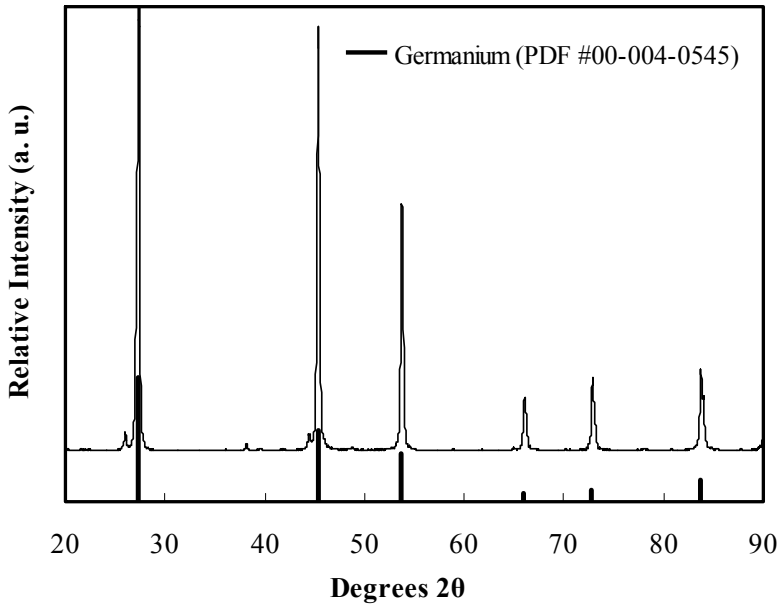

Figure 8.8. XRD pattern from the treated surface of the pure GeO_2 glass treated at 500°C and 700 Torr hydrogen for 2.5 hours.

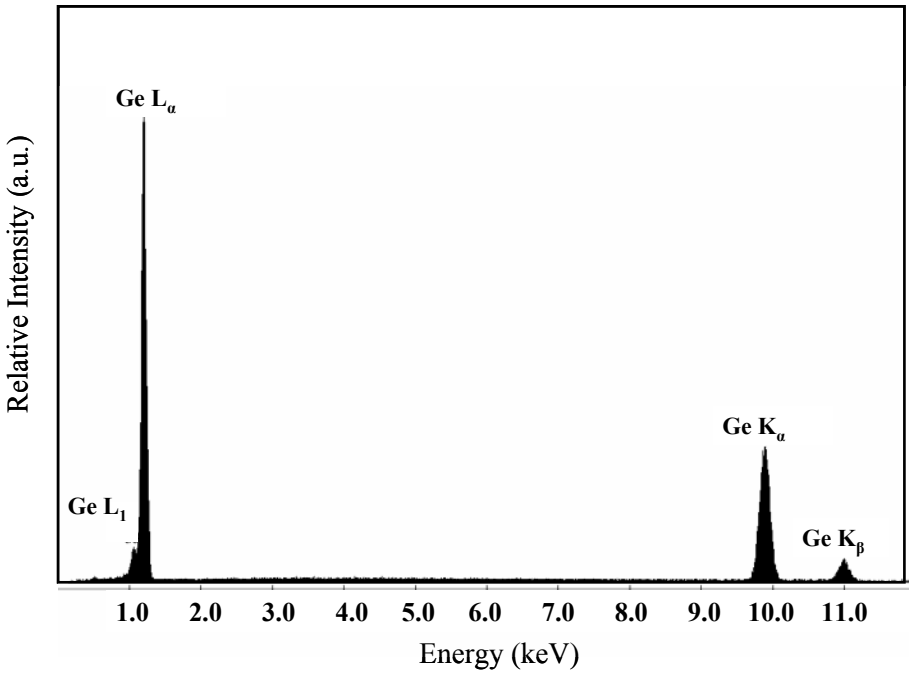

Figure 8.9. EDS spectra from the treated surface of the pure GeO_2 glass treated at 500°C and 700 Torr hydrogen for 2.5 hours

8.3.4. Strange Morphology Observations

The ESEM was also used to investigate the morphology of the crystalline layer at the surface of the treated glass samples. Some rather interesting results were observed. Examination of the layer on the fractured surface reveals a non-faceted morphology with an interconnected morphology. A representative secondary electron and backscatter electron micrograph of the interconnected, non-faceted morphology is shown in Figure 8.10. The secondary electron micrograph (A) shows the topography features of the interconnected morphology. The backscatter electron micrograph (B) was taken in the same area of the sample and has a significantly smaller contrast range than the secondary electron micrograph, indicating that there is no detectable difference in composition or phase in this image. The observation of this non-faceted structure was somewhat unexpected when the XRD pattern of the crystallized surface showed such well developed crystallization.

The most interesting micrographs of the crystallized glass samples developed from a simple mistake during sample preparation. The original placement of the treated

glass sample on the ESEM platform, covered with carbon tape, was not the most favorable position for observation purposes. The sample was removed from the carbon tape, leaving behind a thick layer of crystals where the treated glass sample had separated from the crystallized layer. Examination of this removed layer revealed a diverse collection of multi-faceted crystals with a wide, but fairly organized, size distribution, as shown in Figure 8.11. The reason for the segregation of crystals of different sizes is not known at this time, but it appears that the more developed, larger crystals are clustered in one area while the smaller, less developed crystals are clustered in another area. Closer examination of the smaller crystals (Figure 8.12) shows a fairly uniform morphology similar to, but less developed than, that of the larger crystals. With closer examination, the facets of the individual crystals can be observed more clearly, as shown in Figure 8.13.

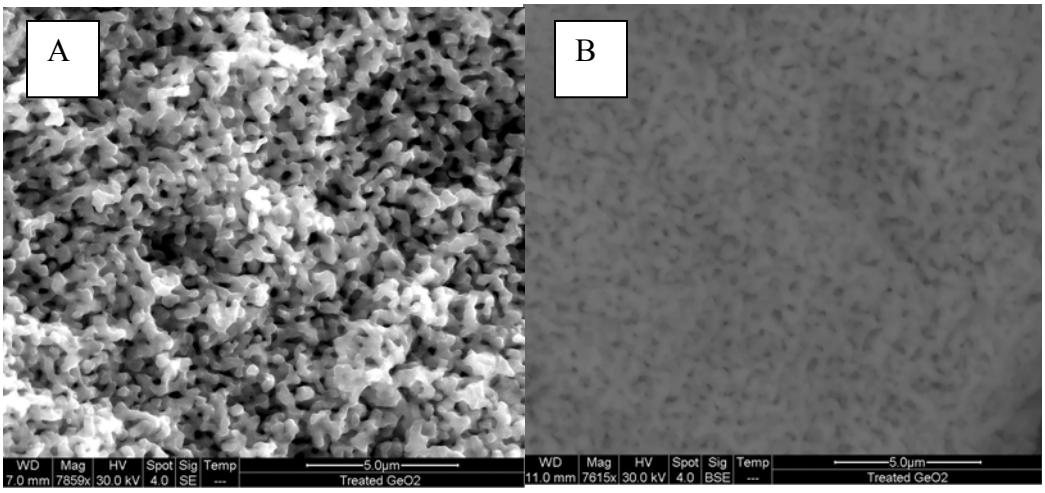

Figure 8.10. A) Secondary electron micrograph and B) backscatter electron micrograph of the treated surface of a GeO_2 glass treated at 500°C and 700 Torr hydrogen for 2.5 hours, taken in low vacuum mode, 7859X and 7615 X magnification, respectively, and a voltage of 30 kV.

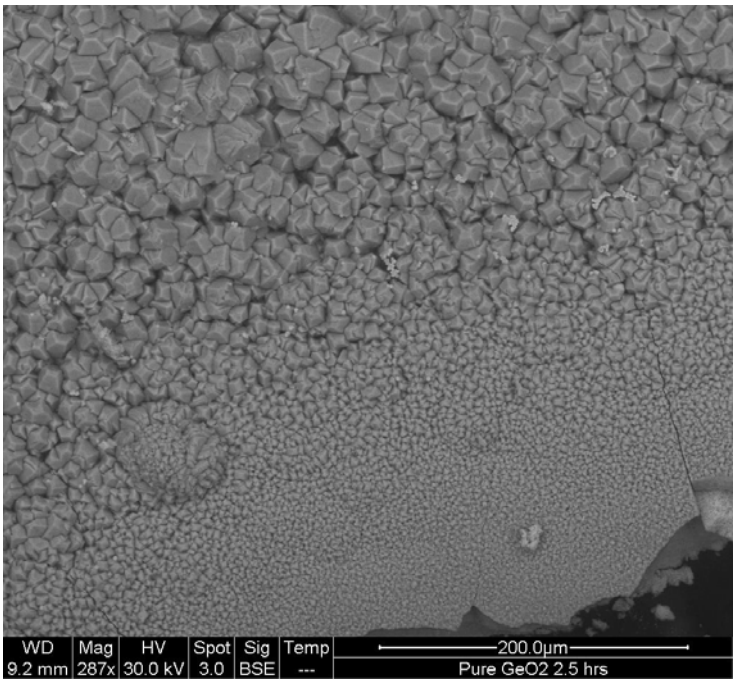

Figure 8.11. Backscatter electron micrograph of the fractured edge of a GeO_2 glass treated at 500°C and 700 Torr hydrogen for 2.5 hours, taken in low vacuum mode, 903X magnification and a voltage of 30 kV.

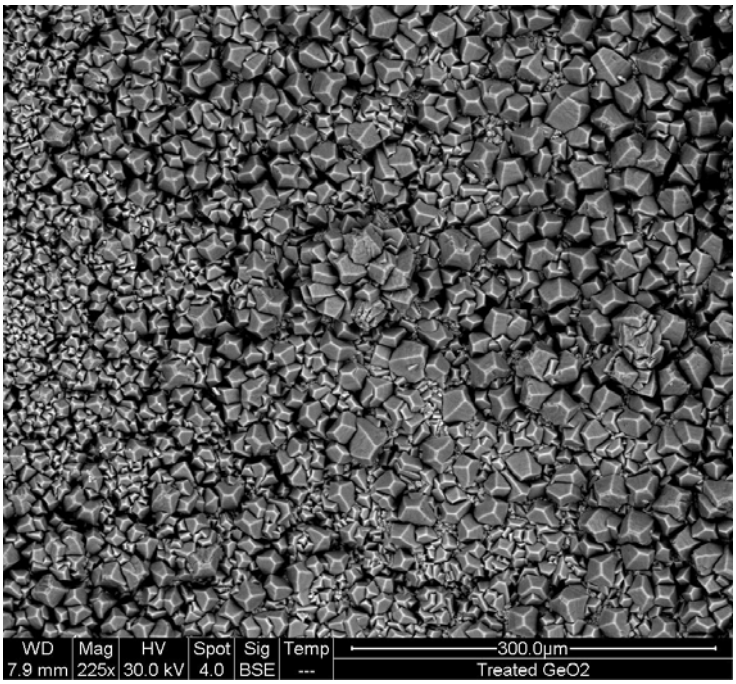

Figure 8.12. Backscatter electron micrograph of the detached surface of a GeO_2 glass treated at 500°C and 700 Torr hydrogen for 2.5 hours, taken in low vacuum mode, 225X magnification and a voltage of 30 kV.

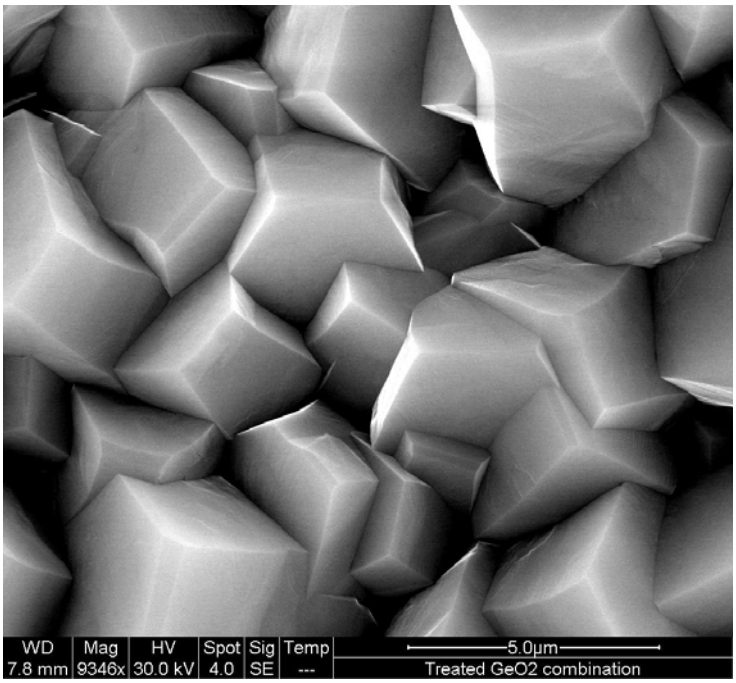

Figure 8.13. Backscatter electron micrograph of the detached surface of a GeO_2 glass treated at 500°C and 700 Torr hydrogen for 2.5 hours, taken in low vacuum mode, 9346X magnification and a voltage of 30 kV.

8.3.5. Progressive Treatment at 400°C, 450°C and 500°C

As-melted GeO_2 glass plates, approximately 1 mm thick, were treated in an atmosphere of hydrogen (700 Torr) at 400°C, 450°C and 500°C to investigate the effect of temperature on this reduction process. Figure 8.14 shows optical micrographs of GeO_2 glass plates treated at A) 400°C, B) 450°C and C) 500°C for the indicated treatment times. Sample treatments were not cumulative, i.e. different samples cut from the same glass melt were used for each treatment. The clear, transparent glass plates show a significant change in optical properties by treatment in hydrogen, with the development of a shiny, opaque crystalline layer, silver/grey in color. Optical absorption spectra were also used to characterize the development of this crystalline layer.

Optical absorption spectra correlate well with the observed change in the optical properties of the treated samples. Figure 8.15 shows the measured optical absorption spectra for each of the glass plates treated at 400°C in 700 Torr of hydrogen, for the indicated treatment times. Minor differences in the baseline value of the optical absorption spectra, more specifically for samples treated for one hour and four hours, can

be explained by differences in the surface condition resulting from small variations in polishing, since different samples were used for each treatment. There is obviously a significant difference in the measured optical properties between the samples treated for four and nine hours. The measured optical absorption spectra for each of the glass plates treated at 450°C in 700 Torr of hydrogen, for the indicated treatment times, are shown in Figure 8.16. The progression of increasing optical absorption with increasing treatment time correlates well with the images shown in Figure 8.14 B. The measured optical absorption for the sample treated for two hours at 450°C was beyond the detectable limits of the spectrometer, i.e. the sample was optically opaque, showing no detectable transmitted light. The measured optical absorption spectra for the samples treated at 500°C are shown in Figure 8.17. The effect of temperature on the reduction and crystallization process is most obvious for treatments at 500°C since there is significant difference in the optical properties of the glass after only fifteen minutes of treatment.

8.3.6. Conductivity Measurements of the Surface Layer

Although the apparatus used in this study was originally designed to measure isothermal direct current electrical resistivity of glasses, it also provides a convenient way to monitor the continuity of a conductive surface film. The apparatus allows for insertion of a glass plate into a series circuit. Insertion of an as-melted glass sample into the circuit will form a barrier to the passage of electric current since glasses are dielectric materials. If a glass sample has a continuous conductive film over the entire surface, the circuit will be complete, resulting in a measurable drop in voltage across the sample. Introduction of the treated samples into the series circuit allows for determination of the on-set of surface conductivity. After a substantial amount of surface crystallization, the treated samples showed a considerable increase in conductivity. Figure 8.18 shows the effect of treatment temperature on the time to detection of conductivity. The range in values indicates the time between observation of the non-conductive sample and the final observation of a fully conductive sample. The onset of conductivity correlates well with the observation of a completely crystalline surface layer on the treated glass. As one would expect, the onset of conductivity occurred at shorter periods of treatment time with increasing treatment temperature.

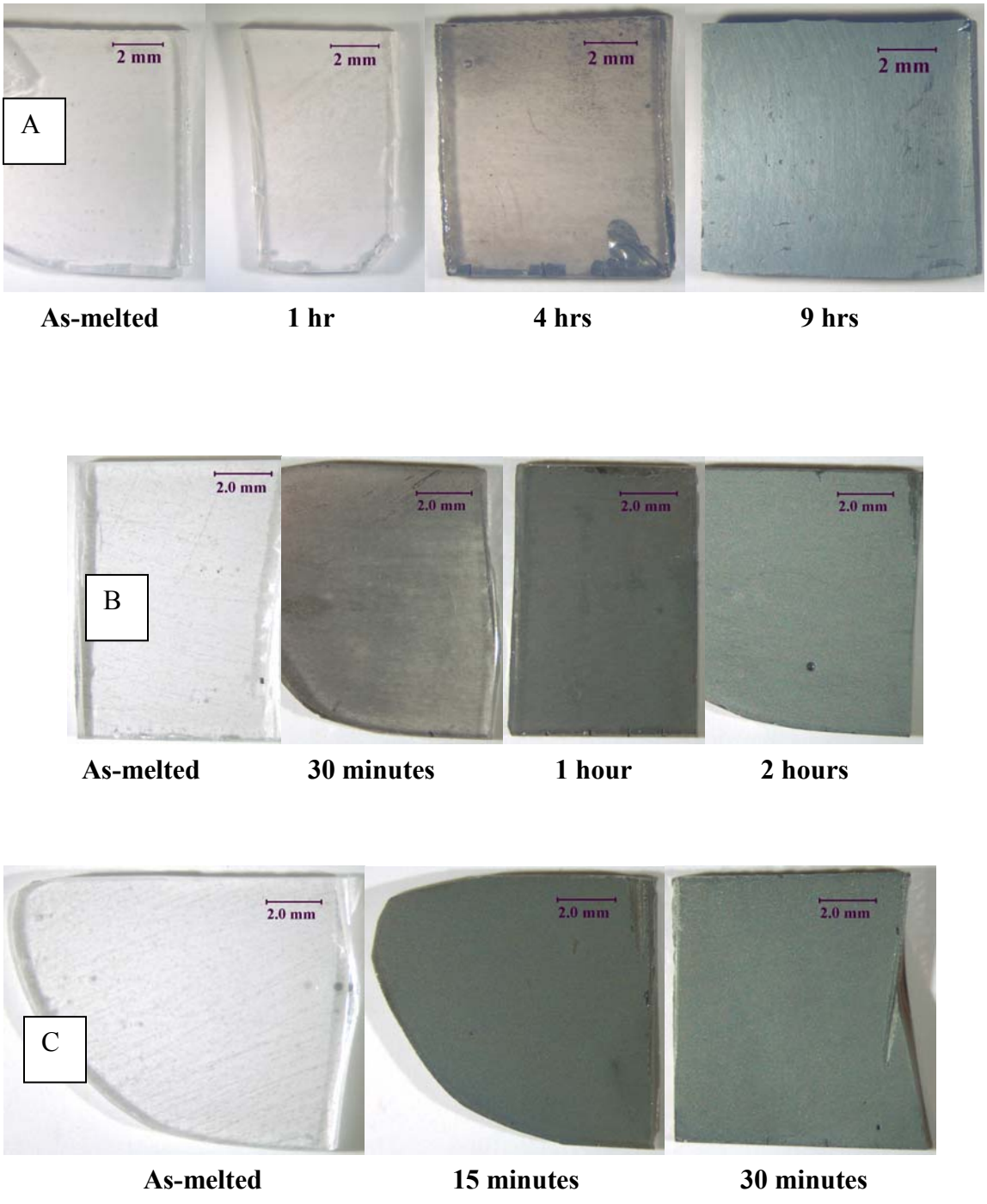

Figure 8.14. Optical micrographs, taken in reflected light with the 6.5 X objective, of GeO_2 glass treated at A) 400°C, B) 450°C and C) 500°C at700 Torr hydrogen for the indicated treatment times.

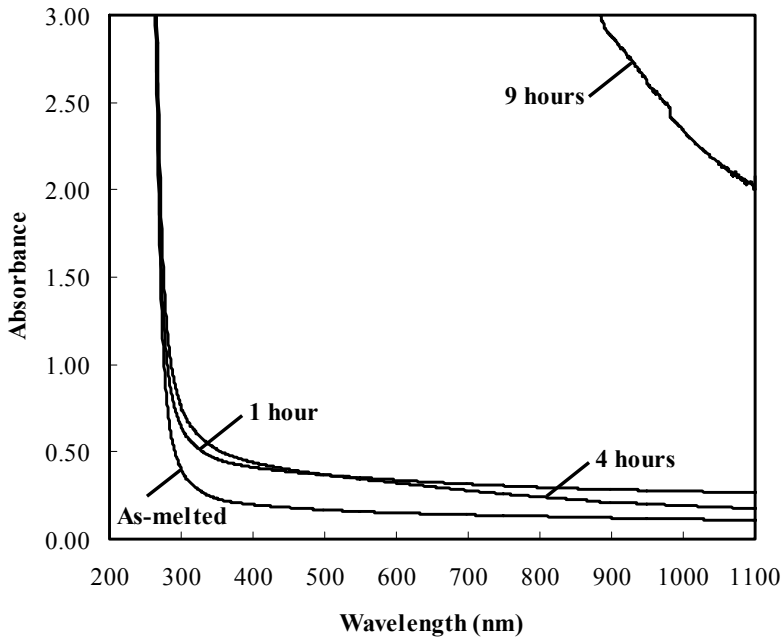

Figure 8.15. Optical absorption spectra for the GeO_2 glass plates treated in hydrogen at 400°C for the indicated treatment times.

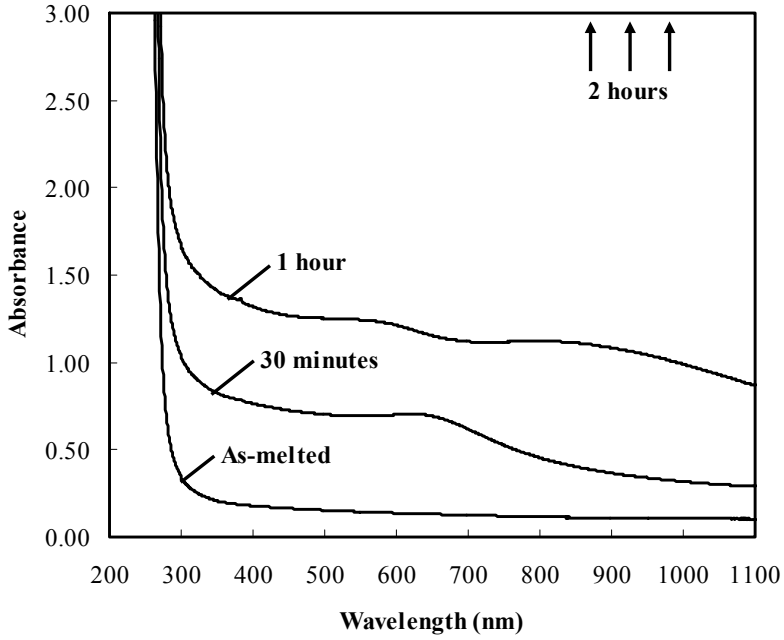

Figure 8.16. Optical absorption spectra for the GeO_2 glass plates treated in hydrogen at 450°C for the indicated treatment times.

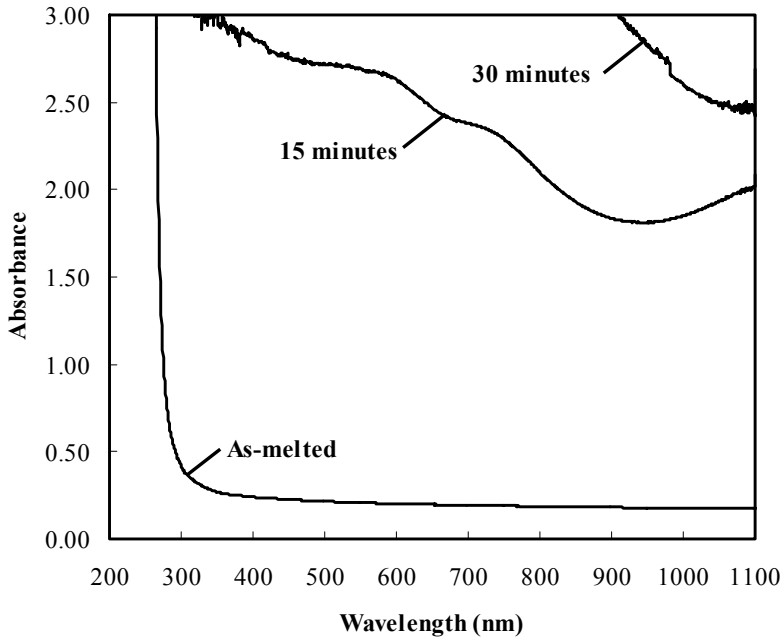

Figure 8.17. Optical absorption spectra for the GeO_2 glass plates treated in hydrogen at 500°C for the indicated treatment times.

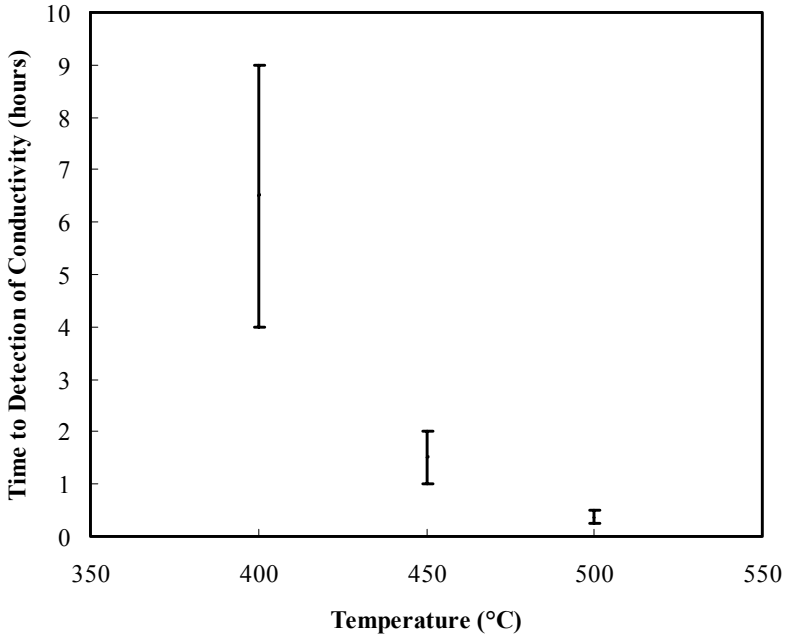

Figure 8.18. The effect of temperature on the time to detection of conductivity for GeO_2 glass plates treated in hydrogen.

8.4. Discussion

8.4.1. Weathering of GeO_2

The discovery that GeO_2 glass turns into crystalline GeO_2 after ~18 years in ambient air storage at room temperature, in and of itself, is very interesting. In crystalline GeO_2 polymorphs the germanium ion can be found in both tetrahedral and octahedral coordination. In this particular case, the weathered product of the GeO_2 glass is hexagonal GeO_2 crystals. The most significant result of this observation is the fact that GeO_2 glass will crystallize at room temperature. This crystallization process probably happens through a chemical reaction following the formation of a gel layer at the surface. The reaction mechanism that results in crystallization of GeO_2 glass at room temperature has not been fully clarified and could potentially lead to information regarding the reduction of germanium species in GeO_2 glass systems.

8.4.2. Formation of Pure Germanium Crystals

The presence of pure germanium crystals at the exposed surfaces of the glass, as determined from both XRD and EDS, is irrefutable. The observation of at least two different morphologies at the surface of crystallized GeO_2 glass has been observed elsewhere.[15] Vergano and Uhlmann observed both non-faceted and faceted interface morphologies at the glass-crystal interface after crystallization induced by undercooloing from the melt. In contrast with the crystallization of pure germanium observed through hydrogen-induced crystallization, Vergano and Uhlmann observed the formation of hexagonal GeO_2 crystals when the GeO_2 glasses were crystallized from the melt. Even though two different crystalline phases where identified through two different crystallization processes, it is interesting but not surprising that both crystallization techniques resulted in the formation of two completely different crystalline morphologies.

8.4.3. Conductivity of the Surface Layer

The use of electric conductivity measurements to observe the reduction and subsequent crystallization of constituent glass species has proven to be a useful technique in the surface characterization of glass samples treated in a reducing environment. Green and Blodgett[17] studied the reduction of Pb, Bi and Sb using electrical conductivity measurements. Glass plates containing Pb, Bi and Sb ions, treated in a hydrogen atmosphere at elevated temperatures within the glass transformation region, had a reduced surface layer on all exposed surfaces. Electrical resistance measurements of the surface layer resulted primarily in electronic conduction as opposed to ionic conduction. The clear, originally colorless glass samples also exhibited color formation, ranging from light brown to black with increased time and temperature of treatment. The color formation was also confined to the exposed surfaces of the samples, where even the most intense black coating was reported to be only 0.001 inches thick.

The results of the present study are similar to those observed by Green and Blodgett[17] in that the electrical resistance measurements of the surface layer on the treated GeO_2 glass plates result in electronic conduction. The presence of an electrically conducting surface layer also supports the observation of a pure germanium crystalline layer, since crystalline GeO_2 would not exhibit the electrical properties observed.

8.4.4. Temperature Dependence of Crystallization

In order to discuss the effect of treatment temperature on the crystallization of the vitreous GeO_2 glasses, discussion of the glass transition temperature is necessary. The measured T_g of this glass is 510°C, as determined from a DSC with a 20 K/min heating rate. A literature survey of reported T_g values for vitreous GeO_2 glass, using Sci-Glass,[k] included 32 different references. The reported values span a range of almost 100 degrees. An interesting analysis of the reported T_g values, adopted from Shelby,[18] is presented in Figure 8.19. The reported values were grouped into ranges of 10 K, i.e. 470°C to 479°C, 480°C to 489°C, etc., from 470°C to 570°C. Each group is labeled with the median of

[k] Taken from 32 references listed by SciGlass, Version 6.5, 1998-2005 SciVision, Inc.

the 10 K range. The histogram showing the distribution of reported values has a maximum in the range of 510°C to 519°C. The measured value of the T_g of the as-melted GeO_2 glass is in good agreement with previously reported values.

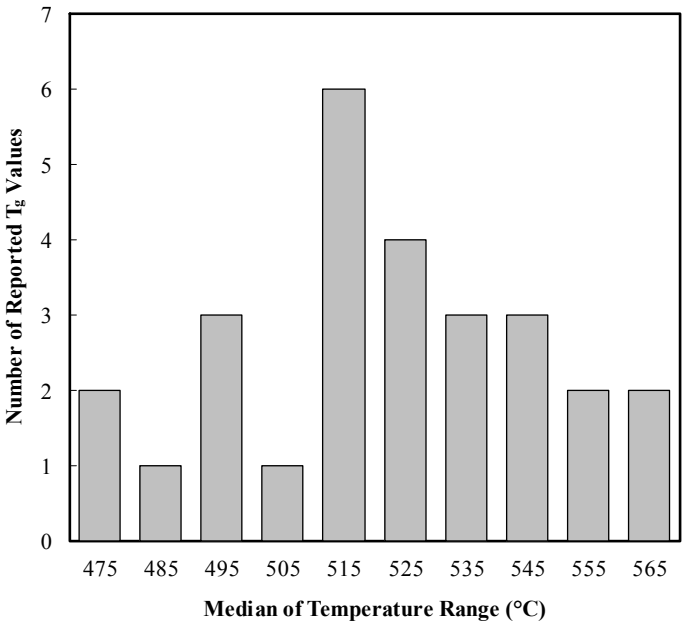

Figure 8.19. Distribution of reported T_g values for vitreous GeO_2 from literature.

Although treatments at 500°C are in the range of the reported T_g values for GeO_2 glass, it appears that treatments at 450°C and 400°C are below any reported T_g values. One would expect crystallization of the glass to occur at a much faster rate at treatment temperatures approaching the T_g of the glass. The optical micrographs shown in Figure 8.14, as well as the optical absorption spectra in Figures 8.15 through 8.17 clearly show the effect of temperature on the formation of pure germanium crystals at the surface of the treated glass samples. The gradual darkening of the glass samples, leading to the formation of an opaque silver/grey continuous crystalline layer, occurs more rapidly as the treatment temperature increases. The formation of fully conductive surface layer also correlates well with these observations, as the formation of continuous surface layer also occurs more rapidly as the treatment temperature increases.

8.5. Conclusion

Unlike pure SiO_2 glass, pure GeO_2 glass is extremely susceptible to weathering. Extended storage of pure GeO_2 glass in an ambient atmosphere results in the formation of GeO_2 crystals on the surface of the glass. Hydrogen reactions with pure GeO_2 glasses below T_g result in the complete reduction of germanium species in the glass. The presence of crystalline germanium was determined using XRD and EDS measurements. Hydrogen reactions with pure GeO_2 glasses resulting in the crystallization of pure germanium are a function of time and temperature.

8.6. References

1. J.E. Shelby, *Introduction to Glass Science and Technology;* pp. 78-97,196. Royal Society of Chemistry, Cambridge, UK, 1997.

2. A.J. Cohen, "Impurity Induced Color Centers in Fused Silica," *J. Chem. Phys.,* **23** [4] 765-6 (1955).

3. A.J. Cohen, "Neutron Specific Color Center in Fused Silica and an Impurity Band of Identical Wave Length," *Phys. Rev.,* **105** [4] 1151-5 (1957).

4. A.J. Cohen and H.L. Smith, "Ultraviolet and Infrared Absorption of Fused Germania," *Phys. Chem. Solids,* **7,** 301-6 (1958).

5. V. Garino-Canina, "Luminescence of Vitreous Silica as a Function of Temperature," *Compt. Rend.,* **238,** 1577-8 (1954).

6. V. Garino-Canina, "A New Phenomenon Relating to the Absorption Band at 2400 A and the Luminescence of Vitreous Silica," *Compt. Rend.,* **240,** 1331-3 (1955).

7. V. Garino-Canina, "Nature of Absorption Centers in Vitreous Silica," *Compt. Rend.,* **240,** 1765-7 (1955).

8. V. Garino-Canina, "The Absorption Band at 2420 A of Vitreous Silica-Germanium Impurity and Oxygen Deficiency," *Compt. Rend.,* **242,** 1982-4 (1956).

9. V. Garino-Canina, "Some Optical Properties of Vitreous Pure Germanium Oxide in the Ultraviolet," *Compt. Rend.,* **247,** 593-6 (1958).

10. V. Garino-Canina, "Diffusion of Oxygen in Vitreous Germanium Oxide," *Compt. Rend.,* **248,** 1319-22 (1959).

11. J.M. Jackson, M.E. Wells, G. Kordas, D.L. Kinser, R.A. Weeks, and R.H. Magruder III, "Preparation Effects on the UV Optical Properties of GeO_2 Glasses," *J. Appl. Phys.,* **58** [6] 2308-11 (1985).

12. J. Nishii, A. Chayahara, K. Fukumi, K. Fujii, H. Yamanaka, H. Hosono, and H. Kawazoe, "Comparison of Formation Process of Ultraviolet Induced Color Centers in GeO_2-SiO_2 Glass Fiber Preform and Ge-Implanted SiO_2," *Nucl. Instrum. Methods Phys. Res., Sect. B,* **116** [1-4] 150-3 (1996).

13. H. Hosono, Y. Abe, D.L. Kinser, R.A. Weeks, K. Muta, and H. Kawazoe, "Nature and Origin of the 5 eV Band in SiO_2:GeO_2 Glasses," *Phy. Rev. B,* **46** [18] 11445-51 (1992).

14. H. Hosono, H. Kawazoe, and K. Muta, "Preferred Concentration Enhancement of Photobleachable Defects Responsible for 5 eV Optical Absorption Band in SiO_2:GeO_2 Glass Preform by Heating in a H_2 Atmosphere," *Appl. Phys. Lett.,* **63** [4] 479-81 (1993).

15. P.J. Vergano and D.R. Uhlmann, "Crystallisation Kinetics of Germanium Dioxide: The Effect of Stoichiometry on Kinetics," *Phys. Chem. Glasses,* **11** [2] 30-8 (1970).

16. K.J. Beales and C.R. Day, "A Review of Glass Fibers for Optical Communications," *Phys. Chem. Glasses,* **21** [1] 5-21 (1980).

17. R.L. Green and K. Blodgett, "Electrically Conducting Glasses," *J. Am. Ceram. Soc.,* **31** [4] 89-100 (1948).

18. J.E. Shelby, "Diffusion and Solubility of Water in Alkali Borate Melts," *Phys. Chem. Glasses,* **44** [2] 106-12 (2003).

CHAPTER 9: RESULTS SUMMARY: POSSIBLE REACTION MECHANISMS

9.1. Introduction

The results presented in the previous chapters are summarized in this chapter. The results of every chapter are considered collectively to provide a more complete understanding of the interactions between hydrogen and binary GeO_2-SiO_2 glasses at elevated temperatures. Suggested reaction mechanisms are discussed. Finally, recommendations for future work are proposed.

9.2. Summary of Results to Determine a Suggested Sequence of Events

The simplest way to address a suggested sequence of events for the phenomena found in this study is to discuss the basic way that hydrogen reacts with the glass sample at elevated temperatures and 700 Torr of hydrogen. Hydrogen molecules enter the sample through the surface and migrate into the bulk of the samples through a diffusion process. Hydrogen molecules react with the glass to form hydroxyl species and reduced germanium species at the exposed surfaces of the glass. With increasing time, hydroxyl species continue to form throughout the thickness of the sample following tarnishing model diffusion behavior. There was no detectable change in the concentration of hydride species in any of the experiments performed in this thesis.

There is sufficient evidence to show that reduced germanium species are also forming throughout the thickness of the sample, however, detectable colloid formation, i.e. nanocrystals of germanium reduced to the atomic state, is restricted to a depth of approximately one μm within the exposed surface of the sample. Even though reduced germanium species are forming throughout the thickness of the sample, the reduced species at the surface of the sample are distinguished from those formed within the bulk. The germanium species at the surface are reduced to the atomic state. This process is followed by diffusion of these species to form colloids or nanocrystals, i.e. small collections of germanium in the atomic state. Reduced germanium species within the bulk of the glass may also be reduced to the atomic state but diffusion to form a colloid could be affected by their position in the sample, i.e. atomic germanium species in the bulk of the glass may not be able to collect through diffusion to form a crystal large enough to be detectable by the instruments used in this study. Another explanation for

the lack of nanocrystal formation in the bulk of the glass sample could simply be that reduced germanium species located deeper within the sample may not be fully reduced to the atomic state. The color formation at the surface of the treated glass samples is a direct result of the colloid, or nanocrystal formation, since color is only observed where detectable crystal formation is present. Color formation does not stop when hydroxyl formation reaches saturation equilibrium, i.e. significant changes in the UV-Vis spectra continue with progressive hydrogen treatment even after changes in the infrared absorption spectra cease.

9.2.1. How Observations Made in This Thesis Compare to Previous Reaction Models

Structural information can be obtained from hydrogen reactions with specific sites in the glass. Knowledge of the sites at which hydrogen reacts in the glass network can lead to information concerning defects or defect precursor sites present in the glass network. Cohen and Smith[1] reported that hydrogen molecules diffusing from the atmosphere preferentially react with germanium species in the glass and form GeOH groups. This suggestion is consistent with the results of this and a number of other studies, since both the final concentration and shape of the hydroxyl band depend on the concentration of germanium in the glass. Mochizuki et al.[2] also claimed that the reaction sites for hydroxyl formation are associated with defect centers in the glass and furthermore, that the defects themselves are associated with the presence of germanium in the glass.

Although Awazu and many others[3-5] have reported formation of hydride species with hydrogen treatment of binary GeO_2-SiO_2 glasses, no significant formation of hydride species was observed in this study. Others[3,5] have proposed a reaction suggesting the formation of hydride species, as well as hydroxyl species;

$$\equiv \text{Ge-O-Si} \equiv + H_2 \rightarrow \equiv \text{GeH} + \equiv \text{SiOH} \qquad (9.1)$$

The absence of a significant formation of hydride species in the glass leads to the conclusion that reaction mechanisms involving the formation of a significant amount of such species can be eliminated from further consideration. Equation 9.1 and similar

reaction mechanisms do not account for the 'excess' formation of OH species necessary to explain the lack of hydride species formation. Reactions including hydride species formation do not fit the results of this study unless a subsequent, independent reaction involving the destruction or elimination of hydride species is included.

Consideration of hydroxyl formation without hydride formation leads to the following suggested sequence of events during thermal treatment in a hydrogen atmosphere. Hydrogen molecules diffuse into the free volume of the glass through the exposed surfaces. The hydrogen subsequently reacts with the glass network at specific reaction sites. The proposed mechanism for the reaction is as follows;

$$\equiv \text{Ge-O-Si} \equiv + H_2 \rightarrow = \text{Ge:} + 2 \equiv \text{TOH} \qquad (9.2)$$

where T represents either Si or Ge. The hydrogen molecule reacts with the glass network to create two hydroxyl species and a germanium lone pair center (GLPC). This defect consists of a Ge^{+2} ion coordinated by two oxygen atoms and two lone pair electrons. This defect is also known as a neutral oxygen divacancy (Ge-NODV). The nature of this defect in binary GeO_2-SiO_2 glasses is fairly well characterized and is discussed in detail in Chapter 6. This reaction corresponds well with the prediction that hydrogen will preferentially react with the glass network at the weaker of the Ge-O-Si bonds. The lower melting temperature of GeO_2 as compared to that of SiO_2, as well as simple ionic field strength arguments, indicate that the Ge-O bond is considerably weaker than the Si-O bond. This reaction also explains the considerable hydroxyl formation without the corresponding formation of hydride species in one simple reaction.

A reaction mechanisms that would explain both the extensive formation of hydroxyl and the growth of the 242 nm band due to oxygen deficient centers is shown in Reaction 9.2. In a single reaction, the hydrogen molecule could react with a network forming bond, breaking the weaker Ge-O bond, resulting in the formation of a Ge-NODV, or lone pair center, with a lone pair of electrons, and various hydroxyl species. This single reaction explains the growth in the 242 nm band, as well as the extensive hydroxyl formation. This reaction is also supported by the observation that, after the colored surfaces are removed by polishing, the 242 nm band does not return to its as-

received intensity, as shown in Figures 6.13 and 6.14, implying that Ge-ODV's are formed throughout the thickness of the sample and are not confined to the near surface. Unfortunately, the observation that the 242 nm band does not grow with a square root time dependency suggests that this is not the correct reaction mechanism for reaction of hydrogen with binary GeO_2-SiO_2 glasses at elevated temperatures. One possible cause for the difference could be further reduction of germanium to the atomic state, which can be explained through a similar, successive step to Reaction 9.3

$$= Ge: + H_2 \rightarrow Ge^0 + 2 \equiv TOH \qquad (9.3)$$

whereby an already reduced Ge-NODV reacts with molecular hydrogen to create atomic germanium and more hydroxyl species, which would change the final concentration of Ge-NODV, making it appear as though the concentration does not have square root time dependence. Reaction 9.3, resulting in atomic germanium formation, could be confined to the surface region where obvious effects of colloid growth are present, however it is possible that atomic germanium is formed throughout the thickness of the sample but only germanium atoms at the surface have the ability to agglomerate and form colloidal species large enough to cause scattering effects. It is also possible that two completely unrelated reactions occur simultaneously with extended treatment time in hydrogen at elevated temperatures.

9.3. Future Work

Although there were many significant observations and conclusions presented in this thesis, there are still many opportunities to advance this research.

9.3.1. Reduction of Germanium Species

The use of XRD and Raman spectroscopy to identify and characterize reduced germanium species confined to the exposed surface of the glasses treated in this thesis provided conclusive evidence that pure germanium species are a product of the reduction reaction. Although the identification of pure germanium crystals is, in and of itself, an

important observation, additional experiments could be performed to provide a more complete characterization of the crystals formed. The kinetics and limitations of the reduction process could be more precisely defined. Treatment of binary GeO_2-SiO_2 glass samples at elevated temperatures in air after significant nucleation has taken place could potentially be used to study the kinetics of crystal growth without excess hydrogen available. High temperature XRD measurements could be used to determine the rate of crystallization.

9.3.2. Use of the Striations to Create NewTechnology

The effect of striations in binary GeO_2-SiO_2 glasses on the reduction of germanium species is profound. If the kinetics of the germanium reduction and subsequent crystal growth process could be more clearly defined, the knowledge could be used to control the size distribution of the germanium crystals. Control over the crystal size distribution, coupled with the unique ability to create striations in VAD glasses, i.e. control the placement of crystal growth, could lead to a significant number of applications.

9.3.3. Observation of Other Related Phenomena that Need Further Attention

The unique response of binary GeO_2-SiO_2 glasses to UV exposure and the affect of this response on the experiments performed here could lead to interesting results. It is well known[6-9] that UV exposure shifts the population of defects related to reduced germanium species, however the effect of this population conversion on the way that binary GeO_2-SiO_2 glasses react with hydrogen has not been extensively studied. A simple experimental design could include exposure of glass samples to intense UV light for variable amounts of time while monitoring changes in UV-Vis absorption spectra, i.e. the 242 nm band attributed to defects related to reduced germanium species. After significant changes have taken place, the effect of defect population conversion on hydrogen reactions could be evaluated using experiments similar to those performed in this study.

Another interesting way to change the concentration of defects related to reduced germanium species is to treat thin samples of binary GeO_2-SiO_2 glasses in an atmosphere

of excess oxygen. It has been shown[8,9] that oxygen can be used to anneal or decrease the concentration of reduced germanium defects, i.e. reduce the intensity of the 242 nm band. As expected, oxygen diffusion is significantly slower than hydrogen diffusion in binary GeO_2-SiO_2 glasses. It would be necessary to use extremely thin samples to see results within a reasonable amount of time. While observation of oxygen diffusion and subsequent reaction with defects related to reduced germanium species, in and of itself, would be a very valuable study, the effect of elimination of reduced germanium species on hydrogen reactions could potentially be an even more important study.

9.3.4. Study Hydroxyl Formation in Other Colloid Forming Glasses

In this particular study, there was no significant relationship found between the formation of bound hydrogen species and formation of colloidal germanium in the glass. It would be interesting to investigate other glass systems that have previously shown formation of colloids with treatment in hydrogen at elevated temperatures, and study the hydroxyl formation behavior. In binary GeO_2-SiO_2 glasses, hydroxyl forms throughout the thickness of the glass while colloids are confined to the surface. Is this reaction mechanism similar in all colloid forming glass systems or do other glass systems show a more direct correlation between hydroxyl formation and colloid growth? For example, the observation of colloids in the surface of certain glass systems that contain lead as a main constituent have shown similar colloid forming behavior. How does colloid formation related to hydroxyl formation in these glasses? Perhaps the addition of information concerning the hydroxyl growth kinetics of colloid forming glass systems could lead to the determination of a relationship between hydroxyl formation and colloid formation.

9.3.5. Further Clarify Anomolies Presented in Reactions of Hydrogen with GeO_2

Perhaps the best way to observe reduction of germanium species in a glass is to examine the reactions between hydrogen and pure GeO_2 glass. There is no question that there are several unexplained results when the reactions between hydrogen and GeO_2 glass are considered. Further characterization of crystal growth on the surface of the

GeO_2 glass merits attention. With the XRD pattern of the crystalline surface showing such well-developed crystallization of pure germanium, the observation of an interconnected, non-faceted morphology in ESEM images was unexpected and remains unexplained. Although a diverse collection of multi-faceted crystals with a wide, but fairly organized, size distribution was observed, the bulk of the crystallized layer exhibited the interconnected, non-faceted morphology. Although challenging, a rather interesting study could be designed around the identification of the interconnected, non-faceted morphology and explanation of the presence of two completely different morphologies.

The use of dc conductivity experiments to determine the onset of conductivity were important to add understanding of the continuity and degree of crystallization. Additional experiments could be performed to further define the properties of the germanium layer. Since germanium is a photoconductor, the conductivity of the germanium film should increase if exposed to light. Since germanium is a semiconductor, the conductivity of the germanium layer should increase with increasing temperature (more charge carriers).

Perhaps one of the most important differences between GeO_2 and SiO_2 is the fact that structural defects are more common in vitreous GeO_2 than in vitreous SiO_2, with a measurable number of Ge-Ge bonds.[10] One particularly interesting study, which follows the same outline as those presented above, would be to study the effect of oxygen treatment on GeO_2 glasses to reduce the concentration of oxygen deficient defects and then study the effect of this reduction on subsequent reactions with hydrogen. Vergano and Uhlmann[11] found that the formation GeO_2 crystals upon quenching had a strong correlation to the reduction state of the glass. Could this same relationship be established for hydrogen treatment of GeO_2 glasses?

9.4. References

1. A.J. Cohen and H.L. Smith, "Ultraviolet and Infrared Absorption of Fused Germania," *Phys. Chem. Solids,* **7,** 301-6 (1958).

2. K. Mochizuki, Y. Namihira, and M. Kuwazuru, "Absorption Loss in Optical Fibers Due to Hydrogen," *Electron. Lett.,* **20** [13] 550-2 (1984).

3. K. Awazu, "Comments on 'Thermal and Photo-Initiated Reactions of H_2 with Germanosilicate Optical Fibers'," *J. Non-Cryst. Solids,* **201** [3] 267-71 (1996).

4. B.I. Greene, D.M. Krol, S.G. Kosinski, P.J. Lemaire, and P.N. Saeta, "Thermal and Photo-Initiated Reactions of H_2 with Germanosilicate Optical Fibers," *J. Non-Cryst. Solids,* **168** [1-2] 195-9 (1994).

5. Q. Zeng, J.F. Stebbins, A.D. Heaney, and T. Erdogan, "Hydrogen Speciation in Hydrogen-Loaded, Germania-Doped Silica Glass: A Combined NMR and FTIR Study of the Effects of UV Irradiation and Heat Treatment," *J. Non-Cryst. Solids,* **258** [1-3] 78-91 (1999).

6. H. Hosono, Y. Abe, D.L. Kinser, R.A. Weeks, K. Muta, and H. Kawazoe, "Nature and Origin of the 5 eV Band in SiO_2:GeO_2 Glasses," *Phy. Rev. B,* **46** [18] 11445-51 (1992).

7. H. Hosono, H. Kawazoe, and K. Muta, "Preferred Concentration Enhancement of Photobleachable Defects Responsible for 5 eV Optical Absorption Band in SiO_2:GeO_2 Glass Preform by Heating in a H_2 Atmosphere," *Appl. Phys. Lett.,* **63** [4] 479-81 (1993).

8. K. Awazu, H. Kawazoe, and M. Yamane, "Simultaneous Generation of Optical Absorption Bands at 5.14 and 0.452 eV in 9 SiO_2:GeO_2 Glasses Heated under an H_2 Atmosphere," *J. Appl. Phys.,* **68** [6] 2713-8 (1990).

9. K. Awazu, H. Onuki, and K. Muta, "Mechanisms of Photo-Bleaching of 5 eV Optical Absorption Band in Hydrogen Loaded Ge-Doped SiO_2," *J. Non-Cryst. Solids,* **211** [1-2] 158-63 (1997).

10. J.E. Shelby, *Introduction to Glass Science and Technology;* pp. 78-97,196. Royal Society of Chemistry, Cambridge, UK, 1997.

11. P.J. Vergano and D.R. Uhlmann, "Crystallisation Kinetics of Germanium Dioxide: The Effect of Stoichiometry on Kinetics," *Phys. Chem. Glasses,* **11** [2] 30-8 (1970).

APPENDIX A

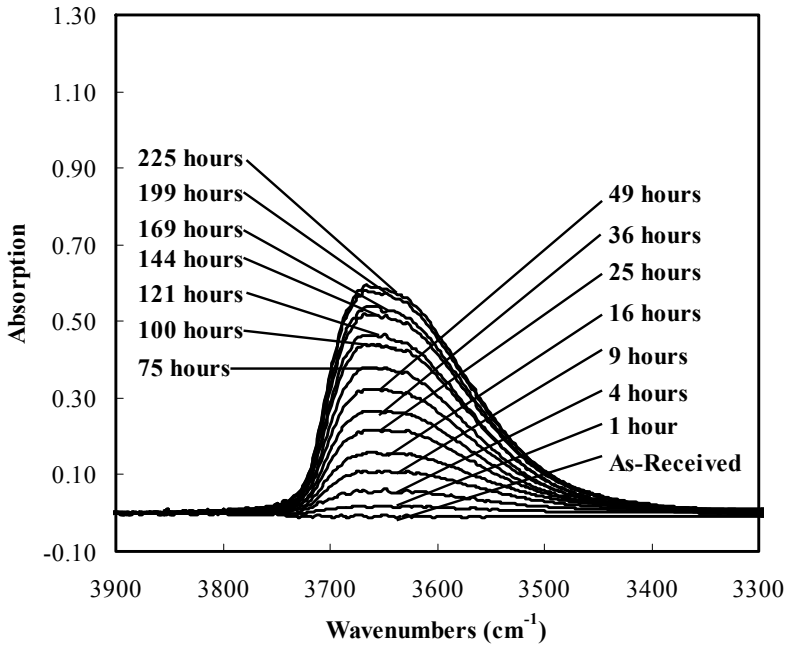

Figure A1. Infrared spectra in the hydroxyl/water region for 6 mol% GeO_2 - 94 mol% SiO_2 glass during progressive hydrogen treatment at 500°C for the indicated cumulative treatment time.

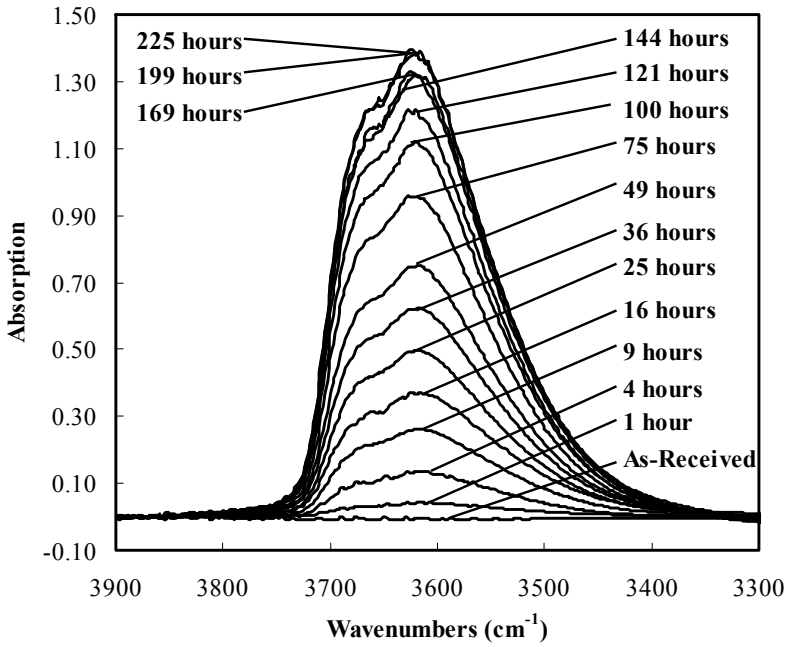

Figure A2. Infrared spectra in the hydroxyl/water region for 14.6 mol% GeO_2 - 85.4 mol% SiO_2 glass during progressive hydrogen treatment at 500°C for the indicated cumulative treatment time.

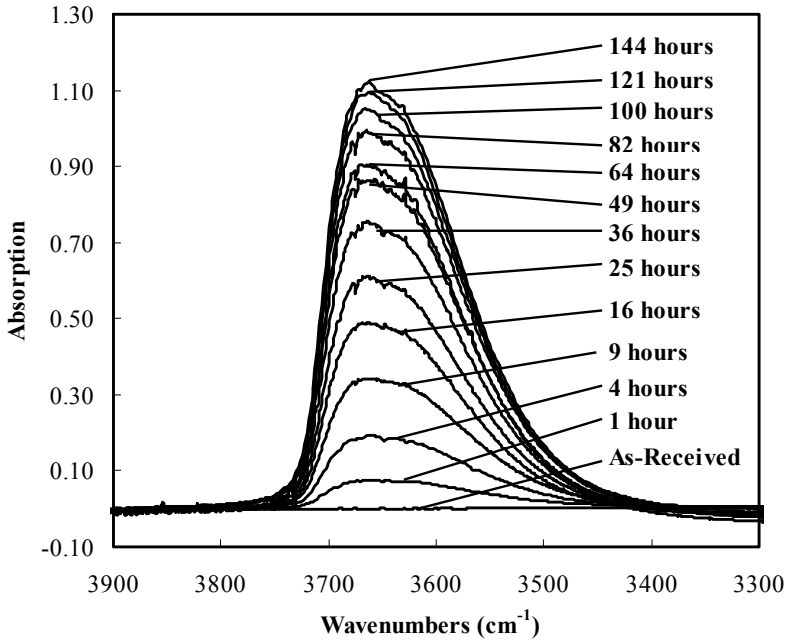

Figure A3. Infrared spectra in the hydroxyl/water region for 6 mol% GeO_2 - 94 mol% SiO_2 glass during progressive hydrogen treatment at 600°C for the indicated cumulative treatment time.

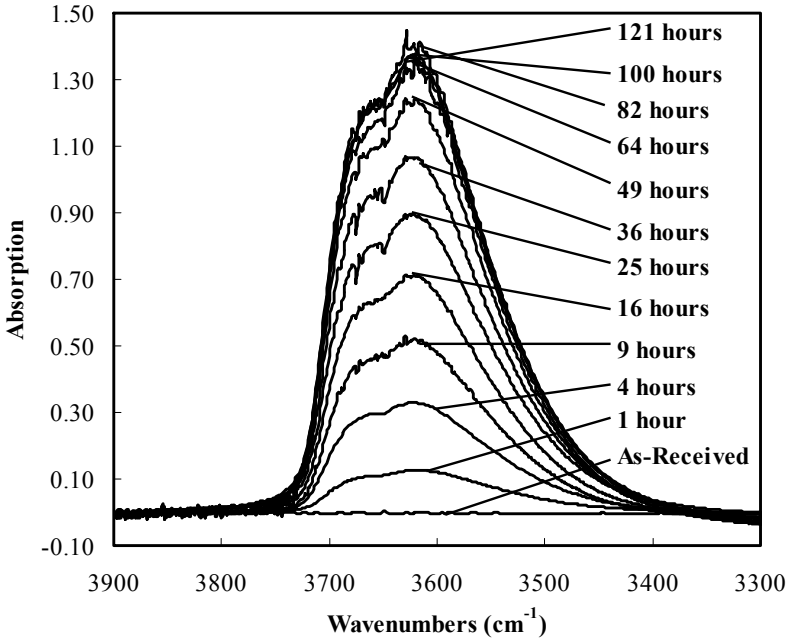

Figure A4. Infrared spectra in the hydroxyl/water region for 14.6 mol% GeO_2 - 85.4 mol% SiO_2 glass during progressive hydrogen treatment at 600°C for the indicated cumulative treatment time.

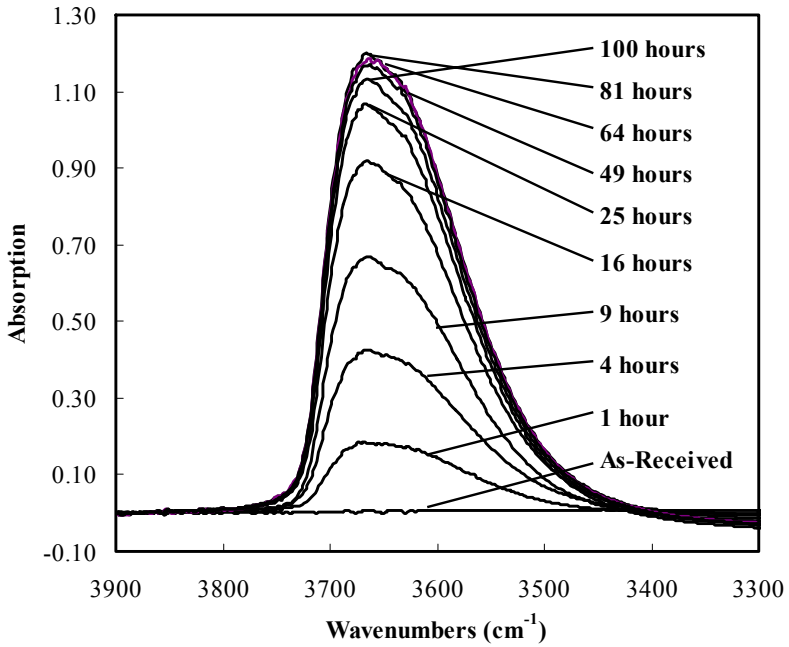

Figure A5. Infrared spectra in the hydroxyl/water region for 6 mol% GeO_2 - 94 mol% SiO_2 glass during progressive hydrogen treatment at 700°C for the indicated cumulative treatment time.

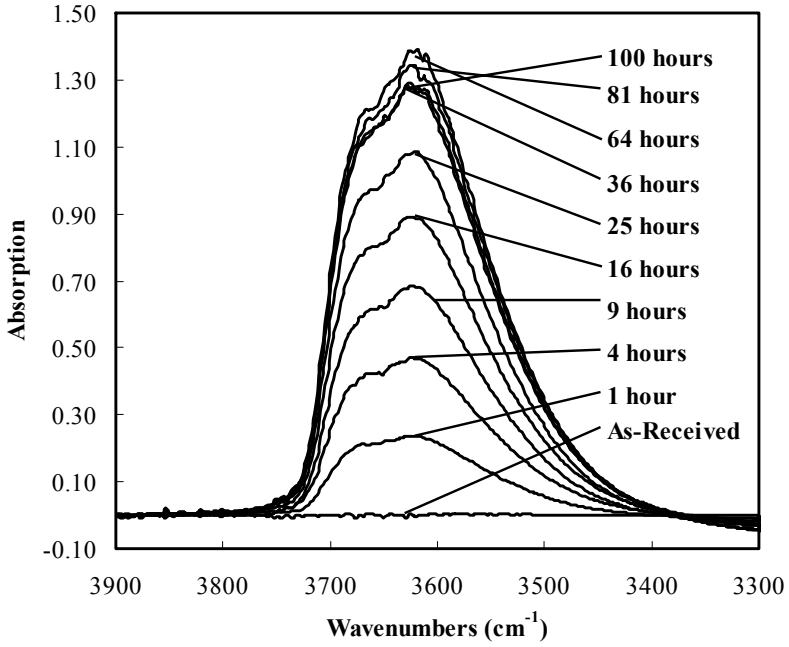

Figure A6. Infrared spectra in the hydroxyl/water region for 14.6 mol% GeO_2 - 85.4 mol% SiO_2 glass during progressive hydrogen treatment at 700°C for the indicated cumulative treatment time.